Steel plate reinforcement of orthotropic bridge decks

Steel plate reinforcement
of orthotropic bridge decks

Dit proefschrift is goedgekeurd door de promotor:
 Prof. ir. F.S.K. Bijlaard

Copromotor:
 Dr. M.H. Kolstein

Samenstelling promotie–commissie:
 Rector Magnificus   voorzitter
 Prof. ir. F.S.K. Bijlaard   Technische Universiteit Delft, promotor
 Dr. M.H. Kolstein   Technische Universiteit Delft, copromotor
 Prof. dr. ir. A.A.A. Molenaar   Technische Universiteit Delft
 Prof. dr. ir. P. van Bogaert   Universiteit Gent
 Prof. Dr.-Ing. M. Feldmann   RWTH Aachen
 Prof. Dr. A. Reis   Instituto Superior Técnico
 Prof. ir. H.H. Snijder   Technische Universiteit Eindhoven
 Prof. ir. A.C.W.M. Vrouwenvelder   Technische Universiteit Delft, reservelid

Printed in the Netherlands

Abstract

Orthotropic steel decks are used in most of the major long span bridges in the world where low dead-weight is an important factor. For the same reason, they are also largely used in movable bridges. In the past decades, severe fatigue cracks have been reported at several welded joints in orthotropic steel bridge decks. One of the main reasons for the fatigue problems is the low stiffness of the deck plate, which is insufficient to deal with the wheel loads of heavy traffic. Moreover, the increase of heavy traffic in the last decades makes the fatigue phenomena an even greater concern.

This research investigates the reinforcement of orthotropic steel bridge decks (OBD) by adding a second steel plate to the existing deck. The main idea is to stiffen the existing deck plate which will reduce the stresses at the fatigue sensitive details and extend the fatigue life of the orthotropic bridge deck. Two reinforcement systems are subject of research, bonded steel plates system and sandwich steel plates system. In the bonded steel plates system, the existing OBD is reinforced by adding the second steel plate using a thin epoxy adhesive layer (approximately 2 mm thick). In the sandwich steel plates system, the existing deck is reinforced by adding a sandwich overlay which is composed of a polyurethane core (PU-core, from 15 mm to 30 mm thick) and the second steel plate. Both reinforcements are considered lightweight solutions (between 50 and 80 kg/m^2), which is of special importance for application on movable bridges.

The strategy used in this research is based on a multi-scale approach, in which the reinforcement behaviour is investigated in three structure-scales: (i) plate-scale, (ii) deck-scale and (iii) bridge-scale. The research was therefore divided into three main parts: Part I (plate-scale), Part II (deck-scale) and Part III (bridge-scale).

In Part I, the mechanical behaviour of the reinforcement system is studied. The material properties of the epoxy-adhesive and of the PU-core were determined at different temperatures. The static and fatigue behaviour of both reinforcement systems were investigated through experiments and numerical simulations, using finite element analysis on reinforced beams. The properties of both the epoxy material and of the polyurethane material are temperature dependent. However, since only 2 mm of adhesive thickness is used on the bonded steel plates reinforced beams, this temperature effect has hardly any influence on the bending stiffness of these beams.

Due to the relatively thick PU-cores used (15 mm to 30 mm), temperature has a significant influence on the bending stiffness of the sandwich steel plates reinforcement. Results show that the static and fatigue damage of the reinforcements are caused by the shear stresses in the adhesive layer, for the bonded system, and by the shear stresses in the faces-to-core interface, for the sandwich system. The fatigue strength of the bonded steel plates reinforced beams is not significantly affected by adhesive thicknesses between 1 and 3 mm. The same can be found for sandwich steel plates reinforced beams with 15 mm and 30 mm PU-core thickness.

In Part II, the behaviour and the effect of the reinforcement system on full-scale orthotropic bridge deck panels are investigated. Tests under realistic wheel loads were performed on deck-panels reinforced with the bonded and the sandwich system. The decks were subjected to static and fatigue wheel loads. In order to better understand the experimental results, linear elastic simulations were carried out on the static behaviour of the reinforced deck panels using finite element analysis. The results show significant stress reduction close to the fatigue sensitive details after applying both reinforcement systems. Considering two reinforcement solutions with approximately the same weight, the local stress reduction close to the welds is higher for the bonded steel plates solutions than for the sandwich steel plates solutions. The sandwich steel plates system reduces the global stresses more than the bonded steel plates system. It can be concluded that wheel loads up to 160 kN cause shear stresses which are considerably lower than the determined fatigue threshold of both reinforcement systems. Therefore, it is expected that wheel loads do not cause fatigue damage in any of the reinforcement systems.

Finally, in Part III, a real case study of reinforcing an orthotropic bridge deck is described. The performance of the bonded steel plates system was investigated during a monitoring campaign performed on a pilot application on the movable orthotropic deck of Scharsterrijn Bridge in the Netherlands. Strain data was recorded during controlled load tests and under normal traffic conditions. The short-term measurements carried out immediately before and after applying the reinforcement show significant stress reduction in the fatigue sensitive details of the bridge deck. By adding the second steel, the fatigue life of the deck-plate-to-stiffener weld is expected to increase 12 times at the deck plate side and 4 times at the stiffener web side. The long-term measurements carried out during the year after applying the reinforcement did not show significant changes on the performance of the reinforcement system.

Overall, the performance of these two light-weight solutions for reinforcing OBD proved to be efficient and durable. A step forward in the design approach to evaluate the reinforcement of OBD has been established.

Contents

List of Symbols

Latin

A_c elongation after fracture
b width of a cross-section
B first moment of area
Bi adhesive i of the bonded system
D flexural rigidity
E Young's modulus
f_y yield strength
f_u ultimate strength
G shear modulus
I second moment of area
K stiffness
L span or length
M bending moment
n cycles
n_f fatigue life
n/e ratio between numerical and experimental values
P load
R ratio between the minimum and maximum applied fatigue load
t thickness
T transverse or shear force
S shear stiffness
Sa surface preparation by blast-cleaning
Si polyurethane i of the sandwich system
w width of a wheel print
$\#$ number of specimens

Greek

ν Poisson's ratio
ρ material density
ε strain
σ stress

τ	shear stress
γ	shear strain
δ	displacement
Δ	amplitude or range

Subscript

a, ad	adhesive
$c, core$	core
$del.$	delamination
eq	equivalent
j	layer
lf	lower face
lp	lower plate
min	minimum
max	maximum
n	nominal
$optm$	optimum
t	tension
r	real
$Reinf.$	reinforced deck
uf	upper face
ult	ultimate
up	upper plate
$Unreinf.$	unreinforced deck
x, y, z	axis direction
y	yield

Supercript

$After$	after applying the reinforcement
$Before$	before applying the reinforcement
th	fatigue threshold

Abbreviations

3pbt	Three-point bending test
4pbt	Four-point bending test
5pbt	Five-point bending test
3D	Three dimensional
CLPT	Classical Laminate Plate Theory
Cb	Crossbeam
del.	delamination
Exp	Experiments

ERF	Strain reduction factor
FEA	Finite element analysis
FE	Finite element
FSDT	First-order Shear Deformation plate Theory
HSDT	High-order Shear Deformation plate Theory
IE	Intelligent Engineering
MA	Mastic asphalt
NDT	Non Destructive Testing
OBD	Orthotropic bridge deck
PU	Polyurethane
RHPC	Reinforced high performance concrete
RSD	Relative standard deviation
RT	Room temperature
sfa	shear failure of the adhesive
SD	Standard deviation
SG	Strain gauges
SN	Stress-cycle
SPS	Sandwich plate system
SRF	Stress reduction factor
tfp	tension failure of the plate
W	Weight
WB	Wheel type B
WC	Wheel type C

Chapter 1

Introduction

1.1 Background

An orthotropic bridge deck (OBD) consists of a deck plate supported in two perpendicular directions by a system of longitudinal stiffeners and transverse crossbeams which are, in turn, spanned by main girders. All these elements are connected by welding.

Fatigue is a well-known phenomenon in orthotropic bridge decks. Several welded details appeared to be extremely sensitive to fatigue loading and shortened drastically the life span of orthotropic bridge decks. One of the most threatening fatigue cracks concerning the traffic safety running on the bridge is the one at the longitudinal welds between the deck plate and trapezoidal stiffener. The main reason is the low stiffness of the deck plate, which is insufficient to deal with the wheel loads of heavy traffic. Moreover, the increase of heavy traffic in the last decades makes the fatigue phenomena an even greater concern. It became clear that existing orthotropic bridge decks needed to be stiffened in order to decrease the stresses at the welds and extend their fatigue life. In the past decades, this subject attracted international attention and several studies have been performed on the fatigue phenomena and on the possible reinforcement systems.

Numerous reinforcement techniques have been suggested. The common idea is to replace the existing wearing course, normally an asphalt layer, by a stiffer overlay. Most of the alternatives up to now were focused on the application for fixed bridges, where the dead-weight of the reinforcement overlay is not a main concern. However, orthotropic steel decks are also largely used in movable bridges. In this case, the reinforcement's dead-weight is a major parameter when choosing the most efficient solution to prolong their life span.

In this thesis, two reinforcements for OBDs are investigated. The reinforcement systems consist of adding a second steel plate to the existing deck. Both alternatives

are promising light-weight solutions for prolonging the life-span of orthotropic bridge decks.

1.2   Aim of the research

The main goal of this thesis is to investigate the performance of reinforcing orthotropic steel bridge decks (OBDs) by adding a second steel plate to the existing deck. The aim of the reinforcement systems is to stiffen the existing deck plate, reducing the stresses at the welds of the deck which results in extending the fatigue life of orthotropic bridge decks. Two reinforcements are subject of research, bonded steel plates system and sandwich steel plates system. In the bonded steel plates system, the second steel plate is bonded to the existing OBD by vacuum-infusing a thin epoxy adhesive layer with a thickness of approximately 2 mm. In the sandwich steel plates system, the existing OBD is reinforced by adding a sandwich overlay which consists of a polyurethane core (PU-core, from 15 mm to 30 mm thick) and the second steel plate. Both reinforcements are considered lightweight solutions for strengthening orthotropic bridges. The reinforcement systems are based on existing technology that has been developed and applied in other type of applications, such as for manufacturing of composite structures in aerospace industry in the case of the vacuum-infused application method or for repair of ferry decks in the naval industry in the case of the sandwich steel plates reinforcement.

1.3   Outline of the thesis

Chapter 2 gives a brief state of the art on orthotropic steel bridge decks. Their fatigue phenomena and especially their possible reinforcement techniques are discussed. Finally, the motivation and strategy of the research are underlined.

The research work has been divided into three main parts. Overall, three reinforcement scales are studied: (i) plate-scale , (ii) deck-scale and (iii) bridge-scale. Each part is dedicated to one scale of the reinforcement structure that has been studied.

Part I describes the research on the behaviour of reinforced steel plates. The plate-scale is the smallest studied and investigates the behaviour of reinforced beams. This part is covered in Chapters 3, 4 and 5. Chapter 3 presents the main findings of an analytical study that was undertaken on the flexural behaviour of the bonded and sandwich steel plates reinforced beams. A parametric study was performed in order to better understand the influence of geometrical, mechanical and structural parameters on the flexural performance of the reinforcements. The results showed the most important parameters and a guidance to the optimum design solutions for both reinforcement systems. Chapters 4 and 5 describe the static and fatigue tests carried out on reinforced beams of the selected solutions of bonded steel plates and sandwich steel plates system, respectively. Linear elastic numerical simulations were performed to better understand the experimental results. In this part of the

research the effect of temperature and load conditions on the static behaviour of the reinforcement are investigated. For each reinforcement, stress-cycle fatigue diagrams are derived from fatigue tests.

Part II is dedicated to the reinforcement behaviour when applied to full-scale orthotropic deck panels. The study includes a characteristic part of an OBD, composed of a deck-plate 5 m long and 2 m wide, three trapezoidal stiffeners and two crossbeams. This part is covered in Chapters 6, 7 and 8. In Chapter 6, the finite element analysis which simulates the behaviour of full-scale reinforced orthotropic steel deck when subjected to wheel loads is described. Chapter 7 presents the full-scale tests carried out on two reinforced orthotropic steel deck panels. One is reinforced with bonded steel plates and another with sandwich steel plates. The aim is to study the effect of the reinforcement on the deck-plate details and to investigate the structural performance of the reinforcement when applied on the orthotropic steel deck loaded by heavy wheels. The finite element analysis (FEA) described in Chapter 6 is validated using experimental data. This chapter also includes the findings of a parametric study which used the FEA to predict the behaviour of different reinforcement scenarios. Finally, Chapter 8 describes the French five-point bending tests that were performed on the sandwich steel plates system. The aim is to understand how well it simulates the fatigue load of an OBD and if it can be used to evaluate the performance of reinforcement systems for OBDs.

In Part III, a real case study of reinforcing an orthotropic bridge deck is described. The performance of the bonded steel plates reinforcement system has been evaluated after being applied on a real bridge. This scale is the largest and evaluates the real reinforcement performance. This part of the research is presented in Chapter 9 and covers the findings of a monitoring campaign carried out during the pilot application of the bonded steel plates reinforcement on the movable orthotropic deck of Scharsterrijn Bridge in the Netherlands.

Finally, the overall conclusions of this research together with recommendations for future work are presented in Chapter 10.

Figure 1.1 shows a schematic overview of the outline of the thesis.

| Chapter 1
Introduction | Problem definition
Goal of the study |
| Chapter 2
Orthotropic steel bridge decks:
Fatigue damage and Renovation | Literature review on OBD |

Part I: Behaviour of the reinforced steel plates (plate-scale)

| Chapter 3
Influence of the interface layer on the behaviour of reinforced steel plates | Chapter 4
Bonded steel plates reinforcement | Chapter 5
Sandwich steel plates reinforcement |
| Parametric study on the influence of geometry and mechanical properties on the bending stiffness of the reinforcement. | Bending static and fatigue behaviour of bonded steel plates reinforced beams. (material testing, bending tests and FEA) | Bending static and fatigue behaviour of sandwich steel plates reinforced beams. (material testing, bending tests and FEA) |

Part II: Behaviour of the reinforced orthotropic steel decks (deck-scale)

| Chapter 6
Numerical simulation of reinforced orthotropic steel decks | Chapter 7
Full-scale behaviour of reinforced orthotropic steel decks | Chapter 8
French 5pbt on sanwich steel plates reinforcement |
| Linear elastic simulation of wheel loads on reinforced OBD using finite element analysis. | Full-scale static and fatigue tests of reinforced deck-panels using realistic wheel loads. | How well do French 5pbt simulate the fatigue behaviour of OBD? Is it possible to use French 5pbt for evaluation of reinforcements systems? |

Part III: Monitoring of a reinforced orthotropic bridge (bridge-scale)

| Chapter 9
Structural monitoring of the reinforced Scharsterrijn Bridge | Pilot application of the bonded steel plates reinforcement on a real bridge.
Short and long term performance evaluation of the reinforcement. |

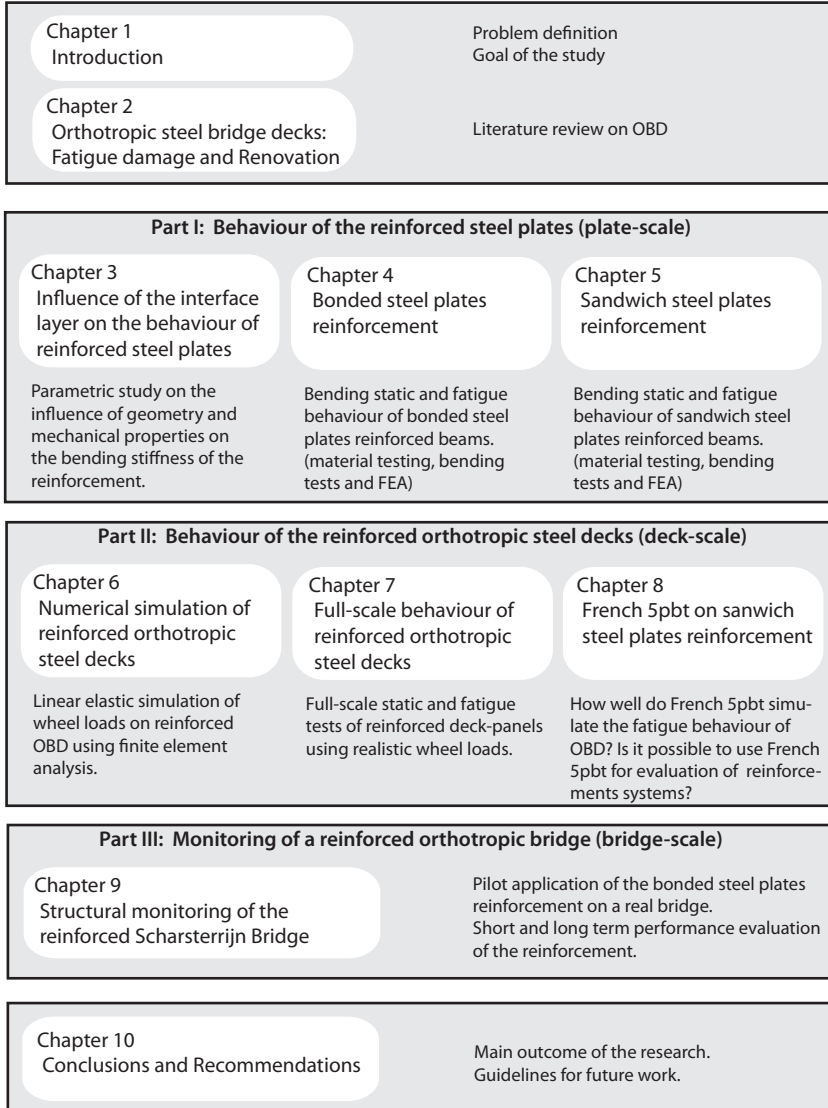| Chapter 10
Conclusions and Recommendations | Main outcome of the research.
Guidelines for future work. |

Figure 1.1: Outline of the thesis.

Chapter 2

Orthotropic steel bridge decks: Fatigue damage and Renovation

2.1   Orthotropic steel bridge decks

Orthotropic steel bridge decks are extremely cost-effective solutions when low dead-weight is an important factor. For this reason they are largely used in most of the major long span bridges in the world and in movable bridges (ASCE, 2008; Huang et al., 2010; Mangus and Sun, 2000).

An orthotropic steel bridge deck consists of a deck plate supported in two mutu-ally perpendicular directions by a system of longitudinal stiffeners and transverse crossbeams. The whole deck is supported by main girders. All these elements are connected by welding. Figure 2.1 shows a schematic drawing of an orthotropic deck (bottom 3D view and typical cross section).

There are two types of longitudinal stiffeners, the open type and the closed type. The closed stiffeners with a trapezoidal shape has been found to be the most practicable and efficient solution (see Figure 2.1(b)). Since they are the most widely used in the deck design, this thesis studies decks which use closed-type trapezoidal stiffeners. The stiffeners are typically spaced 600 mm apart. The transverse crossbeam are usually made of inverted T-sections and they are distanced 3000 mm to 5000 mm from each other. The most common deck plate thicknesses are 10 mm and 12 mm.
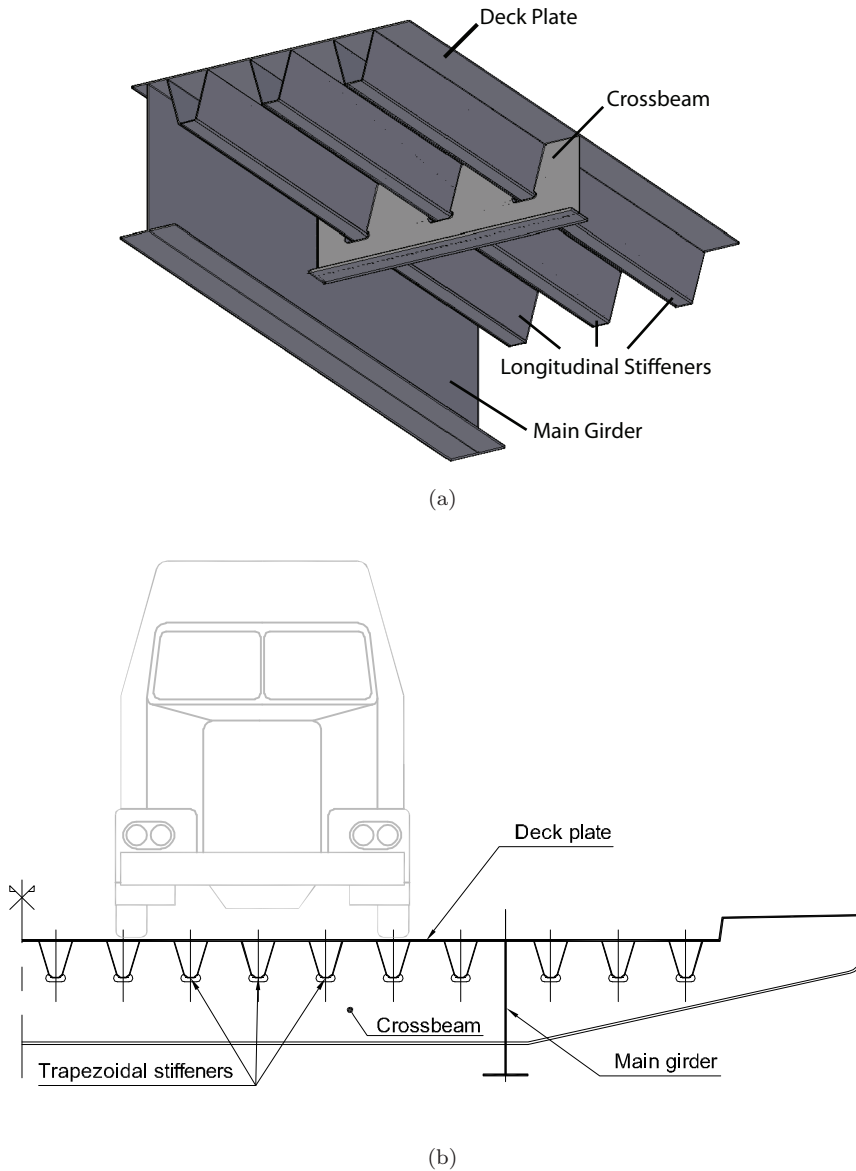
(a)

(b)

Figure 2.1: Orthotropic steel bridge deck (a) bottom 3D view and (b) cross section.

2.2   Fatigue failure modes

The main problem of orthotropic bridge decks is their fatigue life. In the past decades, severe fatigue cracks were found at several welds of orthotropic steel bridge decks. Numerous examples have been reported in Europe (Kolstein et al., 1998; Wolchuk, 1990), in Japan (Sim et al., 2009; Xiao et al., 2006; Yuge et al., 2004), in China (Wang and Feng, 2008) and in Brazil (Pfeil et al., 2005).

Several details suffer from fatigue damage in orthotropic bridge decks (Cheng et al., 2004; Jong, 2004). Investigation on the fatigue behaviour of orthotropic decks has attracted international attention (Janss, 1988; Sim et al., 2009; Tsakopoulos and Fisher, 2003; Uchida et al., 2008) and has led to a better understanding on the fatigue phenomena of the different details and their standard classification (Kolstein, 2007).

One of the most studied fatigue cracks is the one located at the longitudinal welds between the deck plate and the trapezoidal stiffener. When loaded by individual wheel loads, the deck-plate-to-stiffener weld is submitted to local transverse bending moments. If the deck is flexible, the bending moments will cause significant stresses and, therefore, the weld is likely to undergo fatigue cracking (Cullimore and Smith, 1981; Janss, 1988; Miki, 2006). One of the main reasons for these fatigue cracks is the low stiffness of the deck plate, which is insufficient to deal with the wheel loads of heavy traffic. Moreover, the increase of heavy traffic in the last decades makes the fatigue phenomena an even greater concern.

These last fatigue cracks can either start at the weld toe or at the weld root and grow either through the weld throat or through the deck plate thickness. The one starting at the weld root and growing through the deck plate thickness has recently received most attention. Figure 2.2 shows a schematic drawing with the fatigue crack locations in the deck and a detail of the typical crack shape. They are the most dangerous fatigue cracks. Firstly, because the crack initiation point is at the weld root, which makes inspection difficult. Secondly, because as the crack grows through the thickness of the deck plate, it affects the traffic safety running on the bridge. Intensive research on this severe fatigue crack has been performed, for example, by Jong (2006), Xiao et al. (2008), Ya and Yamada (2008), Ya et al. (2011), Inokuchi et al. (2008) and Ishio et al. (2008).

As already mentioned, the main cause of these fatigue cracks is the insufficient stiffness of the deck plate to deal with heavy traffic loading (Jong, 2006; Miki, 2006). The stresses at these longitudinal welds are more severe at the crossbeam location than between crossbeams due to the extra stiffness point induced by the crossbeam web. This stress concentration leads to an even shorter fatigue life of the welds at the crossbeam location than between crossbeams. The consequence of this is that fatigue cracks in the longitudinal welds at the crossbeam location appear in a very early age of the orthotropic bridge decks. A known case-study is the Van Brienenoord Bridge in the Netherlands, where these type of cracks at the crossbeam location were detected after only seven years of service-life (Kolstein et al., 1998).
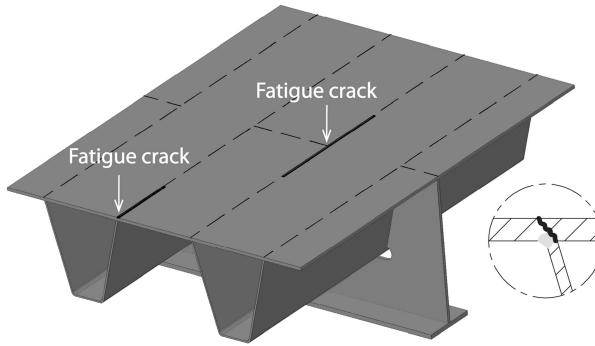
Figure 2.2: Fatigue cracks at orthotropic decks (location and detail).

In order to decrease the stresses at the welds and extend their fatigue life, the bending stiffness of the deck plate needs to be increased. It is therefore clear that renovation techniques are needed to stiffen the deck plate and extend the fatigue life of the existing orthotropic bridge decks.

2.3   Renovation of orthotropic steel bridges

Research projects have studied different renovation systems to strengthen existing orthotropic steel bridge decks. The main idea is to add a stiff layer on the top of the existing deck to increase its total stiffness. The stresses at the existing welds will decrease and their fatigue life will be extended.

Studies have been conducted in order to determine the most efficient renovation system for orthotropic bridge decks. Jong (2006) gives an overview of several ideas for renovation systems. Some of these were selected for further research which was mainly focused on renovation systems for fixed bridges. The renovation system selected for fixed bridges consisted of substituting the common asphalt surfacing by a reinforced concrete overlay.

For movable bridges, Jong (2006) also suggested alternative lightweight renovation systems and proposed using either a similar reinforced concrete overlay as used for the fixed bridges or bonding a second steel plate to the old steel deck plate. However, further research is needed to select the most efficient solution.

In the following sections, the most relevant systems for renovating orthotropic steel bridge decks are reviewed.

2.3.1 Common wearing courses

Several research projects have studied the structural behaviour of the common wearing courses in order to better understand their contribution to the stress reduction in the deck plate. The composite behaviour of the surfacing with the steel deck plate is complex and largely influenced by temperature and load frequencies. Therefore, the stress reduction is difficult to describe and to include in design rules (Kolstein, 2004; Smith and Cullimore, 1987; Wolchuk, 2002).

There are two types of surfacing materials used in wearing courses of orthotropic bridge decks: bituminous-based materials (such as asphalt and mastic asphalt) and polymer-based materials (such as polyurethane pavings and epoxy resins). The most commonly used wearing course in fixed bridges is a thick pavement of bituminous based material (40 mm to 80 mm thick), such as conventional asphalt or mastic asphalt. In movable bridges due to weight restriction a thin polymer based surfacing such as epoxy resins of 6 mm to 10 mm is commonly used.

Intensive research was performed by Medani (2006) in order to characterize the behaviour of bituminous-based materials in an orthotropic bridge deck as well as the membrane materials connecting the mastic asphalt surfacing and the steel deck (Liu et al., 2008; Medani et al., 2008). A design model for the membrane materials together with the mastic asphalt surfacing is proposed. Cong et al. (2009) built a model to help predicting the rutting development of similar mastic asphalt surfacing.

A benchmarking between two types of surfacing for fixed bridges was performed by Jong et al. (2004). The comparison is between a 50 mm mastic asphalt surfacing and a 50 mm polymer-based surfacing called ZOK. When using the asphalt surfacing, field measurements and experiments showed a stress reduction compared with no surfacing of 80% to 10% depending on temperature. When using ZOK surfacing, the experiments showed a reduction compared with no surfacing of 90% to 50% (Jong, 2006). The polyemer-based materials are considerably less temperature dependent than the bituminous-based ones.

New alternatives are also being suggested to upgrade the surfacing performance, for example by combining the asphalt with a layer of glass fibre reinforced mesh (Smith and Bright, 2001) or replacing the asphalt by a neoprene layer (Backer et al., 2008).

2.3.2 Concrete overlay system

An effective renovation system to reduce the stress ranges at the deck plate is to replace the common wearing courses by a concrete overlay. This renovation technique is being applied in several fixed bridges in the world.

In the Netherlands, the common 50 mm thick asphalt surface is being replaced by 50 mm to 100 mm thick Reinforced High Performance Concrete (RHPC) bonded to the deck plate by a thin epoxy layer. Extensive research on this system was performed by Jong (2006). Experiments carried out on bridge deck-panels showed a stress reduction of 90% on the deck plate when compared with no surfacing. Fields

measurements performed during renovations of two orthotropic brides in the Netherlands showed a stress reduction close to the welds of 80% after the reinforcement when compared with no surfacing (Jong and Kolstein, 2004; Kolstein and Sliedrecht, 2008).

A mechanical model of a comparable concrete overlay solution was extensively studied by Walter (2005). The main issue on this type of renovation system is the unavoidable cracking of the concrete overlay which can lead to debonding between the overlay and the steel plate. However, inducing multi-cracking behaviour on the concrete overlay can be the solution to avoid that problem (Walter et al., 2007). The concrete overlay system has also been applied using shear studs to connect the concrete overlay to the steel plate in Brazil (Battista et al., 2008) or shear studs together with an adhesive layer in Japan (Murakoshi et al., 2008).

For movable bridges, alternative renovation systems are required due to weight and height limits. The proposed concrete overlay system replaces the usual epoxy wearing course of 6 mm to 8 mm thick by a layer of reinforced ultra high performance concrete of 20 mm to 30 mm thick. Static bending tests carried out on beams representing the renovated deck show a stress reduction of 70% after renovation, when compared with no surfacing, with an increase of approximately 50 to 60 kg/m^2 to the bridge deck (Boeters et al., 2009; Schrieks, 2006).

2.3.3   Second steel plate reinforcement

The need for more efficient light-weight solutions to reinforce movable bridges led to another very promising system which consists of adding a second steel plate to the existing bridge deck. The reinforcement can simply bond the second steel plate to the existing deck or add it creating a sandwich structure. The second steel plate is generally 5 mm to 8 mm thick.

For the bonding system, the first studies were focused on selecting the right adhesive material to the bonding layer and correspondent application method (Jong, 2006). The first application method consisted of applying Sikadur 30 in the existing deck plate, using a glue comb, and then placing the second steel plate on top. Static and fatigue full-scale tests were performed on deck-panels reinforced by steel plates of 1500 mm by 2600 mm. During the fatigue test delamination occurred on the adhesive layer (Straalen and Hagen, 2003). A similar application method was tested by Corte (2011) using a different adhesive type, PC5800/BL epoxy. Fatigue tests were performed on deck-panels reinforced with two steel plates of 600 mm by 300 mm. After 5 million cycles no fatigue damage was observed on the adhesive layer. Labordus (2006) suggested an alternative application method which consists of vacuum-infusing the adhesive layer between the two steel plates. The adhesive material is a resin epoxy with low viscosity. Static and fatigue tests performed in beams specimens and small parts of OBD showed good fatigue resistance. For the described studies the second steel plate was 6 mm thick.

As an alternative to the bonding system, the second steel plate can be added to the existing deck creating a sandwich structure. The two faces of the sandwich are

the existing deck plate and the second steel plate. The thick core of the sandwich, besides bonding the steel plates together, allows to increase the bending stiffness of the reinforcement. Overduin et al. (1999) studied a renovation solution consisting of a 10 mm thick second steel plate connected with the existing deck by a 30 mm thick synthetic layer. The results showed that the synthetic material used for the core was relatively weak (Young's modulus 32 MPa). A more promising solution is the Sandwich Plate System (SPS) developed by Intelligent Engineering in which the sandwich of two steel plates is separated by a stiffer polyurethane core (Young's modulus approx. 750 MPa at room temperature) (Kennedy et al., 2002). This technology was initially developed to repair and upgrade ferry decks but has been applied in many other fields, such as new bridge decks and repairing of existing bridge decks (Kennedy and Murray, 2004; Vincent and Ferro, 2004). The use of SPS to repair OBD has been studied by Feldmann et al. (2007). The research included experimental and numerical investigation on the reinforcement of OBD using a 6 mm thick second steel plate and a 20 mm to 30 mm thick core (Minten et al., 2007). A pilot application of SPS to strengthen a fixed orthotropic bridge deck was carried out on the Schönwasserpark Bridge near Krefeld in Germany (Friedrich, 2007; Matuschek et al., 2007). SPS applications for new and repairing bridge decks are also being studied in China (Zhang et al., 2011). For both studies, the SPS is used to reinforce fixed bridges and on the top of the SPS overlay there is a 50 mm thick asphalt layer.

2.4   Proposed steel plate reinforcement: Motivation and Strategy

This thesis investigates the second steel plate reinforcement as a strengthening system for orthotropic steel decks, mainly for application in movable bridges. Two alternatives to add the steel plate have been studied: the bonded system and the sandwich system.

The bonded system consists of bonding the second steel plate with a thin adhesive layer. It was decided to further investigate the reinforcement using the previously mentioned application method which uses vacuum infused resin epoxy between the two steel plates. The previous applications undertaken by Labordus (2006) showed good results in terms of the quality of the adhesive layer, but fundamental research is limited. In the thesis, this system is referred to as bonded steel plates reinforcement and a detail is shown in Figure 2.3(a).

The sandwich system consists of adding the second steel plate creating a sandwich structure. The sandwich faces are the existing deck plate and the second steel plate, which are connected by the core of the sandwich. It was decided to study the Sandwich Plate System SPS patented by Intelligent Engineering. Although this system has been applied in different engineering fields all around the world, optimization and fundamental research are needed for further application in orthotropic steel bridge

decks. In the thesis, this system is referred to as sandwich steel plates reinforcement and a detail is shown in Figure 2.3(b).

The motivation for choosing the second steel plate reinforcement is due to its low dead-weight. The concrete overlay systems are often too heavy for application on existing movable orthotropic bridge decks. For these structures, the weight limits are very strict and light-weight reinforcements are the only possible solution. The usual low density of core materials can make the sandwich steel plates system an efficient light-weight solution. The bonded steel plates system is also a light-weight solution and can be the only one to fulfil the height limits required. The strategy used on this thesis is based on a multi-scale approach, in which the reinforcement behaviour is investigated in three structure-scales: (i) plate-scale, (ii) deck-scale and (iii) bridge-scale.
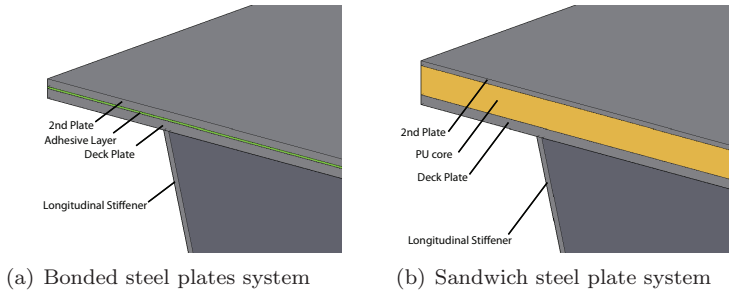

(a) Bonded steel plates system   (b) Sandwich steel plate system

Figure 2.3: Detail of the steel plate reinforcement systems.

Part I

Behaviour of the reinforced steel plates

Chapter 3

Influence of the interface layer on the behaviour of the reinforced steel plates *

3.1   Introduction

The present chapter presents the findings of an analytical study that was performed on the flexural behaviour of the bonded and sandwich steel plates reinforcement. A parametric study was performed in order to better understand the influence of geometrical, mechanical and structural parameters on the performance of the reinforced plates. The thickness of the second steel plate and thickness of the interface layer between the existing deck and the second steel plate are varied as well as the extra weight added to the existing structure. The influence of the mechanical properties of the interface layer is investigated. The aim is to select the most important parameters for the systems' performance for conducting further research. The performance is evaluated by the reinforced plates stiffness and by the stress reduction on the steel plate after applying the reinforcement.

3.2   Materials and Geometry

3.2.1   Materials

Steel grade S355 (f_y = 355 MPa; f_u = 510 MPa; E = 210 GPa; ν = 0.3) was selected for the existing deck plate and the second steel plate (EN1993-1-1, 2006).

---

*This chapter is based on Teixeira de Freitas et al. (2012a).

The materials selection for the interface layer was based on a market prospective of the adhesive materials available. The aim was to work with real inputs for the analytical study, instead of random values for the mechanical properties of the adhesives. Two types of polymer based materials were used for the interface layer: epoxy for the bonded steel plates reinforcement and polyurethane for the sandwich steel plates reinforcement. Four epoxies and four polyurethanes were selected. In the current chapter, both epoxies and polyurethanes will be referred to as adhesives. Table 3.1 lists the adhesives mechanical properties based on the manufacturer data (values for room temperature).

Table 3.1: List of adhesives (E_a Young's modulus; G_a shear modulus; v_a Poisson's ratio; ρ_a density).

Reinforcement	Adhesives	E_a(MPa)	G_a(MPa)	v_a(-)	ρ_a (kg/m^3)
Bonded steel plates	B1	1560	350	0.41	
	B2	1920	483	0.41	
	B3	2100	550	-	1050
	B4	2900	1036	0.4	
Sandwich steel plates	S1	2.9	0.5	-	1150
	S2	840	40	-	
	S3	1580	80	-	
	S4	874	285	0.36	

3.2.2   Geometry

The typical cross-section of the reinforced steel plates has three layers: the lower plate representing the existing steel deck, the upper plate representing the second steel plate and the adhesive layer that bonds the plates together. Figure 3.1 shows a drawing of the typical cross-section, where t_{lp} is the thickness of the lower plate, t_a is the thickness of the adhesive layer and t_{up} is the thickness of the upper plate. The total thickness and width of the cross-section are represented by t and b, respectively.
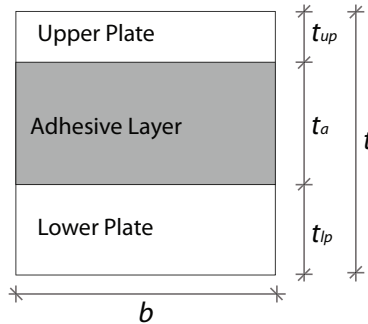

Figure 3.1: Typical cross-section of the reinforced steel plates.

The minimum thickness of the second steel plate was set at 5 mm (t_{up}), since in real applications a minimum robustness of the plate in contact with the wearing course is required. The maximum thickness of the epoxy layer in the bonded steel plates reinforcement was set at 5 mm (t_a). No restrictions were made on the maximum thickness of the polyurethane core in the sandwich steel plates reinforcement since it depends on the height restrictions of each existing deck. The weight of the reinforcement system, i.e. the extra weight added to the existing orthotropic deck (adhesive layer and second steel plate), was varied between 40 to 70 kg/m^2. The study was performed for 10 and 12 mm thick lower steel plate (t_{lp}) since these are the typical deck plate thicknesses of fixed and movable orthotropic steel bridges, respectively, in the Netherlands. Table 3.2 summarizes the main characteristics used for each reinforcement system in the current study.

Table 3.2: Reinforcements' main characteristics.

	Reinforcement	Bonded steel plates	Sandwich steel plates
Plates	Geometry	$t_{up.min}$=5 mm	
		t_{lp}=10 mm and 12 mm	
	Material	steel	
Adhesive	Geometry	$t_{a.max}$=5 mm	no limits
	Material (see Table 3.1)	Epoxies: B1 to B4	Polyurethane: S1 to S4
Weight – W		40 to 70 kg/m^2	

3.3   Analytical study

An analytical study was carried out in order to determine the stiffness and stress reduction factor of the two reinforcements: bonded and sandwich steel plates. The model used for carrying out the analytical study is a simply supported beam, subjected to three point bending. Such a simple model enables studying numerous parameters and a wide range of values in each parameter. More complex models can only be applied after selecting the most important parameters and their more efficient values. Even though the quantitative results obtained for this model cannot be compared or extrapolated for the real structures, the model used is valuable for the main aim of this study, which is to check the important parameters, optimize the structure and compare both reinforcements.

Figure 3.2 shows the beam-model where x, y, z are the axes in the direction of the length, width and thickness, respectively. The beam with span L is subjected to three-point loading by a load P. The beam cross-section is the one presented in Figure 3.1 with 100 mm width (b=100 mm).
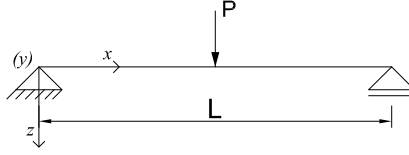
Figure 3.2: Beam model for analytical study.

The normal strain ε_x, normal stress σ_x, shear stress τ_{xz} and shear strain γ_{xz} were determined by Equations (3.1), (3.2), (3.3) and (3.4), respectively.

$$\varepsilon_x = \frac{M_x}{D} \cdot z \tag{3.1}$$

$$\sigma_{x,j} = \frac{M_x}{D} \cdot z \cdot E_j \tag{3.2}$$

$$\tau_{xz} = \frac{T_x}{D} \cdot B \tag{3.3}$$

$$\gamma_{xz,j} = \frac{\tau_{xz}}{G_j} \tag{3.4}$$

where M_x and T_x are the bending moment and transverse force, respectively, of the cross-section x, and j numbers each layer of the cross-section (E_j and G_j are the Young's modulus and shear modulus of layer j, respectively).

The flexural rigidity of the cross-section D is defined by Equation (3.5) which normally is the product of the elastic modulus E and the moment of inertia I, but as the Young's modulus E varies along the thickness, it cannot be removed outside integral in Equation (3.5). The first moment of area B is defined by Equation (3.6) and the shear stiffness S by Equation (3.7).

$$D = b \cdot \int \left(E \cdot z^2 \right) \, \mathrm{d}z \tag{3.5}$$

$$B = \int \left(E \cdot z \right) \, \mathrm{d}z \tag{3.6}$$

$$S = \frac{T_x^2}{b \cdot \int \left(\frac{\tau_{xz}^2}{G} \right) \, \mathrm{d}z} \tag{3.7}$$

The shear modulus of each material was determined by Equation (3.8).

$$G = \frac{E}{2 \cdot (1 + \nu)} \tag{3.8}$$

3.3.1   Stiffness

The beam stiffness was determined using equivalent single layer theories. The beam representing the bonded steel plates was analysed using Classical Laminate Plate Theory (CLPT). The beam representing the sandwich steel plates was analysed using First-order Shear Deformation plate Theory (FSDT). Both theories assume full connection between the layers and linear elastic behaviour of the material. The CLPT assumes that a line originally straight and normal to the reference axis remains straight and normal to the reference axis during deformation. The deformation is entirely due to bending and the shear deformation γ_{xz} is neglected. The FSDT assumes that a line originally straight and normal to the reference axis remains straight during deformation but not necessarily perpendicular to the reference axis. The displacement consists of two parts, one due to pure bending and one due to transverse shear. In the FSDT the transverse shear strains γ_{xz} are constant through the thickness (Reddy, 2004).

For both reinforcements the shear displacement occurs mainly in the adhesive layer as the adhesive material has much lower shear stiffness than the steel. The CLPT was used for determining the displacement of the bonded steel plates reinforcement since the shear strain of the thin epoxy layer can be neglected. The FSDT was used for the sandwich steel plates reinforcement. As the thickness of the polyurethane core is significant in the total reinforcement thickness, its shear displacement must be taken into account (Zenkert, 1997).

Considering the equilibrium equations of the beam model, constitutive equations of each material and strain-displacements relations of each theory CLPT and FSDT, the bending displacement and shear displacement at the middle span cross-section of the beam are given by Equation (3.9) and (3.10), respectively.

$$\delta_{bending;midspan} = \frac{P \cdot L^3}{48 \cdot D} \tag{3.9}$$

$$\delta_{shear;midspan} = \frac{P \cdot L}{4 \cdot S} \tag{3.10}$$

The total displacement of the bonded steel plates reinforcement using the CLPT is equal to the bending displacement (Equation (3.11)). The total displacement of the sandwich steel plates reinforcement using the FSDT is equal to the bending displacement plus the shear displacement (Equation (3.12)).

$$\delta_{bondedsteelplates} = \delta_{CLPT} = \delta_{bending} \tag{3.11}$$

$$\delta_{sandwichsteelplates} = \delta_{FSDT} = \delta_{bending} + \delta_{shear} \tag{3.12}$$

For each theory, the stiffness K was determined by the ratio between the load and the displacement at middle span – Equation (3.13).

$$K = \frac{P}{\delta_{midspan}} \tag{3.13}$$

3.3.2 Stress reduction factor

The aim of adding a second steel plate to the existing steel deck is to reduce the stress range at the welded joints that generates the fatigue cracks. Therefore, the stress reduction on the deck plate after applying the reinforcement is extremely important. The stress reduction factor SRF was determined by the ratio between the maximum stress in the deck plate after the reinforcement and before the reinforcement (steel plate with no surfacing) – Equation (3.14). The stresses on the deck plate are represented by the stresses on the lower steel plate of the beam (σ_{lp}).

$$SRF = \left(1 - \frac{\sigma_{lp}^{After}}{\sigma_{lp}^{Before}} \right) \cdot 100 \tag{3.14}$$

3.4 Results

The analytical solutions were applied to the model representing the reinforced steel plates. In order to better understand the models and reinforcement used, one example will be presented hereinafter.

The results of one bonded steel plates solution and one sandwich steel plates solution will be shown. Both solutions have approximately the same weight of 70 kg/m^2 and the same 12 mm lower plate thickness. The bonded steel plates solution consists of a 5 mm thick Epoxy B4 (see Table 3.1) and an 8 mm thick upper steel plate. The sandwich steel plates solution consists of a 30 mm thick S4 polyurethane (see Table 3.1) and a 5 mm thick upper steel plate. The beam has a 1000 mm span and is loaded with 1 kN at middle span. The results of the bonded and sandwich solutions are presented in Figures 3.3 and 3.4, respectively.

The longitudinal strains ε_x along the thickness at the middle span cross-section are presented in Figures 3.3(a) and 3.4(a). Both strain distributions are straight lines with a constant slope along the thickness, since full connection and elastic material behaviour is assumed. The normal stresses σ_x along the thickness at the middle span cross-section are presented in Figures 3.3(b) and 3.4(b). The values are almost zero at the adhesive layer, as the adhesive has a much lower Young's modulus than the steel. Figures 3.3(c) and 3.4(c) show the shear stresses τ_{xz} along the thickness of one cross-section between the load and the support point. For both reinforcements, the maximum shear stress is reached at the adhesive layer where it remains constant along the thickness. Finally, Figures 3.3(d) and 3.4(d) plot the displacement along the beam's length of the bonded and sandwich steel plates reinforcement, respectively.

The strains, stresses and total displacement of the sandwich steel plates solution are lower than the bonded steel plates solution. The stiffness increases by a factor two and the stress is reduced by a factor three when using the sandwich steel plates solution instead of the bonded steel plates solution, maintaining the same weight and increasing the height by 20 mm.

3.4.1 Parametric study

The analytical solutions were used to perform a parametric study in order to better understand the influence of different parameters on the stiffness and on the stress reduction of the reinforcement systems. The reinforcement efficiency, which aims at extending the lifespan of the deck plate, depends largely on the stiffness and on the stress reduction factor.

The following geometrical parameters were varied: thickness of the lower plate, t_{lp}, thickness of the adhesive, t_a and thickness of the upper plate, t_{up}. Although some of the thickness values cannot be used in real applications, using their total range enables a better understanding of the reinforcement's behaviour. Thickness limits, listed in Table 3.2, and height limits should be considered for real applications. The
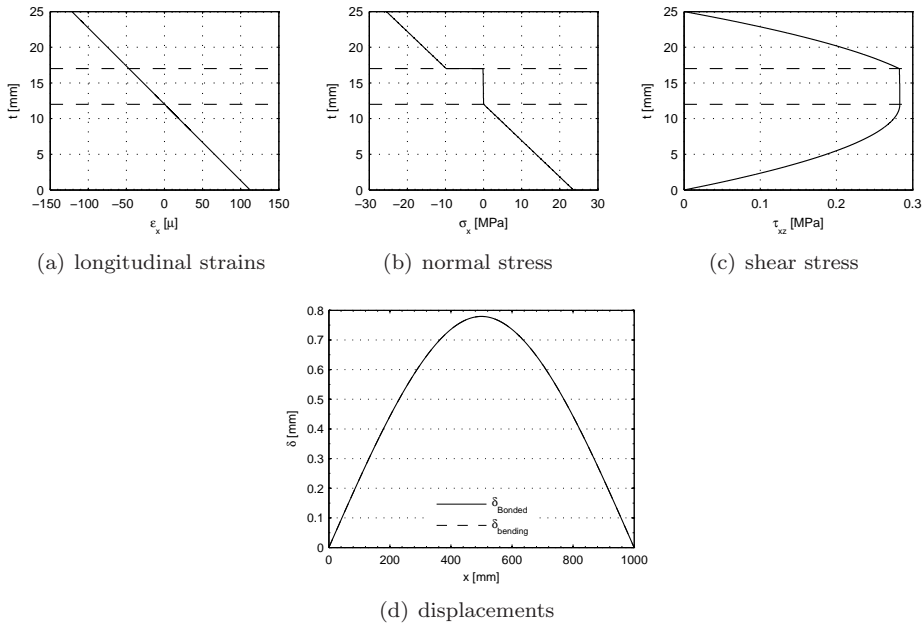
(a) longitudinal strains   (b) normal stress   (c) shear stress

(d) displacements

Figure 3.3: Bonded steel plates solution results (t_{lp}=12 mm; B4: t_a=5 mm; t_{up}=8 mm).

(a) longitudinal strains   (b) normal stress   (c) shear stress
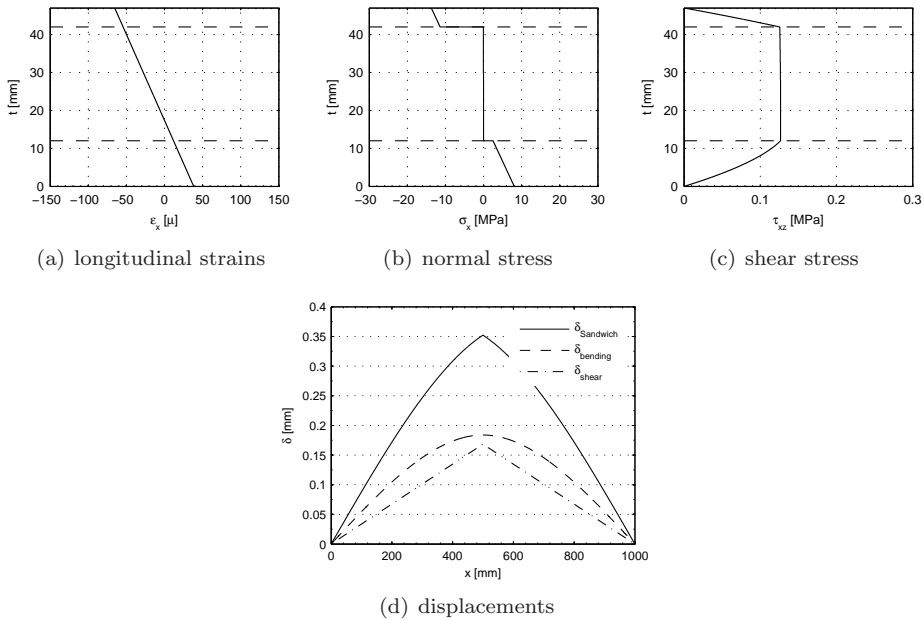

(d) displacements

Figure 3.4: Sandwich steel plates solution results (t_{lp}=12 mm; S4:t_a=30 mm; t_{up}=5 mm).

weight W of the reinforcement system was varied between 40 and 70 kg/m^2. The mechanical properties of the adhesive layers were varied according to the different materials presented in Table 3.1. The parametric study was carried out for two spans L of the beam model presented in Figure 3.2, one representing short beams with 500 mm span and another representing long beams with 1000 mm span. The aim is to study different ratios between normal stress and shear stress on the cross-section (σ_x/τ_{xz}), varying the importance of the adhesive layer on the total displacement of the beam. For short beams this ratio is lower than for long beams. The load applied to both models is 1 kN ($P = 1$ kN).

The extra weight W of each renovation solution is given by Equation (3.15).

$$W = t_a \cdot \rho_a + t_{up} \cdot \rho_{steel} \tag{3.15}$$

Due to their importance for the optimization of the reinforcement system, the weight and the adhesive thickness were chosen as independent parameters and therefore the thickness of the upper plate (second steel plate) is given by Equation (3.16).

$$t_{up} = \frac{W - t_a \cdot \rho_a}{\rho_{steel}} \tag{3.16}$$

The stiffness K and the stress reduction factor SRF of the reinforcement system are defined as functions of the different parameters as shown in Equations (3.17) and (3.18).

$$K = K\left(t_{lp}, t_a, W, L, G_a, E_a\right) \tag{3.17}$$

$$SRF = SRF\left(t_{lp}, t_a, W, E_a\right) \tag{3.18}$$

The SRF (Equation (3.14)) is only dependent on the flexural rigidity D of the reinforced plates (Equation (3.5)) and therefore is independent of the beam's span L and of the adhesive's shear modulus G_a.

The results of the parametric study are presented varying one of the parameters continuously and the remaining ones are either fixed or discretely varied.

Effect of the adhesive thickness t_a

Figure 3.5 shows the influence of the adhesive thickness on the stiffness of the reinforced steel plates. Figure 3.5(a) plots the stiffness of the bonded steel plates using adhesive B4 and Figure 3.5(b) of the sandwich steel plates using adhesive S4. The stiffness values are presented for four different weight restrictions (40, 50, 60 and 70 kg/m^2) and were determined using a 12 mm thick lower steel plate and a beam span of 1000 mm (long beams). The upper steel plate thickness t_{up} (Equation(3.16)) was varied from 1 to 9 mm for the sandwich steel plates and from 4 to 9 mm for the bonded steel plates. As already mentioned, although some of these values cannot be used in real applications, using their total range enables a better understanding of each reinforcement's behaviour.

(a) bonded steel plates, epoxy B4   (b) sandwich steel plates, polyurethane S4
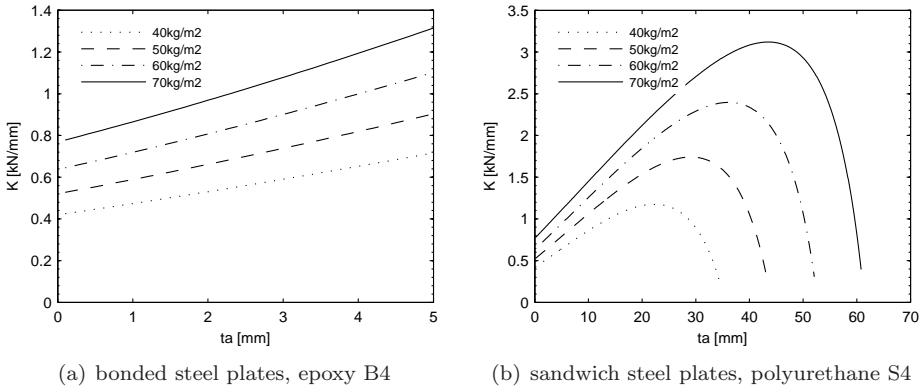
Figure 3.5: Reinforced steel plates stiffness when varying the adhesive thickness t_a for different weight restrictions (t_{lp}=12 mm; L=1000 mm).

Increasing the thickness of the epoxy layer increases the stiffness of the bonded steel plates, see Figure 3.5(a). Allowing more total weight to the reinforcement shifts the stiffness function up. The maximum stiffness and maximum SRF are obtained for solutions with 4 to 8 mm upper steel plate thickness and 5 mm adhesive thickness. The maximum SRF values are between 70% and 80% (the highest is obtained for the heaviest solution – 70 kg/m^2).

The sandwich steel plates stiffness increases with the increase of core thickness until reaching a maximum value. The core thickness for this maximum stiffness is the optimum core thickness. For core thicknesses higher than the optimum value, the stiffness starts to decrease (see Figure 3.5(b)). The maximum stiffness is reached when the decrease of bending displacement starts not to compensate the increase of shear displacement. On the one hand, increasing the core thickness increases the flexural rigidity D (Equation (3.5)), and therefore decreases the bending displacement (Equation (3.9)). On the other hand, increasing the core thickness decreases the shear stiffness S (Equation (3.7)) and therefore increases the shear displacement

(Equation (3.10)). The optimum solutions consist of a 2 to 3 mm thick upper steel plate and a 20 to 50 mm thick core. The maximum stress reduction factor is also achieved for the same thickness combinations and varies between 90% and 95% (the highest to the heaviest solution – 70 kg/m^2).

Effect of the beam span L

Figure 3.6 plots the stiffness for short and long beams using epoxy B4 and polyure-thane S4, and a weight limit of 70 kg/m^2. As expected, short beams have higher stiffnesses than the long beams both for the bonded steel plates, Figure 3.6(a) and for the sandwich steel plates, Figure 3.6(b). For the bonded steel plates, the optimum adhesive thickness is 5 mm for both models (maximum allowed). For the sandwich steel plates the optimum adhesive thickness slightly increases when decreasing the span (43 mm and 48 mm for long and short beams, respectively). For practical applications, this difference is insignificant.

(a) bonded steel plates, epoxy B4   (b) sandwich steel plates, polyurethane S4
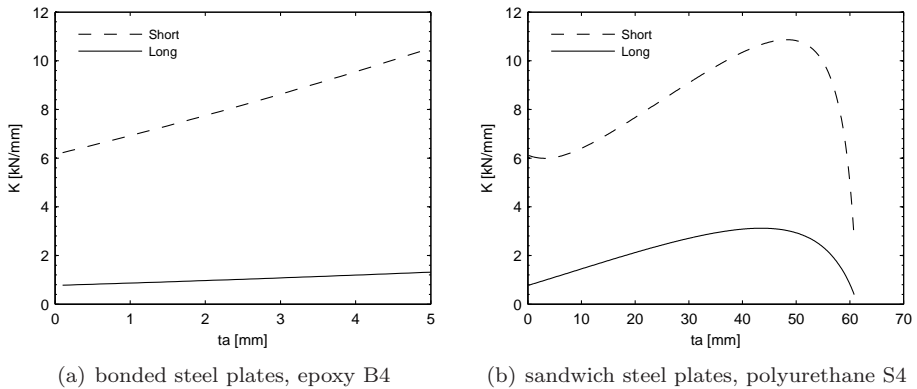
Figure 3.6: Reinforced steel plates stiffness when varying the adhesive thickness t_a for different spans L (t_{lp}=12 mm; W=70 kg/m^2).

Effect of the deck plate thickness t_{lp}

Figure 3.7 plots the stiffness considering 10 mm and 12 mm of lower plate thickness. Figure 3.7(a) shows the results for the bonded steel plates and Figure 3.7(b) for the sandwich steel plates. The stiffness values were determined for long beams (L = 1000 mm), 70 kg/m^2 weight and using epoxy B4 and polyurethane S4. The optimal solution for a 10 mm thick steel deck plate is the same as for a 12 mm thick steel deck plate. As expected, if the same reinforcement is applied on a 10 mm or on a 12 mm thick deck plate, the 12 mm deck plate will have a higher stiffness.
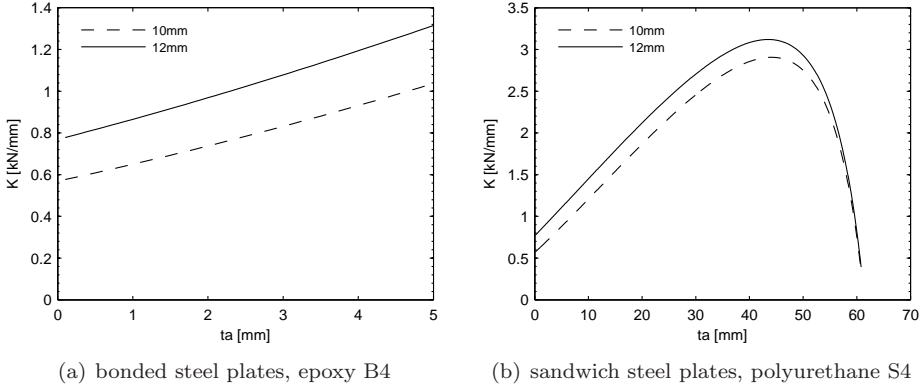
(a) bonded steel plates, epoxy B4   (b) sandwich steel plates, polyurethane S4

Figure 3.7: Reinforced steel plates stiffness when varying the adhesive thickness t_a for different lower plate thicknesses t_{lp} (W= 70 kg/m^2; L=1000 mm).

Effect of the adhesive mechanical properties

Figure 3.8 plots the reinforced steel plates stiffness for the different adhesives presented in Table 3.1. The stiffness values were determined for long beams (L = 1000 mm), 70 kg/m^2 weight and a 12 mm thick lower steel plate.

As shown in Figure 3.8(a) the adhesive mechanical properties do not significantly affect the stiffness of the bonded steel plates. The four series B1, B2, B3 and B4 are coincident. Since the adhesive has a much lower Young's modulus than the steel and the adhesive layer is much thinner than the total thickness of the steel plates, the contribution of the adhesive material is almost insignificant to the flexural rigidity D of the bonded steel plates. The maximum SRF is 80% and is obtained using a 8 mm thick upper steel plate and 5 mm of adhesive thickness (solution with maximum stiffness).

Figure 3.8(b) shows that the core properties significantly affect the stiffness of the sandwich steel plates. The most important property is the core's shear modulus G_a: higher values as for polyurethane S4 (see Table 3.1) achieve higher stiffnesses than S1, S2 and S3. As the sandwich stiffness depends also on the shear displacement, higher polyurethane shear modulus leads to lower shear displacement and therefore higher stiffness. For a very low shear modulus as for the polyurethane S1 (G_a=0.5 MPa) the stiffness drastically decreases as soon as the thickness of the core increases. The shear displacement for this polyurethane is too high to compensate any solution of core thickness. The stress reduction factor is not significantly affected by the core mechanical properties because it is only dependent on the flexural rigidity D. Excluding polyurethane S1, the maximum SRF is 95%. The maximum values are reached when using 2 to 3 mm upper steel plate thickness and 40 to 50 mm core thickness.
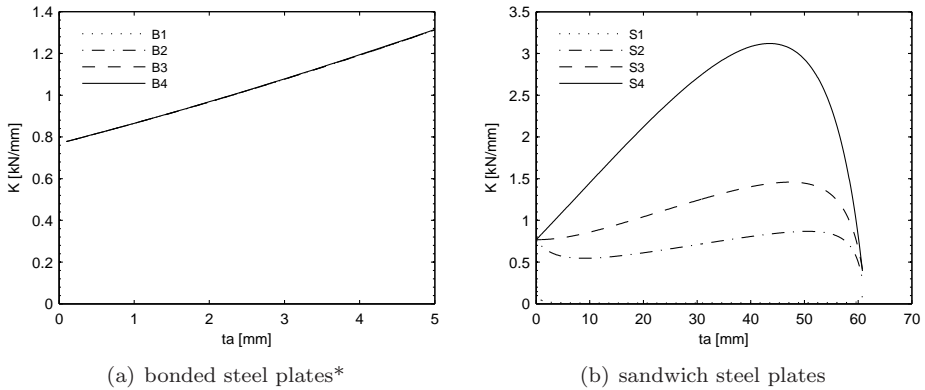
(a) bonded steel plates*   (b) sandwich steel plates

Figure 3.8: Reinforced steel plates stiffness when varying the adhesive thickness t_a for different adhesives ($*B1 \equiv B2 \equiv B3 \equiv B4$; t_{lp}=12 mm; W=70 kg/m^2; L=1000 mm).

Figure 3.9 plots the bonded and the sandwich steel plates stiffness in the same graph, Figure 3.9(a) for long beams (L = 1000 mm) and Figure 3.9(b) for short beams (L = 500 mm). The weight limit is 70 kg/m^2 and the lower plate thickness is 12 mm. As shown in Figure 3.9(a), for long beams the sandwich steel plates reinforcement leads to higher stiffnesses than the bonded steel plates reinforcement as long as G_a is higher than a certain limit ($G_a > G_a(S3)$). This limit is drastically increased for short beams, Figure 3.9(b). For short beams, the bonded steel plates present a very similar performance as the sandwich steel plates, even when using the highest core shear modulus S4. The sandwich steel plates reinforcement behaves better for long beams than for short beams, i.e., when shear displacement is lower.

Figure 3.10 plots the maximum stiffnesses of the bonded steel plates (B) and sandwich steel plates (S), when varying the shear modulus of the adhesive G_a. The aim is to determine the minimum shear modulus $G_{a.min}$ of the core of the sandwich steel plates that leads to a higher stiffness than the bonded steel plates. The maximum stiffness (K_{max}) is determined using the optimum thicknesses solution ($t_{a.optm}$; $t_{b.optm}$) for 70 kg/m^2 weight, 12 mm of lower steel plate thickness and a constant adhesive's Young's modulus E_a (adhesive S4). The optimum solution is a 8 mm thick upper steel plate and a 5 mm thick adhesive for the bonded steel plates, and a 2 to 3 mm thick upper steel plate and 40 to 50 mm thick core for the sandwich steel plates.
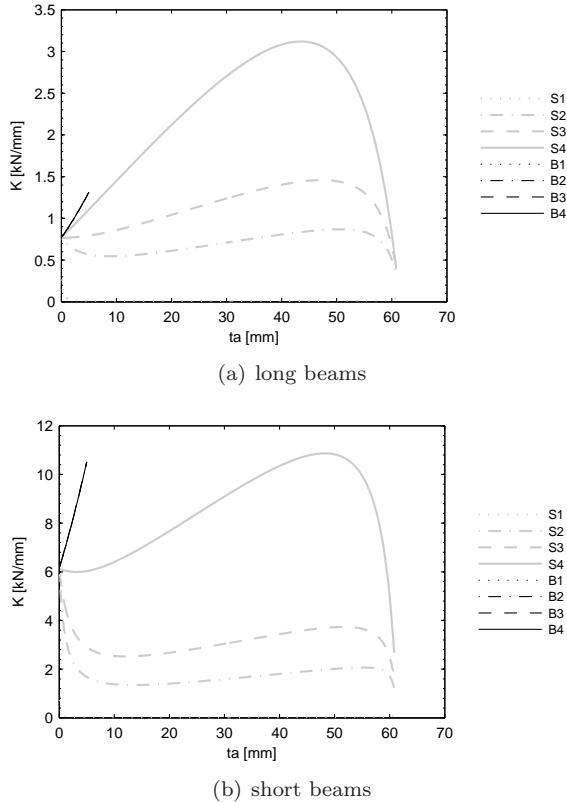
(a) long beams

(b) short beams

Figure 3.9: Reinforced steel plates stiffnesses when varying the adhesive thickness t_a for different adhesives and spans ($B1 \equiv B2 \equiv B3 \equiv B4$; t_{lp}=12 mm; W=70 kg/m^2).

Figure 3.10(a) plots the results for long beams and Figure 3.10(b) for short beams. As shown before, the stiffness of the bonded steel plates is independent of the adhesive's mechanical properties. The maximum stiffness of the sandwich steel plates tends to increase with the increase of the shear modulus until maximum limit. This limit at the upper right part of the graphs corresponds with the stiffness where the shear deformation is zero ($\delta_{shear} \to 0$ when $G_a \to \infty$) and therefore the total displacement is constant and entirely due to bending. The shear modulus at the intersection between the bonded steel plates (B) and sandwich steel plates (S) is the minimum required to the polyurethane core for the sandwich to be stiffer than the bonded steel plates. This minimum value is higher for short beams than for long beams, 270 MPa and 70 MPa, respectively. For a given steel deck plate with its weight limit and structure, minimum mechanical properties can be required for the polyurethane core of the sandwich steel plate reinforcement.
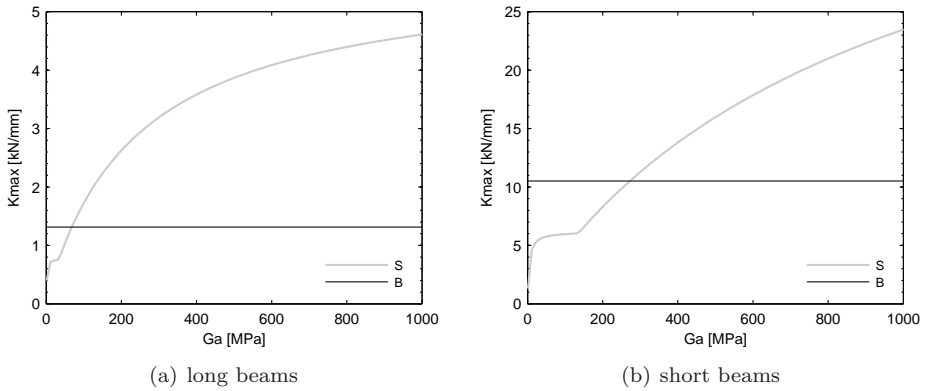
(a) long beams

(b) short beams

Figure 3.10: Reinforced steel plates maximum stiffness when varying the adhesive shear modulus G_a for different spans (S: sandwich steel plates; B: bonded steel plates; t_{lp}=12 mm; W=70 kg/m^2).

3.5 Conclusions

A parametric study based on analytical solutions was carried out in order to better understand the behaviour of two types of reinforcements for orthotropic steel bridge decks: bonded steel plates and sandwich steel plates. Both reinforcements include a new second steel plate bonded to the existing bridge deck in order to reduce the stresses on the deck and extend the lifespan of orthotropic bridge decks.

The optimization of the bonded steel plates system can only be achieved by maximizing the second steel plate thickness. The variation of the adhesive thickness is limited at 2 mm in real applications, but thicker adhesive layers up to 5 mm increase the reinforcement stiffness. For 70 kg/m^2, the optimum solution for the bonded steel plates is a 8 mm thick upper steel plate which reduces the stresses on the lower steel plate by 80%. The optimum combination of thickness of the sandwich steel plates is achieved by maximizing the core thickness until a certain maximum limit. For cores thicker than this maximum value, the increase of shear displacement of the core counterbalances the increase of the moment of inertia of the sandwich section. For 70 kg/m^2, the optimum solution is a 2 to 3 mm thick upper steel plate and 40 to 50 mm thick polyurethane core. This solution reduces the stresses on the lower steel plate by 95%. However, for real applications the minimum thickness of the steel plate is 5 mm and, for maintaing the same weight, the core thickness is reduced to 30 mm and the SRF to 94%.

The mechanical properties of the epoxy adhesive do not significantly affect the stiffness of the bonded steel plates. The stiffness of the sandwich steel plates is affected by the polyurethane shear modulus (G_a). Higher values of the shear modulus lead to higher stiffness. The SRF is not significantly affected by the mechanical properties of the adhesive or core.

The sandwich steel plates reinforcement decreases its performance as the shear increases its role in the flexural behaviour of the reinforced structure. The minimum shear modulus for the polyurethane that makes the sandwich steel plates stiffer than the bonded steel plates is much higher for short beams than for long beams. This minimum value depends on the weight limit.

The bonded and sandwich steel plates reinforcements look promising solutions for reinforcing orthotropic bridge decks. Nevertheless, lower stress reduction factors are expected on the real structure due to the complex geometry of an orthotropic bridge deck.

Chapter 4

Bonded steel plates reinforcement

4.1 Introduction

In the present chapter, the behaviour of the bonded steel plates reinforcement is investigated. The technique consists in bonding with a thin resin epoxy layer a second steel plate to the existing deck. An experimental program was carried out in order to evaluate the static and fatigue flexural behaviour of the reinforced plates. The influence of the thickness of the adhesive layer, environmental temperature and loading conditions are investigated. Part of the contents presented in this chapter is also available in Teixeira de Freitas et al. (2010).

4.2 Technique

The manufacturing and application of the bonded steel plates reinforcement was performed by Lightweight Structures B.V. A more detailed description of the technology and manufacturing process is given in Chapter 7. The application procedure of the specimens used in the current Chapter consisted of the following steps:

1. steel surfaces treatment: grit blast and clean the steel surfaces to be free from rust, grease and dust – cleaning grade Sa 2 1/2 according to ISO-8501 (2007);

2. primer application on the cleaned steel surfaces;

3. glue steel spacers with the adhesive thickness to the lower plate (nominally 2 mm thick);

4. place the upper plate above the spacers;

5. prepare the cavity between the plates to create vacuum;

6. vacuum inject the adhesive in the cavity;

7. cure during 16 hours between $40\,°C$ and $50\,°C$.

4.3   Materials

4.3.1   Steel plates

Steel grade S355 was selected for both steel plates which represent the existing steel plate and the second steel plate. According to EN1993-1-1 (2006) the nominal values for S355 steel grade are 355 MPa for the yield strength (f_y) and 510 MPa for the ultimate strength (f_u). The design Young's modulus for steel is 210 GPa (E) and Poisson's ratio is 0.3 (ν), according to the same standard. Four different steel plate thicknesses were used: 6 mm and 8 mm, for the second steel plate, and 10 mm and 12 mm, for the existing steel plate.

Tensile tests

In order to characterize the mechanical properties of the steel plates, four series of tensile tests were performed, one for each plate thickness. The specimens and test procedure were in accordance with EN10002-1 (2001). Table 4.1 shows the average±standard deviation values of the mechanical properties obtained from the tensile tests. The average values for the Young's modulus E, yield strength f_y, ultimate strength f_u, ratio between ultimate strength and yield strength fu/fy and percentage elongation after fracture A_c are given.

Overall, the average tensile strengths are higher than the nominal values recommended in EN1993-1-1 (2006), except for the plate thicknesses 6 mm and 10 mm, of which the average ultimate strength is lower than the nominal value recommended 510 MPa. All steel plates fulfil the minimum ductility requirement concerning the ratio $f_u/f_y > 1.10$, recommended in EN1993-1-1 (2006). On average, the Young's modulus are in agreement with the design value 210 GPa.

Table 4.1: Tensile mechanical properties of the steel plates.

Plate thickness	#	E (GPa)	f_y (MPa)	f_u (MPa)	f_u/f_y	A_c (%)
6 mm	3	205.1 ± 2.9	374.1 ± 1.7	502.5 ± 1.4	1.34 ± 0.01	29.7 ± 1.1
8 mm	3	207.4 ± 5.0	426.8 ± 3.2	531.3 ± 0.6	1.24 ± 0.01	29.6 ± 0.9
10 mm	3	211.1 ± 1.2	374.9 ± 4.3	480.6 ± 1.1	1.28 ± 0.01	25.9 ± 0.5
12 mm	3	213.6 ± 1.8	387.2 ± 7.8	551.2 ± 1.1	1.42 ± 0.03	26.4 ± 0.7

4.3.2 Adhesive

The adhesive material is a low-viscosity epoxy resin - Epikote resin EPR 04908 with hardener Epikure curing agent EPH 04908. This epoxy is the adhesive B4 presented in Chapter 3, Table 3.1. The adhesive characteristics based on the manufacturer's data are presented in Table 4.2.

Table 4.2: Characteristics of the adhesive material at room temperature given by the manufacturer.

Characteristics	EPR 04908+EPH 04908
Manufacturer	Hexion
Curing process	Curing at room temperature for 24h, post-curing at 60 °C for 12h
Density (kg/m^3)	1150
ν (-)	0.4
E_t (MPa)	2900
σ_{tmax} (MPa)	74
ε_{tmax} (%)	9.4

Tensile tests

Tensile tests were performed on the adhesive material in order to characterize its mechanical properties. The tests were performed at three different temperatures: low temperature (-10 °C), room temperature (RT: $+20$ °C to $+23$ °C) and high temperature ($+50$ °C). Material testing was carried out by displacement control using a testing machine with a maximum test load of 10 kN. A climate chamber was fitted to the testing machine to enable testing under different temperatures. Six specimens were submitted to tensile load up to failure for each temperature (-10 °C, RT and $+50$ °C). The experimental procedure was in accordance with ASTM-D638 (2008). A mechanical extensometer was used to measure the elongation of the specimens.

Figure 4.1 shows three representative stress-strain curves of the adhesive at each tested temperature. It is clearly shown that the behaviour of the adhesive can be considered brittle at low temperatures and ductile at high temperatures. Table 4.3 presents the maximum, minimum and the average values of the mechanical properties determined by the tensile tests at the three temperatures: tensile modulus (E_t), tensile strength (σ_{tmax}) and tensile failure strain (ε_{tmax}). As expected, the mechanical properties of the adhesive are affected by temperature. The tensile modulus is higher at -10 °C than at room temperature, while the tensile failure strain is lower. The results obtained for the tensile strength at -10 °C show a significant scatter, which is a characteristic of brittle material behaviour (high sensitivity to small defects). This significant scatter can explain the unexpected higher average value of the tensile strength at RT than at -10 °C. This fact does not occur for

the maximum values of the tensile strength. The tensile modulus is lower at $+50\,^{\circ}\mathrm{C}$ than at room temperature. The tensile strength is considerably reduced at this temperature, while the tensile failure strain is much higher. The adhesive mechanical properties from the tensile tests at room temperature are in accordance with the ones given by the manufacturer (see Table 4.2).
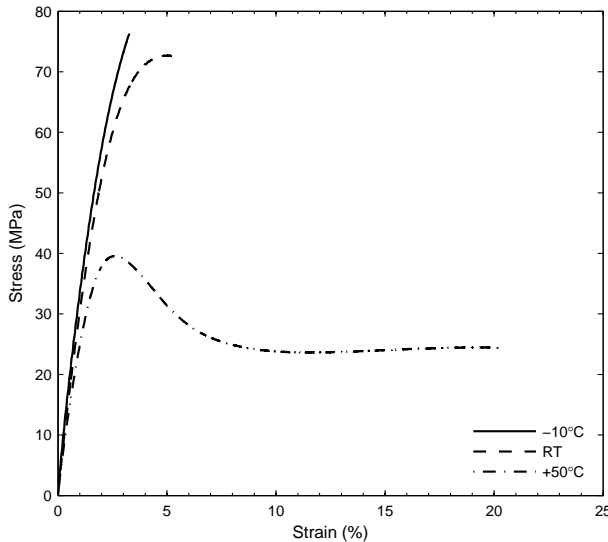

Figure 4.1: Adhesive tensile stress-strain curves.

Table 4.3: Tensile mechanical properties from adhesive material testing and from the manufacturer (* Table 4.2).

	Temperature	Average	Maximum	Minimum	Manufacturer*
	$-10\,^{\circ}\mathrm{C}$	3378	3585	3131	–
E_t(MPa)	RT	2929	3129	2728	2900
	$+50\,^{\circ}\mathrm{C}$	2451	2585	2308	–
	$-10\,^{\circ}\mathrm{C}$	69.01	75.97	59.83	–
σ_{tmax}(MPa)	RT	69.28	72.69	62.80	74
	$+50\,^{\circ}\mathrm{C}$	43.34	49.66	39.47	–
	$-10\,^{\circ}\mathrm{C}$	2.56	3.27	2.07	–
ε_{tmax}(%)	RT	4.88	7.11	3.57	9.4
	$+50\,^{\circ}\mathrm{C}$	19.51	25.42	15.95	–

4.4   Bonded steel plates specimens

Five bonded steel plates reinforcement configurations were used in the testing. The thickness of the steel plates and adhesive were varied according to the expected real applications. In the Netherlands, the steel deck plate of orthotropic bridge decks is typically 12 mm thick in movable bridges and 10 mm thick in fixed bridges. In the present study, both thicknesses were used in combination with 6 mm and 8 mm thick second steel plate. Two nominal adhesive thicknesses were used: 2 mm and 5 mm. For real application the nominal thickness is 2 mm, but often due to unflatness of the existing orthotropic deck, the final thickness can vary a lot and therefore it was included in the experimental program specimens with 5 mm adhesive thickness.

Table 4.4 shows the five configurations tested. The specimen configuration is referred to as "Baabc", where "aa", "b" and "c" represent the nominal thicknesses of the lower plate (t_{lp}), the adhesive layer ($t_{a,n}$) and the upper plate (t_{up}), respectively. The lower plate represents the existing steel deck plate and the upper plate represents the second steel plate added. Since this research is mainly focused on movable bridges, the adhesive thickness was only varied when using it with 12 mm thick lower steel plates. Moreover, the results from the parametric study carried out in Chapter 3 show that there is no significant difference in the flexural behaviour of the reinforcement when using 10 mm or 12 mm lower steel plate. The weight of each reinforcement configuration W is also presented in Table 4.4.

Table 4.4: Configuration of the bonded steel plates specimens and their characteristics.

Configuration	t_{lp} (mm)	$t_{a,n}$ (mm)	t_{up} (mm)	W (kg/m^2)
B1226	12	2	6	49
B1256	12	5	6	53
B1228	12	2	8	65
B1026	10	2	6	49
B1028	10	2	8	65

The specimens were manufactured by Lightweight Structures B.V. which was responsible for the adhesive material and its application. The fabrication procedure followed the technique described in section 4.2. The specimens geometry are simple beams with 100 mm width and variable lengths.

One resin/epoxy injection was performed for each reinforcement configuration. The steel plates were manufactured large enough to extract more than one specimen of each configuration (1000 x 800 mm^2). After cutting the specimens to their final dimensions, the actual adhesive thickness $t_{a,r}$ was determined for each specimen by measuring the total thickness of the specimen and extracting the thicknesses of the steel plates. The actual thickness of the steel plates corresponds with its nominal thickness (t_{lp} and t_{up}). However, the actual adhesive thickness presents significant deviations from its nominal value. Table 4.5 presents the average actual adhesive thickness ($average$), standard deviation (SD) and relative standard devia-

tion (RSD). The average actual thickness ($t_{a,r}$) tends to be lower than the nominal one ($t_{a,n}$) and the relative standard deviation between specimens can be as much as 24% (specimen B1026).

Table 4.5: Adhesive actual thickness.

$t_{a,r}$	$average$ (mm)	SD (mm)	RSD (%)
B1226	1.30	0.28	22
B1256	3.18	0.20	6
B1228	1.05	0.22	21
B1026	1.49	0.35	24
B1028	1.24	0.08	7

All specimens were carefully checked by using an ultrasonic Non Destructive Testing C-scan in order to detect any flaws or delamination areas created during the fabrication or the cutting process. The ultrasonic technique used was the water column testing. In this technique, the sound is projected from the traducer to the specimen through a column of flowing water (Grandt, 2004). The sound frequency used was 10 MHz.

4.5   Static behaviour

The aim of this part of the study is to better understand the static bending behaviour of the bonded steel plates reinforcement. The experimental program that has been carried out is presented and discussed in the following sections.

4.5.1   Experimental procedure

Static tests were performed on the five different reinforcement configurations, using a four-point bending rig. The static tests were carried out at three temperatures: low temperature ($-10\,^{\circ}\mathrm{C}$), room temperature (RT: $+20\,^{\circ}\mathrm{C}$ to $+23\,^{\circ}\mathrm{C}$) and high temperature ($+50\,^{\circ}\mathrm{C}$), chosen according to the conditions expected to occur in the Dutch bridges. The tests were carried out at displacement control using a testing machine with a maximum test load of 100 kN. A climate chamber was fitted to the testing machine to enable testing under different temperatures. Two types of load configuration were used: short and long beams. The short beams load configuration was quarter point loading with 400 mm support span and 200 mm load span. The long beams load configuration was third point loading with 750 mm support span and 250 mm load span. The aim was to better understand the flexural behaviour of the reinforcement when subjected to different ratios between the normal stress at the steel plates and the shear stress at the adhesive layer ($\sigma_{steelplates}/\tau_{adhesive}$) and hence change the importance of the adhesive layer on the total behaviour of the beam. The specimens were 850 mm long and 100 mm wide. The bending tests were

performed at a constant displacement rate of 1 mm/min and 3 mm/min for short and long beams load configuration, respectively.

Firstly, a non-destructive test was carried out in the elastic range using two specimens of each geometry. Each specimen was tested under the six test conditions mentioned above (3 temperatures x 2 load configurations). Secondly, the configurations B1228, B1026 and B1028 were tested to final failure. The failure tests were carried out under the three different temperatures and for the short beams load configuration.

Figure 4.2 shows a photo of the test set-up. The load actuator is at the lower side of the specimen. Therefore, the specimen is positioned upside down (lower plate up and upper plate down). Figure 4.3(a) shows a schematic drawing of the test set-up where $L1$ is the load span and $L2$ is the support span. The displacements of the middle span cross-section were measured by two potentiometers, one on each side of the specimen's width (see Figure 4.3(a)). Temperature sensors were used to measure the climate chamber and the specimen temperature. The specimens' middle span cross-section was instrumented with strain gauges measuring longitudinal strains. Figure 4.3(b) shows a detail of the middle span cross-section where the strain gauges were applied. The strains along the specimen's thickness were measured by five strain gauges, three on the lower plate and two on the upper plate. The strains along the specimen's width were measured by three strain gauges at the surface of the lower plate and three strain gauges at the surface of the upper plate.
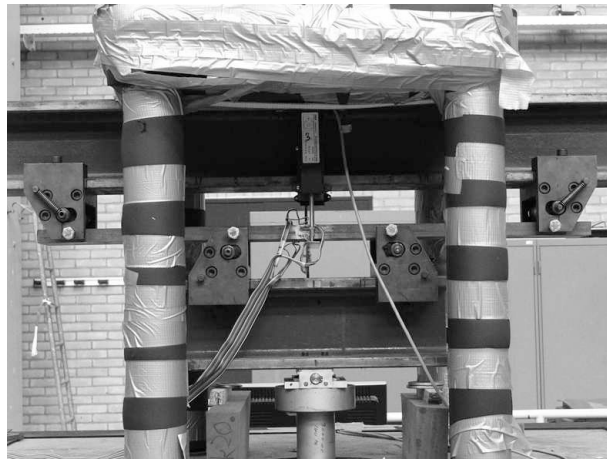
Figure 4.2: Test set-up used for the bending tests.

(a) Test set-up   (b) Strain gauges at middle span
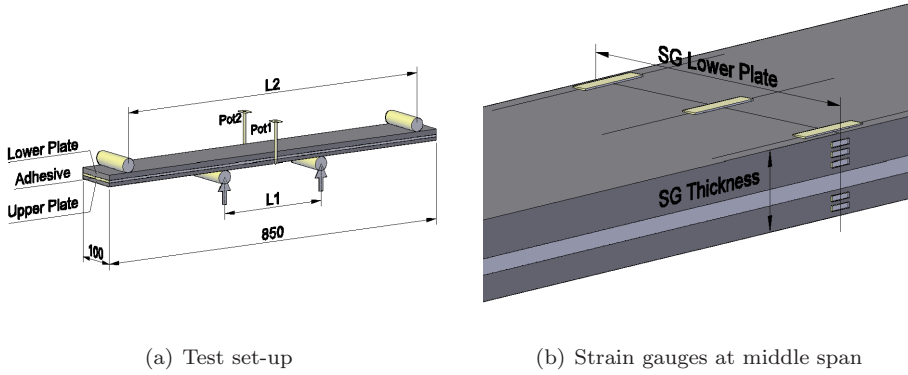
Figure 4.3: Isometric drawing of the bending test set-up and instrumentation (L1 – load
span; L2 – support span; Pot1/2 – potentiometers).

4.5.2   Results and Discussion

The results of the experimental program carried out on the static behaviour of the
bonded steel plates reinforcement are divided into three sub results: elastic flexural
behaviour, failure flexural behaviour and stress reduction factor. The experimental
results are compared with analytical results obtained from the analytical solutions
discussed in Chapter 3, applied to the bending tests. A summary of the analytical
study is given hereinafter.

Analytical study

Analytical study was performed on the bonded steel plates specimens to simulate the
bending tests of the experimental program. The elastic flexural behaviour of the spe-
cimens at low temperature ($-10\,^{\circ}\mathrm{C}$), room temperature (RT) and high temperature
($+50\,^{\circ}\mathrm{C}$) for short and long beams is studied.

The model is a beam subjected to four-point loading bending test where x, y, z are
the axes in the direction of the length, width and thickness, respectively. The normal
strain ε_x, normal stress σ_x, shear stress τ_{xz} and shear strain γ_{xz} were determined
by the Equations (3.1), (3.2), (3.3) and (3.4) presented in Chapter 3 (page 18).

The cross-section of the bonded steel plates specimens consists of three layers: two
steel plates and one adhesive layer in between. The Young's modulus and Pois-
son's ratio of the steel were defined in accordance with EN1993-1-1 (2006), as no
significant difference was found on the tensile material testing performed on the
steel plates. The adhesive material properties were defined by the tensile Young's
modulus obtained from the tensile tests and by the Poisson's ratio given by the
manufacturer.

In order to include temperature effects, the actual mechanical properties of the adhesive at each temperature were used to determine the flexural rigidity of the cross-section D (Equation (3.5) in Chapter 3, on page 18) and the first moment of area B (Equation (3.6) in Chapter 3, on page 18). The mechanical properties of the steel are considered constant within the tested temperature range.

The specimens stiffness was determined using the two equivalent single layer theories described in Chapter 3: Classical Laminate Plate Theory (CLPT) and the First-order Shear Deformation plate Theory (FSDT). The analysis was carried out using both theories in order to understand whether or not shear deformation is important to the total deformation of the beams. The bending displacement and shear displacement at the middle span cross-section are given by Equation (4.1) and (4.2), respectively:

$$\delta_{bending;midspan} = \frac{P \cdot L^3}{k_1 \cdot D} \tag{4.1}$$

$$\delta_{shear;midspan} = \frac{P \cdot L}{k_2 \cdot S} \tag{4.2}$$

where P is the applied load, L is the beam span and k_1 and k_2 are functions of the support and load span.

The total displacement using the CLPT is equal to the bending displacement – Equation (4.3). The total displacement using the FSDT is equal to the bending displacement plus the shear displacement – Equation (4.4), as presented in Chapter 3.

$$\delta_{CLPT} = \delta_{bending} \tag{4.3}$$

$$\delta_{FSDT} = \delta_{bending} + \delta_{shear} \tag{4.4}$$

For each theory, the specimen stiffness K was determined by the ratio between the load and the displacement at middle span – Equation (4.5).

$$K = \frac{P}{\delta_{midspan}} \tag{4.5}$$

Bonded steel plates elastic flexural behaviour

This section presents the results from the non-destructive tests performed in the elastic ranges of the specimens. Figure 4.4 shows the typical load-displacement graph, measured on a B1256 specimen under the six test conditions: three temperature levels ($-10\,°C$, RT and $+50\,°C$) and two load configurations (S - short beams, L - long beams). Both for short and for long beams, the results show that temperature has hardly any effect on the bonded steel plates stiffness. Only the adhesive material is significantly affected by temperature within the considered range and B1256 has the thickest adhesive layer (5 mm) from the geometries that were studied. Therefore, for a smaller adhesive thickness, the temperature effect is even less. As expected, due to the loading conditions, the stiffness is higher for short beams than for long beams.
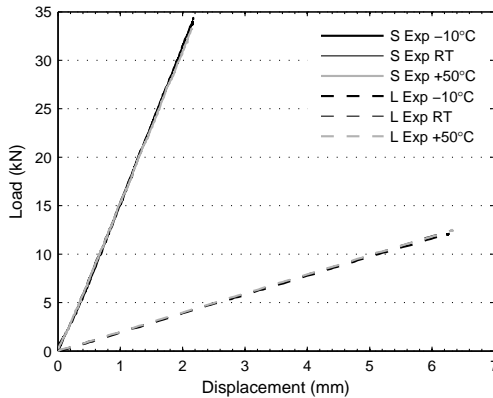
Figure 4.4: Load displacement graphs measured for B1256 (S – short beams, L – long beams).

Figure 4.5 and Figure 4.6 show the strains measured at the middle span cross-section along the thickness of one specimen B1256 and one specimen B1226, respectively, for short and long beams. The strains measured by strain gauges are plotted for the three temperatures, Exp T$=-10\,°C$, Exp RT and Exp T$=+50\,°C$. The only difference between the two geometries is the adhesive thickness (2 mm thick for B1226 and 5 mm thick for B1256). The results show that the experimental strains are not significantly affected by temperature. Contrary to what was expected, the influence of the temperature is slightly greater for the thinner adhesive layer (B1226) than for the thicker adhesive layer (B1256). These results are in accordance with the load-displacement graphs (Figure 4.4) which show that the stiffness is not significantly affected by temperature. The experimental values are compared with the strain distribution predicted by CLPT (see Equation (3.1) in Chapter 3, on page 18). The strain distribution was determined for the three temperatures, CLPT T$=-10\,°C$, CLPT RT and CLPT T$=+50\,°C$. The temperature effect is included in the flexural

rigidity of the cross-section D (see Equation (3.5) in Chapter 3, on page 18) by the adhesive's mechanical properties at the three temperatures. The strain distributions at the three temperatures by CLPT are coincident for all cases presented. The series CLPT T=-10 °C, CLPT RT and CLPT T=$+50$ °C have hardly any difference. The analytical and experimental results are in considerable agreement.

(a) Short beams (15 kN) (b) Long beams (6 kN)
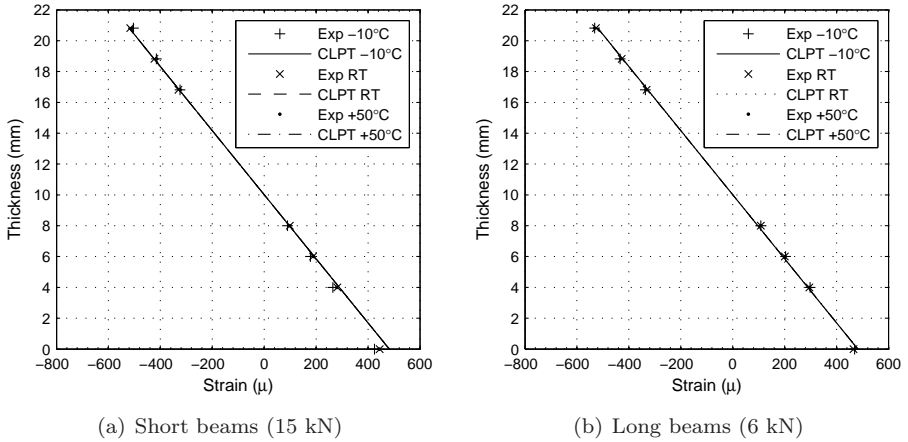
Figure 4.5: B1256 longitudinal strains (ε_x) at the middle span cross-section.

(a) Short beams (15 kN) (b) Long beams (6 kN)
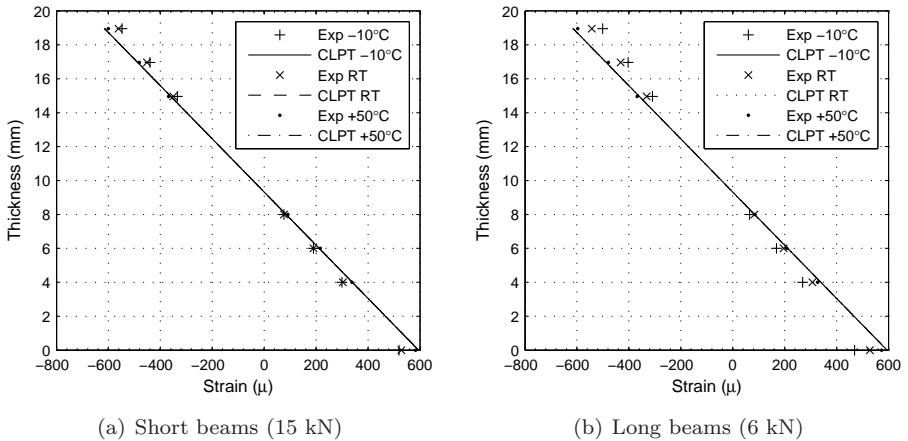
Figure 4.6: B1226 longitudinal strains (ε_x) at the middle span cross-section.

Figure 4.7 shows the typical load-displacement graphs of the five geometries at room temperature for short and long beams. In both graphs, the highest stiffness is measured for B1228 geometry. Similar values were measured for the geometry B1256. B1256's weight is considerably lower than B1228 (53 kg/m^2 and 65 kg/m^2 as shown in Table 4.4) and therefore the first is a more efficient configuration than the latter. For the geometries with a 10 mm thick lower plate, the solution using an 8 mm thick upper steel plate (B1028) is stiffer than the one using a 6 mm thick upper steel plate (B1026), as expected.

(a) Short beams   (b) Long beams
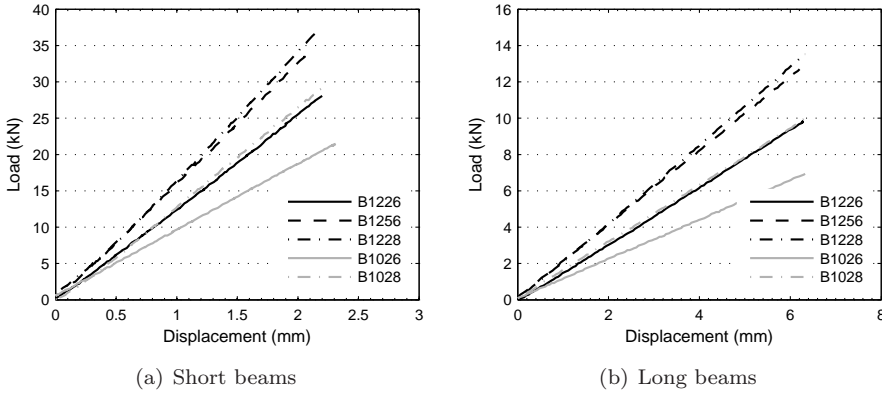
Figure 4.7: Load displacement graphs measured at room temperature.

A complete set of experimental stiffnesses is presented in Table 4.6 considering all geometries, temperatures and load configurations. The results are the average stiffness measured from two specimens per geometry. The experimental results are compared with the analytical stiffnesses determined from CLPT and FSDT. The analytical calculations were performed using the actual adhesive thickness for each specimen instead of the nominal one, and the actual mechanical properties determined from the tensile tests.

As expected, for short beams, the stiffness is higher than for long beams load configuration. The temperature effect is higher in short beams than in long beams for all geometries. Only the adhesive material is significantly affected by temperature within the considered range and is responsible for the shear displacement. As the shear displacement plays a more important role in short beams than in long beams, the temperature effects were expected to be higher in the short beams than in the long beams ($\sigma_{steelplates}/\tau_{adhesive}$ lower for short than for long beams). The temperature effect within the same geometry is generally less than 10%, with the exception of the B1026 specimens (approximately 20%). This geometry presents a significant scatter in the adhesive actual thickness (approximately 20% – see Table 4.5, on page 36) which contributes to a greater scatter in the stiffness results.

The difference between CLPT and FSDT is greater for short beams (approximately

6%) than for long beams (2%). Results can be explained through the shear displacement, which is higher in short beams than in long beams. The difference between the two theories decreases with temperature due to the fact that the adhesive tensile modulus E_t is higher for low temperatures (see Table 4.3), leading to lower shear deformations.

The difference between the analytical stiffnesses and the experimental stiffnesses is, in most of the cases, less than 5%. B1026 and B1228 specimens are the only two exceptions. The high scatter at the actual adhesive thickness present in these two geometries might contribute significantly to these results (see Table 4.5).

Table 4.6: Stiffness results from the bending tests (Exp), from CLPT and FSDT.

K		$-10\,°\mathrm{C}$			RT			$+50\,°\mathrm{C}$	
(kN/mm)		Exp	CLPT	FSDT	Exp	CLPT	FSDT	Exp	CLPT	FSDT
	B1226	12.31	13.04	12.53	12.84	13.03	12.46	12.07	13.03	12.36
	B1256	14.92	16.80	15.35	16.01	16.79	15.15	15.65	16.78	14.87
Short beams	B1228	15.40	17.49	16.69	17.09	17.48	16.59	16.86	17.48	16.44
	B1026	7.60	9.72	9.34	9.58	9.71	9.29	7.82	9.71	9.21
	B1028	12.04	13.47	12.85	13.44	13.47	12.76	12.32	13.46	12.64
	B1226	1.66	1.60	1.58	1.58	1.60	1.57	1.52	1.59	1.57
	B1256	2.06	2.06	2.00	2.02	2.06	1.99	1.95	2.05	1.98
Long beams	B1228	2.17	2.14	2.11	2.22	2.14	2.11	2.04	2.14	2.10
	B1026	1.16	1.19	1.18	1.15	1.19	1.17	1.00	1.19	1.17
	B1028	1.56	1.65	1.63	1.63	1.65	1.62	1.51	1.65	1.62

Bonded steel plates failure flexural behaviour

In order to determine the flexural strength and failure mechanism at different temperatures, B1228, B1026 and B1028 were tested to final failure. B1226 and B1256 were not included in this testing since the specimens were used in the fatigue experimental program that is described in section 4.6.

The bending static tests were carried out for short beams load configuration at the three temperatures ($-10\,°\mathrm{C}$, RT and $+50\,°\mathrm{C}$). Short beams load configuration was chosen in order to test lower ratios between normal stress and shear stress ($\sigma_{steelplates}/\tau_{adhesive}$), increasing the importance of the adhesive layer on the total strength of the beam.

Figure 4.8 shows the representative load-displacement curves at the three temperatures for B1228 and B1026. Tables 4.7 and 4.8 present the average loads and displacement at yield and failure, respectively. The elastic limit of the bonded steel plates beams is not significantly affected by temperature, while the ultimate load and its displacement are higher at low temperature ($-10\,°\mathrm{C}$) than at high temperature ($+50\,°\mathrm{C}$). As the mechanical properties of the steel plates are not affected by temperature within the considered range, these results indicate that yielding is highly affected by the steel plates and the ultimate failure by the adhesive layer. Temperature effects on the ultimate strength can be explained by the much lower

adhesive strength at high temperatures than at low temperatures (see Figure 4.1). As the normal stresses at the adhesive layer are almost zero (near the neutral axis and low Young's modulus compared to steel), the dominant failure mode at the adhesive is due to shear stresses. This is shown in Figure 4.9 by the failure mode of one B1026 specimen, where the shear failure of the adhesive layer next to the loading point is visible.
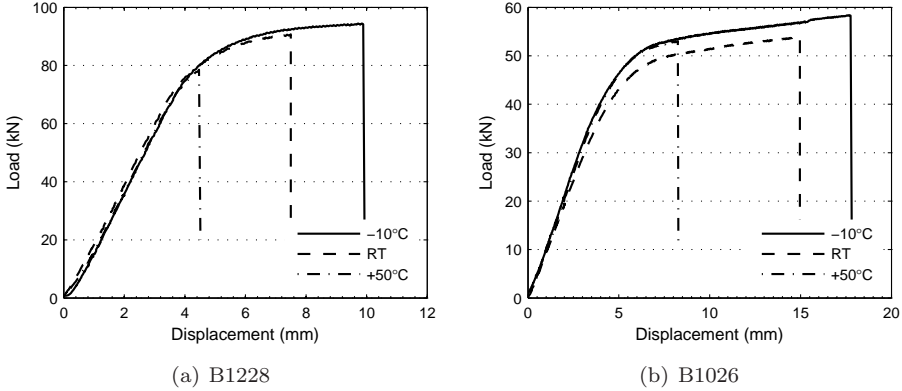

(a) B1228

(b) B1026

Figure 4.8: Load-displacement curves.

Table 4.7: Average yield loads and displacements (* not tested).

	−10 °C		RT		+50 °C	
(kN,mm)	P_y	δ_y	P_y	δ_y	P_y	δ_y
B1228	72.1	3.8	70.5	3.7	68.7	3.6
B1028	*	*	51.4	3.4	50.2	3.5
B1026	37.6	3.6	38.0	3.8	38.0	3.7

Table 4.8: Average failure loads and displacements (* not tested).

	−10 °C		RT		+50 °C	
(kN,mm)	P_{ult}	δ_{ult}	P_{ult}	δ_{ult}	P_{ult}	δ_{ult}
B1228	94.5	9.7	90.7	7.5	78.6	4.5
B1028	*	*	74.5	8.1	65.1	5.5
B1026	58.4	17.7	54.3	14.9	53.0	8.2
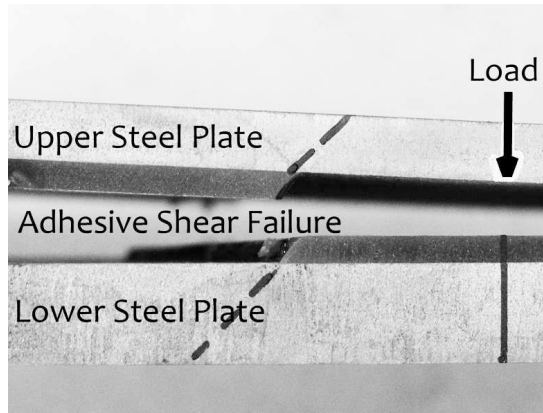
Figure 4.9: Shear failure of the adhesive layer on specimen B1026 tested at $+50\,^{\circ}\mathrm{C}$.

Figure 4.10 shows the representative load-displacement curves of the three geometries at room temperature. As expected, the stiffness and the yield load are different for each geometry due to their different flexural rigidity values (D - see Equation (3.5), Chapter 3). Figure 4.11 shows the normal and shear stress distribution along the normalized thickness at the yield load for each geometry. The normal stresses were determined at the middle span cross-section (highest values) using Equation (3.2). The shear stresses were determined at a cross-section between the load and the support of the beams (highest values) using Equation (3.3). The normal stress distribution shows that the adhesive's normal stress is negligible when compared to steel stress due to its low Young's modulus. It can also be observed that for all geometries the yield load of the beams corresponds approximately with the average yield stress of the steel plates shown in Table 4.1, $\overline{f_y} = 390$ MPa (normal stresses at $z/t = 0$ and $z/t = 1$ are around 360 MPa). As the steel material properties are independent of temperature, the yield load is not significantly affected by temperature, as already shown in Figure 4.8. Additionally, for the three geometries presented, the level of shear stress at the yield load is lower than the shear strength of the adhesive determined from the tensile strength presented in Table 4.3 using Von Mises criterion ($\tau = \sigma/\sqrt{3} = 69/\sqrt{3} = 39.8$ MPa). The lowest shear stress level occurs in B1026 geometry and the highest in B1228. This can explain why the adhesive failure is achieved with much more deformation after yielding for the B1026 than for B1228 geometries, as shown in Figure 4.10.
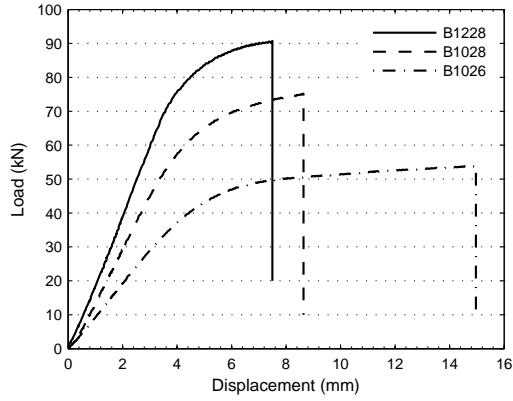
Figure 4.10: Load-displacement curves at room temperature.

(a)   (b)
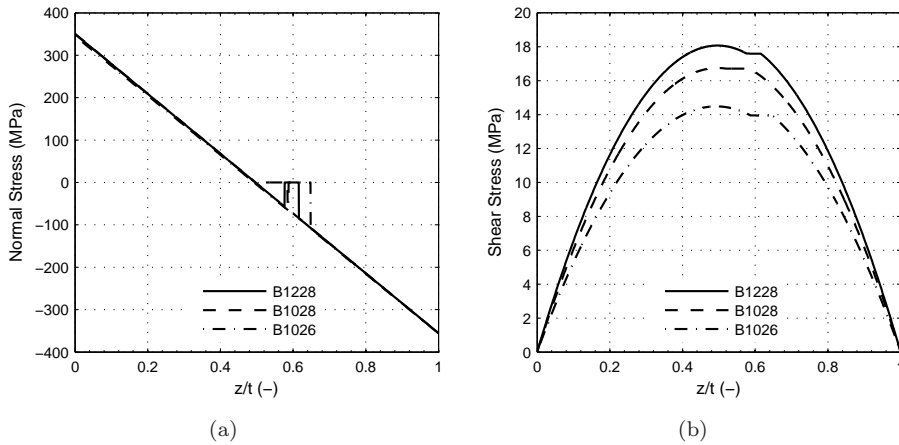
Figure 4.11: Stresses at RT at the yield load.

Stress reduction factor

The stress reduction factor SRF was determined by the ratio between the maximum stress in the lower steel plate after the reinforcement and before the reinforcement (steel plate with no surfacing). The stress before the reinforcement was determined using Equation (3.2) for a steel beam with no reinforcement subjected to the same load conditions. For the experimental values (Exp), the stress after the reinforcement was determined by the measured strains along the width of the lower steel plate during tests. For the analytical values (Ant), the stress after the reinforcement was determined using Equation (3.2) using the actual adhesive thickness and mechanical properties. Equation (4.6) presents the general expression used for determining the stress reduction factor of the bonded steel plates specimens.

$$SRF = \left(1 - \frac{\sigma_{lp}^{After}}{\sigma_{lp}^{Before}} \right) \cdot 100 = \left(1 - \frac{\sigma_{Baabbc}}{\sigma_{aa}} \right) \cdot 100 \tag{4.6}$$

The results are presented in Table 4.9 for all geometries, temperatures and load configurations. The experimental values of SRF are an average of the results for the specimens tested in each test condition.

Table 4.9: Average SRF results from bending tests and determined from analytical solution.

SRF		$-10\,°\mathrm{C}$		RT		$+50\,°\mathrm{C}$	
(%)		Exp	Ant	Exp	Ant	Exp	Ant
Short beams	B1226	65	60	65	60	63	60
	B1256	71	67	70	67	70	67
	B1228	71	67	71	67	71	67
	B1026	69	67	69	67	68	67
	B1028	75	73	76	73	75	73
Long beams	B1226	65	60	63	60	62	60
	B1256	70	67	69	67	68	67
	B1228	70	67	71	67	68	67
	B1026	67	67	68	67	63	67
	B1028	75	73	75	73	73	73

As the analytical stress reduction factor depends only on stress, and therefore only on the flexural rigidity (D), its value is independent of the load conditions (short and long beams). The analytical SRF is exactly the same for long and short beams load configurations, for each geometry. The differences presented between long and short beams on the experimental stress reduction factor, determined for each geometry, are mainly due to the variability on experimental data. Once again the influence of the temperature is very small on the stress reduction factor.

Overall, the stresses can be reduced by 60% to 75% when a 6 mm to 8 mm thick second steel plate is added to an unreinforced steel plate of 10 to 12 mm thickness.

4.6   Fatigue behaviour

Fatigue tests have been carried out in order to better understand the fatigue behaviour of the bonded steel plates reinforcement. The experimental program was performed using the first two of the five configurations listed in Table 4.4: B1226 and B1256. The aim was also to investigate the influence of the adhesive thickness on the fatigue behaviour of the reinforcement.

4.6.1   Experimental procedure

Two reinforcement configurations were tested on fatigue: B1226 and B1256, i.e., a 12 mm thick lower plate and a 6 mm thick upper plate bonded with a nominal adhesive thickness of 2 mm and 5 mm. All fatigue tests were performed at room temperature at the same test rig as the one used for the static tests. Two load configurations were used: four point bending and three point bending. The four point bending test was equivalent to the short beams load configuration used on the static tests: 200 mm load span and 400 mm support span. The three point bending test was a mid point loading with 200 mm support span. The B1226's specimens were subjected to four point bending tests and the B1256 specimens were subjected to four and three point bending tests. The change in load configuration had to do with the limited number of specimens available. In order to increase the number of specimens, the long specimens of 850 mm length designed for the four point bending tests were cut into several shorter specimens of 250 mm length and tested in three point bending tests.

Figure 4.12 shows the fatigue load configurations and the strain gauges used. The strain gauges measured longitudinal strains at the bottom side of the lower plate and at the top side of the upper plate, in the middle of the strip. The strain gauges were applied at midspan and between the load and the support points. Static results showed that the shear failure of the adhesive occurs between the load and the support point, where the shear stress is the highest. Therefore it is important to monitor this area during fatigue tests to detect a possible failure.

In all fatigue tests, the load was controlled and the applied load ratio R – defined as the ratio of the minimum applied load to the maximum applied load P_{min}/P_{max} – was 0.1. The wave form was sinusoidal with a frequency of 8 Hz. Fatigue tests were performed at three load levels, at a maximum load (P_{max}) between 70% and 40% of the relevant static failure load (P_{ult}). Static tests were initially performed to obtain relevant load levels for the fatigue tests. The static tests were carried out at room temperature at a constant displacement rate of 1 mm/min. Due to the reduced number of specimens available, one specimen within each configuration and test set-up, was tested in static loading.
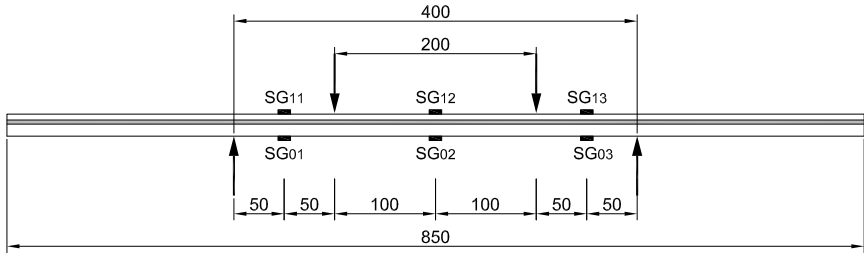
(a) four point bending test – 4pbt
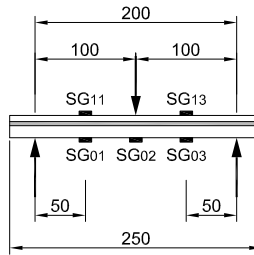
(b) three point bending test – 3pbt

Figure 4.12: Fatigue load configurations and specimens' instrumentation (SG - strain gauges; dimensions in mm).

4.6.2   Results

The results from the static test initially performed on each configuration (B1226, B1256) and test set-up (4pbt and 3pbt) are shown in Table 4.10. The failure mode is the same as described in the previous section 4.5.2 for the static tests (page 45): yield of the steel plates and shear failure of the adhesive at the ultimate load.

Table 4.10: Static yield and ultimate loads and displacements at room temperature.

(kN,mm)	P_y	δ_y	P_{ult}	δ_{ult}
B1226 – 4pbt	59.1	4.3	69.7	12.7
B1256 – 4pbt	67.8	4.0	80.6	14.7
B1256 – 3pbt	53.0	1.4	88.7	4.4

Fatigue failure mode

Two failure modes were observed during the fatigue tests. The majority of the tests failed by shear of the adhesive layer. The failure occurred between the support and load points. The failure mode was similar to the one observed at the static tests but in this case the shear failure of the adhesive occurred without any yield of the steel plates. The second fatigue failure mode observed was at the steel plate in tension. The failure occurred at midspan and generally the steel crack started at the edge of the strip. Table 4.11 shows pictures of the two failure modes and respective fracture areas at each load configuration, 4pbt and 3pbt.

Figure 4.13 shows one typical example of the displacement and strain ranges measured during fatigue tests on each failure mode. The displacement range is measured by the piston of the load cell δ_{piston} and the strains are measured by the strain gauges applied on the specimen (see Figure 4.12). The examples shown are both from B1256's specimens using 3pbt configuration under 0.48 and 0.56 P_{max}/P_u load level.

Table 4.11: Fatigue failure modes.

Failure mode	Load configuration: fracture area
Shear failure of the adhesive – sfa	4pbt: between supports and loads 3pbt: between supports and load
Tension failure of the plate – tfp	3pbt: midspan at the tension steel plate
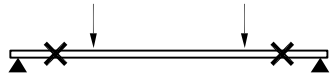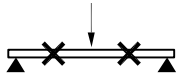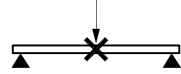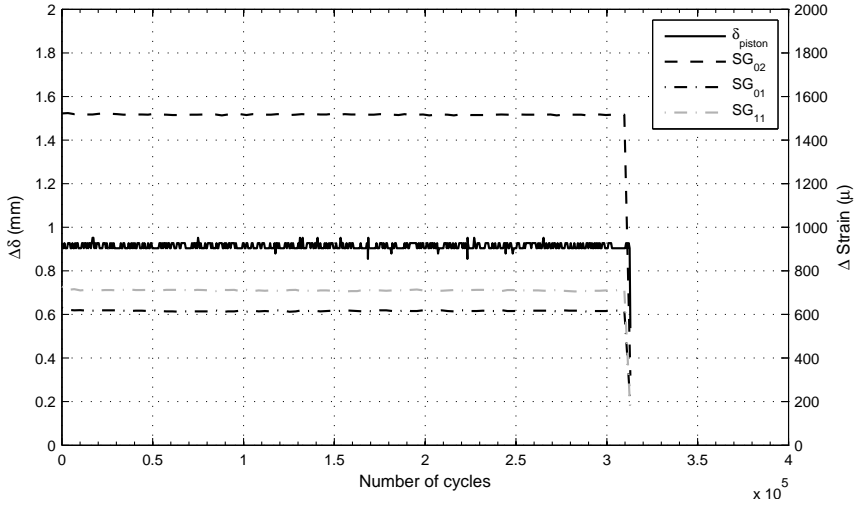
(a) Shear failure of the adhesive (load level $0.48 \cdot P_{max}/P_{ult}$)
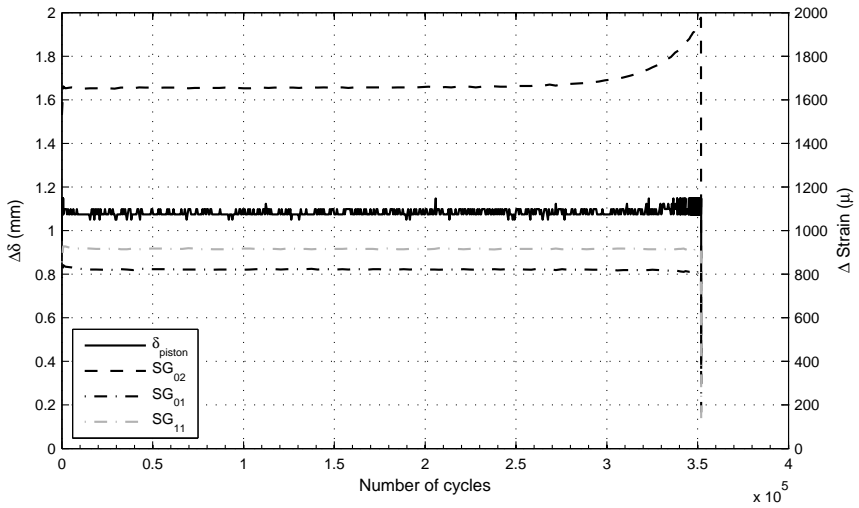
(b) Tension failure of the plate (load level $0.56 \cdot P_{max}/P_{ult}$)

Figure 4.13: Displacement and strain ranges versus number of cycles recorded during B1256 three point bending fatigue tests.

On the specimens which failed by shear of the adhesive (Figure 4.13(a)), there is no significant stiffness degradation during the fatigue test until final failure. The failure occurs suddenly at approximately $3.1 \cdot 10^5$ cycles. Neither the displacement nor the strains have significant changes during the test. The crack initiation could not be detected before the final fracture of the specimen. The fatigue life of these specimens is defined as the number of cycles that corresponds with the final failure of the specimens.

On the specimens which failed by tension of the steel plate (Figure 4.13(b)), the strain gauge at the midspan (SG_{02}) where the fatigue crack occurred, started to show the crack initiation at the steel plate between $2.5 \cdot 10^5$ and $3.0 \cdot 10^5$ cycles. During this crack initiation and propagation there is almost no stiffness degradation. The fatigue life of these specimens is defined as the number of cycles that corresponds with an increase of 10% of the initial strain range at the strain gauge SG_{02}.

Fatigue life

Table 4.12 presents the experimental results of the fatigue life of all fatigue tests performed. The fatigue life corresponding to each load level is presented to each studied specimens configuration. Figure 4.14 shows the relationship between the ratio P_{max}/P_{ult} and the fatigue life n_f for both configurations.

Five B1226 specimens were tested at three load levels under four-point cyclic loading – Figure 4.14(a). The four specimens tested at load levels higher than 60% failed by shear failure of the adhevive ('sfa'). The specimen tested at the lowest load level 50% did not show any damage after 3 million cycles. Due to the limited number of specimens, only one load level had more than one specimen. At this load level (around 60%), there is a considerable scatter on the fatigue life.

Seven B1256 specimens were tests at four load levels under three-point cyclic loading – Figure 4.14(a): '3pbt'. The specimens failed in two different modes: shear failure of the adhesive ('sfa') and tension failure of the plates ('tfp'). At load levels higher than 50%, the specimens failed on the steel plate in tension ('tfp'). The higher stress concentration at midpsan under three-point bending tests induced higher strains in the tensile steel plates than on the four-point bending tests and therefore the steel plate in tension failed before the adhesive layer. At the load level around 50%, two specimens failed on the adhesive and one specimen reached 3 million cycles without any damage. There is once again a considerable scatter on the fatigue life at this load level. Finally one specimen at 40% load level failed on the adhesive at 2.5 million cycles. The fatigue life of the B1256 configuration under four-point cyclic loading (Figure 4.14(a) – '4pbt') was only tested with one specimen at 50% load level, which reached 6 million cycles without any damage.
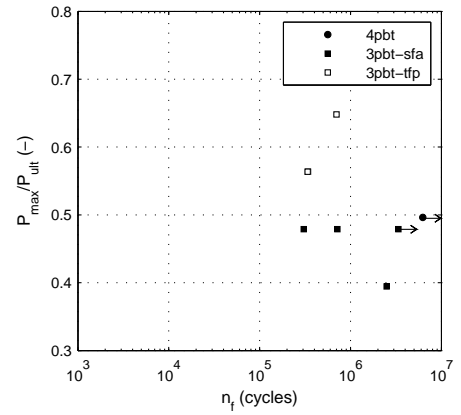
Overall, the fatigue life of the bonded steel plates reinforcement presents a significant scatter.

Table 4.12: Experimental results of the fatigue life (sfa – shear failure of the adhesive; tfp – tensile failure of the plates).

	P_{max}/P_{ult}	n_f (cycles)	failure
	0.72	11621	sfa
		9483	sfa
B1226 – 4pbt	0.61	2427	sfa
		244038	sfa
	0.50	> 3005735	run out
B1256 – 4pbt	0.50	> 6242504	run out
	0.65	701147	tfp
	0.56	340161	tfp
		337751	tfp
B1256 – 3pbt		715806	sfa
	0.48	306298	sfa
		> 3370955	run out
	0.39	2502631	sfa
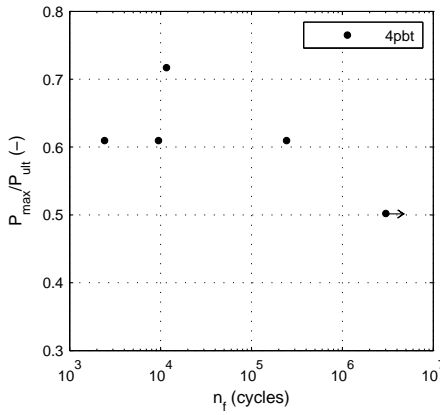
(a) B1226

(b) B1256

Figure 4.14: Experimental results given by the relationship between the ratio P_{max}/P_{ult} and the fatigue life n_f.

4.6.3   Discussion

Results show that shear failure of the adhesive is the major fatigue failure mode of the bonded steel plates reinforced beams. Therefore, the evaluation of the fatigue life will be focused on the behaviour of the adhesive layer. The shear stress distribution at the adhesive layer is used to evaluate the fatigue life.

In order to determine the stress distribution at the adhesive layer, linear elastic finite element analysis (FEA) was performed on the bonded steel plates specimens. The FEA is explained in the following section.

Stress distribution: FEA

Numerical simulations were performed on the specimens under static four and three point bending test. The analysis was performed with various adhesive thicknesses, from 1 mm to 5 mm. Although the nominal adhesive thickness was 2 mm for B1226 configuration and 5 mm for B1256 configuration, the actual thicknesses were between 1 mm and 1.5 mm for B1226 configuration and between 3 mm and 3.5 mm for B1256 configuration, as presented earlier in Table 4.5. Therefore, for the simulation to fit the actual testing as much as possible, models with 1 mm, 1.5 mm, 2 mm, 3 mm, 3.5 mm and 5 mm adhesive thickness were performed and fitted to each specimen actual adhesive thickness.

The analysis is fully elastic and under constant loading. The ABAQUS finite element code was used. The Young's modulus and Poisson's ratio of the steel were defined in accordance with EN1993-1-1 (2006), as no significant difference was found on the tensile material testing performed on the steel plates ($E_{steel} = 210$ GPa and $\nu = 0.3$). The adhesive mechanical properties were defined by the tensile Young's modulus obtained from the tensile tests at room temperature ($E_{adhesive} = 2929$ MPa – see Table 4.3) and by the Poisson's ratio given by the manufacturer ($\nu = 0.4$ – see Table 4.2).

The boundary conditions and the loads were applied directly on the element nodes. Both the steel plates and the adhesive layer were modelled using continuum 20-nodes brick (solid) elements, quadratic (second-order) with reduced integration. These elements are available in the ABAQUS library as C3D20R. These elements show accurate results when the elements are under shear and bending loads and avoid errors due to shear locking (a problem in fully integrated, first-order, solid elements) (ABAQUS, 2008). The mesh was refined until the numerical results converged. The 100 mm width was divided into elements of 5 mm wide. The thicknesses of the steel plates were divided into elements of 1.5 mm thickness. The adhesive layer is simulated with one element along the thickness. After performing mesh convergency studies with 1, 2, 3 and 4 elements per adhesive thickness which showed insignificant differences, it was decided to keep 1 element per adhesive thickness. In the model of the four-point bending tests (4pbt), only 425 mm length of the specimen was modeled since both geometry and loading are symmetric (see Figure 4.12(a)). The specimen length was divided into three mesh areas: the most refined mesh is between

the supports and the loads with elements 2.5 mm long; the second area is between the load and the symmetric axis with elements 5 mm long, and finally the coarsest mesh in the unloaded areas of the specimen with elements 10 mm long. The 4pbt model has 105819 nodes and 23920 elements. In the model of the three-point bending tests (3pbt), the complete specimens length was modeled (see Figure 4.12(b)). The 250 mm specimens length was divided into elements of 2.5 mm length. The 3pbt model has 117229 nodes and 26520 elements.

The maximum aspect ratio of the elements is 5, which is enough to avoid errors due to artificial stiffening. Figure 4.15 shows an example of a 3D finite element model of a bonded steel plates specimen under three-point bending and a detail of the mesh.

(a) 3D model   (b) mesh detail
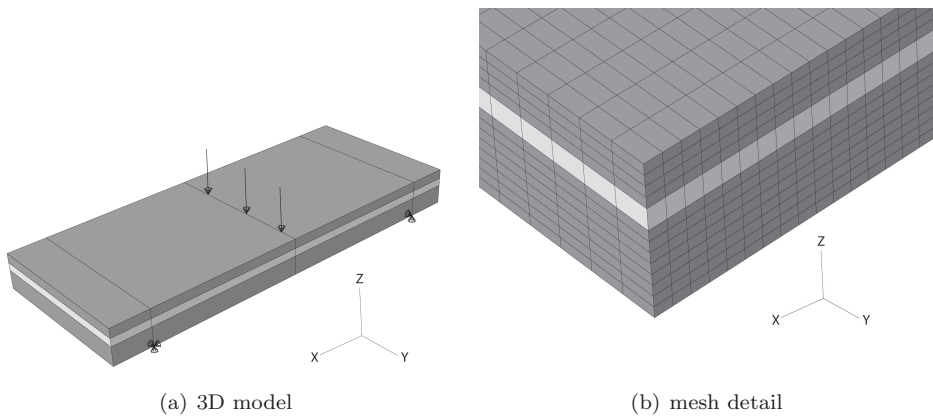
Figure 4.15: 3D finite element model of a bonded steel plates specimen under 3pbt.

To verify the accuracy of the numerical simulations, the results from the FEA were compared with the experimental results under static bending loads. The strains measured during the static test at the strain gauges located at the midspan cross-section were compared with the respective 3D FE models. Table 4.13 presents the experimental (Exp) and numerical (FEA) results of the strain gauges at the upper plate and lower plate, SG_{12} and SG_{02}, respectively, and the deviation of the numerical results. The experimental results from the 'B1226 – 4pbt' static tests are compared with the model 'B12'1'6 – 4pbt' because its actual adhesive thickness is 1 mm and not 2 mm. The same is valid for the other two specimens: 'B1256 – 3pbt' static tests are compared with the model 'B12'3'6 – 4pbt' and 'B1256 – 3pbt' static tests are compared with the model 'B12'3'6 – 3pbt'. The simulated results are close to the measured values, with maximum deviations of 10%. Figure 4.16 shows the comparison between the simulated and measured longitudinal strains along the thickness at the midspan cross-section of the 'B12'2'6 – 4pbt'.

Labordus (2006) performed similar fatigue tests on bonded steel plates reinforced specimens. Specimens with B1226 configuration were subjected to a sinusoidal fatigue load at 10 Hz frequency and 0.1 ratio. The set-up was a three-point bending

Table 4.13: Validation of the FEA with experimental data.

Static Test	Model	P (kN)	SG	Exp (μ)	FEA (μ)	dev.
B1226 – 4pbt	B12'1'6 – 4pbt	50	SG_{12}	-1927	-2053	6.5%
			SG_{02}	1789	1983	10.8%
B1256 – 4pbt	B12'3'6 – 4pbt	57	SG_{12}	-1995	-2038	2.1%
			SG_{02}	1699	1864	9.7%
B1256 – 3pbt	B12'3'6 – 3pbt	40	SG_{02}	1577	1594	1.1%
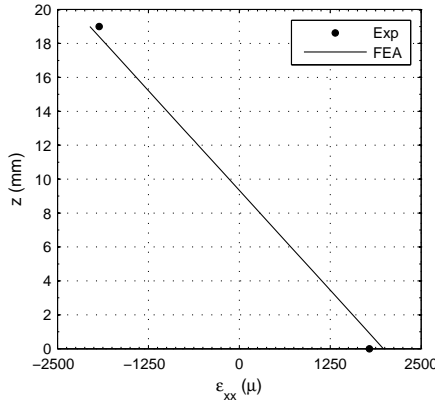
Figure 4.16: B1226 – 4pbt longitudinal strains along the thickness at the midspan cross-section.

test, similar to the one presented in Figure 4.12(b), but with asymmetric support loads, 100 mm and 50 mm instead of even 100 mm. FEA was performed on the specimens tested by Labordus (2006) in order to compare these results with the ones tested in this thesis. FEA was performed using the nominal adhesive thickness of 2 mm and using the same mechanical properties mentioned earlier in this section.

SN diagram

Figure 4.17 shows the shear stress distribution τ_{xz} obtained from the FEA of several reinforcement configurations at four-point bending under 10 kN static load. Figure 4.17(a) shows the stress distribution at the adhesive layer along the length of the specimens. This shear stress is maximum at the cross-section between the support and load point ($y/L = 0.325$ and $y/L = 0.625$). The shear stress at the adhesive decreases as the adhesive thickness increases. Figure 4.17(b) shows the shear stress distribution along the total thickness of the reinforcement at those cross-sections with maximum shear stress. At the adhesive layer, the shear stress is constant. The shear stress at the 12 mm steel plate is higher than at the adhesive layer.
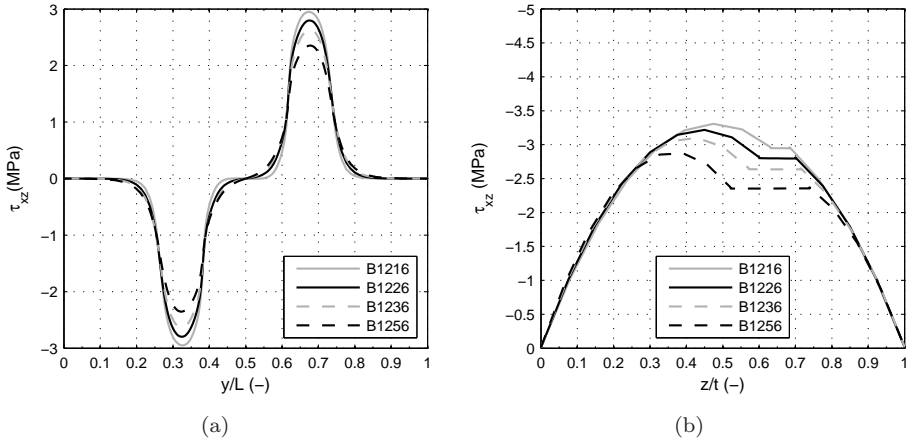
Figure 4.17: Shear stress distribution τ_{xz} under four-point bending tests at 10 kN load (a) along the normalized total length (L) at the adhesive layer ($z/t \approx 0.65$) and (b) along the normalized total thickness (t) at the cross-section between support and load points ($y/L \approx 0.325$).
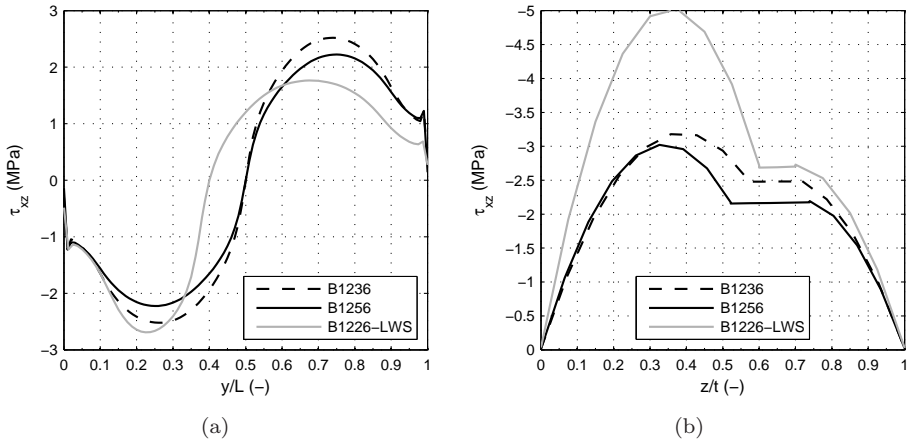
Figure 4.18: Shear stress distribution τ_{xz} under three-point bending tests at 10 kN load (a) along the normalized total length (L) at the adhesive layer ($z/t \approx 0.65$) and (b) along the normalized total thickness (t) at the cross-section between support and load points ($y/L \approx 0.2 - 0.3$).

Figure 4.18 shows the corresponding results for the three-point bending test also at 10 kN load. The cross-section where the shear stress at the adhesive is maximum is also between the support and load points (y/L between 0.2 and 0.3). The series 'B1226LWS' shows the results from the specimens tested by Labordus (2006). As in this case the load is asymmetric, the shear stress is higher at the shortest support span.

The shear failure of the adhesive occurred at the cross-section where the FEA predicts highest shear stresses. This means that using the adequate parameter to evaluate the fatigue life, in this case the shear stress at the adhesive layer, can predict the potential locations of failure.

The shear stress distribution at the adhesive layer during the fatigue tests is related to its fatigue life in a stress-cycles diagram. Figure 4.19 shows the stress-cycle SN diagram of all fatigue tests performed on the bonded steel plates reinforcement beams that failed at the adhesive. The SN diagram was determined from the fatigue results presented in Table 4.12 and Figure 4.14. The adhesive shear stress range ($\Delta\tau_{ad}$) is the average adhesive shear stress along the width at the area where the fatigue failure occurred at the amplitude load ($\Delta \cdot P = 0.9 \cdot P_{max}$). The fatigue life of each specimen n_f is plotted against its adhesive shear stress range $\Delta\tau_{ad}$.

The results taken from Labordus (2006) are apparently better than those from the present study. It is important to mention that those results are from literature and many important parameters for the fatigue life are missing.

The fatigue life does not change significantly when varying the adhesive thickness between 1 mm and 3.5 mm. No significant difference was found between the fatigue results from B1226 and B1256 specimens.

Overall, the results are considerably aligned except for the two points that failed before 10^4 cycles at 12.6 MPa adhesive shear stress range. In order to investigate the cause of these two earlier failures, Figure 4.20 shows the results from the C-scan before testing and photos after testing of one of these specimens. The C-scan shows significant air flaws before testing, Figure 4.20(a). These air flaws are particularly large at the edge of the strip. However, this 'edge air flaw' is outside the loaded area of the strip and therefore does not interfere with the fatigue results. On the loaded area, the air flaws are significantly smaller ('air flaws'). The C-scan also shows the steel spacers position on the strip. After testing, the specimen was open and Figure 4.20(b) shows a photo of the failure zone at the interfaces between the adhesive layer and the 12 mm and 6 mm thick steel plates. The same air flaws and steel spacers detected on the C-scan can be observed on this photo. The specimen failed by shear of the adhesive earlier than expected. The fatigue "beach marks" observed at both interfaces indicate that the fatigue crack initiated at the steel spacer. Hence, the earlier fatigue failures shown in Figure 4.19 are caused by the stress concentration at the steel spacers and/or air flaws present in the adhesive layer before testing.
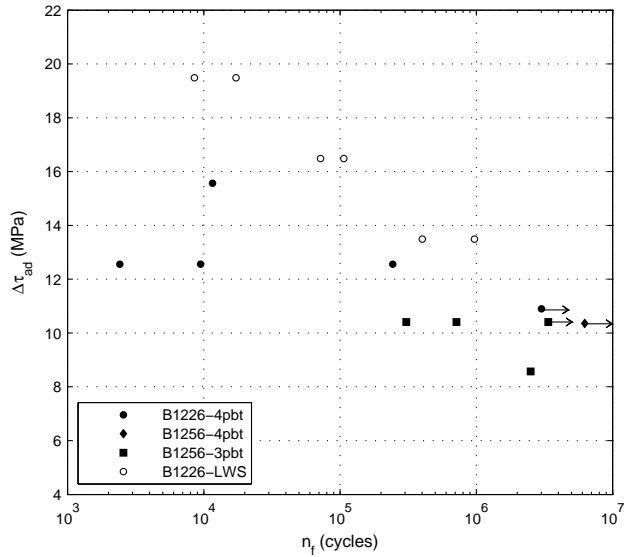
Figure 4.19: SN diagram of the bonded steel plates reinforcement.
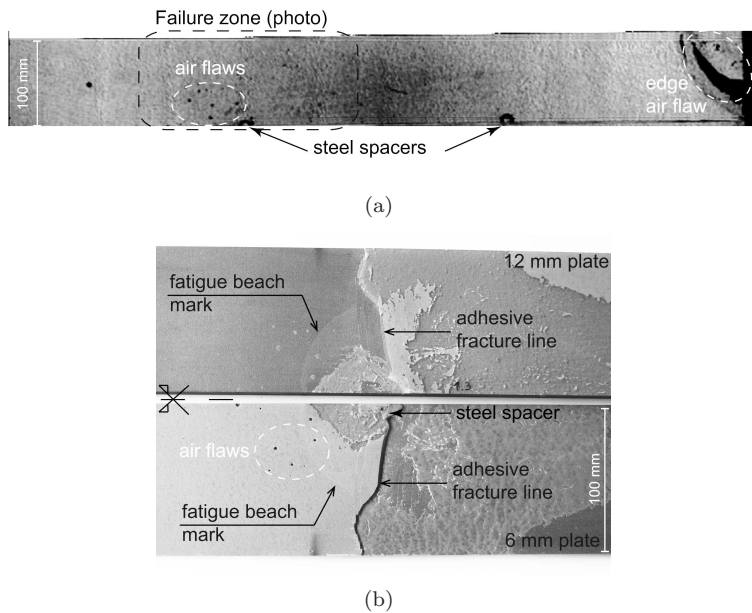

(a)

(b)

Figure 4.20: Specimen (a) C-scan before testing and (b) photos of the failure zone after testing ($\Delta\tau_{ad} = 12.6$ MPa, $n_f = 10^4$ cycles).

Fatigue threshold

The fatigue threshold, $\Delta\tau^{th}$ is defined as the stress level below which no damage will initiate or if a damage has already formed, no further propagation will take place. A limited number of cycles was set at 3 million cycles. Three specimens reached this limit without any damage. The shear stress on the adhesive at those tests is around 10-11 MPa. However, two other fatigue tests failed before one million cycles at the same stress range. One specimen even failed at 2.5 million cycles at a lower stress level around 9 MPa. These results indicate that we are very close to the border between limited and unlimited fatigue life. Despite the limited number of fatigue data, it can be said that the fatigue threshold of the adhesive shear stress range is approximately 8 MPa.

4.7   Conclusions

An assessment of the behaviour of the bonded steel plates reinforcement has been made through an experimental program. The flexural static and fatigue behaviour of the reinforcement has been studied by three- and four-point bending tests.

The stiffness and the elastic limit of the bonded steel plates reinforcement is not significantly affected by temperatures between $-10\,^{\circ}$C and $+50\,^{\circ}$C. Both the Classical Laminate Plate Theory (CLPT) and the First-order Shear Deformation Plate Theory (FSDT) applied to beams fit to simulate the elastic behaviour of the bonded steel plates beams. In comparison with no reinforcement, the stresses can be reduced by 65% to 75% after reinforcement. The static failure mode is characterized by yielding of the steel plates followed by the shear failure of the adhesive layer at the ultimate load.

The major fatigue failure mode of the bonded steel plates specimens is shear failure of the adhesive. The damage occurs at the cross-section where the shear stress is the highest. There is no significant stiffness degradation until the final failure. Therefore, the stiffness may not be a good monitoring measure for the 'health' of a specimen. The fatigue life of the bonded steel plates reinforcement is not significantly affected by adhesive thicknesses between 1 mm and 3.5 mm. The fatigue behaviour is determined by shear stress at the adhesive layer, $\Delta\tau_{ad}$. Concerning this parameter, the fatigue threshold of the adhesive layers is approximately $\Delta\tau_{ad}^{th} = 8$ MPa.

The fatigue life of the specimens is sensitive to the quality of the adhesive layer. The presence of air flaws or steel spacers on the adhesive layer can decrease the fatigue life of the reinforcement, specially at stress levels higher than the fatigue threshold.

Chapter 5

Sandwich steel plates reinforcement

5.1 Introduction

In the present Chapter the behaviour of the sandwich steel plates reinforcement is studied. The technique consists of adding a second steel plate creating a sandwich structure, in which the faces are the existing steel plate and the second steel plate, and the polyurethane layer is both the core and the adhesive of the sandwich. An experimental program was carried out aiming at a better understanding of the influence of several parameters such as core thickness, environmental temperature, etc, on the sandwich flexural behaviour. Static and fatigue bending tests were performed in sandwich beams representing the sandwich steel plates reinforcement. Part of the contents presented in this chapter is also available in Teixeira de Freitas et al. (2011).

5.2 Technique

The sandwich steel plates reinforcement was developed by Intelligent Engineering (IE) and patented as Sandwich Plates System (SPS). All manufacturing and application of SPS were performed by IE. A more detailed description of the technology and manufacturing process is given in Chapter 7. The application procedure of the sandwich specimens used on the current study consists of the following steps:

1. steel surfaces treatment: grit blast and clean the steel surfaces to be free from rust, grease and dust – cleaning grade Sa 2 1/2 according to ISO-8501 (2007);

2. weld steel bars (with the design core thickness) on the perimeter of the lower steel plate;

3. place the upper steel plate on the top of the perimeter bars and fillet weld through the perimeter forming a cavity;

4. inject the polyurethane into the cavity through small holes previously drilled in the top plate;

5. cure at room temperature during 48 h.

5.3   Materials

5.3.1   Steel plates

Steel grade S355 was selected for both steel plates, the existing steel plate and the second steel plate. According to EN1993-1-1 (2006) the nominal values for S355 steel grade are 355 MPa for the yield strength (f_y) and 510 MPa for the ultimate strength (f_u). According to the same standard, the design Young's modulus for steel is 210 GPa (E) and Poisson's ratio is 0.3 (ν). Four different steel plate thicknesses were used: 5 mm and 6 mm for the second steel plate, and 10 mm and 12 mm for the existing steel plate.

Tensile tests

In order to characterize the mechanical properties of the steel plates, four series of tensile tests were performed, one for each plate thickness. The specimens and test procedure were in accordance with EN10002-1 (2001). Table 5.1 shows the average±standard deviation mechanical properties obtained from the tensile tests. The values for the Young's modulus E, yield strength f_y, ultimate strength f_u, ratio between ultimate strength and yield strength fu/fy and percentage elongation after fracture A_c are given.

The average yield strengths are higher than the nominal value 355 MPa recommended in EN1993-1-1 (2006). The average ultimate strength are lower than the nominal value 510 MPa recommended in the same standard. All steel plates fulfil the minimum ductility requirement concerning the ratio $f_u/f_y > 1.10$, recommended in EN1993-1-1 (2006). The Young's modulus are on average 8% lower than the recommended design value, 210 GPa.

Table 5.1: Tensile mechanical properties of the steel plates.

Plate thickness	#	E (GPa)	f_y (MPa)	f_u (MPa)	f_u/f_y	A_c (%)
5 mm	4	205.9 ± 2.1	431.1 ± 2.9	504.2 ± 4.1	1.17 ± 0.00	27.0 ± 3.1
6 mm	3	186.2 ± 10.5	407.3 ± 2.5	494.3 ± 2.5	1.21 ± 0.01	31.3 ± 2.1
10 mm	4	204.1 ± 15.2	427.6 ± 5.2	486.7 ± 1.4	1.14 ± 0.02	31.8 ± 1.1
12 mm	3	179.7 ± 2.6	405.0 ± 2.6	500.3 ± 3.8	1.24 ± 0.01	31.7 ± 2.1

5.3.2 Core

The sandwich core is polyurethane (solid polymer) with density 1150 kg/m^3. This polyurethane is the material S4 presented in Chapter 3, Table 3.1. Table 5.2 shows the polyurethane characteristics given by the manufacturer, including the tensile mechanical properties at three temperature ranges (σ_{ty}, yield strength at 0.2% offset; ε_{tmax}, tensile failure strain).

Table 5.2: Characteristics of the core material given by the manufacturer.

Characteristics	Polyurethane elastomer		
Manufacturer	Elastogran GmbH		
Curing process	Room temperature during 48 h		
Density (kg/m^3)	1150		
ν (-)	0.36		
Temp.	$-20\,^\circ$C	$+23\,^\circ$C	$+60\,^\circ$C
E_t (MPa)	1164	874	436
σ_{ty} (MPa)	23.0	16.1	8.1
ε_{tmax} (%)	15.1	32.1	43.1

Tensile tests

Tensile tests were performed on the core material in order to characterize its mechanical properties. The tests were performed at three different temperatures: low temperature ($-10\,^\circ$C), room temperature (RT: $+20\,^\circ$C to $+23\,^\circ$C) and high temperature ($+50\,^\circ$C). Tests were conducted in an environmental chamber of a testing machine with a maximum test load of 250 kN. At each temperature five specimens were submitted to tensile load up to failure. The experimental procedure was in accordance with ISO-527 (1996). Experiments were performed under displacement control at cross-head speed of 5 mm/min. A mechanical extensometer was used to measure the elongation of the specimens.

The average±standard deviation results obtained from the core tensile testing at low temperature ($-10\,^\circ$C), room temperature (RT) and high temperature ($+50\,^\circ$C) are presented in Table 5.3. The corresponding stress-strain curves are shown in Figure 5.1.

The polyurethane core tensile behaviour is significantly affected by temperature within the considered range. The polyurethane is stiffer at low temperatures than at high temperatures. The Young's tensile modulus (E_t) increases by approximately 45% at $-10\,^\circ$C and decreases by approximately 35% at $+50\,^\circ$C when compared to room temperature. The same tendency is observed for the yield strength at 0.2% offset (σ_{ty}) and the tensile strength (σ_{tmax}), higher values at low temperatures than at high temperatures. The tensile failure strain (ε_{tmax}) presents the opposite behaviour with lower values at low temperatures than at high temperatures, although

at a lower rate of approximately 20% for both temperature extremes when compared to room temperature.

The results fit well to the mechanical properties given by the manufacturer (see Table 5.2).

Table 5.3: Tensile mechanical properties from the core material testing.

Temp	E_t(MPa)	σ_{ty}(MPa)	σ_{tmax}(MPa)	ε_{tmax}(%)
$-10\,^\circ$C	1049 ± 70	22.0 ± 0.5	37.6 ± 1.0	21.2 ± 4.1
RT	721 ± 54	15.1 ± 0.3	25.0 ± 1.1	26.6 ± 4.8
$+50\,^\circ$C	471 ± 52	9.1 ± 0.4	17.7 ± 0.6	31.4 ± 2.0
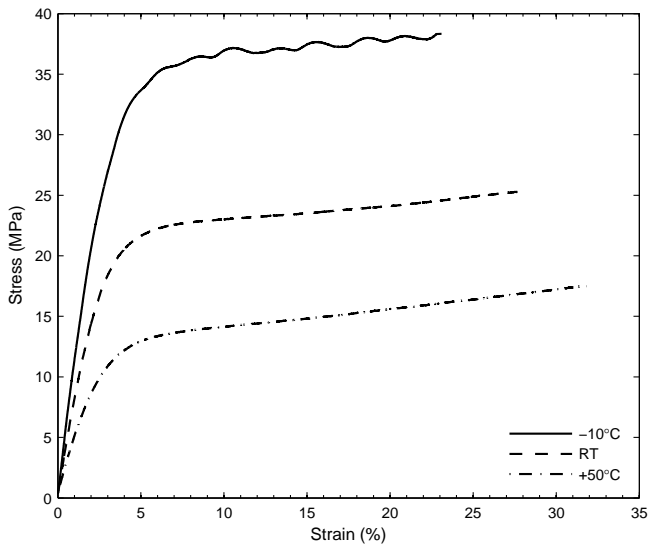
Figure 5.1: Core tensile stress-strain curves.

5.4   Sandwich steel plates specimens

The sandwich specimens are simple beams representing the sandwich steel plates reinforcement. Five configurations were tested. The thickness of the steel faces and core were varied according to the expected real applications.

Although stiffer sandwich structures are achieved when minimizing faces thickness and maximizing core thickness, for this specific application several limitations must be considered. In the Netherlands, the steel deck plate of orthotropic bridge decks is typically 12 mm thick in movable bridges and 10 mm thick in fixed bridges. In the present study, both thicknesses were used for the lower steel face. In addition, the thickness of the second steel plate cannot be less than 5 mm. In real applications, a minimum robustness is needed for this second steel plate, for preventing damage of the interface layer (for example when repairing wearing courses). Therefore, thicknesses of 5 and 6 mm were used for the upper steel face. The thickness of the core was selected according to the most common limitations on weight for movable bridges. The extra weight added to the structure (W: weight of the core and upper steel face) was varied between 60 and 80 kg/m^2. Taking these values into account, the thickness of the polyurethane core was varied from 15 mm to 30 mm. Although the height limit on a movable bridge might be exceeded using these values, the thickness variation allows to investigate the influence of the core thickness on the bending behaviour and extend the applicability of the research (for example to fixed bridges).

Specimens with five different cross-sections were manufactured using different combinations of thicknesses. Table 5.4 shows the characteristics of the specimens, including lower and upper face thickness (t_{lf} and t_{uf}), core thickness (t_c), ratio between core thickness and average face thickness ($t_c/\bar{t}_f$) and weight (W). The specimens' configuration is referred to as "Saabbc", where "aa" represents the lower face thickness (t_{lf}), "bb" the core thickness (t_c) and "c" the upper face thickness (t_{uf}). The sandwich geometry was mainly varied using a 12 mm thick lower steel face, because this study is mainly focused on reinforcement systems for movable bridges.

The specimens were manufactured by Elastogran GmbH, by order of Intelligent Engineering, which was responsible for the core material and its application. The fabrication procedure followed the technique described in section 5.2.

Table 5.4: Configuration of the sandwich steel plates specimens and their characteristics.

Specimen	t_{lf} (mm)	t_c (mm)	t_{uf} (mm)	$t_c/\bar{t}_f$ (-)	W (kg/m^2)
S12305	12	30	5	3.5	74
S12155	12	15	5	1.8	57
S12206	12	20	6	2.2	70
S12306	12	30	6	3.3	82
S10306	10	30	6	3.8	82

One sandwich box was manufactured per sandwich configuration. The sandwich boxes were manufactured large enough to extract more than one specimen from each box. The boxes were water-jet cut to obtain the specimens final dimensions, 100 mm wide and 850 mm long.

After cutting the specimens, the thicknesses of the faces and core were carefully measured. No significant difference was found between the real and the nominal values.

5.5   Static behaviour

The aim of this part of the study is to better understand the static bending behaviour of the sandwich steel plates reinforcement. The experimental program that has been carried out is presented and discussed in the following sections. The experimental program is similar to what was performed on the bonded steel plates reinforcement presented in Chapter 4.

5.5.1   Experimental procedure

The flexural behaviour of the sandwich specimens at low temperature ($-10\,°$C), room temperature (RT) and high temperature ($+50\,°$C) was determined from static four-point bending tests in accordance with ASTM-C393 (2006). Two types of load configuration were used: short and long beams. The short beams load configuration was quarter point loading with 400 mm support span and 200 mm load span. The long beams load configuration was third point loading with 750 mm support span and 250 mm load span. The aim was to better understand the flexural behaviour of the sandwich beams when subjected to different ratios between normal stress of the steel faces and shear stress of the core ($\sigma_{steelfaces}/\tau_{core}$). The bending tests were performed under displacement control at cross-head speeds of 1 and 3 mm/min for the short beams and long beams load configuration, respectively.

Firstly, the elastic flexural behaviour was determined from non-destructive bending tests performed up to a certain elastic load. Two specimens per geometry were subjected to six test conditions: three environmental temperatures ($-10\,°$C, RT and $+50\,°$C) at two load configurations (short and long beams). Tests were conducted in an environmental chamber of a testing machine with a maximum test load of 100 kN.

Secondly, the failure flexural behaviour of the sandwich beams S12206, S12306 and S10306 was determined at $-10\,°$C, RT and $+50\,°$C for short beams load configuration. For this second part of the experimental program six specimens were tested per geometry (two specimens per test condition). Tests were conducted in an environmental chamber of a testing machine with a maximum test load of 600 kN.

Figure 5.2 shows the test set-ups used for elastic (Figure 5.2(a)) and failure (Figure 5.2(b)) bending tests. The sandwich specimens are positioned upside down (lower

face up) since the load actuator is at the bottom side. The displacement at middle span was measured by two potentiometers, one at each side of the specimen (see Figure 5.2(a)). The middle span longitudinal strains of the steel faces were measured by strain gauges placed along the thickness of the faces as shown in Figure 5.3(a). Rosettes were positioned half way between the supports and the load points at the short beams load configuration in order to measure the shear strain of the polyurethane core (see Figure 5.3(b)). The climate chamber's and the specimen's temperature were measured by temperature sensors.

(a) elastic behaviour   (b) failure behaviour
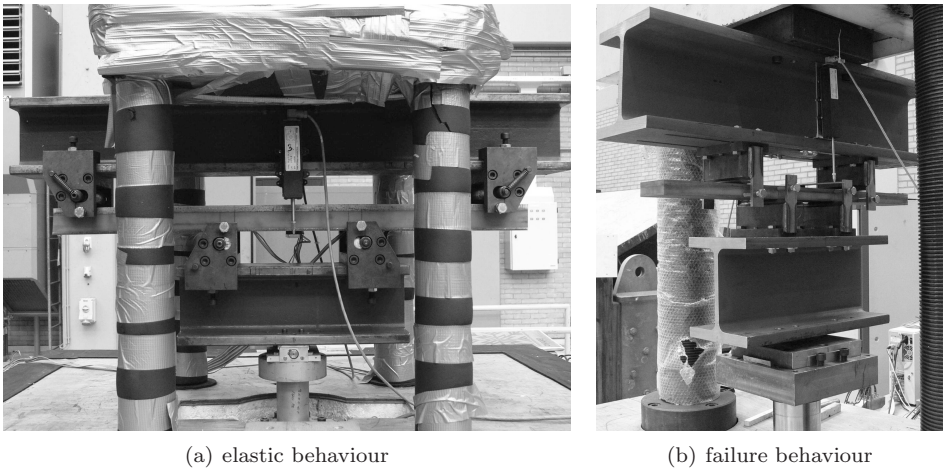
Figure 5.2: Test set-ups used for bending tests.

(a) strain gauges on the faces   (b) rosette on the core
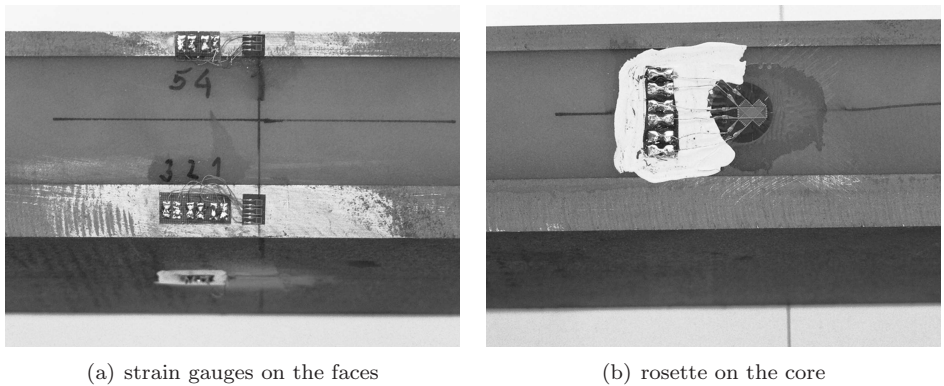
Figure 5.3: Strain gauges applied on the sandwich specimen.

5.5.2   Analytical and Numerical Analyses

Analytical and numerical analyses were performed to verify the elastic flexural behaviour at low temperature ($-10\,°\text{C}$), room temperature (RT) and high temperature ($+50\,°\text{C}$) of short and long sandwich beams. The analyses are fully elastic, under constant loading and assume perfect bonding conditions between the core and the faces of the sandwich. The analytical stiffness of the sandwich beams was determined using the First-order Shear Deformation Theory (FSDT). Numerical simulations of the elastic bending tests were performed using finite element analysis (FEA).

The Young's modulus and Poisson's ratio of the steel were defined in accordance with EN1993-1-1 (2006), as no significant difference was found between the real and design values. The core material properties were defined by the tensile Young's modulus obtained from the tensile tests and by the Poisson's ratio given by the manufacturer.

First-order Shear Deformation Theory

Many theories have been developed to predict the flexural behaviour of sandwich beams. One of the most popular is the First-order Shear Deformation Theory (FSDT), also known as classical sandwich theory, already presented in Chapter 3. The FSDT is an equivalent single layer theory which assumes that a line originally straight and normal to the reference axis remains straight during deformation, but not necessarily perpendicular to the reference axis. The displacement consists of two parts, one due to pure bending and one due to transverse shear.

The model used to simulate the sandwich bending tests is a beam subjected to four-point loading bending tests where x, y, z are the axes in the direction of the length, width and thickness, respectively. In the FSDT, the normal strains ε_x are linear through the thickness of the laminate and the transverse shear strains γ_{xz} are constant through the thickness (Reddy, 2004). The normal strain ε_x, normal stress σ_x, shear stress τ_{xz} and shear strain γ_{xz} were determined by the Equations (3.1), (3.2), (3.3) and (3.4) presented in Chapter 3 (page 18).

According to FSDT, the sandwich beam total displacement is the sum of the bending displacement of the faces and the shear displacement of the core. The total displacement at middle span is given by Equation (5.1), the bending displacement by (5.2) and the shear displacement by (5.3).

$$\delta_{midspan} = \delta_{bending;midspan} + \delta_{shear;midspan} \tag{5.1}$$

$$\delta_{bending;midspan} = \frac{P \cdot L^3}{k_1 \cdot D} \tag{5.2}$$

$$\delta_{shear;midspan} = \frac{P \cdot L}{k_2 \cdot S} \qquad (5.3)$$

where P is the applied load, L is the beam span and k_1 and k_2 are functions of the support and load span. The sandwich stiffness K was determined by the ratio between the load and the displacement at middle span – Equation (5.4).

$$K = \frac{P}{\delta_{midspan}} \qquad (5.4)$$

Finite element analysis

Finite element analysis (FEA) was performed to better understand the elastic flexural behaviour of the sandwich beams. The ABAQUS finite element code was used. Figure 5.4 shows the 3D finite element model of S12305 specimen subjected to long beams and short beams load configuration, Figures 5.4(a) and 5.4(b), respectively. The coordinate system is the same as the one used in FSDT, x, y and z in the direction of the length, width and thickness of the specimen. The boundary conditions and the loads were applied directly on the element nodes. Both faces and core were modelled using continuum 20-nodes brick (solid) elements, quadratic (second-order) with reduced integration. These elements are available in the ABAQUS library as C3D20R. These elements show accurate results, especially when the elements are under shear and bending loads and avoid errors due to shear locking (a problem with fully integrated, first-order, solid elements) (ABAQUS, 2008). A mesh convergency study was performed until the difference in stresses between two refined meshes was insignificant (less than 0.5%). The elements thicknesses were varied from 1.25 mm to 1.5 mm on the faces and from 3 to 6 mm on the core (5 elements per core thickness). The elements width was 5 mm (20 elements per specimen width). The specimen length was divided into elements of 10 mm length except for the short beams load configuration between supports where the mesh was refined to 5 mm element length. The long beams model has 127773 nodes and 29240 elements. The short beams model has 186693 nodes and 42840 elements. The maximum aspect ratio of the elements is 5, which is enough to avoid errors due to artificial stiffening. A detail of the mesh is shown in Figure 5.5. Simulations were carried out at the three environmental temperatures and for the five geometries tested.

(a) Long beams

(b) Short beams
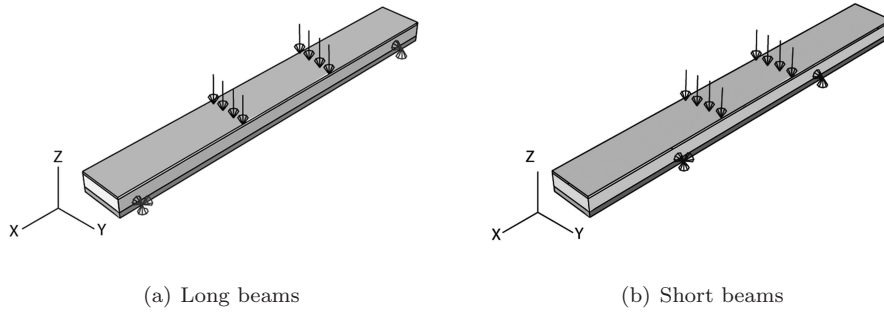
Figure 5.4: S12305 3D FE model.

(a) Mesh detail

(b) Mesh refinement at short beams
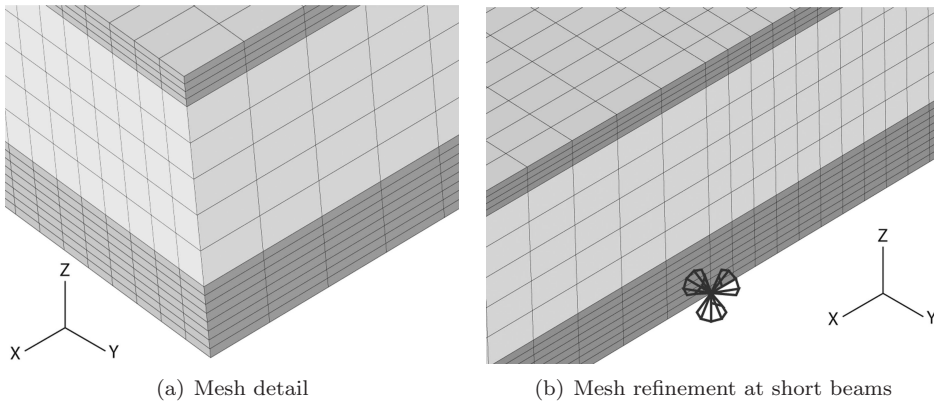
Figure 5.5: S12305 FE model mesh.

5.5.3 Results and Discussion

The results of the experimental program carried out on the static behaviour of the sandwich steel plates reinforcement are divided into three sub results: elastic flexural behaviour, failure flexural behaviour and stress reduction factor. The experimental results are compared with the analytical and numerical results presented in the previous section.

Sandwich steel plates elastic flexural behaviour

The load-displacement graphs at room temperature of the five tested sandwich geometries are presented in Figure 5.6, for long beams load configuration. The ratio between core thickness and face thickness influences the stiffness of the different geometries. Specimens with higher ratios (S12305: 3.5; S12306: 3.3; S10306: 3.8) are stiffer than specimens with lower ratios (S12206: 2.2; S12155: 1.8). It can also be observed that reducing by 1 mm or 2 mm the steel face thickness (S12306, S12305 and S10306) has much less influence on the stiffness than reducing the core thickness by 10 or 5 mm (S12306, S12206 and S12155). Moreover, considering that 1 mm steel face and 5 mm PU-core have approximately the same weight, the reduction is more significant when reducing by 5 mm the core thickness from S12206 to S12155 than when reducing by 1 mm the upper steel face from S12305 to S12306. Therefore, if weight reduction must be made it should be on the steel faces rather than on the core thickness. Stiffer sandwich steel plates solutions can be achieved by putting the extra weight on the core thickness rather than on the face thickness.
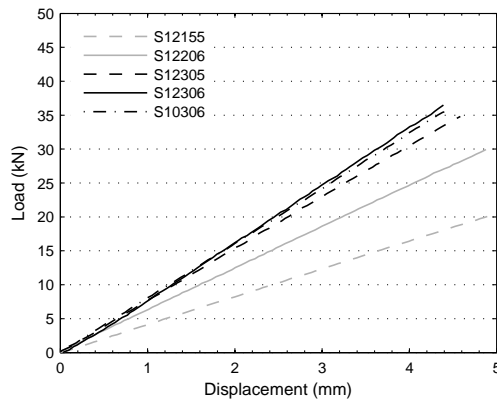
Figure 5.6: Load-displacement graphs measured at room temperature for long beams.

The load-displacement graphs for the sandwiches S12305 and S12155 at low temperature ($-10\,^\circ$C), room temperature (RT) and high temperature ($+50\,^\circ$C) are presented in Figure 5.7 both for short and long beams load configuration. These two geometries have extreme values of the ratio between core thickness and face thickness (S12305: 3.5; S12155: 1.8). With regard to other geometries, similar ratios have similar flexural behaviour (S12306 and S10306 similar to S12305) and in between ratios have in between flexural behaviour (S12206 in between S12305 and S12155).

(a) S12305   (b) S12155
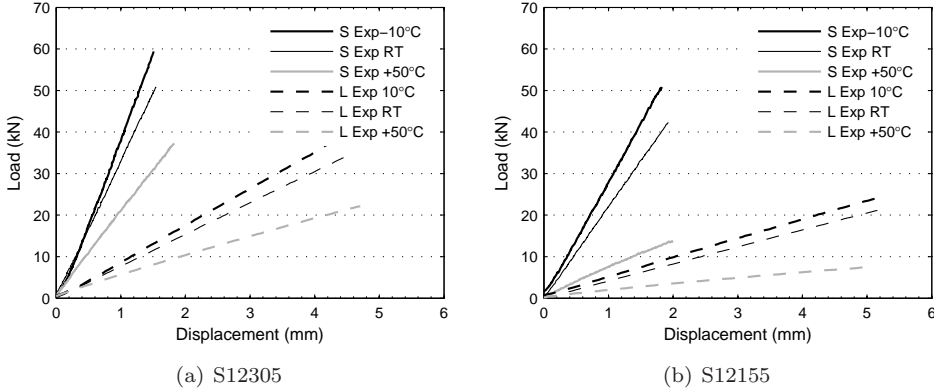
Figure 5.7: Load-displacement graphs (S–short beams; L–long beams).

The temperature significantly affects the sandwich stiffness, within the considered range. The sandwich beams are stiffer at low temperatures ($-10\,^\circ$C) than at high temperatures ($+50\,^\circ$C). The stiffness increases by approximately 25% and 15% at $-10\,^\circ$C for short and long beams, respectively, when compared with room temperature. The stiffness decreases by approximately 50% and 45% at $+50\,^\circ$C for short and long beams, respectively, when compared with room temperature. The bending stiffness is more affected by temperature variations in short beams than in long beams. Only the core behaviour is temperature dependent and it plays a more important role in short beams than in long beams ($\varepsilon_{steelfaces}/\gamma_{core}$ lower in short beams than in long beams). When compared with room temperature, the bending stiffness decreases significantly more at $+50\,^\circ$C than increases it at $-10\,^\circ$C. According to Gibson and Ashby (1997), increasing the temperature of a polymer based material gives time-dependent strain beyond the further drop in the Young's modulus. The significant visco-elasticity at high temperatures justifies more notable temperature effects at high temperatures than at low temperatures. This phenomenon is relatively more significant on the experimental results of thinner cores than of thicker cores. This effect might be caused by the low thermal conductivity of the polyurethane where thinner cores ensure better temperature distribution along the beam than thicker cores.

The average stiffness results (K) from all geometries tested at low temperature ($-10\,^\circ$C), room temperature (RT) and high temperature ($+50\,^\circ$C) are presented in

Table 5.5 both for short and long beams load configuration. In Table 5.5 the experimental results are compared with the results from the First-order Shear Deformation Theory and from the FEA simulations.

Table 5.5: Stiffness results from sandwich bending tests (Exp), FSDT and FEA.

K		$-10\,°C$			RT			$+50\,°C$		
(kN/mm)		Exp	FSDT	FEA	Exp	FSDT	FEA	Exp	FSDT	FEA
Short beams	S12305	39.4	30.3	36.4	32.3	22.6	29.1	20.2	15.8	22.5
	S12155	28.2	19.6	23.2	22.0	15.5	19.7	9.0	11.4	16.2
	S12206	38.3	24.4	29.8	29.6	18.5	24.5	13.3	13.1	19.5
	S12306	46.2	31.2	38.6	37.1	23.0	30.6	19.0	15.9	23.6
	S10306	42.7	29.8	34.0	34.2	22.1	26.6	16.2	15.4	20.1
Long beams	S12305	8.8	7.8	8.1	7.6	6.4	6.8	4.5	4.9	5.3
	S12155	4.6	4.1	4.2	4.2	3.6	3.8	2.0	3.0	3.2
	S12206	7.0	5.8	6.1	6.2	4.9	5.2	2.9	3.8	4.2
	S12306	9.9	8.4	8.9	8.5	6.7	7.3	4.7	5.1	5.7
	S10306	9.4	7.8	8.0	8.0	6.3	6.6	4.3	4.8	5.1

With regard to the accuracy of FSDT it can be observed that only for long beams at $-10\,°C$ and RT there is reasonable agreement between FSDT and experiments. The FSDT predicted stiffness is approximately 15% lower than experimental results at these tests conditions. For short beams the deviation between the FSDT stiffness and experiments grows to 30% at $-10\,°C$ and RT. At $+50\,°C$ the experimental results show less analogy with the FSDT results.

The FEA simulations are generally more in accordance with the experimental results. At $-10\,°C$ and RT, the predicted stiffnesses for short beams are approximately 20% lower than the experimental results and for long beams 15% lower. At $+50\,°C$, FEA predicted stiffnesses are on average 25% higher than the experimental results. The deviation of the FEA at high temperatures is higher for specimens with thinner cores (30% and 40%) than for specimens with thicker cores (10% and 20%) because, as discussed earlier, the experimental results of thinner cores are more affected by high temperatures.

In order to better understand these results, the through-thickness variation of longitudinal strains at the middle span cross-section was measured experimentally (Exp) and determined using FSDT and FEA. The results are given in Figures 5.8 and 5.9 for S12305 and S12155 for short beams at 12 kN load and for long beams at 7 kN load.

(a) long beams   (b) short beams
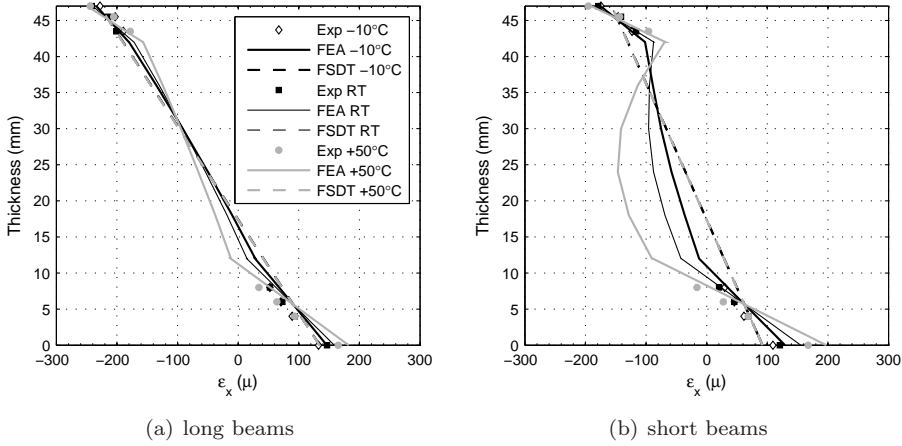
Figure 5.8: S12305 longitudinal strains (ε_x) at the middle span cross-section.

(a) long beams   (b) short beams
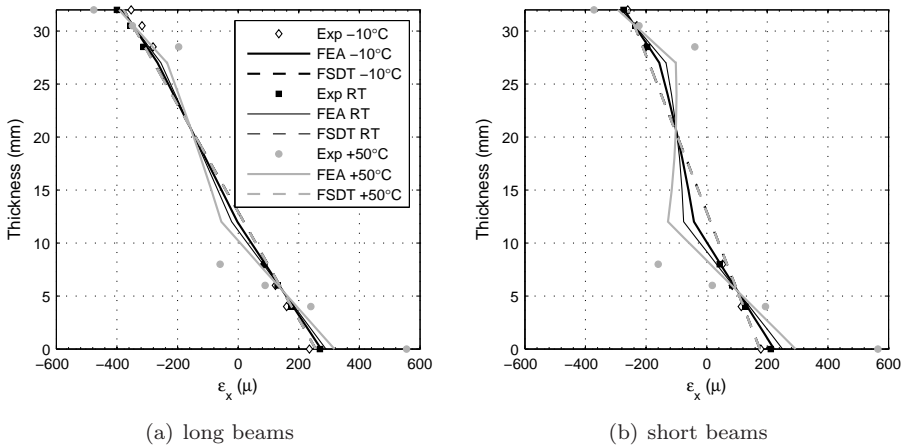
Figure 5.9: S12155 longitudinal strains (ε_x) at the middle span cross-section.

The Exp and FEA results indicate that the plane-sections-remain-plane criterion assumed in FSDT is only valid for long beams at $-10\,^{\circ}$C and RT (Figures 5.8(a) and 5.9(a)) and clearly invalid for short beams at any temperature range (Figures 5.8(b) and 5.9(b)). The FSDT cannot predict the discontinuity at the interfaces core-steel-face and the non-linearity at the core present on the longitudinal strains for the short beams load configuration. Higher order shear deformation theories (HSDT) are needed to better model the sandwich bending behaviour on these load conditions. At $+50\,^{\circ}$C the experimental results present greater deviations with the FSDT results

than at lower temperatures. The visco-elasticity present in the polyurethane at high temperatures, which fails the elastic assumption, might be the reason for the increase of deviation.

FEA simulations result in a better analogy with the experimental results. This is especially observed for short beams load configuration (Figures 5.8(b) and 5.9(b)). In both geometries S12305 and S12155, the results from FEA predict the slope discontinuity measured on the longitudinal strains at all temperatures tested. The difference of mechanical properties between the steel faces and the core causes a discontinuity of the deformed core-steel-face planes at the interface. This is also known as 'zig-zag' effect and has been subject of several studies in sandwich composite structures (Brischetto et al., 2009; Carrera, 2003; Cho and Averill, 2000). The 'zig-zag' effect increases with temperature as the discontinuities in the mechanical properties between faces and core increase. At short beams load configuration, the 'zig-zag' effect becomes stronger than at long beams because the transverse shear strain is higher in short beams than in long beams.

Besides this discontinuity, FEA simulations of the geometry S12305 present an extra warping of the core at short beams load configuration. The warping gets stronger for high temperatures and is less significant for S12155 geometry. This effect might be caused by secondary effects of short beams already observed by Hardy and Pipelzadeh (1991) when studying static analysis of short beams with homogeneous cross-section. As the ratio between span and thickness of the cross-section increased, the distribution became less distorted. This might be the reason for the less significant warping on the distribution along the S12155 geometry.

For the results at $+50\,^\circ$C, the percentage of deviation between FEA and experiments is approximately 15% for S12305 and 40% for S12155. The simulations are stiffer than the experiments because the FEA took only the decrease of Young's modulus into account and ignored the extra effect of time-dependent strain.

The shear strain was measured during tests by rosettes at half way between the support and the load for short beams load configuration. The results are shown in Figure 5.10 for S12305 and S12155 at all temperatures tested and compared with FSDT and FEA. As already observed, FEA is more in agreement with experimental results than FSDT. At $-10\,^\circ$C and RT, the predicted shear strains are higher than the ones measured, both for FSDT and FEA. At $+50\,^\circ$C, and mainly at thinner cores, greater deviation is observed between measured values and predicted values.

(a) S12305   (b) S12155
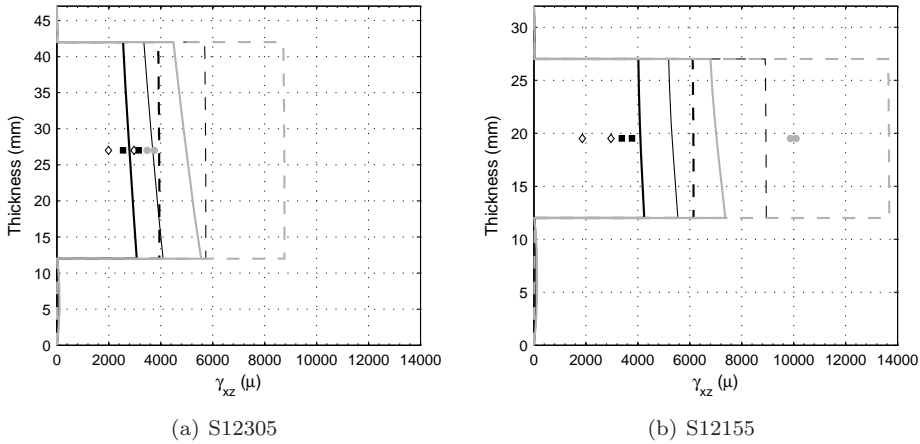
Figure 5.10: Shear strain (γ_{xz}) at half way between the support and the load for short
beams load configuration (see Fig. 5.9 for key).

Sandwich steel plates failure flexural behaviour

The failure flexural behaviour of the sandwich beams S12206, S12306 and S10306
was determined at $-10\,^{\circ}\mathrm{C}$, RT and $+50\,^{\circ}\mathrm{C}$ for short beams load configuration. The
representative load-displacement curves at room temperature of the three sandwich
geometries are presented in Figure 5.11. It can be observed that the lower steel face
thickness, 12 mm or 10 mm (S12306 to S10306), has less influence on the flexural
strength than the core thickness, 30 mm or 20 mm (S12306 to S12206).
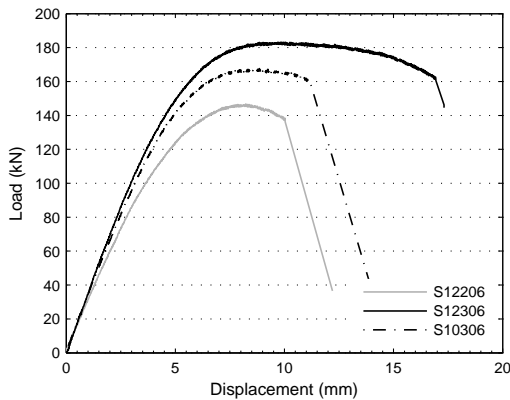
Figure 5.11: Load-displacement curves at room temperature.

The representative load-displacement curves for geometries S12206 and S10306 at the three temperatures ranges are shown in Figure 5.12. The average yield loads and delamination loads and corresponding displacements are presented in Table 5.6. The delamination between the faces and PU-core was detected by monitoring the bending tests taking pictures at every displacement step. This procedure was carried out only when no climate chamber was used. Therefore, there are only delamination values for RT tests. Table 5.7 shows the average maximum loads and failure displacements.

At $-10\,^{\circ}$C the behaviour is brittle and almost linear. Failure occurs at high load levels and small displacements. No significant plastic deformation is observed as the yield and failure occur at similar displacement values.

At RT the plastic deformation increases but the yield and maximum load values are not significantly affected. The delamination loads are higher than the yield loads, which indicates that the sandwich beams yield before delamination occurs between the PU-core and the faces.

At $+50\,^{\circ}$C the behaviour is non-linear with significant plastic deformation. The maximum load decreases and the failure displacement increases.

Temperature significantly affects the flexural strength of the sandwich beams within the considered range. The behaviour observed indicates that the PU-core has a significant influence on the flexural behaviour of the sandwich beams. Temperature effects can be explained by the temperature dependency of the PU material, lower strength and higher failure strain at high temperature than at low temperatures (see Table 5.3).

(a) S12206   (b) S10306
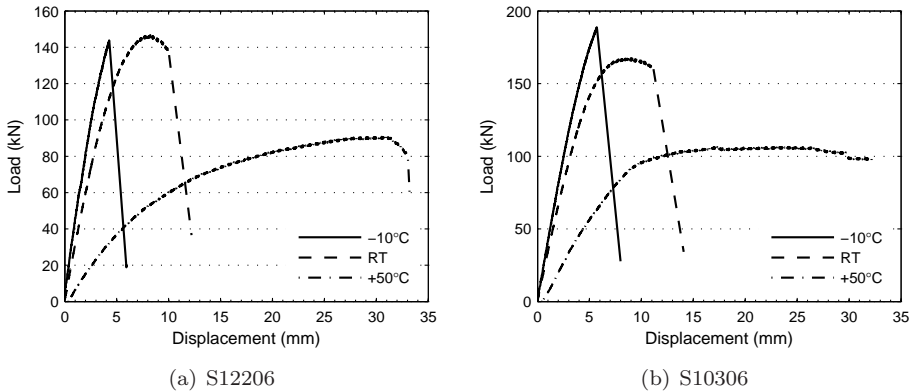
Figure 5.12: Load-displacement curves.

Table 5.6: Average yield loads and delamination loads and corresponding displacements.

(kN,mm)	$-10\,^{\circ}\mathrm{C}$		RT				$+50\,^{\circ}\mathrm{C}$	
	P_y	δ_y	P_y	δ_y	P_{del}	δ_{del}	P_y	δ_y
S12206	110.7	3.2	97.9	3.6	135.7	6.0	40.4	5.7
S12306	146.4	3.8	130.2	4.1	131.3	4.2	72.9	5.8
S10306	135.4	3.5	120.2	4.0	134.7	4.9	70.3	7.4

Table 5.7: Average maximum loads and failure displacements.

(kN,mm)	$-10\,^{\circ}\mathrm{C}$		RT		$+50\,^{\circ}\mathrm{C}$	
	P_{ult}	δ_{ult}	P_{ult}	δ_{ult}	P_{ult}	δ_{ult}
S12206	133.7	5.8	148.0	12.6	91.4	37.4
S12306	234.3	13.5	182.8	16.7	119.9	42.3
S10306	197.9	9.2	167.7	17.0	102.7	40.1

Figure 5.13 shows pictures of S10306 specimens after failure. The failure modes at $-10\,^{\circ}\mathrm{C}$ and at RT are faces-to-core delamination and core shear failure (Figures 5.13(b) and 5.13(c)). Although the final failure of the specimens is core shear failure, delamination started before. This is confirmed by the delamination load measured at RT which occurred before failure. It can also be observed in Figures 5.13(b) and 5.13(c) that the plastic deformation after failure is more significant on the steel faces than on the PU-core. For both temperatures the lines drawn on the PU-core surface remain straight after failure. The failure mode at $+50\,^{\circ}\mathrm{C}$ is faces-to-core delamination (Figure 5.13(d)). At high temperatures the PU-core allows more deformation before failure than at low temperatures. This can be observed by the significant warping of the lines drawn on the PU-core at $+50\,^{\circ}\mathrm{C}$ when compared to $-10\,^{\circ}\mathrm{C}$ and RT (Figures 5.13(b) to 5.13(d) – perpendicular lines before test). The deformation needed for the complete delamination of the interface between PU-core and faces can only be achieved before shear failure of the PU-core at $+50\,^{\circ}\mathrm{C}$ and not at $-10\,^{\circ}\mathrm{C}$ and RT.

Figures 5.14, 5.15 and 5.16 show the normal stress and the shear stress distribution along the normalized thickness at the yield load of each geometry, respectively, at $-10\,^{\circ}\mathrm{C}$, RT and $+50\,^{\circ}\mathrm{C}$. The normal stress σ_x is at the middle span cross-section and the shear stress τ_{xz} at the cross-section half way between load and support points. The experimental values (Exp) were determined by Equations (5.5) and (5.6) using the strain values measured during tests by strain gauges applied on the steel faces and rosettes on the PU-core.

$$\sigma_{x.exp}^{steel} = \varepsilon_x \cdot E_{steel} \tag{5.5}$$

$$\tau_{xz.exp}^{PU} = \gamma_{xz} \cdot G_{PU} \tag{5.6}$$

(a)

(b) $-10\,^{\circ}\mathrm{C}$

(c) RT

(d) $+50\,^{\circ}\mathrm{C}$
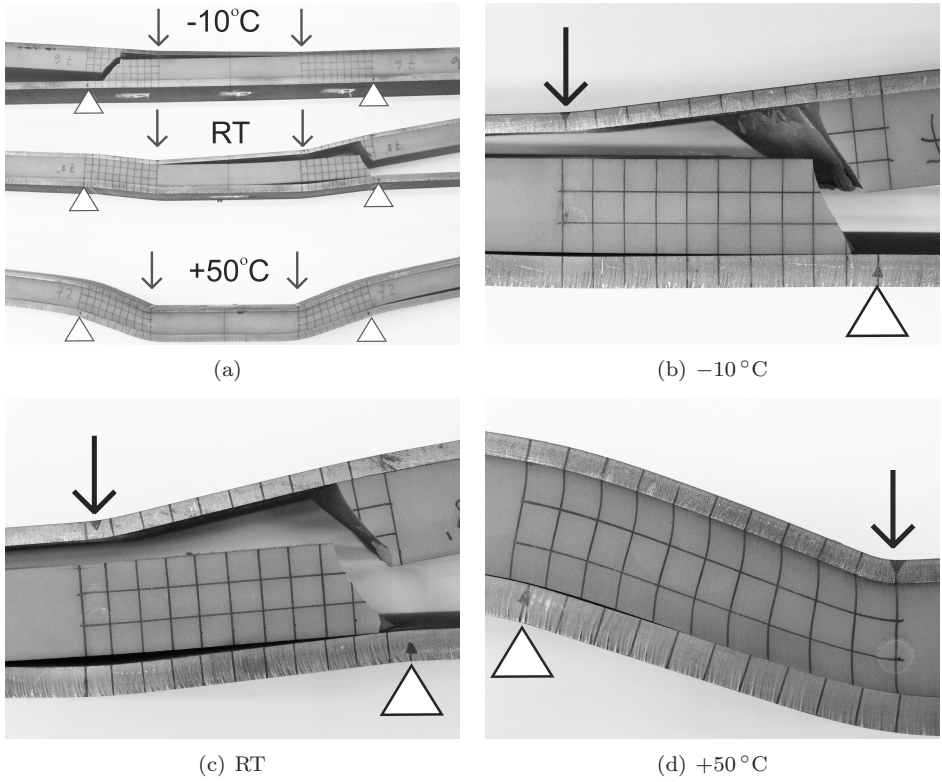
Figure 5.13: S10306 specimens after failure.

(a)

(b)
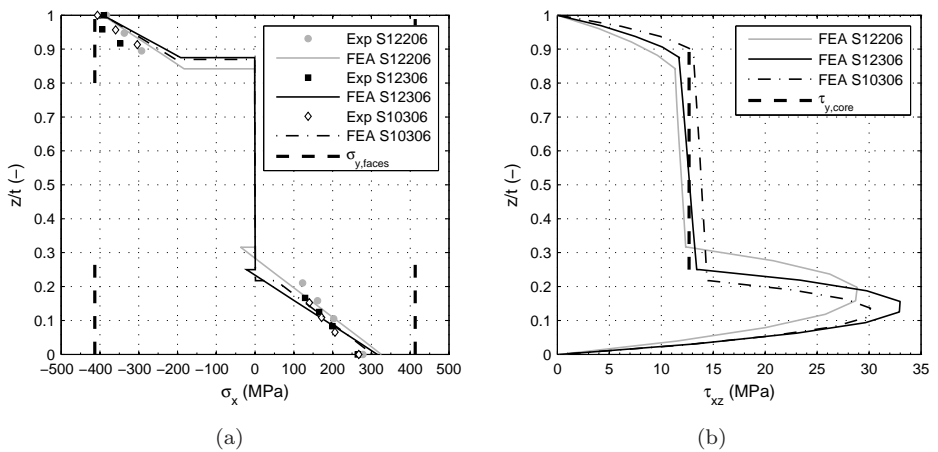
Figure 5.14: Stresses at $-10\,^{\circ}\mathrm{C}$ at the yield load.
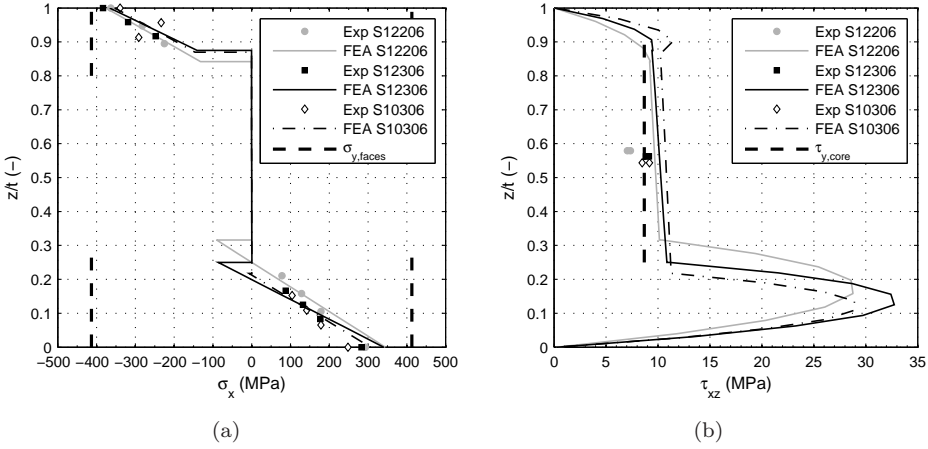
Figure 5.15: Stresses at RT at the yield load.
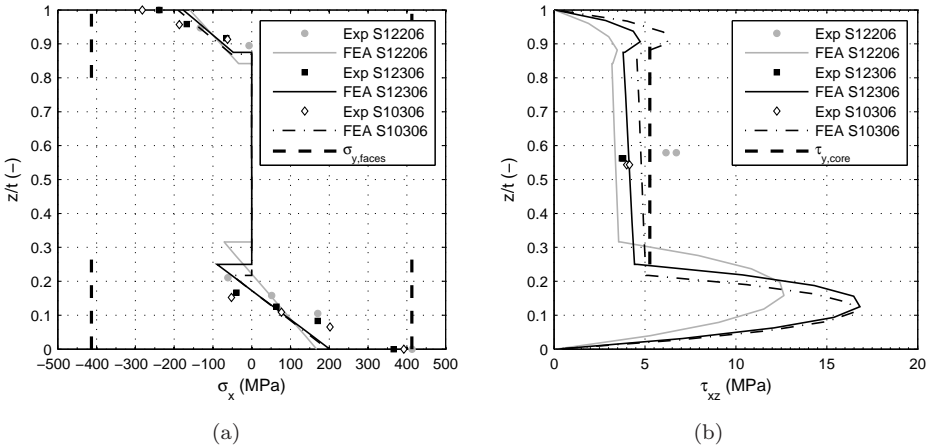
Figure 5.16: Stresses at +50 °C at the yield load.

The steel Young's modulus was defined in accordance with EN1993-1-1 (2006) (E_{steel} = 210 GPa). The shear modulus of the PU was determined by Equation (3.8) using the tensile Young's modulus obtained from the tensile tests at each temperature and by the Poisson's ratio given by the manufacturer.

The experimental results are compared with FEA results. Both results are compared with the average yield stress of the faces ($\sigma_{y,faces}$ – Table 5.1, for 6, 10 and 12 mm: $\overline{f_y}$ = 413 MPa) and the yield shear stress of the PU-core using Von Mises criterion ($\tau_{y,core} = \sigma_{ty}/\sqrt{3}$).

For the yield load at $-10\,^\circ$C and RT, the upper steel face and PU-core are close to yielding. At $-10\,^\circ$C and RT, there is good agreement between the experimental values and the FEA. At $-10\,^\circ$C no experimental results are available for the shear strain of the PU-core. At $+50\,^\circ$C, the lower steel face and the PU-core are close to yielding. The considerable deformation of the PU-core at this temperature decreases the connection between the steel faces. Therefore, the stresses on the lower steel face increase considerably. Meanwhile, the PU-core is also close to yielding. At $+50\,^\circ$C a greater deviation is observed between experimental results and FEA than at $-10\,^\circ$C and RT. For all temperatures tested, the yield load of the sandwich beams occurred when one of the steel faces and the PU-core were close to yielding.

Stress reduction factor

The stress reduction factor SRF for the sandwich beams was determined by the ratio between the maximum stress in the lower steel face (midspan location) before the reinforcement and after the reinforcement – Equation (5.7). The stress before was determined using Equation (3.2) for a steel beam with no reinforcement subjected to the same load conditions. The stresses after the reinforcement were determined from the strain gauge measurements during tests using Equation (5.5) and from the FEA.

$$SRF = \left(1 - \frac{\sigma_{lf}^{After}}{\sigma_{lf}^{Before}}\right) \cdot 100 = \left(1 - \frac{\sigma_{Saabbc}}{\sigma_{aa}}\right) \cdot 100 \qquad (5.7)$$

The SRF from the experimental tests (average values) and from the FEA at $-10\,^\circ$C, RT and $+50\,^\circ$C are presented in Table 5.8 both for short and long beams load configurations. Stresses at the steel plate can be reduced by 60% to 95% after reinfocement. The SRF is significantly affected by temperature, within the considered range. The temperature increase, from RT to $+50\,^\circ$C, decreases the SRF by up to 20%. The temperature decrease, from RT to $-10\,^\circ$C, increases the SRF by up to 3%.

The most efficient combination is 30 mm PU-core and 5 mm or 6 mm upper steel face: rows S12305, S12306 and S10206. These combinations can result in an SRF between 80% and 90%. Decreasing the PU-core thickness from 30 mm to 20 mm or 15 mm (rows S12205 and S12155) can reduce the SRF to 75% or 65%, respectively. The FEA results are in good agreement with the experimental results.

Overall, the SRF is higher for long beams than for short beams load configuration. As shown in Figures 5.8 and 5.9, decreasing the span from long to short increases the 'zig-zag' effect present at the strains of the sandwich beams. As the 'zig-zag' effect becomes stronger, the desirable composite action between the three layer becomes weaker (more than one neutral axis) and, therefore the SRF decreases.

The bonded and sandwich steel plates reinforcements can be compared with the ultra high performance concrete alternative studied by Schrieks (2006) and Boeters

Table 5.8: Average *SRF* results from sandwich bending tests and determined from FEA.

	SRF	$-10\,^{\circ}$C		RT		$+50\,^{\circ}$C	
	(%)	Exp	FEA	Exp	FEA	Exp	FEA
Short beams	S12305	91	89	90	87	84	83
	S12155	85	81	83	79	62	75
	S12206	89	86	87	83	74	80
	S12306	92	90	90	87	83	84
	S10306	94	93	94	91	89	89
Long beams	S12305	92	92	92	91	90	89
	S12155	86	84	85	83	75	82
	S12206	90	88	89	88	83	86
	S12306	93	92	92	91	90	90
	S10306	95	94	94	94	92	93

et al. (2009) in terms of stress reduction factors. Tests were performed on small beams similar to the present study. The results show a stress reduction of 70% on the steel plate adding $50\,\mathrm{kg/m^2}$ (25 mm of concrete overlay). For approximatelly the same weight, the *SRF* obtained for the bonded steel plates reinforcement is 60%-65% adding a 6 mm thick upper steel plate using 2 mm adhesive nominal thickness and for the sandwich steel plates reinforcement is 75%-85% adding a 5 mm thick upper steel plate using 15 mm core thickness.

5.6   Fatigue behaviour

Fatigue tests have been carried out in order to better understand the fatigue behaviour of the sandwich steel plates reinforcement. The experimental program was performed using the first two of the five configurations listed in Table 4.4: S12305 and S12155.

5.6.1   Experimental procedure

Fatigue tests were performed in two sandwich beam geometries. Both have 12 mm and 5 mm lower and upper steel face thicknesses, respectively. The difference between the two tested geometries is the core thickness, 30 mm and 15 mm. The maximum and minimum values for the core thickness were tested to enable any further interpolation for the fatigue behaviour of the thickness in between.

The fatigue tests were performed at room temperature on the test rig used for the static tests (see Figure 5.2(a)), with a maximum capacity of 100 kN. The tests were four-point loading equivalent to the short beams load configuration used for the static tests: 200 mm load span and 400 mm support span.

Strain gauges were applied at the bottom side of the lower steel face and at the top side of the upper steel face in the middle of the strip's width. The strain gauges

measured longitudinal strains at the midspan cross-section and at the cross-section between the load and the support points. It was decided to monitor the latter region, since core shear failure was expected to occur where the core shear stress is the highest. Figure 5.17 shows a drawing of a specimen S12305 under the fatigue load configuration and the strain gauge positions.
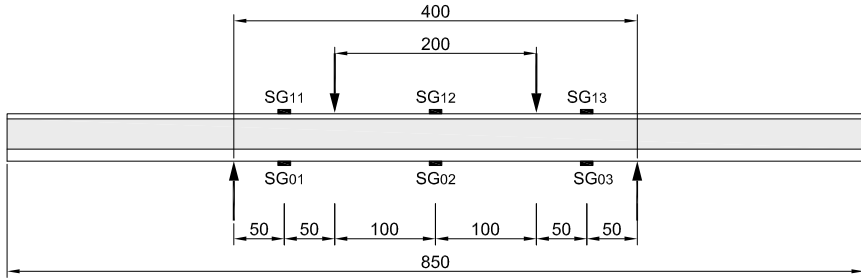
Figure 5.17: Fatigue load configuration and specimens instrumentation (SG - strain gauges; dimensions in mm).

The fatigue tests were carried out in load control with a constant applied load ratio $R = 0.1$ ($R = P_{min}/P_{max}$). The aim was to perform tests at different load levels, at a maximum load (P_{max}) between 60% and 30% of the respective static failure load (P_{ult}). The wave form was sinusoidal.

Cyclic loading on sandwich beams with large strain variation creates an increase in the temperature of the core material, that will not be released due to its very low thermal conductivity. This temperature increase results in a degradation of the core properties, as observed in the previous section, and hence has a decremental effect on the fatigue life of the sandwich beams (Sharma et al., 2006). Therefore, attention must be paid to temperature increases at the core material during fatigue loads in order to avoid any negative influence on the fatigue life of the sandwich beams.

In order to ensure that the fatigue life determined in this study is not influenced by any thermal effects during the fatigue tests, a pre-study was conducted varying the frequency of testing. Temperature sensors were glued to the free surface of the sandwich core. The evaluation was based on the criterion that the core temperature should not rise more than $5\,°C$ from its initial temperature (Burman and Zenkert, 1997; Shenoi et al., 1995). After testing between 5 Hz and 2 Hz frequency, it was concluded that at 2 Hz the temperature was not increasing more than $4\,°C$ to $5\,°C$ from its initial temperature. Therefore it was decided to conduct all the fatigue tests on the sandwich steel plates at a constant frequency of 2 Hz.

Static tests were initially performed to obtain relevant load levels for the fatigue tests. Static tests were performed at room temperature, at a constant displacement rate of 1 mm/min and using exactly the same load configuration as for the fatigue tests. Due to the small amount of specimens available for the fatigue experimental

program, only one specimen within each sandwich geometry was tested in static loading.

5.6.2   Results

The results from the static test initially performed on the sandwich beams S12305 and S12155 are shown in Table 5.9. The static failure mode was first delamination at the interface between the core and the faces and finally core shear failure at the ultimate applied load (see Figure 5.13(c)).

Table 5.9: Static yield and ultimate loads and corresponding displacements at room temperature.

(kN,mm)	P_y	δ_y	P_{ult}	δ_{ult}
S12305	111.9	3.6	174.8	16.4
S12155	81.1	3.8	127.5	20.2

Fatigue failure mode

All the fatigue failures occurred in the area between the support and the load point of the sandwich beam, where the transverse shear force is constant. All the fatigue final failure modes were core shear failures. Figure 5.18 shows a typical example of displacement and strains range values measured during one fatigue test until failure. The displacement range is measured by the piston of the load cell δ_{piston} and the strains are measured by the strain gauges SG_{01} and SG_{11} (see Figure 5.17), located close to the area where final failure occurred. The example shown is from a S12155 sandwich configuration under 0.35 P_{max}/P_{ult} load level.

The displacement and strain range are constant in the greater part of the fatigue test, until a certain point when the fatigue damage starts. For the example shown in Figure 5.18, the damage starts at approximately 1.8 million cycles. At this point the strain of both strain gauges starts to increase. This is the start of the fatigue damage and corresponds with the beginning of the delamination between the 12-mm-steel-face (tension face) and the core, which was visually observed. For all the fatigue tests performed, the delamination was the first damage event observed. The starting point of the delamination is detected by the strain gauges, but it does not affect the displacement significantly. As the delamination propagates throughout the interface, the displacement starts to increase.

The second damage event is the kink of the delamination crack through the core thickness. The starting point of the crack kink was difficult to be detected visually due to the high crack propagation rate. Nevertheless it is believed that the kink of the crack and following progression through the core thickness occurs approximately when the strain range of SG_{11} starts to decrease.
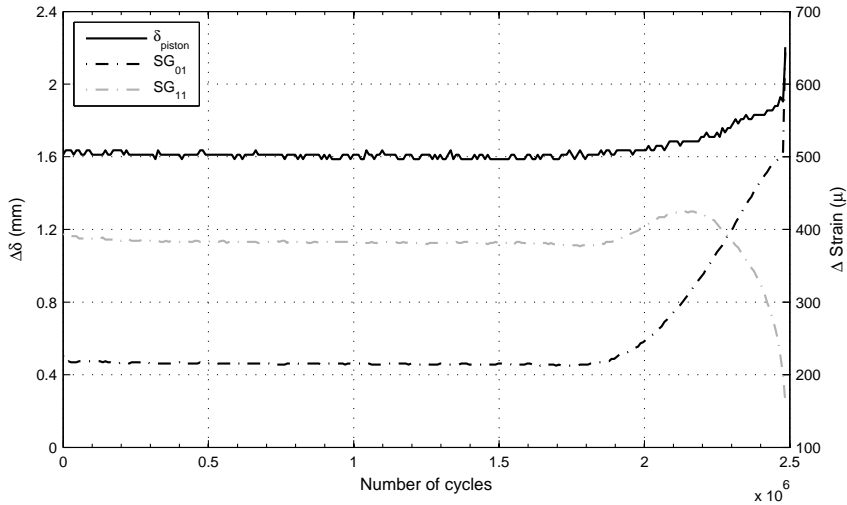
Figure 5.18: Displacement and strain range versus number of cycles measured at S12155 fatigue test under $0.35 \cdot P_{max}/P_{ult}$ load level.

The third and last damage event is when the crack progresses through the core thickness and reaches the interface with the 5-mm-steel-face (compression face), causing the displacement and strain to increase exponentially and finally to the failure of the specimen (close to 2.5 million cycles).

These three fatigue damage events occurred in all fatigue tests performed both for S12305 and S12155.

Very similar fatigue damage progression was already observed in previous research on fatigue of sandwich structures found in literature. Kulkarni et al. (2004) and Shenoi et al. (1995) described very similar fatigue damage on sandwich panels with PVC foams (polyvinyl chloride) under three-point bending fatigue tests. Gibson (2011) reports the core crack progression in the same way for sandwich beams with Rohacell foam cores. A very good summary of the research that has been performed on fatigue of sandwich beams is reported in Sharma et al. (2006).

Looking at what the failure and cracks look like during fatigue damage, two distinct 'core shear crack shapes' were identified based on the angle of the crack in the core of the sandwich: type A and type B.

Figure 5.19 shows examples of type A crack on S12305 and S12155. On type A crack, after progression of the delamination between the tension face and core (this delamination can be detected on the right hand side of Figure 5.19(a) and left hand side of Figure 5.19(b)), the crack kinks to the core thickness with an angle clearly larger than 45°, rather between 70° and 80°. The crack progresses through the core thickness decreasing the angle and finally reaches the compression face at an angle

of approximately 55°. The crack is asymmetrical considering the mid core thickness plan.

Kink angles larger than 45° were also observed in shear fatigue tests performed on sandwich beams with polymer foams reported in Zenkert and Burman (2009). Analytical studies performed by the same author state that kink angles higher than 45° occur when an interface delamination is present just prior to the core crack (Zenkert, 1991), which is exactly the case with the damage progression observed at the tested sandwich beams.

Figure 5.20 shows examples of type B crack on S12305 and S12155. The initial crack angle (kink angle) is also between 70° and 80° just like type A crack. However, when the crack reaches the mid thickness of the core, the angle decreases to approximately 45°. This is especially evident on the S12305 specimen in Figure 5.20(a). When the crack reaches the compression face, the angle returns to its initial shape, but now with the compression face. In Figure 5.20(c), prior to the crack, there is delamination on both interfaces between the core and the tension face and the core and the compression face. The delamination with both faces is thought to be the cause of the symmetrical kink angle and symmetrical crack shape.

Fatigue crack growth and fracture mechanics on sandwich structures has been subject of several research studies for many years, such as Prasad and Carlsson (1994), Shipsha et al. (1999) and Berggreen and Carlsson (2010). In these studies, analyses are carried out to better understand and explain the fracture mechanism of sandwich beams.

Fatigue life

The fatigue life is defined as the number of cycles that corresponds to 10% of stiffness degradation. In all failure fatigue tests, this point occurred after the delamination event but before the final failure. For the example shown in Figure 5.18, the delamination occurred around 1.8 million cycles, the 10% stiffness degradation at 2.3 million cycles and the final failure at 2.48 million cycles.

Table 5.10 presents the experimental results of the fatigue life of all tested sandwich beams. The fatigue life n_f corresponding to the load level (P_{max}/P_{ult}) of each test is presented, as well as the moment when delamination was detected in terms of percentage of the fatigue life ('del. ($\% n_f$)'). For specimens with a fatigue life lower than 1 million cycles, the delamination occurs quite early, approximately 50% to 70% of the fatigue life. For specimens with longer lives, the delamination occurs mainly after 80% of the fatigue life.

Figure 5.21 shows the relationship between the ratio P_{max}/P_{ult} and the fatigue life n_f for the S12305 and the S12155 sandwich configurations.

(a) S12305 $(0.54 \cdot P_{max}/P_{ult})$

(b) S12155 $(0.42 \cdot P_{max}/P_{ult})$
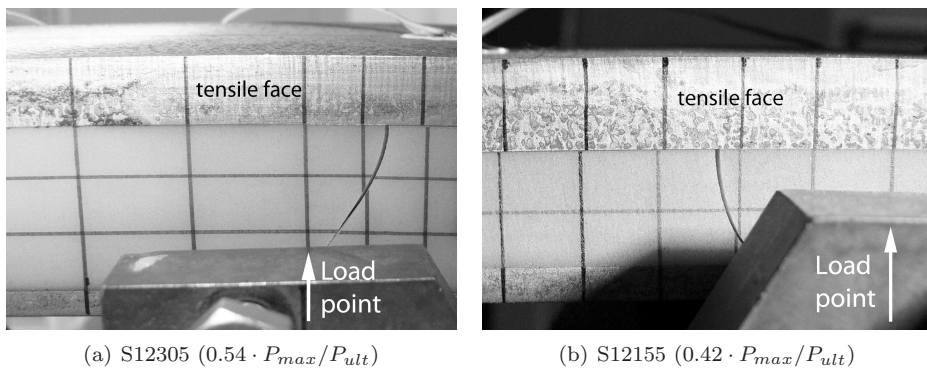
Figure 5.19: Type A core shear crack : delamination and core crack progression.

(a) S12305 – crack progression

(b) S12305 – final failure

(c) S12155 – delamination prior to crack

(d) S12155 – final failure
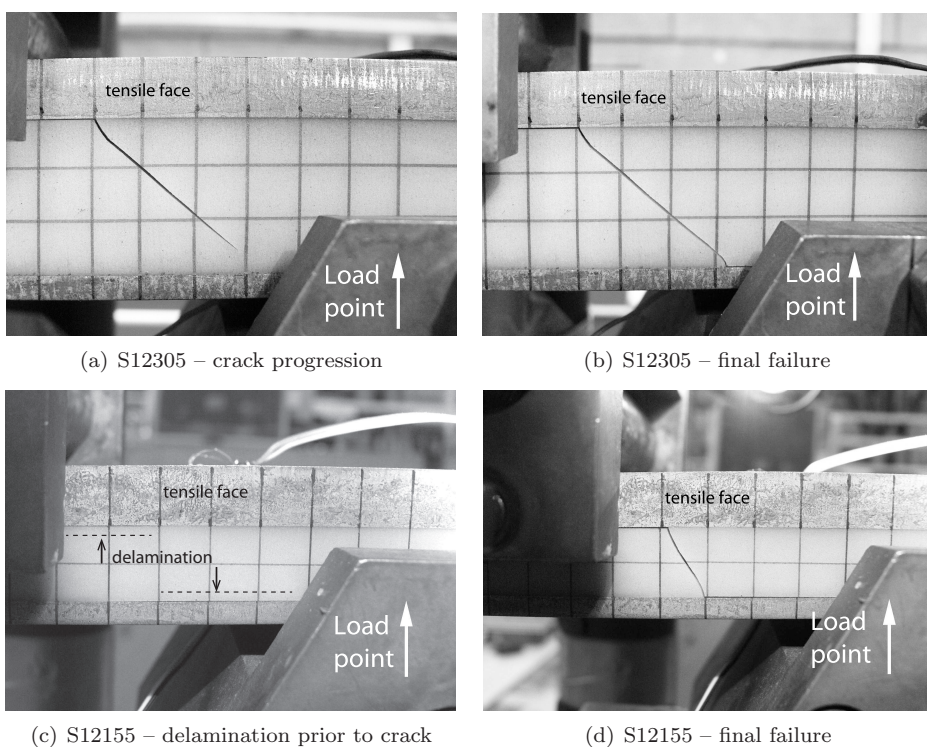
Figure 5.20: Type B core shear crack – (a) and (b) $0.43 \cdot P_{max}/P_{ult}$, (c) and (d) $0.42 \cdot P_{max}/P_{ult}$.

Table 5.10: Experimental results of the fatigue life of the sandwich beams (* delamination not detected).

	P_{max}/P_{ult}	n_f (cycles)	del. ($\% \, n_f$)
	0.54	209282	72%
		103191	68%
	0.43	283672	71%
S12305		2593862	94%
		2976665	89%
	0.34	> 4674438	(run out)
		> 5363733	(run out)
	0.63	11107	*
	0.47	243604	57%
		379407	*
		308479	55%
	0.42	1093497	87%
S12155		1448238	76%
		1438322	90%
		2303967	78%
	0.35	2878979	83%
		> 3638481	(run out)
	0.31	> 4165831	(run out)
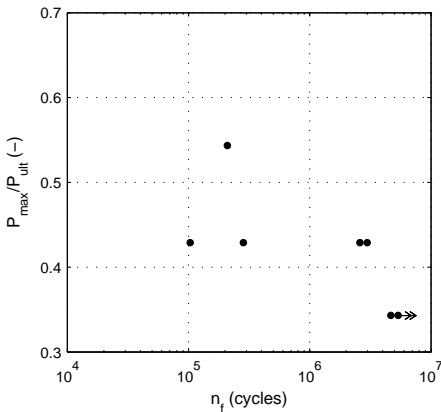
(a) S12305
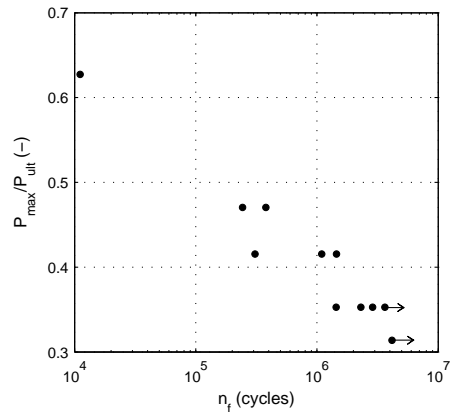
(b) S12155

Figure 5.21: Experimental results given by the relationship between the ratio P_{max}/P_{ult} and the fatigue life n_f.

Seven S12305 specimens were tested at three different load levels (Figure 5.21(a)). The specimen tested at the highest load level failed before half a million cycles. At the intermediate load level between 0.4 and 0.5, two specimens failed before half a million cycles and two specimens failed after 2.5 million cycles. There is a considerable scatter at this intermediate level. At the lowest load level (0.34) two specimens reached approximately 5 million cycles without any damage.

Eleven S12155 specimens were tested at five different load levels (Figure 5.21(b)). The only specimen tested at the highest load level had a very early failure, around 10.000 cycles. From the five specimens tested between 0.4 and 0.5 load level, three failed before half a million cycles and two failed around 1 million cycles. At the lower load levels two specimens failed between 2 and 3 million and two specimens reached almost 4 million cycles without any damage. One specimen at this load level failed earlier than the other ones, at 1.4 million cycles.

5.6.3   Discussion

SN diagram

Results show that delamination between the core and the steel faces followed by shear failure of the core is the major fatigue failure mode of the studied sandwich beams. Therefore the shear stresses through the interfaces and through the core thickness are the parameters used to evaluate the fatigue life.

The stress distribution at the sandwich beams was obtained from the static FEA explained in the previous section 5.5.2. Figure 5.22 shows the shear stress distribution τ_{xz} under four-point bending tests at 10 kN load (by equilibrium $\tau_{zx}{=}\tau_{xz}$) . The cross-section along the length with the maximum shear stress is located between the load and support points (Figure 5.22(a) – $y/L = 0.35$). It was at this cross-section where all the fatigue failures were experimentally observed. Using the adequate parameter to evaluate the fatigue life, in this case the shear stress at the interface between the core and the 12 mm thick steel plate, can predict the potential locations of failure.

The distribution along the sandwich thickness (Figure 5.22(b)) shows that the shear stress at the interface between the core and the 12 mm thick steel plate is 17% higher than at the interface with the 5 mm thick steel plate, both for S12305 and S12155. This explains why the delamination was mainly observed at the interface between the core and the 12 mm thick steel face. The shear stress at the S12155 sandwich configuration is approximately 39% higher than at the S12305 sandwich configuration.

(a)   (b)
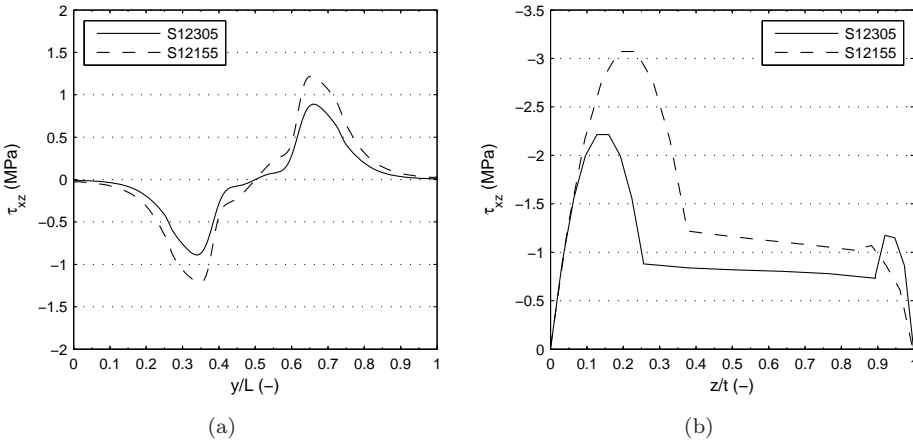
Figure 5.22: Shear stress distribution τ_{xz} under four-point bending tests at 10 kN load (a) along the normalized total length (L) at the interface between core and 12 mm steel face ($z = 12$ mm) and (b) along the normalized total thickness (t) at the cross-section between support and load points ($y/L = 0.35$).

Figure 5.23 shows the stress-cycle SN diagram of all fatigue tests performed on the sandwich steel plates reinforcement beams. The SN diagram was determined from the fatigue results presented in Figure 5.21. The fatigue life of each test n_f is plotted against the interface shear stress range $\Delta\tau_c$. This stress range is the shear stress τ_{xz} at z=12 mm (interface between the 12 mm steel plate and the core – see Figure 5.22(b)), multiplied by the amplitude load ($\Delta \cdot P = 0.9 \cdot P_{max}$) in each fatigue test.

There is a good agreement between the fatigue life of the two sandwich configurations, S12305 and S12155. The fatigue life of both configuration end at approximately the same area, depending on the load level, except for one specimen S12305 that failed too early at 10^5 cycles. This might be caused by less quality adherence between the core and the interface at this specific specimen. The fatigue life of the sandwich steel plates reinforcement might be influenced by the quality of the interface between the core and the steel faces. Increasing the core thickness does not have direct influence on the fatigue life of the sandwich beams since this is dominated by the interface life.
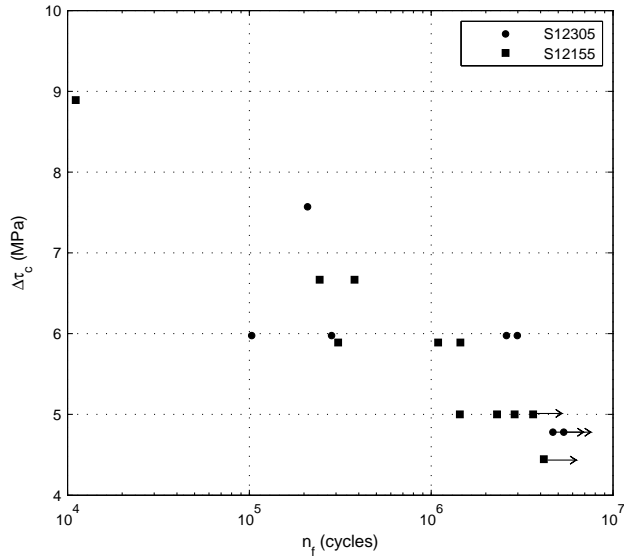
Figure 5.23: SN diagram for sandwich steel plates reinforcement.

Fatigue threshold

The fatigue threshold, $\Delta\tau^{th}$ is defined as the stress level below which no damage will initiate or if a damage has already formed, no further propagation will take place. Four specimens reached 3 to 5 million cycles without any damage. The shear stress at the interface at those tests is between 4 and 5 MPa. At 5 MPa, three other tests failed after 1.4 million cycles. This indicates that the fatigue threshold is lower than 5 MPa. Despite the small number of fatigue data without any damage, it can be said that the fatigue threshold of the interface shear stress range lays somewhere between 4 and 5 MPa. Moreover, the fatigue threshold is not significantly influenced by the core thickness.

5.7   Conclusions

An assessment of the behaviour of the sandwich steel plates reinforcement has been made through an experimental program and finite element analysis (FEA). The flexural static and fatigue behaviour of the reinforcement has been studied by four point bending tests.

The static behaviour of the sandwich steel plates reinforcement is significantly affected by temperatures between $-10\,°$C and $+50\,°$C. The increase of the temperature decreases the sandwich stiffness. When compared to RT, the bending stiffness of the sandwich beams increases on average 20% at -10 °C and decreases on average 50% at $+50\,°$C. At $+50\,°$C the viscoelastic behaviour present in the PU-core at high temperatures plays an important role in the flexural behaviour of the sandwich beams and decreases the sandwich stiffness. Experimental results reveal some agreement with FSDT only at $-10\,°$C and RT for long beams. Overall, FEA is in good agreement with the experimental results. The increase of the temperature decreases the sandwich strength and increases the deformation capacity before failure. At $-10\,°$C and RT the static failure mode of the sandwich beams starts by yielding of the steel plates and near yielding of the PU-core, subsequently by delamination of the faces-to-core interfaces and, finally by shear failure of the core. At $+50\,°$C the PU-core deformation increases considerably. The static failure mode at this temperature also starts by yielding of the steel plates and near yielding of the PU-core, but the final failure is the complete delamination of the interface between core and faces. Stresses on the steel plate can be reduced from 60% to 95% after the reinforcement. When using the 30 mm PU-core and 5 to 6 mm upper steel face, a maximum stress reduction of 80% to 95% is achieved.

The fatigue failure mode of the sandwich beams has three damage events. It starts by delamination of the interface between the core and the steel faces. In the second phase, the delamination crack progresses through the core thickness and in the last stage the crack crosses the complete core thickness (shear failure of the core). The stiffness degradation starts with the delamination event. The strain gauges applied to the steel faces are a good monitoring method for identifying the fatigue damage. There is significant stiffness degradation as the damage progresses.

Increasing the core thickness does not increase the fatigue life of the sandwich beams. The fatigue behaviour is determined by shear stress at the interface $\Delta\tau_c$. Considering this parameter, the fatigue threshold is approximately $\Delta\tau_c^{th} = 4$ MPa.

Part II

Behaviour of the reinforced orthotropic steel decks

Chapter 6

Numerical simulation of reinforced orthotropic steel decks

6.1 Introduction

This Chapter describes the finite element analysis (FEA) conducted to simulated the behaviour of the reinforced orthotropic bridge decks. Linear elastic simulations are performed to better understand the structural behaviour of the bridge deck-panels when subjected to wheel loads. The FEA are also needed to set up an experimental program for the full-scale tests (presented in Chapter 7), revealing the most relevant load cases and typical stress patterns due to wheel loading. Furthermore, after the appropriate validation with experimental data, it is an excellent tool to simulate different scenarios as an extension of the experimental program. The present chapter describes the main characteristics of the finite element model, such as geometry, materials, wheel loads and boundary conditions. After selecting the appropriate elements and mesh for the analysis, numerical results are presented as a preparation for the full-scale experimental program.

6.2 Model description

The numerical simulations are performed in order to predict the structural behaviour of an orthotropic bridge deck when subjected to wheel loading. The fatigue damage at the deck-plate-to-stiffener welds is caused by local transverse-bending moments due to individual wheel loads (Cullimore and Smith, 1981). Therefore, as the present study aims at extending the fatigue life of the mentioned welds, the structural behaviour is focused on local stress and strain fields due to individual wheel loads.

FEA are frequently used to characterize the stress fields on orthotropic bridge decks. The numerical results are needed to evaluate the fatigue behaviour of several deck details which are critical for the fatigue life of the bridge deck (Choi et al., 2008; Choi and Kim, 2008; Kiss and Dunai, 2002; Xiao et al., 2008; Ya and Yamada, 2008; Zhang et al., 2011).

In this study it is not only important to characterize the stresses at the steel deck details but also on the reinforcement structures. On the one hand it is important to quantify the stress reduction at the critical OBD details due to the reinforcement in order to predict the extended fatigue life of the welds. On the other hand, the stress fields at the adhesive layer of the bonded steel plates reinforcement and at the core of the sandwich steel plates reinforcement need to be characterized when applied to orthotropic bridge deck panels and subjected to wheel loads. Only then the real fatigue performance of the reinforcement can be evaluated. Therefore the numerical models should be accurate on both fronts, orthotropic steel deck and reinforcements. Three models were built, one for each deck status: unreinforced bridge deck, bonded steel plates reinforced bridge deck and sandwich steel plates reinforced bridge deck. The unreinforced bridge deck model is the reference model and allows the prediction of the stress reduction at the deck details.

The prediction of stress reduction and fatigue life of orthotropic bridge decks due to renovation systems using FEA is also popular in this research area. Walter et al. (2007) simulated the performance of a concrete overlay system at FarøBridge using FE models. FEA were also used by Pover (2002, 2004) to evaluate and compare performances of different renovation solutions. The behaviour of asphalt surfacing on orthotropic bridge decks was also studied by FEA calibrated with materials testing by Huurman et al. (2004), Medani et al. (2008) and Liu et al. (2008).

The fatigue damage at the deck-plate-to-stiffener welds has been observed both at the crossbeam location and at midspan between crossbeams. Both deck locations are therefore important to investigate and are included in this numerical study. The FE model consists of a 12 mm deck plate supported by three trapezoidal stiffeners and by two crossbeams 3000 mm apart. Several individual wheel loads were positioned at the crossbeam location and at midspan between crossbeams in order to select the most adequate load case for the experimental program, presented in Chapter 7.

The simulations were performed using the commercial FEA program ABAQUS. Abaqus/CAE software application was used for the pre- and post-processing. Abaqus/ Standard, a finite element analyser that employs implicit integration scheme, was used to run the analysis.

6.3   Calibration of the model

The calibration of the FE model was based on the experimental program carried out during this study. The actual mechanical properties of the materials are used in the FEA, based on the results from the materials testing presented in Chapters 4 and

5. The geometry, wheel loads and boundary conditions are simulating as much as possible the full-scale test set-up that will be presented in Chapter 7.

6.3.1   Geometry

The geometry of the model is directly related to the bridge deck-panels tested in the full-scale testing program (Chapter 7).

The deck plate is 12 mm thick, 5000 mm long and 2000 mm wide (deck plate area: 10 m^2). The deck plate is supported by three trapezoidal stiffeners and by two crossbeams 3000 mm apart. Figure 6.1 shows a longitudinal view of the deck-panels and Figure 6.2(c) a typical transverse cross-section at the crossbeam location. The trapezoidal stiffeners are 6 mm thick and 325 mm high. The crossbeam is an inverted T-section 10 mm thick and 788 mm high. The two reinforcement systems were applied in two identical deck panels. The bonded steel plates FE model consists of an orthotropic bridge deck reinforced with 6 mm thick second steel plate and 2 mm thick adhesive layer. The sandwich steel plates FE model consists of an orthotropic bridge deck reinforced with 5 mm thick second steel plate and 15 mm thick core thickness. In both cases, the second steel plate and the interface layer do not include any joint.

The nominal geometry of the several parts of the OBD were used in the model, namely, deck plate, second steel plate and interface layer thicknesses. The welds were not specifically modelled. They were simulated with the geometrical connection between the different elements (deck plate, stiffeners and crossbeams).

6.3.2   Materials

All materials were modelled as linear elastic. The mechanical properties of the steel are defined in accordance with EN1993-1-1 (2006), i.e., Young's modulus is 210 GPa and Poisson's ratio is 0.30. The mechanical properties of the epoxy adhesive in the bonded steel plates reinforcement are defined by the Young's modulus at room temperature obtained from the tensile material testing $E_a = 2929$ MPa and by the Poisson's ratio given by the manufacturer $\nu_a = 0.40$ (Chapter 4, pages 33 and 34). The mechanical properties of the polyurethane core in the sandwich steel plates reinforcement are defined by the Young's modulus at room temperature obtained from the tensile material testing $E_c = 721$ MPa and by the Poisson's ratio given by the manufacturer $\nu_c = 0.36$ (Chapter 5, pages 63 and 64).

6.3.3   Loads and Boundary conditions

The loads and boundary conditions of the model were defined in order to simulate the local transverse bending moments at the deck plate due to individual wheel loads. These local moments are the main cause for the fatigue problems, since they induce the high stress ranges at the deck-plate-to-stiffener weld which lead to fatigue

cracking. Taking this into account, the effect of the bending of the crossbeams has been neglected. The two crossbeam supporting the deck-panel are fully clamped to the floor. Although this is not exactly the real situation, the most important effect on this research is the bending of the deck-plate between stiffener webs, which is present in the model, and not the bending of the crossbeams between main girders.

The FEA simulates OBD when loaded with wheel prints at the crossbeam location and at midspan between crossbeams. The wheel prints dimensions are in accordance with the set of 'standard' lorries defined at the Fatigue Load Model 4 of EN1991-2 (2003). Two types of wheel prints were used, a single tyre wheel type C (super-single) and a double tyre wheel type B. The wheel type A was not used in this study since it causes similar stress levels as the wheel print type C (Jong et al., 2004). Table 6.1 presents the dimensions of each wheel print.

Figure 6.1 shows a schematic drawing of the longitudinal view of the global-model loaded at the crossbeams with the wheel type C and at midspan between crossbeams with the wheel type B. The load conditions presented are only one example, since both wheel prints were simulated at both locations, crossbeam and midspan. As shown in Figure 6.1 the global model has symmetric geometry and symmetric loading and therefore only half of the model was subjected to analysis with the corresponding symmetric boundary conditions. Two models were built according to the load location as shown in Figure 6.2. One model simulates loads at the crossbeam location (Crossbeam-FE model: Figures 6.2(a) and 6.2(c)) and the second model simulates loads at midspan location (Midspan-FE model: Figures 6.2(b) and 6.2(d)). The symmetry simplification saves enormous computational time and memory. This allows to implement a more refined mesh close to the critical areas of the FE model, such as loading areas and high stress gradient areas, which leads to more accurate results.

Figure 6.3 shows an overview of the three-dimensional finite element model.

Table 6.1: Dimensions of the wheel prints.
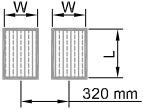
Wheel type	Geometry	w - width (mm)	L - length (mm)
B		220	320
C		270	320
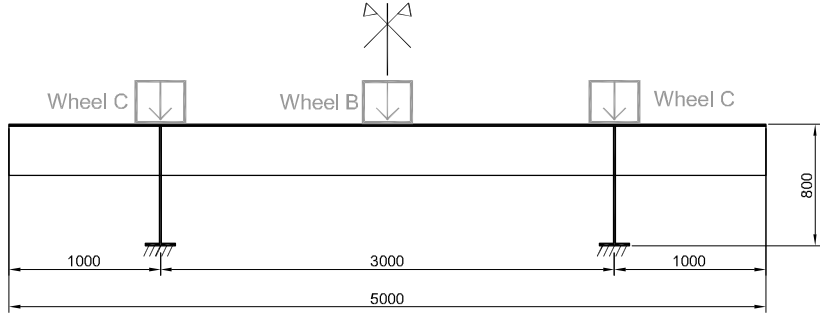
Figure 6.1: Longitudinal view of the global model loaded with the wheel type C at the crossbeams and the wheel type B at midspan between crossbeams.
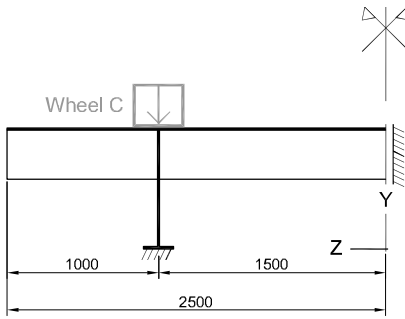
(a) Crossbeam-FE model: longitudinal view
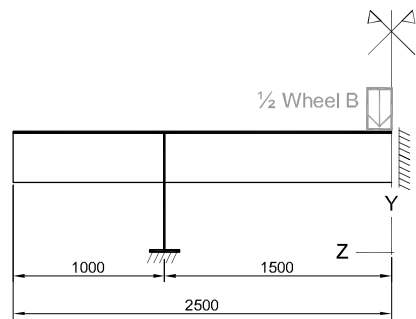
(b) Midspan-FE model: longitudinal view
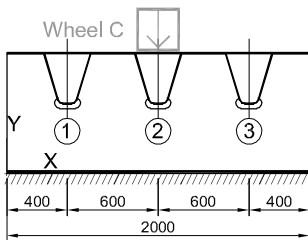
(c) Crossbeam-FE model: transverse view
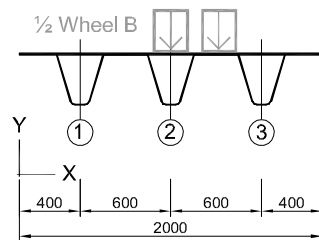
(d) Midspan-FE model: transverse view

Figure 6.2: Symmetry simplification for wheel loads at the crossbeam (a) and (c) and at midspan (b) and (d).
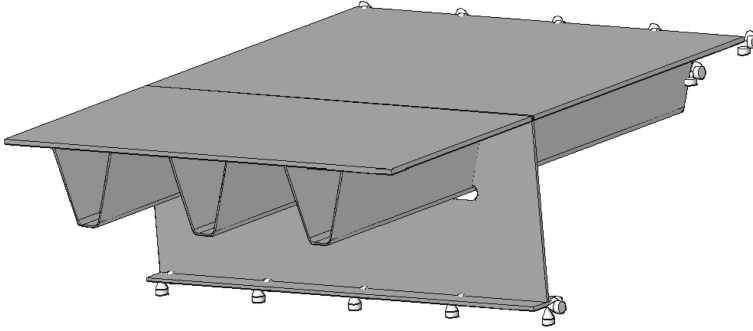
Figure 6.3: Three-dimensional finite element model overview.

6.4   Mesh and Element type

The model of the reinforced orthotropic bridge decks were built using three-dimensional elements. All the parts of the structure, crossbeams, troughs, deck plate and reinforcement, were modelled using continuum 20-nodes brick (solid) elements, quadratic (second-order) with reduced integration. These elements are available in the ABAQUS library as C3D20R (Continuum 3-Dimensional 20-nodes Reduced integration elements). Quadratic elements were used in order to avoid problems of shear locking. Shear locking affects the performance of linear elements subjected to bending loads. In this analysis the elements are subjected to bending and shear loads. The quadratic reduced-integration elements are not susceptible to locking, even when subjected to complicated states of stress (ABAQUS, 2008). Quadratic fully integrated elements were not used in this analysis since they are only needed when a very high stress gradient exists in coarse meshes.

As mentioned in the previous section, two models were built, one for loads at midspan and another for loads at the crossbeams. In each of these models, the three deck states were modelled: unreinforced, bonded steel plates reinforced and sandwich steel plates reinforced. Therefore six models were built in total.

An overview of the meshes used in this analysis is shown in Figure 6.4 for the Midspan-FE model and in Figure 6.5 for the Crossbeam-FE model. The meshes were refined close to the loading areas and where high stress levels were expected, such as close to the crossbeams and at the deck-plate-to-stiffener weld. Coarser meshes were used where the stress level were low or irrelevant for the analysis. The maximum aspect ratio of an element is 5, in order to avoid artificial stiffening, except in the areas of coarser meshes where the stress level is low and far from the loading area.
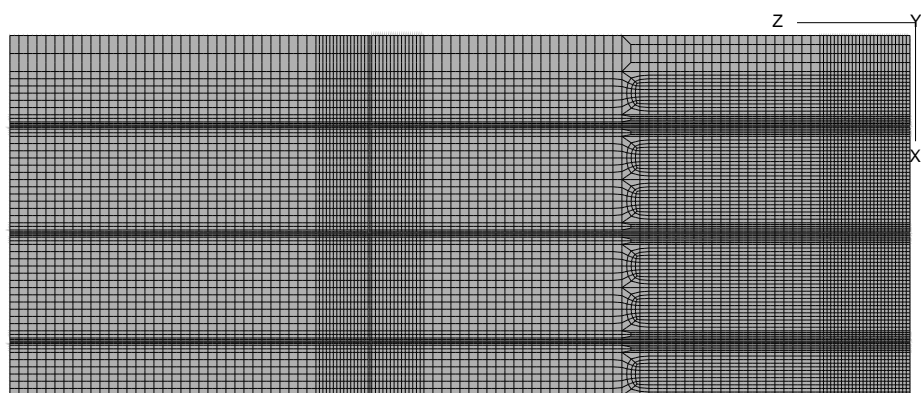
(a) half of the deck plate (top view)
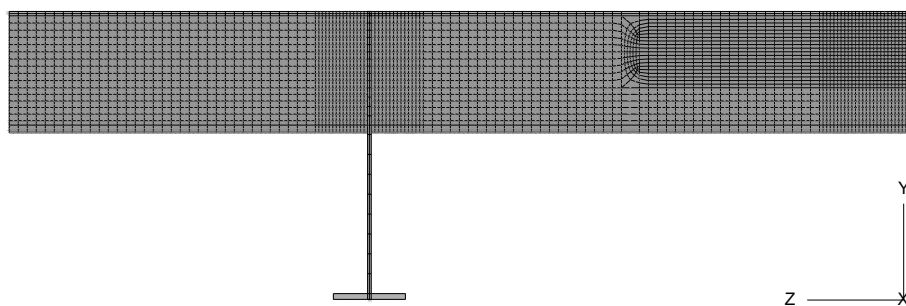
(b) trough (longitudinal view)
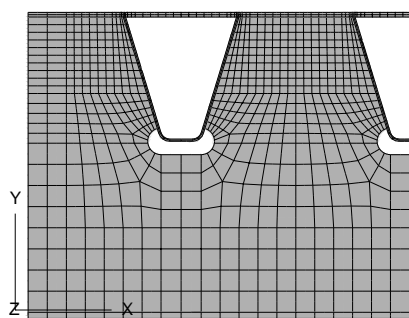
(c) half of the crossbeam web (z=1500 mm; transverse view)
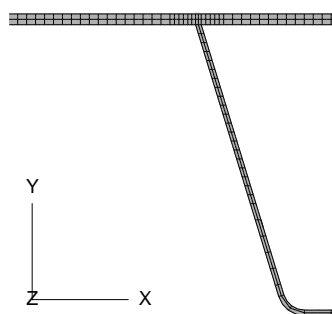
(d) weld detail at midspan (z=0 mm)

Figure 6.4: Mesh of the Midspan-FE model.

(a) half of the deck plate (top view)

(b) trough (longitudinal view)
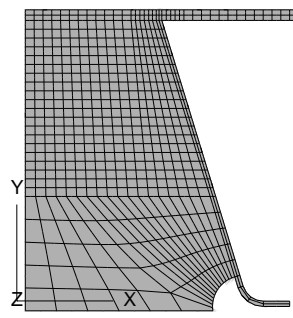
(c) half of the crossbeam web (z=1500 mm; (d) weld detail at the crossbeam (z=1500 transverse view)   mm)

Figure 6.5: Mesh of the Crossbeam-FE model.

Figure 6.6 shows the mesh details along the unreinforced and reinforced deck plate thickness. The existing deck plate was modelled with two elements per thickness – Figure 6.6(a). The bonded steel plate reinforcement was modelled with one element per epoxy layer thickness and two elements per second steel plate thickness – Figure 6.6(b). The sandwich steel plate reinforcement was modelled with four elements per core thickness and two elements per second steel plate thickness – Figure 6.6(c). The troughs and the crossbeams web were modelled with two elements per thickness. The FE models of the reinforced decks have between 720000 and 1000000 nodes and between 150000 and 215000 elements. The mesh of the finite element model satisfies a mesh convergency study presented in Appendix A which proves the mesh independency of the results.

(a) unreinforced deck   (b) bonded reinforced deck   (c) sandwich reinforced deck
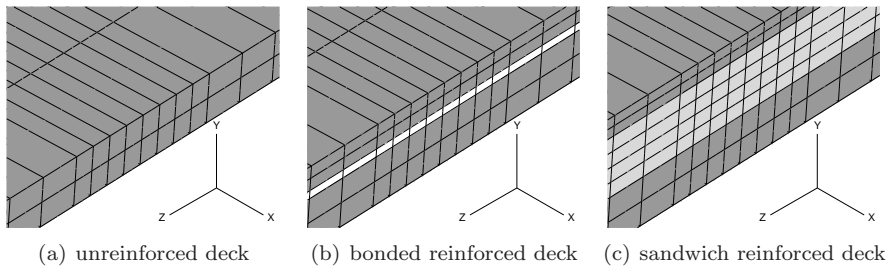
Figure 6.6: Mesh details along the deck plate thickness (Y-axis).

6.5 Numerical results

As an example, the results of the unreinforced steel deck FE model are presented in this section (steel plate 12 mm thick without any reinforcement). These results were used for setting up the full-scale experimental program, selecting the most severe load cases and preparing an instrumentation plan. These numerical results are predictions of the actual behaviour of the structure and further in Chapter 7, they will be validated using experimental data.

Figures 6.7 and 6.8 show the load cases simulated in the Crossbeam-FE model and in the Midspan-FE model, respectively. In the Crossbeam-FE model, the load is aligned with the crossbeam, Figure 6.7(a), and in the Midspan-FE model the load is at midspan between crossbeams, Figure 6.8(a). In both models, two load cases were simulated: in the first the wheel type C was aligned with the middle trough and in the second the wheel type B was centred at the deck-plate-to-stiffener weld (see Figures 6.7(b) and 6.8(b)).

(a) longitudinal view　　　　　　　　　　　(b) transverse view
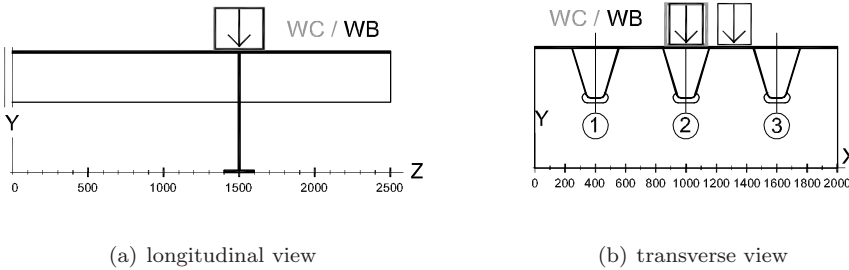
Figure 6.7: Crossbeam load cases: wheel type C (WC) and wheel type B (WB).

(a) longitudinal view　　　　　　　　　　　(b) transverse view
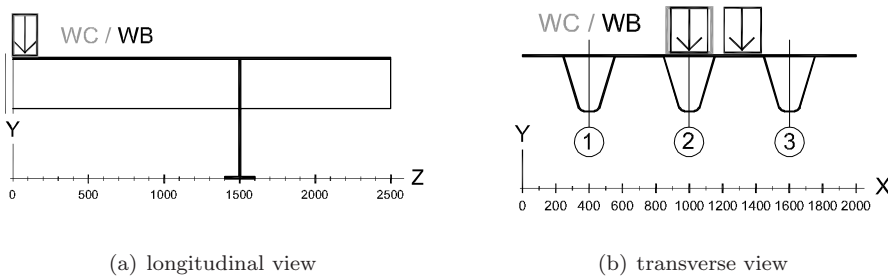
Figure 6.8: Midspan load cases: wheel type C (WC) and wheel type B (WB).

Figure 6.9 shows the stresses and correspondent strains at the bottom side of the unreinforced deck plate due to 100 kN wheel loads applied at the crossbeam location (Crossbeam-FE model).

Figure 6.9(a) shows the results along the crossbeam cross-section for the wheel type C and the wheel type B load cases. Both transverse and longitudinal stresses are shown for the load case wheel type C, σ_{xx} and σ_{zz}, respectively. It can be observed that wheel loads cause higher transverse stresses than longitudinal stresses and those are the main source for the fatigue cracking at the deck-plate-to-stiffener weld.

Comparing σ_{xx} due to the wheel type C and due to the wheel type B, the most severe load case is clearly the wheel type C. The stresses at the deck-plate-to-stiffener welds are considerably higher for the wheel type C than for the wheel type B. Also the stresses at the deck plate between the welds (x = 1000 mm) are higher for the wheel type C than for the wheel type B. Wheel loads at the crossbeam location cause mainly stresses on the loaded area close to the middle trough. Immediately outside the loaded area, the stresses are almost zero. The stress concentration is extremely

high close to the deck-plate-to-stiffener welds. The high stress concentration is caused by the singularity of the crossbeam web. The peak stresses occur at the weld root. Actually, the stresses at the peaks are unrealistic because at more than 400 MPa, the steel already yielded. The stresses that should be taken into account at the welds are the ones 10 to 15 mm away from the peak.

Figure 6.9(b) shows the transverse stresses along the length of the deck-panel for the wheel type C (worse load case). The results along the deck-plate-to-stiffener weld-root (point P2) show a very high stress concentration when the weld crosses the crossbeam web (known as 'hot-spot' point). This high stress concentration is the main cause for the extremely short fatigue life of the welds at this location. The stresses are significantly lower between stiffener webs (point P1) than close to the welds.

Figure 6.10 shows the stresses and correspondent strains when the wheel loads are at midspan between crossbeam (Midspan-FE model).

Figure 6.10(a) shows the results along the midspan cross-section for the wheel type C and for the wheel type B load cases (100 kN wheel load). Once more, it can be observed that wheel loads cause higher transverse stresses than longitudinal stresses and those are the main source for the fatigue cracking at the deck-plate-to-stiffener weld. However at midspan between crossbeams, the transverse stresses at the deck-plate-to-stiffener welds are higher for wheel type B than for wheel type C. Moreover, the stress concentration close to the welds is lower than at the crossbeam location.

Figure 6.10(b) shows the transverse stresses along the length of the deck-panel for the wheel type B, as this is the worst load case for the welds. In this case, with the wheel load at midspan, the stresses at the welds show lower stress gradients than at the crossbeam location.
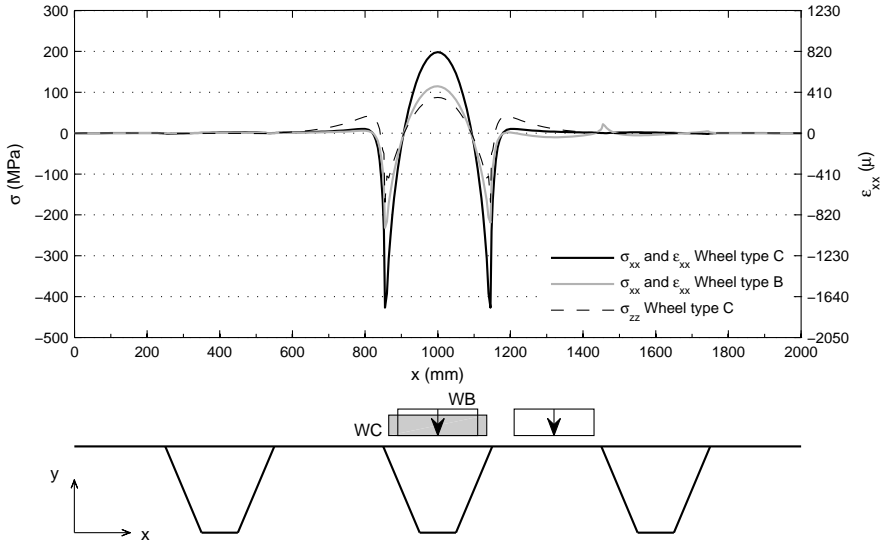
(a) along the models width at the crossbeam cross-section – x-axis
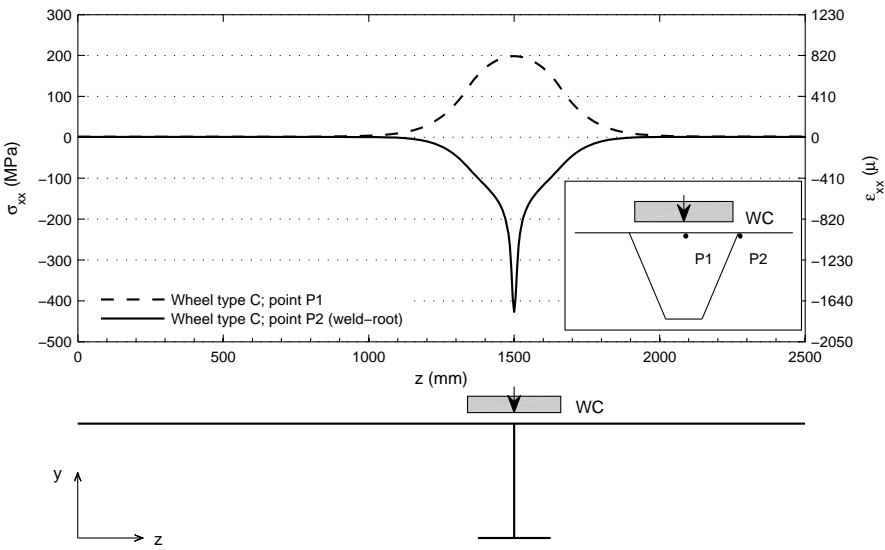
(b) along the model length – z-axis

Figure 6.9: Stresses at the bottom side of the unreinforced deck plate due to wheel loads of 100 kN applied at the crossbeam location, Crossbeam-FE model (WC – wheel type C and WB – wheel type B).
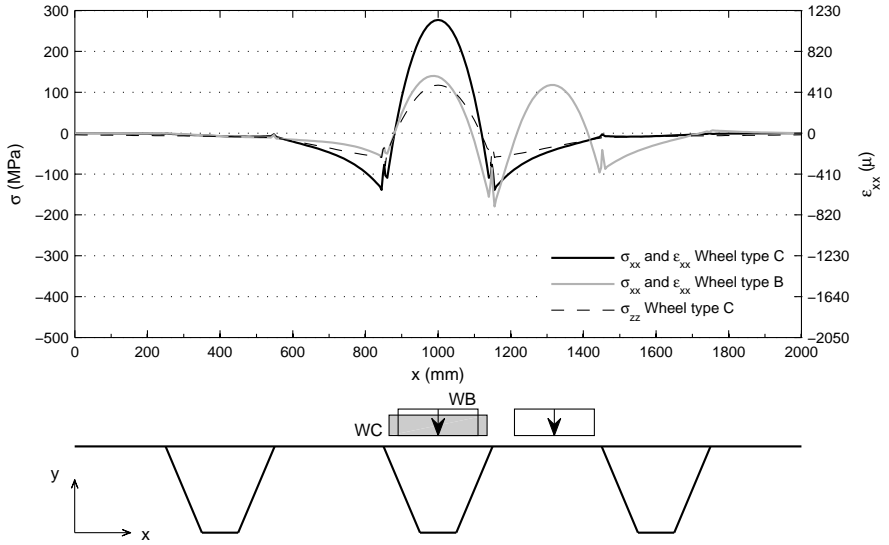
(a) along the model width at midspan cross-section
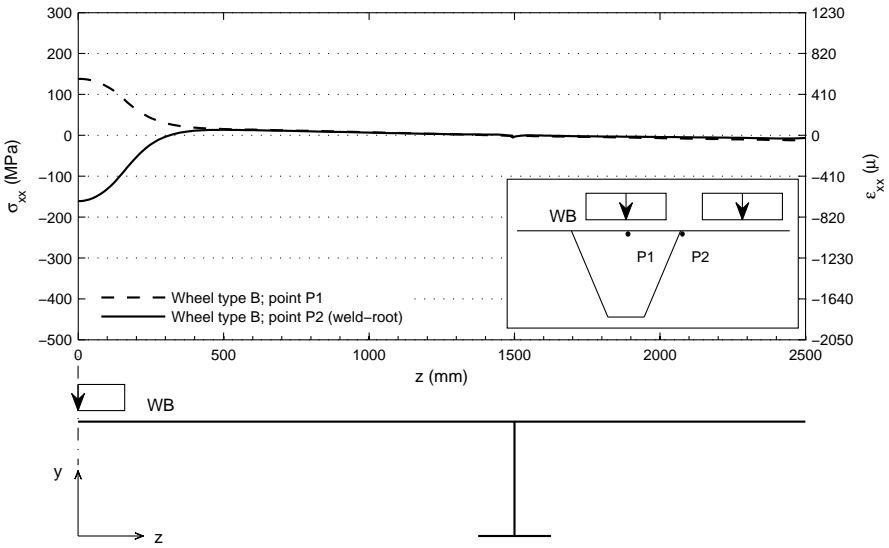
(b) along the model length (axis of symmetry at z = 0 mm)

Figure 6.10: Stresses at the bottom side of the unreinforced deck plate due to wheel loads of 100 kN applied at midspan between crossbeams, Midspan-FE model (WC – wheel type C and WB – wheel type B).

Chapter 7

Full-scale behaviour of reinforced orthotropic steel decks

7.1 Introduction

In the present chapter the full-scale behaviour of the reinforced orthotropic steel decks is studied. The first part of Chapter (Section 7.2) describes the actual application of the bonded steel plates and the sandwich steel plates reinforcements on two orthotropic deck-panels with 10 m^2. Section 7.3 describes the full-scale static tests carried out on these reinforced decks. The specimens were subjected to individual wheel loads. The goal is to determine the effect of the reinforcement on the full-scale deck-panels. The experimental results are presented and compared with the numerical simulations of the reinforced OBD presented in the Chapter 6. The numerical results are validated using the experimental data. Section 7.4 presents the results from the full-scale fatigue tests carried out in the same deck specimens. The aim is to determine the fatigue behaviour of the reinforcement when subjected to wheel loads. In both Sections 7.3 and 7.4, the reinforcements' behaviour is compared with the static and fatigue behaviour of the reinforced beams studied in Chapters 4 and 5. Finally, Section 7.5 presents the main findings of a parametric study which used FEA to predict the behaviour of different reinforcement scenarios.

7.2 Bridge deck specimens

Two orthotropic deck-panels were built in order to perform the full-scale tests. The two decks have exactly the same geometry and one was reinforced using the bonded steel plates technique and the second one using the sandwich steel plates technique.

7.2.1 Geometry

Figure 7.1 shows the geometry of the orthotropic steel deck specimens. The deck panels are 5000 mm long and 2000 mm wide. The deck plate is 12 mm thick and it is supported in the longitudinal direction by three trapezoidal stiffeners and in the transverse direction by two crossbeams 3000 mm apart. In the actual situation, the traffic is running in the longitudinal direction on the top of the deck plate. All the elements of the OBD were manually welded together in a common steel workshop. The orthotropic deck is made of steel grade S355 (EN1993-1-1, 2006).
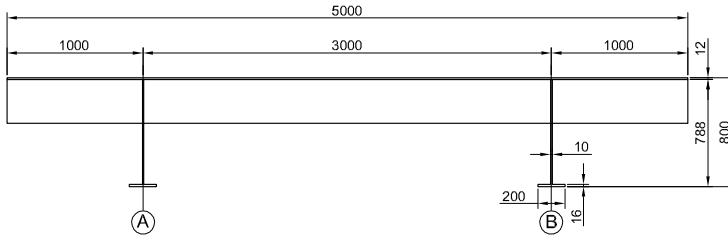
(a) longitudinal view
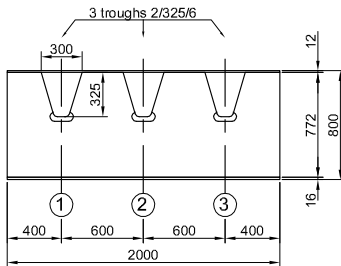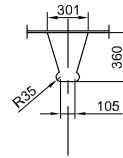
(b) transverse view   (c) hole detail on crossbeam

Figure 7.1: Geometry of the orthotropic steel deck specimens.

7.2.2 Reinforcement

The application of the bonded and sandwich steel plates reinforcements followed exactly the same procedure as described previously in Chapter 4 (page 31) and in Chapter 5 (page 61), respectively. The bonded steel plates reinforcement was applied by Lightweight Structures B.V. and the sandwich steel plates reinforcement by Intelligent Engineering (IE) – Sandwich Plates System SPS. Tables 7.1 and 7.2 describe the application procedure followed for the bonded steel plates and sandwich steel plates reinforcements, respectively.

From the several reinforcement geometries studied in Part I, the lightest solutions were chosen for the full-scale application. Figure 7.2 shows a detail of the solutions applied on the deck specimens. After validating the numerical simulations presented in Chapter 6 with the experimental data, predictions can be made for different solutions.

In the bonded steel plates, the 12 mm thick deck plate was reinforced with a 6 mm thick second steel plate and a 2 mm thick adhesive layer (nominal thickness). This reinforcement is referred to as 'B1226' (Bonded, 12 mm existing steel plate, 2 mm adhesive and 6 mm second steel plate). The second steel plate is made of steel grade S355 (EN1993-1-1, 2006). The adhesive material is exactly the same epoxy as presented in Chapter 4 - Epikote resin EPR 04908 with hardener Epikure curing agent EPH 04908. The mechanical properties determined from material testing and obtained from the manufacturer data are presented in Tables 4.2 and 4.3, pages 33 and 34.

In the sandwich steel plates, the 12 mm thick deck plate was reinforced with a 5 mm thick second steel plate and a 15 mm thick polyurethane core. This reinforcement is referred to as 'S12155' (Sandwich, 12 mm existing deck plate, 15 mm core and 5 mm second steel plate). The second steel plate is also made of steel grade S355 (EN1993-1-1, 2006). The core material is exactly the same polyurethane as presented in Chapter 5. The mechanical properties determined from material testing and obtained from the manufacturer data are presented in Tables 5.2 and 5.3, pages 63 and 64.

The end details of the reinforcements were not taken into account on the behaviour of the deck-panels. Wheel loads are the main cause for the fatigue problems and, as it was presented before in Chapter 6, they cause very local stresses on the deck. On the area just outside the wheel load (100 mm frame-thickness, approximately), the stresses decrease to almost zero. Therefore, the influence of the end details such as the perimeter bars in the sandwich steel plates reinforcement that are positioned at least 200 mm from the wheel loads, can be neglected. In the actual situation these end details are positioned far away from the loaded areas of the deck (traffic lines).
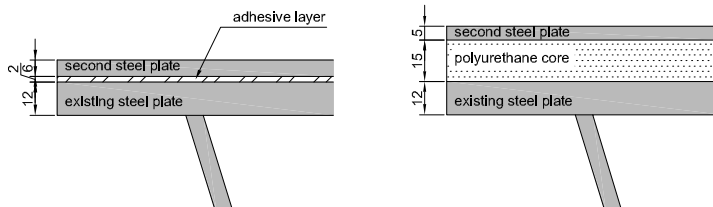
(a) bonded steel plates reinforcement   (b) sandwich steel plates reinforcement

Figure 7.2: Reinforcement systems (dimensions in mm).

Table 7.1: Application procedure of the bonded steel plates reinforcement on the deck specimen.

1	steel surfaces treatment: grit blast and clean the steel surfaces to be free from rust, grease and dust (Sa 2 1/2)	
2	primer application on the cleaned steel surfaces	
3	glue steel spacers on the top of the existing deck plate with the adhesive thickness (nominally 2 mm); the spacers grid is chosen in order to avoid the weld location on the deck (high stress levels), such as crossbeams and troughs webs	
4	place the second steel plate carefully on the top of the existing deck plate, above the steel spacers	
5	prepare the cavity between the steel plates to create vacuum	
6	vacuum inject the adhesive into the cavity	
7	cure during 16 hours between $40\,^\circ$C and $50\,^\circ$C (the deck is covered with a thermal insulation blanket and heated with electrical heaters). The procedure is the same in the real structure.	
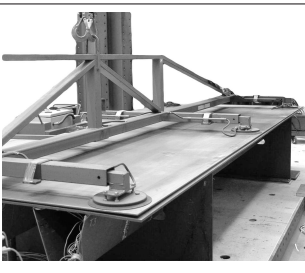
Table 7.2: Application procedure of the sandwich steel plates reinforcement on the deck specimen.
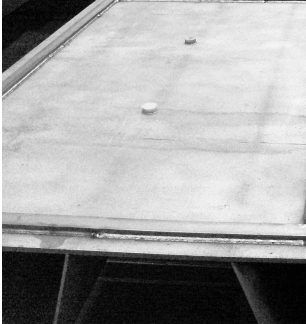
1	steel surfaces treatment: grit blast and clean the steel surfaces to be free from rust, grease and dust (Sa 2 1/2)	
2	weld steel bars on the perimeter of the existing deck plate (the bar thickness is the nominal core thickness)	
3	glue PU spacers with the core thickness on the existing deck plate	
4	place the second steel plate on the top of the perimeter bars and fillet weld through the perimeter forming a cavity	
5	inject the liquid PU into the cavity through small holes previously drilled on the second steel plate	
6	cure at room temperature during 48 h	
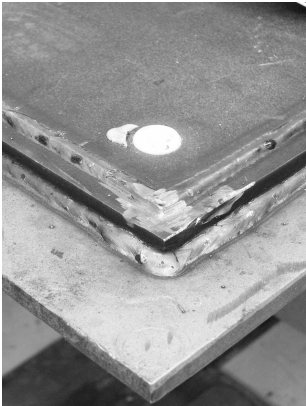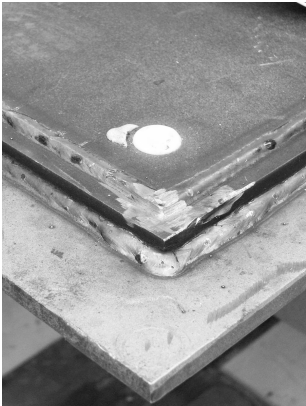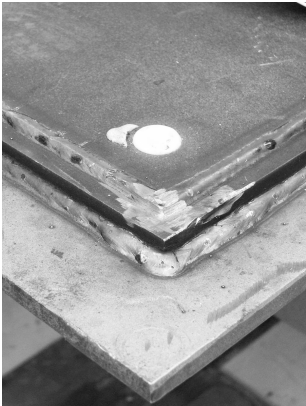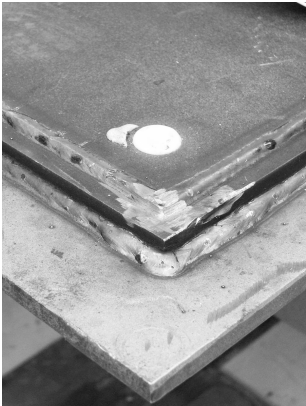
7.2.3 Instrumentation

The instrumentation plan consisted mainly of applying strain gauges to the steel deck. The strain gauges were used to monitor the behaviour of the deck-panel during testing. This is specially important during fatigue testing, in which changes of the measured strains can indicate fatigue damage of the reinforced deck. Moreover, the measured strains were used to validate the FEA described in Chapter 6. At reference points of the deck-panels, the strains measured during static tests were compared with the strains predicted by the FEA.

The strain gauges were applied to three cross-sections of the deck-panel: crossbeam A, crossbeam B and midspan between both crossbeams (see Figure 7.1). These sections represent the two typical cross-section of an orthotropic deck and therefore they were selected to conducted static and fatigue tests.

Figures 7.3 and 7.5 show the strain gauges applied at midspan and at crossbeam cross-sections, respectively. All strain gauges measured transverse strains except strain gauges 26, 27 and 28 at midspan cross-section (Figure 7.3(a)) which measured longitudinal strains at the bottom of the trough. Figure 7.4 shows the position of the strain gauges close to the deck-plate-to-stiffener welds.

(a) Midspan cross-section
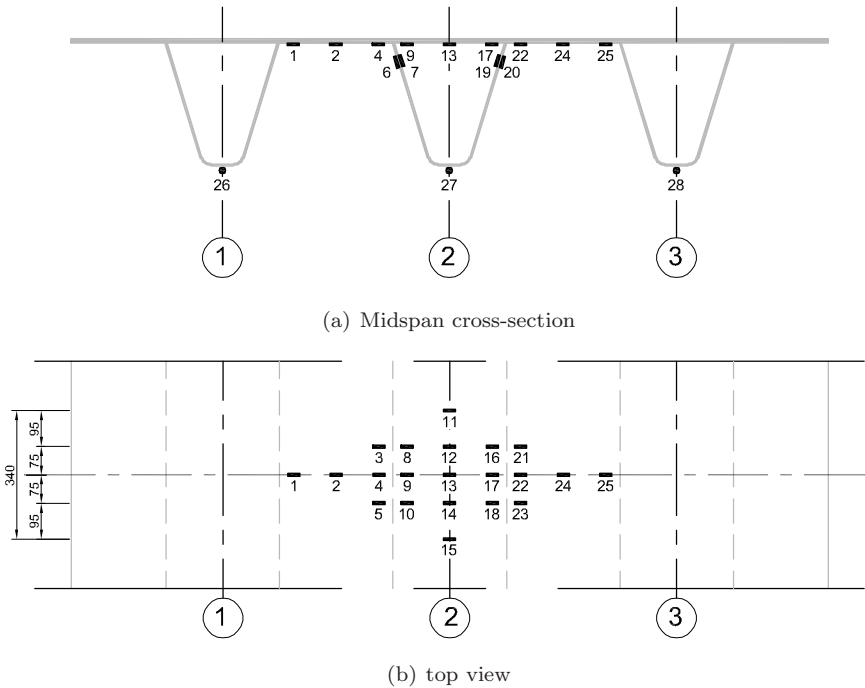
(b) top view

Figure 7.3: Strain gauges at midspan between both crossbeams.
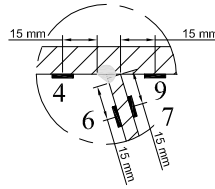
Figure 7.4: Strain gauges close to the deck-plate-to-stiffener weld at midspan between cross-beams.
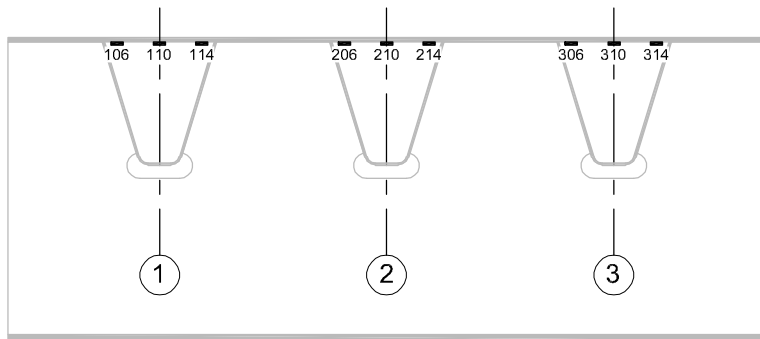
(a) crossbeam cross-section
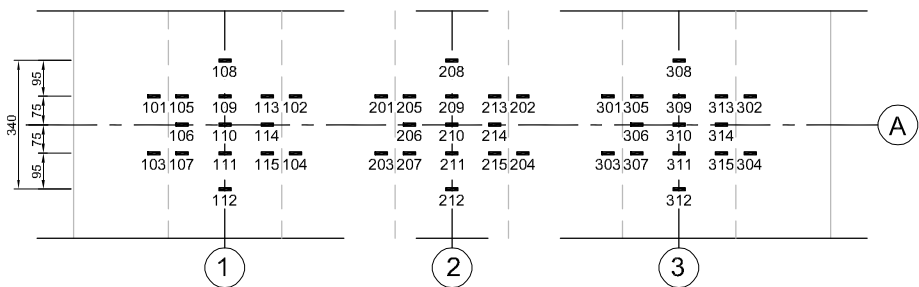
(b) top view

Figure 7.5: Strain gauges at crossbeam A.

The instrumentation plan was exactly the same for both reinforced deck specimens: sandwich and bonded steel plates.

The position and distribution of the strain gauges were chosen in accordance with the stress patterns predicted by the FEA due to individual wheel loads (see Figures 6.9 and 6.10 in Chapter 6, pages 106 and 107). The strain gauges should cover the area with the most significant stress values.

Considering the midspan cross-section when loaded at the middle trough, the area with more significant stresses is approximately 900 mm wide in the transverse direction and 400 mm long in the longitudinal direction (see Figures 6.10 on page 107). Figure 7.3 shows the strain gauges distributed in an area 850 mm wide and 340 mm long, in the transverse and longitudinal direction, respectively. The strain gauges at this location are numbered from 1 to 28.

Considering the crossbeam cross-sections when loaded at the middle trough, the area with more significant stresses is approximately 400 mm wide in the transverse direction and 400 mm long in the longitudinal direction (see Figures 6.9 on page 106). The effect of the wheel load at the adjacent troughs (trough 1 and 3) is negligible. Only a very limited area around the loaded trough has significant stress values. Therefore, several tests were conducted at each crossbeam section. More specifically, three tests, one per trough, were performed on each crossbeam cross-section, since there is no interaction between the stresses.

As shown in Figure 7.5, the strain gauges were distributed along an area 400 mm wide and 340 mm long centred in each trough, on the transverse and longitudinal direction, respectively.

In each deck specimen a total of six tests were performed at the crossbeam locations: three troughs times two crossbeams. The strain gauges at these locations are numbered from 100 to 615 (the first digit indicates the trough-to-crossbeam location, 1 to 6; the last two digits indicate the strain gauge location at the deck).

In order to apply the strain gauges inside the troughs, such as numbers 8 to 18 at midspan (Figure 7.3(b)) and 105 to 115 at the crossbeam (Figure 7.5(b)), part of the troughs was cut out. After applying the strain gauges the cut-outs were welded back to the deck. Figure 7.6 shows pictures of the troughs cut-outs.

It was decided not to instrument the interface layer of the reinforcement. Both adhesive and core are in a closed cavity and therefore of difficult access after manufacturing. The possibility of including any instrumentation inside the layers installed during manufacture, could create initial imperfections which would lead to stress concentrations. These undesirable stresses could influence the test results. The strain/stress field at the interface layers of the reinforcements are determined by the FEA after it has been validated with experimental results.

The integrity of the bonded steel plates reinforcement was monitored using an ultrasonic Non Destructive Testing A-scan. The scan was performed before testing, during fatigue testing at specific cycles-intervals and after testing. The aim is to detect any initial flaws and imperfections before testing and monitored them during fatigue testing. NDT was already used before in the beams specimens presented in

(a) trough cut-outs close to the cross-beam

(b) trough cut-out at midspan
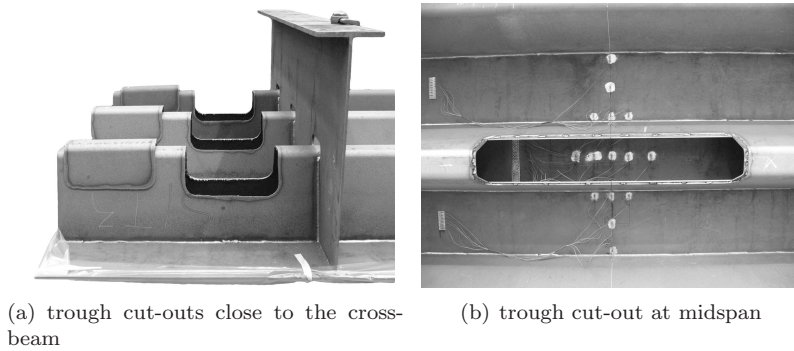
Figure 7.6: Troughs cut-outs for instrumentation.

Chapter 4. For the full-scale application, the pulse-echo technique was used since the access was limited to one single side of the reinforcement (the top side of the second steel plate). The pulse echo technique uses a pulsed ultrasonic beam that is reflected back to the original transducer by a surface or flaw at the tested object (Grandt, 2004). The frequency used was 2.25 MHz. The frequency is lower than the one used in the beam specimens, which increases the penetration length, but decreases the testing resolution (minimum flaw area detected). NDT was performed at the tested areas, at each trough-to-crossbeam joint and at midspan between crossbeams. Areas of approximately 500 mm by 500 mm were monitored with a minimum grid of 50 mm by 50 mm. Figure 7.7 shows a picture of the A-scan set-up on the top surface of the deck.

Figure 7.7: Non Destructive Testing A-scan.

7.3 Static behaviour

This part of the study describes the full-scale static tests performed on the bridge deck specimens. The experimental results are used to validate the numerical analysis and to determine the stress reduction factor after the reinforcement.

7.3.1 Experimental procedure

The static tests were performed at the crossbeam location and midspan between crossbeams. The specimens were loaded with wheel prints type B and type C. The wheel prints dimensions are shown in Table 7.3. They are in accordance with the wheel prints defined at the fatigue load models of EN1991-2 (2003).

Table 7.3: Dimensions of the wheel prints.
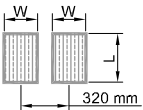
Wheel type	Geometry	w - width (mm)	L - length (mm)
B		220	320
C		270	320

At the crossbeam, static tests were performed at each trough-to-crossbeam joint loaded by one wheel type C aligned with the trough. The numerical results of the Crossbeam-FE model presented in Chapter 6 showed that the wheel type C is the worst load case at the crossbeam location (see Figure 6.9(a), page 106). Therefore, the wheel type B load case was excluded from the static tests at the crossbeam. The six trough-to-crossbeam joints, present at each deck specimen, were tested one by one. Figure 7.8 shows one example of a static test performed at trough 2 to crossbeam A joint.

At midspan between crossbeams, two static tests were performed, one using wheel type C aligned with trough 2 and a second one using wheel type B (double-tyre) with one of the tyres aligned with trough 2. The numerical results of the Midspan-FE model presented in Chapter 6 showed that the stresses at the deck-plate-to-stiffener weld are higher for the wheel type B than for the wheel type C load cases. However, the stresses between stiffener webs are higher for the wheel type C than for the wheel type B (see Figure 6.10(a), page 107). Therefore, it was decided to perform static test using both wheel prints. Figure 7.9 shows the static test performed using wheel type B.
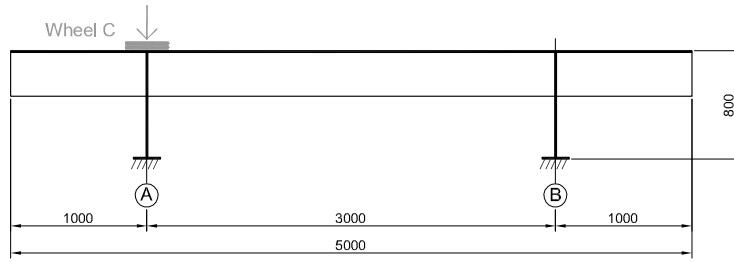
(a) longitudinal view
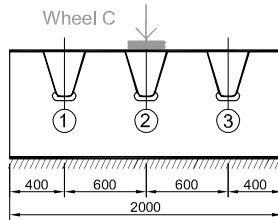
(b) crossbeam A cross-section
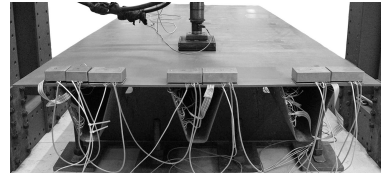
(c) photograph of the test

Figure 7.8: Static tests at crossbeam location (wheel type C).

In the experimental program, two bridge deck specimens were tested. Specimen 1 is the bonded steel plates reinforced bridge deck B1226 and specimen 2 is the sandwich steel plates reinforced bridge deck S12155. Static tests were performed on specimen 1 before and after being reinforced. The static tests on the unreinforced deck are the reference tests. Specimen 2 was tested only after being reinforced with the sandwich steel plates. The maximum wheel load on the static tests was 50 kN for the unreinforced deck and 100 kN for the reinforced decks. The load level was lower at the unreinforced deck in order to prevent any damage before applying the reinforcement.

The deck specimens were clamped to the ground at the bottom flange of the two crossbeams. The load was applied by a metallic frame which held the hydraulic jack. A photo overview of the test set-up is given in Figure 7.10(a).

Two test-rigs were used, one for the bonded deck specimen and another for the sandwich deck specimen. The tests were load controlled and the testing speed was 0.3 kN/s. The load was applied on the deck by the following sequence: hydraulic jack, load cell, a rectangular-shaped steel plate 30 mm thick and three layers of 10 mm thick rubber with the same rectangular shape. The rectangular area is the size of the wheel prints. A photo of the wheel print is given in Figure 7.10(b).
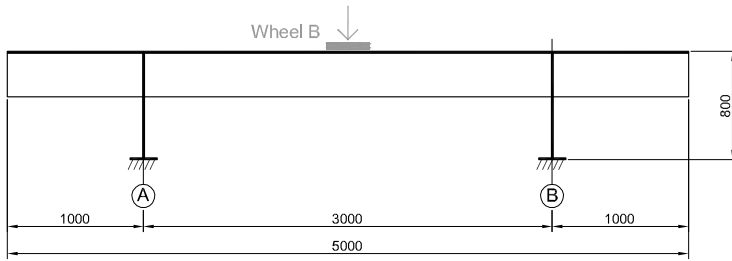
(a) longitudinal view
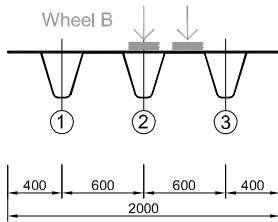
(b) midspan cross-section
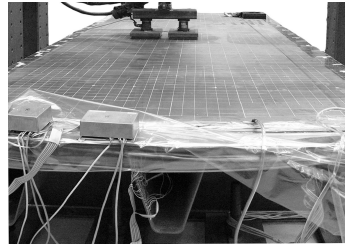
(c) photograph of the test

Figure 7.9: Static tests at midspan between crossbeams (wheel type B).

(a) overview

(b) wheel print detail

Figure 7.10: Photos of the test set-up

The rubber layers are used to evenly distribute the load over the wheel print. During static tests, pressure sensitive papers were used between the last rubber layer and the deck-plate. The goal was to have a qualitative indication of the pressure distribution over the wheel print during the static tests. The pressure sensitive paper used was 'Pressure measurement film PRESCALE' from Fujifilm.

The pressure sensitive paper results showed several load distributions along the wheel prints. For some tests the distribution is rather uniform over the wheel print, for others the load pressure was higher at the centre of the wheel print than at the edges. After a qualitative evaluation of the available pressure sensitive papers at each static test, several pressure distributions were defined. These pressure distributions were used in the FEA for the pressure load of the wheel prints. The results from the pressure sensitive papers and corresponding load distribution used in FEA are presented in Appendix B.

7.3.2   Experimental results and numerical validation

The static test results are presented for the unreinforced deck, for the bonded steel plates reinforced deck and for the sandwich steel plates reinforced deck. The experimental results are strains recorded by the strain gauges at the maximum static load: 50 kN for the unreinforced deck and 100 kN for the reinforced decks. The experimental values are compared with the corresponding strain distribution obtained from the FEA, presented in Chapter 6.

For the static tests at the crossbeams, the results at all six trough-to-crossbeam joints are very consistent. Therefore, as an example, the results for the wheel type C aligned with the middle trough are presented. The results for the wheel loads aligned with trough 1 and 3 are presented in Appendix B, for both bonded and sandwich steel plates reinforced decks.

For the static tests at midspan between crossbeams, both the results for the wheel type C and the wheel type B load cases are presented.

The numerical simulations are evaluated by the average ratio between the numerical values (n) predicted for the strain gauges and the experimental values (e) recorded at the strain gauges during testing, n/e.

Unreinforced steel deck

Figure 7.11 shows the results of the unreinforced steel deck when it is loaded at the crossbeam. The wheel load is 50 kN and it is aligned with the middle trough. The wheel print is type C.

The graph plots the transverse strain distribution at the bottom side of the steel deck plate (ε_{xx}) along the width of the specimen (x-axis). The experimental values are the strains recorded by the strain gauges during the static test (Exp). The numerical distribution is given by the Crossbeam-FE model of the unreinforced deck described in Chapter 6 (FEA).

Figure 7.11(a) shows the results at the crossbeam cross-section. The strains given by the strain gauges close to the deck-plate-to-stiffener welds are very high, around -600μ. The results 75 mm from the crossbeam cross-section, given in Figure 7.11(b), show a significant decrease of strains close to these welds. The strain values close to troughs 1 and 3 are almost zero. The numerical prediction fits well with the experimental values ($n/e = 1.01 \pm 0.09$).

Figure 7.12(a) shows the results of the unreinforced deck when it is loaded at midspan between crossbeams. Figure 7.12(a) shows the results using a wheel print type C and Figure 7.12(b) using a wheel print type B. The total wheel load for both cases is 50 kN.

For both wheel prints, the strains recorded by the strain gauges close to the deck-plate-to-stiffener welds (approx. 200 μ to 300 μ) are significantly lower than the same strain gauges at the crossbeam cross-section. The strain values close to these welds are slightly higher for the wheel type B than for the wheel type C. The strain values between trough webs are lower for the wheel type B than for the wheel type C ($x \approx 1000\,mm$).

For both wheel prints, the strain distribution given by the FEA fits well with the experimental values ($n/e = 0.95 \pm 0.09$ and $n/e = 0.89 \pm 0.08$, wheel type C and B, respectively).
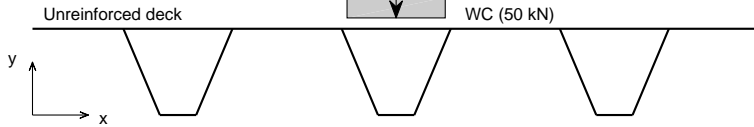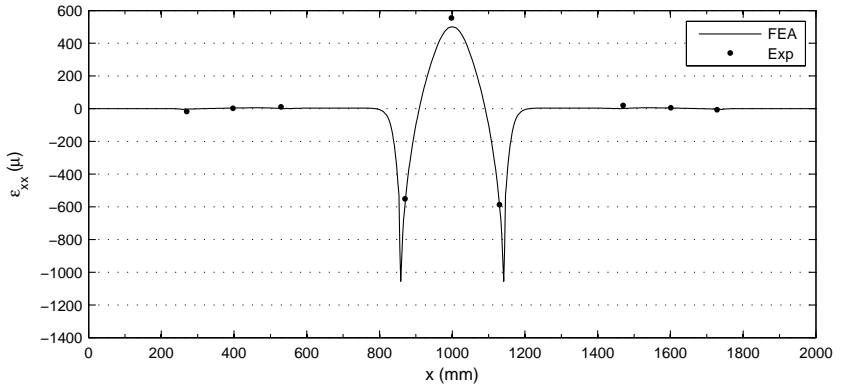
(a) crossbeam cross-section
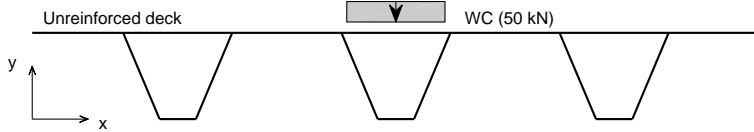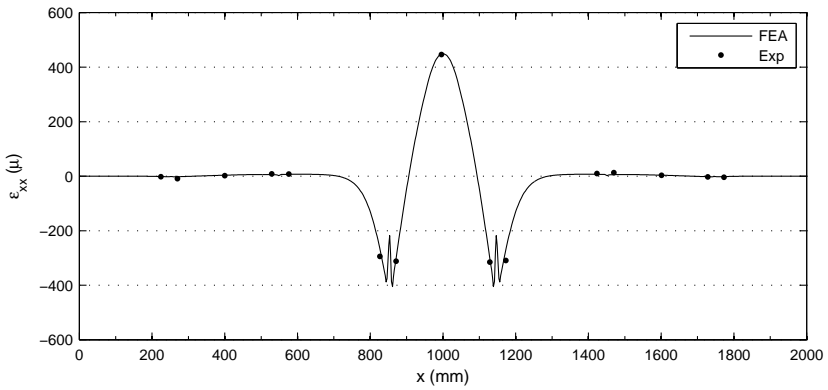
(b) 75 mm from crossbeam cross-section

Figure 7.11: Transverse strains ε_{xx} at the bottom side of the unreinforced steel deck plate recorded during testing (Exp) and predicted by the FEA (50 kN wheel load type C aligned with middle-trough at the crossbeam).

(a) wheel type C at midspan between crossbeams

(b) wheel type B at midspan between crossbeams
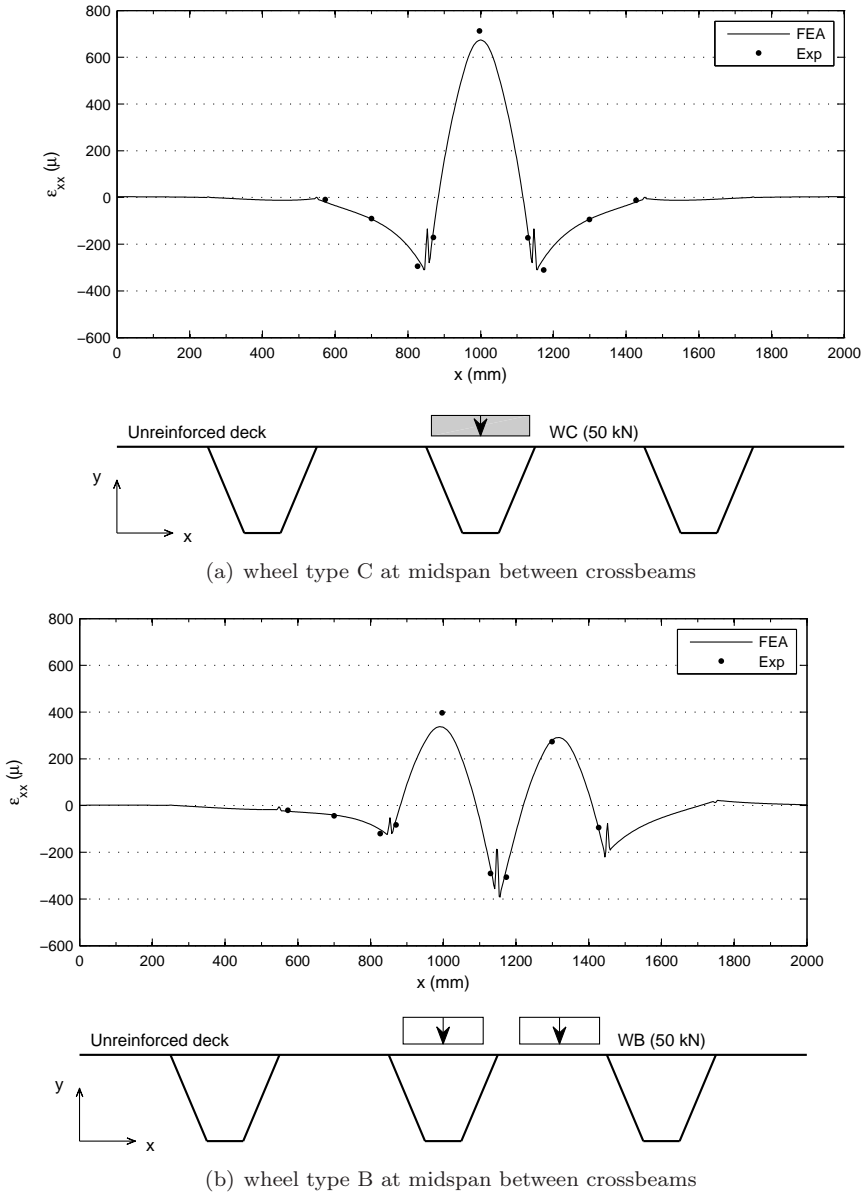
Figure 7.12: Transverse strains ε_{xx} at the bottom side of the unreinforced steel deck plate recorded during testing (Exp) and predicted by the FEA (50 kN wheel load at midspan between crossbeams).

Bonded steel plates reinforced steel deck

Figure 7.13 shows the results of the bonded steel plates reinforced deck when it is loaded at the crossbeam. The wheel load is 100 kN and it is aligned with the middle trough. The wheel print is type C. The experimental values (Exp) are the strains recorded by the strain gauges during the static test. The numerical distribution is given by the FEA of the bonded steel plates reinforced deck described in Chapter 6.

Figure 7.13(a) shows the transverse strains along the crossbeam cross-section and Figure 7.13(b) along the cross-section 75 mm from the crossbeam. The strain distribution is similar to that of the unreinforced deck. It is important to notice that the wheel load at this tests is 100 kN, which is twice the load used in the unreinforced deck tests. The strain values are of the same order when compared with the unreinforced deck for twice the load (50 kN for the unreinforced and 100 kN for the reinforced). This indicates that the strain values decrease by approximately 50% after the reinforcement. Overall, the numerical prediction fits well with the experimental values ($n/e = 0.96 \pm 0.09$).

Figure 7.14 shows the results when the deck is loaded at midspan between crossbeams. Figure 7.14(a) shows the results using wheel print type C and Figure 7.14(b) using wheel print type B. The total wheel load for both cases is 100 kN. Both strain distributions are once again similar to the corresponding strains of the unreinforced deck. The strain distribution given by the FEA fits well with the experimental values ($n/e = 0.91 \pm 0.10$ and $n/e = 0.93 \pm 0.09$, wheel type C and B, respectively).

Sandwich steel plates reinforced steel deck

Figure 7.15 shows the results of the sandwich steel plates reinforced deck when it is loaded at the crossbeam. The wheel load is 100 kN and it is aligned with the middle trough. The wheel print is type C. The experimental values (Exp) are the strains recorded by the strain gauges during the static test. The numerical distribution is given by the FEA of the sandwich steel plates reinforced deck described in Chapter 6.

Figure 7.15(a) shows the transverse strains along the crossbeam cross-section and Figure 7.15(b) along the cross-section 75 mm from the crossbeam. The strain distribution is similar to the ones previously presented at the crossbeam location. Overall, the numerical prediction fits well with the experimental values ($n/e = 1.09 \pm 0.07$).

Figure 7.16 shows the results when the deck is loaded at midspan between crossbeams. Figure 7.16(a) shows the results using wheel print type C and Figure 7.16(b) using wheel print type B. The total wheel load for both cases is 100 kN.

The strain distribution is similar to the ones previously presented at midspan location. However in comparison with the previous results, this case has one of the highest deviation, although it is still acceptable ($n/e = 1.06 \pm 0.16$ and $n/e = 1.01 \pm 0.19$ wheel C and wheel B, respectively).
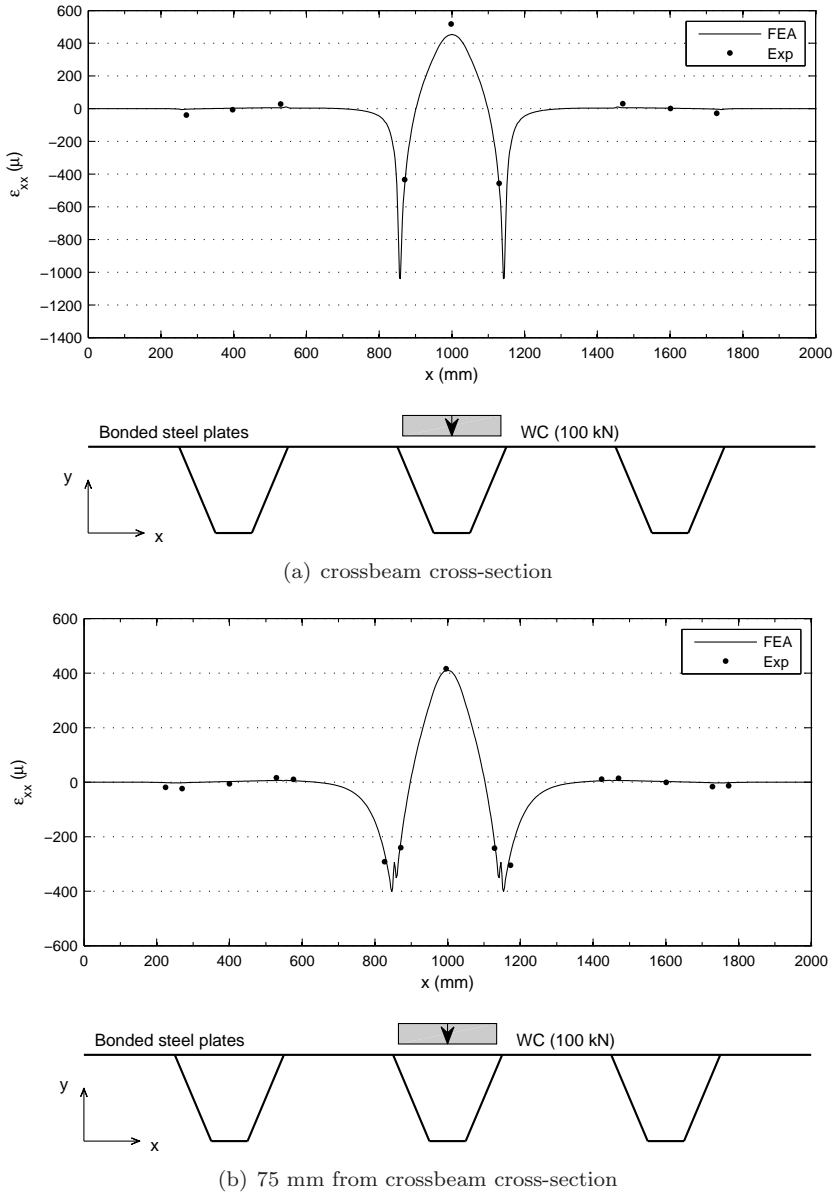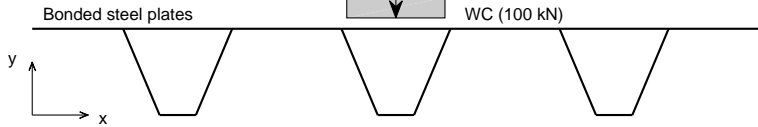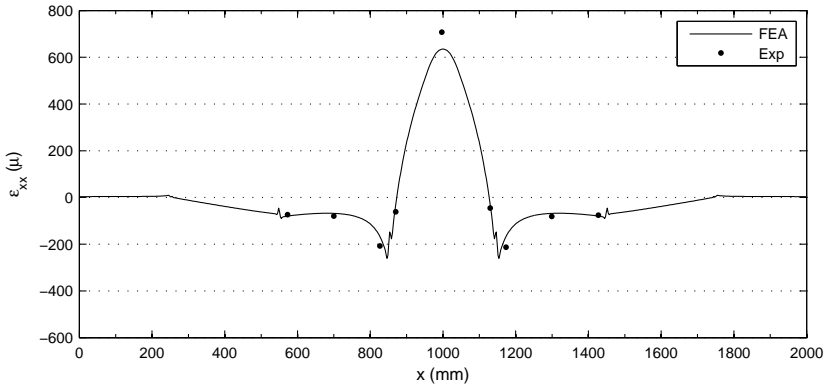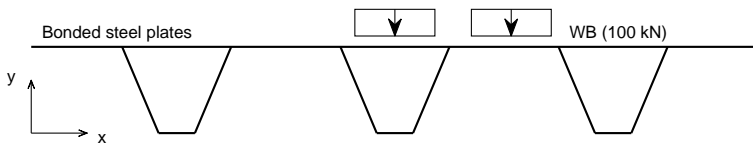
(a) crossbeam cross-section

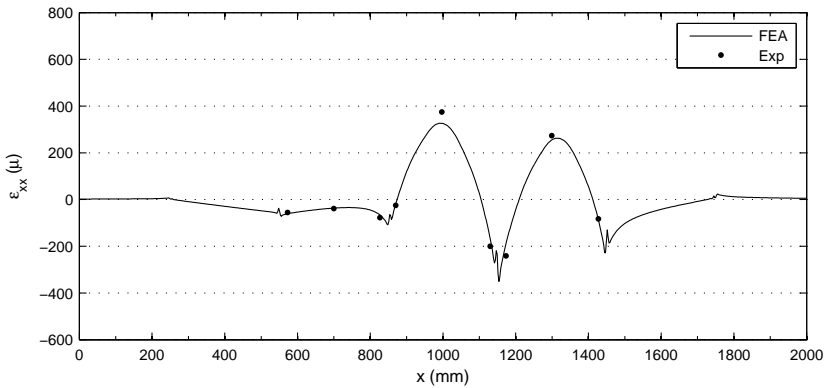(b) 75 mm from crossbeam cross-section

Figure 7.13: Transverse strains ε_{xx} at the bottom side of the bonded steel plates reinforced deck plate recorded during testing (Exp) and predicted by the FEA (100 kN wheel load type C aligned with middle-trough at the crossbeam).
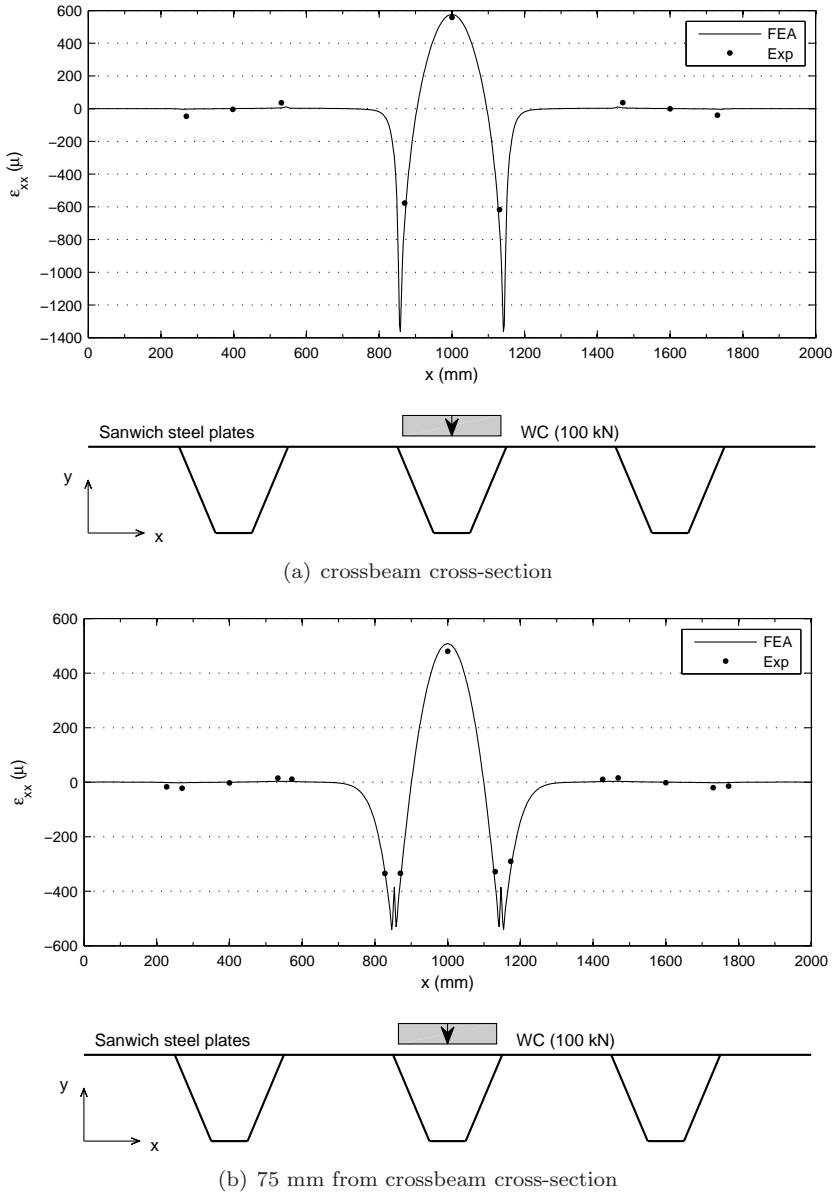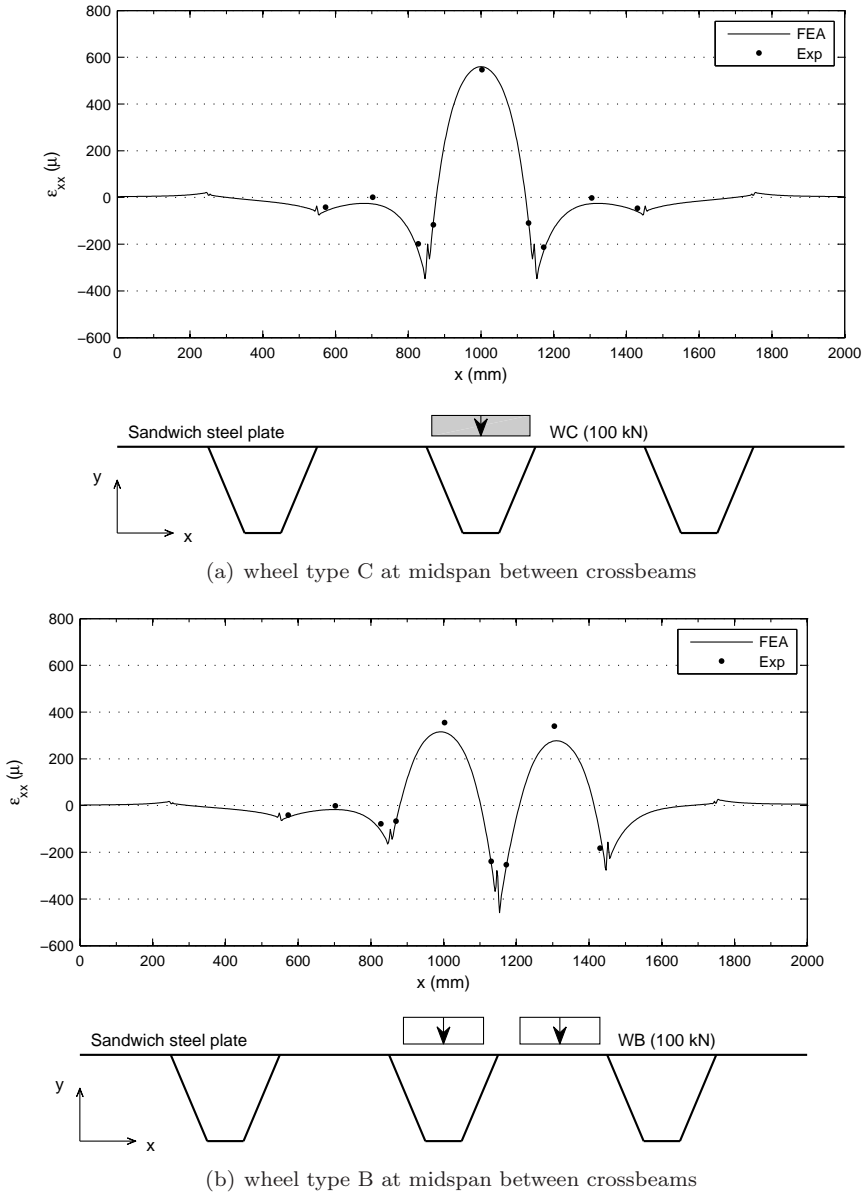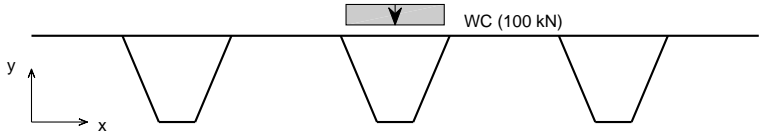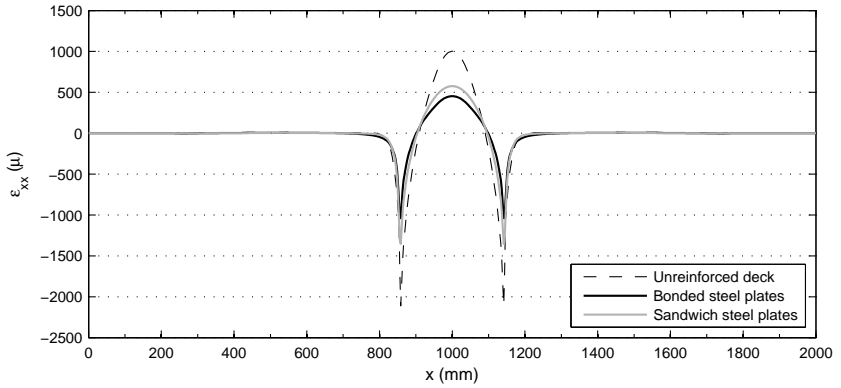
(a) wheel type C at midspan between crossbeams

(b) wheel type B at midspan between crossbeams

Figure 7.14: Transverse strains ε_{xx} at the bottom side of the bonded steel plates reinforced deck plate recorded during testing (Exp) and predicted by the FEA (100 kN wheel load at midspan between crossbeams).

(a) crossbeam cross-section

(b) 75 mm from crossbeam cross-section

Figure 7.15: Transverse strains ε_{xx} at the bottom side of the sandwich steel plates reinforced deck plate recorded during testing (Exp) and predicted by the FEA (100 kN wheel load type C aligned with middle-trough at the crossbeam).

(a) wheel type C at midspan between crossbeams

(b) wheel type B at midspan between crossbeams

Figure 7.16: Transverse strains ε_{xx} at the bottom side of the sandwich steel plates reinforced deck plate recorded during testing (Exp) and predicted by the FEA (100 kN wheel load at midspan between crossbeams).

Summarizing, the transverse strains at the bottom side of the deck plate decrease significantly after reinforcement, both close to the deck-plate-to-stiffener welds and between stiffener webs. The FEA proved to be a good simulation of the actual full-scale behaviour of the deck panels. Therefore the FEA are validated for further studies.

Figure 7.17 compares the transverse strains at the bottom side of the deck plate between the unreinforced deck, bonded steel plates reinforced deck and sandwich steel plates reinforced deck. The results are given by the validated FEA. The wheel load is 100 kN and the wheel print is type C.

Figure 7.17(a) compares the strain distribution at the crossbeam cross-section. The transverse stresses close to the deck-plate-to-stiffener weld are extremely high for all deck states. The peak values occur at the weld root. The strain values are unrealistic at these peak points. In reality the steel would yield before reaching those values. The stresses to take into account at the welds are the ones 10 to 15 mm away from those peak points. The strains close to the deck-plate-to-stiffener welds and between stiffener webs ($x = 1000\,mm$) are higher for the sandwich steel plates reinforcement than for the bonded steel plates reinforcement.

Figure 7.17(b) compares the strain distribution at midspan between crossbeams. Also at this deck location, the transverse stresses close to the deck-plate-to-stiffener weld are higher for the sandwich steel plates reinforcement than for the bonded steel plates reinforcement. However, the strains between stiffener webs ($x = 1000\,mm$) are lower for sandwich steel plates reinforcement than for the bonded steel plates reinforcement.

The fact that the sandwich steel plates perform less well close to the welds is related with the high shear forces present at this deck location. In Chapter 3, after a parametric study performed on bonded and sandwich steel plates reinforced beams, it was concluded that the sandwich beams decrease their bending performance when shear increases its role on the bending behaviour of the beam. This is why the sandwich steel plates have better results at midspan between crossbeam than at the crossbeam, and better results between stiffener webs than close to the welds. The bending performance of sandwich steel plates is much better if bending moments play a more important role than shear forces on the behaviour of the reinforced deck.

(a) wheel type C at crossbeam cross-section
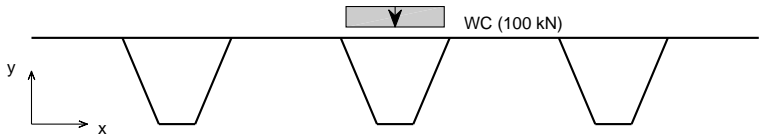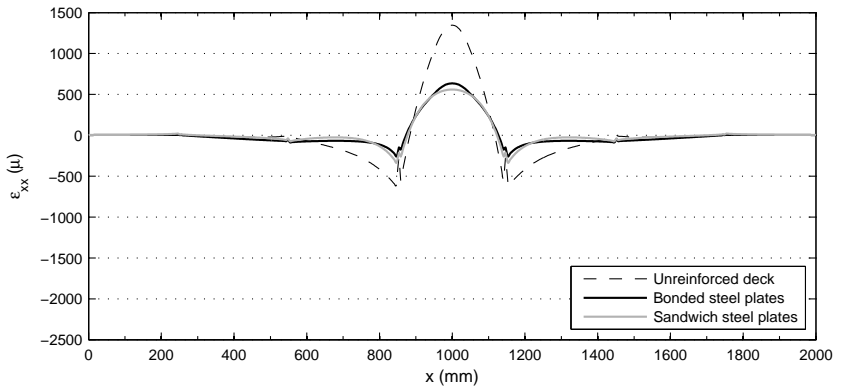
(b) wheel type C at midspan between crossbeams

Figure 7.17: Transverse strains ε_{xx} at the bottom side of deck plate for the unreinforced deck, the bonded steel plates reinforced deck the sandwich steel plates reinforced deck (100 kN wheel load type C).

7.3.3   Strain reduction factor

In order to quantify the decrease of strain values at the deck after applying the reinforcements, the strain reduction factor ERF was determined for each strain gauge applied to the deck by equation 7.1.

$$ERF = 1 - \frac{\varepsilon_{Reinforced\ deck}}{\varepsilon_{Unreinforced\ deck}} \tag{7.1}$$

The ERF was determined using the recorded strains during testing (Exp) and using the predicted strains by the FEA. From these results, three strain reduction factors were determined, ERF^{Exp1}, ERF^{Exp2} and ERF^{FEA}, equations 7.2, 7.3 and 7.4, respectively.

$$ERF^{\text{Exp1}} = 1 - \frac{\varepsilon_{Reinf.}^{\text{Exp}}}{\varepsilon_{Unreinf.}^{\text{Exp}}} \tag{7.2}$$

$$ERF^{\text{Exp2}} = 1 - \frac{\varepsilon_{Reinf.}^{\text{Exp}}}{\varepsilon_{Unreinf.}^{\text{FEA}}} \tag{7.3}$$

$$ERF^{\text{FEA}} = 1 - \frac{\varepsilon_{Reinf.}^{\text{FEA}}}{\varepsilon_{Unreinf.}^{\text{FEA}}} \tag{7.4}$$

ERF^{Exp1} compares experimental strains obtained from the static tests. This factor was only determined for a limited amount of strain gauges on specimen 1 (B1226), since only on this specimen static tests were performed before and after the reinforcement. This strain reduction factor is not available for specimen 2 (S12155). ERF^{Exp2} was determined using the experimental strain values of the reinforced decks and the numerical values of the unreinforced deck. This factor was determined for all the strain gauges applied to specimen 1 – B1226 and specimen 2 – S12155. Finally, ERF^{FEA} compares the strain values predicted by the FEA of the unreinforced and reinforced decks. This factor was determined for all the strain gauges applied to specimen 1 – B1226 and specimen 2 – S12155.

The results from the strain gauges were gathered in four groups of deck locations. Figure 7.18 shows a drawing where the four details are defined. Table 7.4 gives the list of strain gauges included in each group of results, at the crossbeam (see Figure 7.5, page 115) and at midspan between crossbeams (see Figure 7.3, page 114).

Some strain gauges at midspan location were not included in this analysis because the load case applied at midspan was not the most severe for those strain gauges.

Therefore their strain values are not significant and not appropriate to determine the strain reduction factor. This is the case for strain gauges 1, 2, 6, 7, 19, 20, 24 and 25. For the same reason, only strain gauge 27 is considered in group IV. The most important groups for the fatigue life of the OBD are II and III, since they indicate the reduction close to the deck-plate-to-stiffener welds.
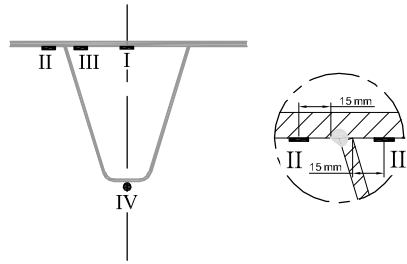

Figure 7.18: Groups of strain gauges according to the deck location: trough and close to the welds.

Table 7.4: Strain gauges groups at the crossbeam and at midspan between crossbeams.

Group	Crossbeam	Midspan
I	_08, _09, _10, _11, _12	11, 12, 13, 14, 15
II	_01, _02, _03, _04	3, 4, 5, 21, 22, 23
III	_05, _06, _07, _13, _14, _15	8, 9, 10, 16, 17, 18
IV	—	27

Tables 7.5 and 7.6 show the average±standard deviation values of the strain reduction factors on each group of strain gauges at the crossbeam location and at midspan between crossbeams for the bonded steel plates and the sandwich steel plates reinforcement, respectively.

At the crossbeam location, the bonded steel plates reinforcement reduces by approximately 45% to 60% the strain values close deck-plate-to-stiffener welds (groups II and III). At midspan, the reduction is higher than at the crossbeam, between 60% and 80%. The standard deviation is considerably higher at midspan, especially for group III, because at this location two load cases are considered, the wheel type C and the wheel type B. Group IV has the lowest strain reduction factor, approximately 20%. These results indicate that the reinforcement has more influence on the local strains (transverse strains, groups I, II and III) than on the longitudinal strains. The bonded steel plates reinforcement has little influence on the global behaviour of the bridge deck (longitudinal strains, strain gauge 27).

The sandwich steel plates reinforcement reduces by approximately 40% to 55% the transverse strains at the existing deck. The differences between midspan and cross-

beam are not as significant as for the bonded steel plates reinforcement. The longitudinal strains at the bottom of the stiffener are reduced by about 30% (group IV). This value is higher than for the bonded steel plates. The sandwich steel plates reinforcement influences not only the local behaviour, but also the global behaviour of the deck.

The sandwich steel plates can be considered as a global reinforcement system while the bonded steel plates is more a local reinforcement system.

Table 7.5: Strain reduction factors of the bonded steel plates reinforcement B1226.

ERF (%)	Crossbeam			Midspan		
	Exp1	Exp2	FEA	Exp1	Exp2	FEA
I	46 ± 5	56 ± 5	56 ± 0	50 ± 3	48 ± 3	51 ± 1
II	45 ± 3	45 ± 3	51 ± 0	66 ± 3	61 ± 3	68 ± 1
III	58 ± 3	62 ± 4	62 ± 1	83 ± 10	81 ± 12	86 ± 10
IV	—	—	—	18 ± 5	23 ± 1	21 ± 3

Table 7.6: Strain reduction factors of the sandwich steel plates reinforcement S12155.

ERF (%)	Crossbeam			Midspan		
	Exp1	Exp2	FEA	Exp1	Exp2	FEA
I	—	47 ± 7	46 ± 6	—	45 ± 9	49 ± 3
II	—	37 ± 8	42 ± 4	—	56 ± 3	50 ± 4
III	—	48 ± 7	46 ± 6	—	48 ± 14	51 ± 9
IV	—	—	—	—	36 ± 4	27 ± 3

The strain reduction factors for both reinforced decks are considerably lower than the ones determined for the beam-type specimens studied in Chapters 4 and 5. The results from the bending tests performed at room temperature on the reinforced beams showed a stress reduction of approximately 60% for the bonded steel plates B1226 and 80% for the sandwich steel plates S12155 (see Table 4.9, page 47 and Table 5.8, page 82, respectively).
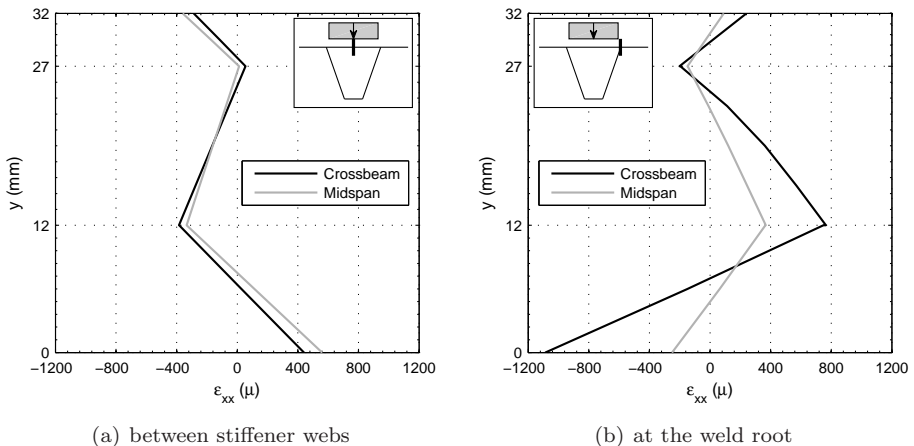
Figure 7.19 shows the transverse strains along the thickness of the sandwich steel plates reinforcement when the deck-panel is loaded at the crossbeam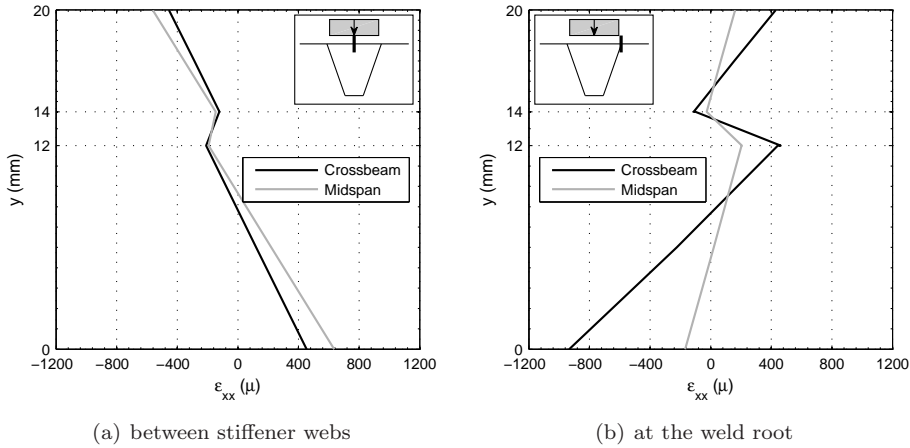 or at midspan between crossbeams by 100 kN wheel type C. Figure 7.19(a) shows the distribution between stiffener webs and Figure 7.19(b) at the root of the deck-plate-to-stiffener weld. Both strain distributions present a 'zig-zag' shape. This is a characteristic of the 'zig-zag' effect that causes the existence of two neutral axis on the cross-section instead of one. The 'zig-zag' is stronger at the weld root than between stiffener webs (Figure 7.19(b) and 7.19(a), respectively). This 'zig-zag' effect had been already observed in the 4pbt performed on the sandwich beams, described in Chapter 5 (see Figure 5.9, page 74). In those tests, the effect was stronger for short beams than for long beams. The effect is exactly the same in the beam tests and in the full-scale

tests. The 'zig-zag' is stronger when shear forces are high. This is the reason why it is stronger in the the short beams in comparison with the long beams, on the beam specimens, and it is stronger in the weld root in comparison with between the stiffener webs. The same is applied to justify the stronger 'zig-zag' for the crossbeam than for midspan between crossbeams, at the weld root (Figure 7.19(b)): higher shear forces at the crossbeam than at midspan.

Figure 7.20 shows the corresponding results for the bonded steel plates reinforcement. The only strain distribution which presents a strong 'zig-zag' shape is at the weld root when the load is at the crossbeam. However in none of the distribution the 'zig-zag' is as strong as in the sandwich steel plates. This shape was not observed at the beam tests of the bonded steel plates, presented in Chapter 4 (see Figure 4.6, page 41). This gives once more the indication that the shear forces are much higher close to the weld (specially at the crossbeam cross-section) due to the high stiffness of the existing deck in comparison with an unstiffened steel plate (beam tests).

This phenomena is the main reason for the difference between the stress reduction factors of the beam specimens and of the deck-panels. The 'zig-zag' effect is dependent on the span, on the loading and on the stiffness of the structure. All these parameters are different when comparing the beams tests with the full-scale tests.

The geometry of an orthotropic bridge deck is complex and each detail has a different strain reduction factor, which not only depends on the detail geometry but even on the load case applied to the deck. The simple beam geometry can be used to predict the influence of different parameters on the reinforcement performance, but not for predicting the absolute value of the stress reduction at weld details of orthotropic bridge decks.

(a) between stiffener webs

(b) at the weld root

Figure 7.19: Transverse strains along the thickness of the sandwich steel plates reinforcement when the deck-panel is loaded at the crossbeam or at midspan between crossbeams by 100 kN wheel type C.

(a) between stiffener webs　　　　　　　　　(b) at the weld root

Figure 7.20: Transverse strains along the thickness of the bonded steel plates reinforcement when the deck-panel is loaded at the crossbeam or at midspan between crossbeams by 100 kN wheel type C.

7.4　Fatigue behaviour

This part of the study describes the fatigue tests performed on the full-scale reinforced deck panels. The aim of this experimental program was to evaluate the fatigue behaviour of the bonded and sandwich steel plates reinforced deck panels when subjected to wheel loads. The fatigue tests were mainly focused on the fatigue behaviour of the reinforcement, the composite structure of the adhesive or core and second steel plate, rather than on the fatigue life of the welds present on an orthotropic bridge deck.

As studied in Chapter 4, Section 4.6, the main fatigue failure mode of the bonded steel plates reinforcement is adhesive shear failure. For the sandwich steel plates reinforcement, the main fatigue failure mode is delamination between the steel face and the core, as shown in Chapter 5, Section 5.6. Hence, the fatigue behaviour of the bonded and sandwich reinforcements depends on the shear stress in the adhesive layer and at the interface between the steel face and the core, respectively. The full-scale fatigue tests should be performed using the load cases that lead to the highest shear stresses at these locations.

Before describing the experimental procedure and corresponding results, the following section presents the shear stresses in the reinforcements when subjected to wheel loads, based on FEA.

7.4.1   Shear stress distribution in the reinforcement

The FEA validated in the previous section were used to determine the shear stress distribution in the adhesive and at the interface between the steel face and the core. The shear stress distribution was determined when the deck panels are subjected to wheel loads at the crossbeam and at midspan between crossbeams. Two shear stresses were determined, τ_{xy} and τ_{zy}, being x-axis along the specimen width, y-axis along the specimen thickness and z-axis along the specimen length. The coordinated system is based on the FEA described in Chapter 6 (see Figure 6.4, page 101). Besides these two shear stresses, an equivalent shear stress τ_{yeq} was determined that combines those two stress components. τ_{yeq} was determined by Equation 7.5 (by equilibrium $\tau_{yx} = \tau_{xy}$ and $\tau_{yz} = \tau_{zy}$).

$$\tau_{yeq} = \sqrt{\left(\tau_{yx}\right)^2 + \left(\tau_{yz}\right)^2} \tag{7.5}$$

Figure 7.21 shows the shear stresses τ_{xy} and τ_{zy} in the adhesive layer (mid-thickness) when the bonded steel plates reinforced deck is loaded at the crossbeam by wheel type C or at midspan by wheel type C or B (100 kN wheel load). The shear stress τ_{xy} is shown along the x-axis (specimen width), Figure 7.21(a). The shear stress τ_{zy} is shown along the specimen length z-axis between stiffener webs – point P (Figure 7.21(b). At the crossbeam it is clear that the wheel type C is the most severe load case for the adhesive layer. This load case is also the worst for the deck-plate-to-stiffener welds at this location (see Figure 6.9 in Chapter 6 on page 106). At midspan between crossbeams, the wheel type C is the worst load case for the adhesive layer. However for the deck-plate-to-stiffener welds the worst load case is wheel type B (see Figure 6.10 in Chapter 6 on page 107).

As the fatigue tests were focused on the fatigue behaviour of the reinforcement layers rather than on the welds, the fatigue tests on the bonded steel plates reinforced deck were performed using the heel load type C both at the crossbeam and at midspan between crossbeams.

The corresponding results at the interface between the 12 mm thick steel plate and the core of the sandwich steel plates reinforced decks are shown in Figure 7.22. They are in accordance with the ones for the bonded steel plates: the wheel type C is the worst load case, both at the crossbeam and at midspan between crossbeams. Therefore the fatigue tests on the sandwich steel plates reinforcement deck were also performed using wheel type C both at the crossbeam and at midspan between crossbeams.

Figures 7.23(a) and 7.23(b) show the stress distribution of τ_{yeq} in the adhesive layer over the loaded area at the crossbeam and at midspan between crossbeams, respectively. The maximum values are approximately 8 MPa and 7 MPa for crossbeam and midspan, respectively. The predominant shear stress at both locations is τ_{xy}.

Figures 7.24(a) and 7.24(b) show the stress distribution of τ_{yeq} at the interface between the steel plate and the core over the loaded area, at the crossbeam and at
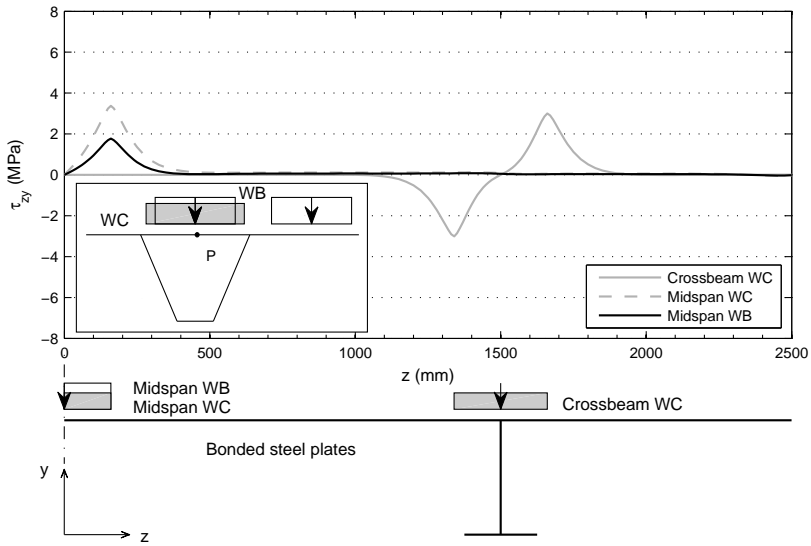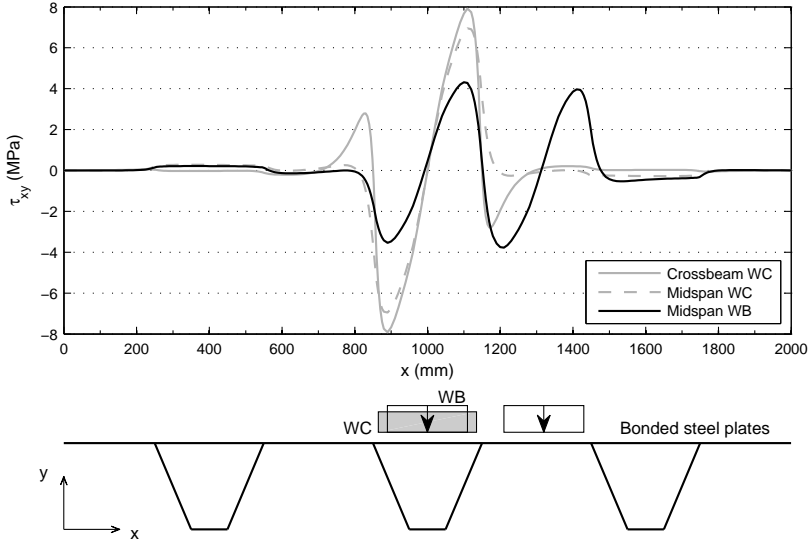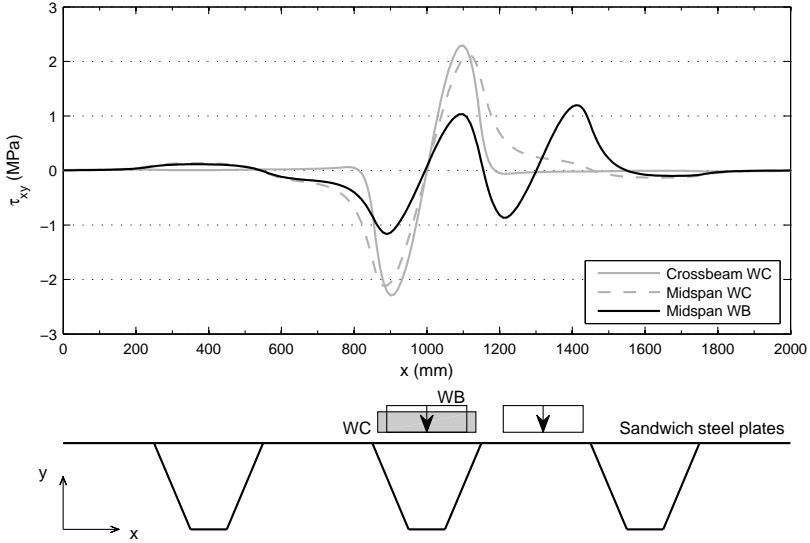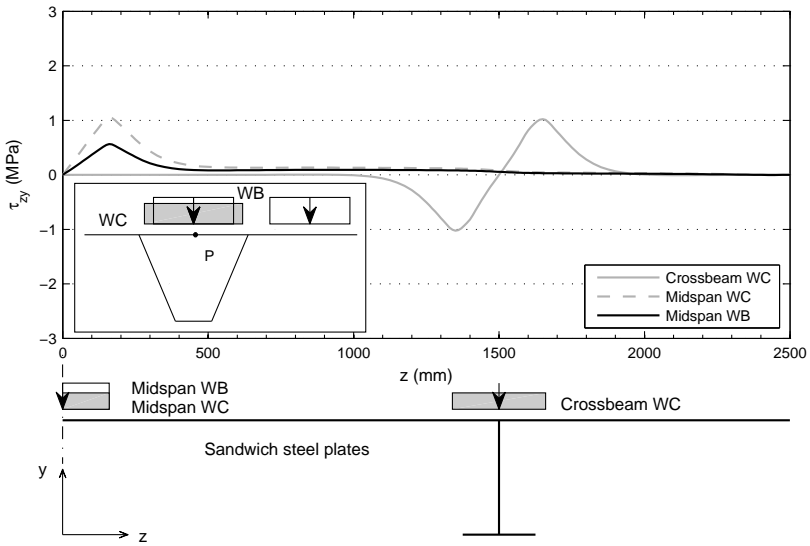
(a) crossbeam and midspan cross-sections

(b) longitudinal cross-section (axis of symmetry at z = 0 mm)

Figure 7.21: Shear stresses τ_{xy} and τ_{zy} in the adhesive layer (mid-thickness) when the bonded steel plates reinforced deck is loaded at the crossbeam by wheel type C or at midspan by wheel types C or B (100 kN wheel load).

(a) crossbeam and midspan cross-sections

(b) longitudinal cross-section (axis of symmetry at z = 0 mm)

Figure 7.22: Shear stresses τ_{xy} and τ_{zy} at the steel-core interface when the sandwich steel plates reinforced deck is loaded at the crossbeam by wheel type C or at midspan by wheel types C or B (100 kN wheel load).

(a) crossbeam (z = 1500 mm)   (b) midspan (z = 0 mm)
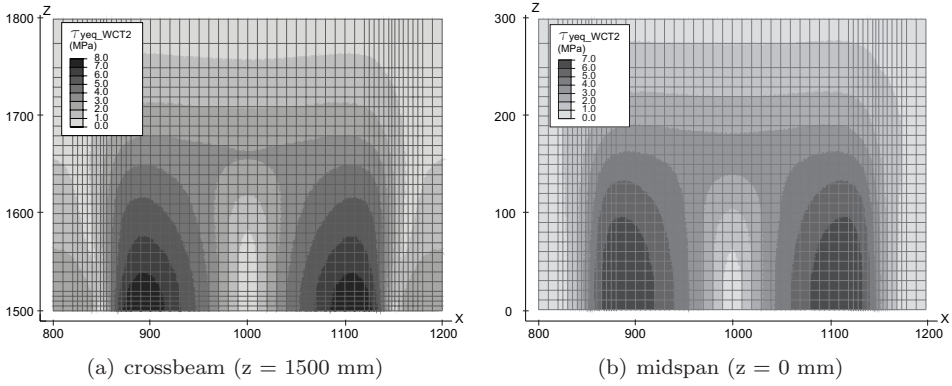
Figure 7.23: Shear stress distribution τ_{yeq} in the adhesive layer (mid-thickness) over the loading area when the bonded steel plates reinforced deck is loaded at the crossbeam or at midspan by wheel type C (100 kN wheel load).

(a) crossbeam (z = 1500 mm)   (b) midspan (z = 0 mm)
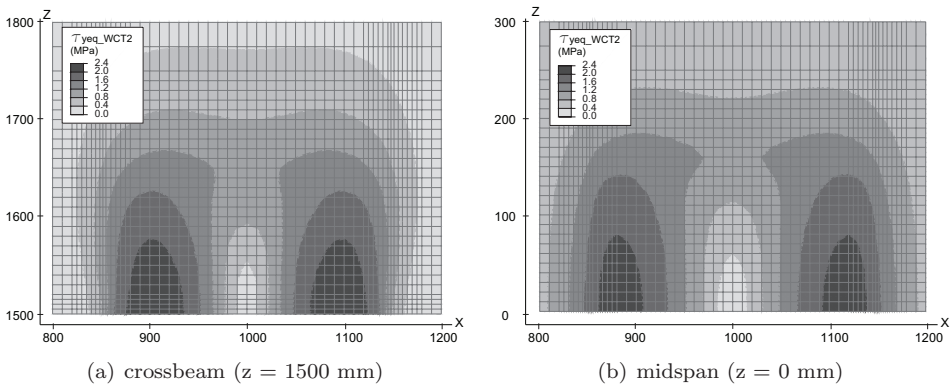
Figure 7.24: Shear stress distribution τ_{yeq} at the steel-core interface over the loading area when the sandwich steel plates reinforced deck is loaded at the crossbeam or at midspan by wheel type C (100 kN wheel load).

midspan between crossbeams, respectively. The maximum values are approximately 2.4 MPa both at the crossbeam and at midspan. The predominant shear stress at both locations is also τ_{xy}. The shear stress values at the steel-core interface are considerably lower than at the adhesive layer of the bonded steel plates reinforced deck.

7.4.2   Experimental procedure

In total seven fatigue test were performed on each deck specimen. At the crossbeams, six fatigue tests were performed in total, one on each trough-to-crossbeam joint. The wheel type C was aligned with the crossbeams web and with each trough, as shown in Figure 7.8 (page 119) for the static tests. At midspan between crossbeams, one fatigue test was performed. The wheel type C was aligned with the middle trough at midspan between crossbeams. The seven fatigue tests on each deck specimen were performed one by one. The load cases used were the same for both deck specimens, bonded and sandwich steel plates reinforced deck.

The fatigue tests were carried out in load control with a constant applied load ratio $R = 0.1$ ($R = P_{min}/P_{max}$). The wave form was sinusoidal. The tests were conducted in the same test rigs as for the static tests. The bonded steel plates specimen was loaded at a frequency of 7 and 5 Hz at the crossbeam and at midspan between crossbeams, respectively. The sandwich steel plates specimen was loaded at a frequency of 2 Hz at both locations.

The tests were performed at three load levels. The maximum loads P_{max} were 160 kN, 110 kN and 90 kN ($\Delta P = 144$ kN, 99 kN and 81 kN, respectively). At the crossbeams, two tests were performed at each load level. At midspan between crossbeams, the bonded steel plates specimen was tested at $P_{max} = 160$ kN and the sandwich steel plates at $P_{max} = 110$ kN. Chronologically, the bonded steel plates specimen was tested first, and at midspan a fatigue crack appeared in an early stage of the tests at the weld of the trough made for the instrumentation holes (cut-outs shown in Figure 7.6). The test had to be stopped, the trough was cut out once again but this time a larger piece in order to reduce the stresses at the welds. After re-welding the new trough-piece, the test was restarted. In order to avoid this problem, on the sandwich steel plates specimen, the maximum load level was decreased to 110 kN at midspan between crossbeams. No fatigue crack was detected at the trough of this specimen.

The load levels used in the fatigue tests are higher than the ones recommended at the fatigue load model 2 of EN1991-2 (2003). On this model the maximum wheel load of type C is 60 kN. The loads used in the fatigue tests are from 1.5 to 2.67 times higher than the ones prescribed by the fatigue model.

Ultrasonic NDT A-scan was performed at the loaded areas of the bonded steel plates reinforced specimen. The scanning was performed before the fatigue tests. Every million cycles the fatigue tests were stopped to perform another scanning.

7.4.3 Results

The fatigue results are presented for each specimen: bonded steel plates reinforced deck and sandwich steel plates reinforced deck. The strain ranges measured by the strain gauges during testing are presented.
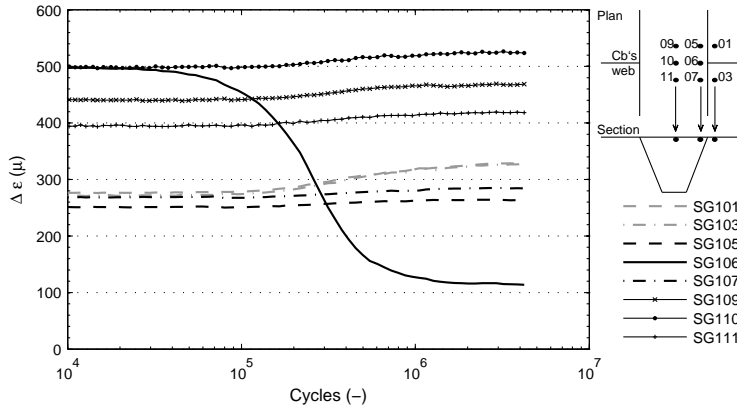
Bonded steel plates reinforced deck

Figure 7.25 shows the strain ranges measured during fatigue tests at the crossbeam location on the bonded steel plates reinforced deck. The presented results are from a selection of strain gauges which represent the typical results of each fatigue test: strain gauges close to the deck-plate-to-stiffener weld root SG_05, SG_06 and SG_07 and close to the weld toe, SG_01 and SG_03; and strain gauges between the stiffener webs, SG_09, SG_10 and SG_11. Figures 7.25(a), 7.25(b) and 7.25(c) show the results for the three load levels, $P_{max} = 160$ kN, 110 kN and 90 kN, respectively.

At all load levels, the biggest change in the strain range occurred in strain gauge SG_06. This strain gauge is aligned with the crossbeam close to the deck-plate-to-stiffener weld root. The range started to decrease in an early stage of the fatigue tests. As a response to that decrease, the strain range of strain gauges SG_01 and SG_03 increased. Strain ranges of strain gauges SG_09, SG_10 and SG_11 also increased, but on a lower magnitude than the previous ones. The increase of the strain ranges of these strain gauges is a consequence of stress redistribution due to the local loss of stiffness close to strain gauge SG_06.

The results of the repeated tests at the same load level are very similar to the ones presented.
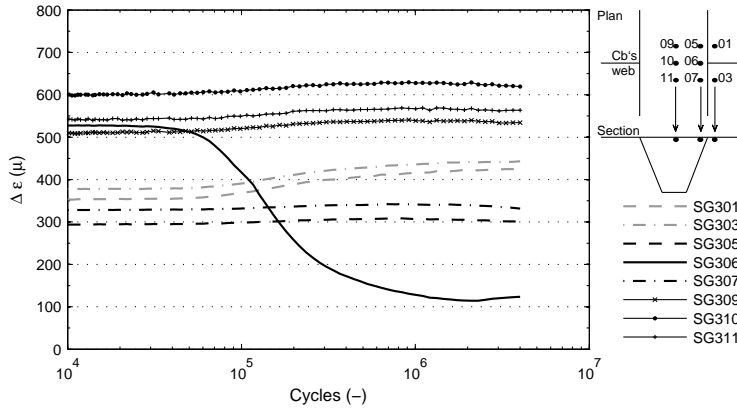
(a) crossbeam trough 3 $P_{max} = 160$ kN ($\Delta P = 144$ kN)

(b) crossbeam trough 1 $P_{max} = 110$ kN ($\Delta P = 99$ kN)
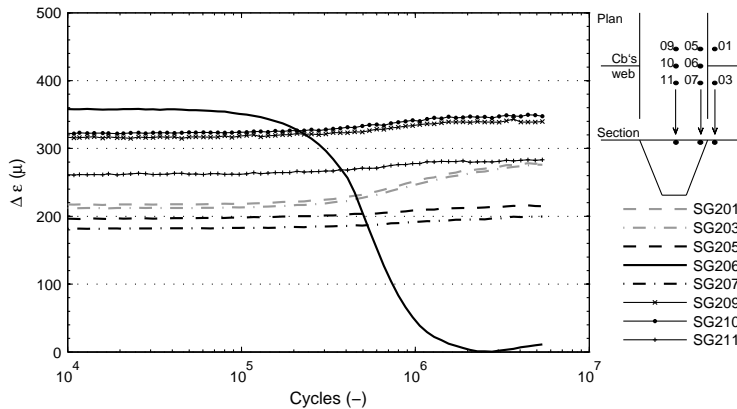
(c) crossbeam trough 2 $P_{max} = 90$ kN ($\Delta P = 81$ kN)

Figure 7.25: Strain ranges measured by strain gauges (SG) during fatigue tests at the crossbeam on the bonded steel plates reinforced deck specimen.
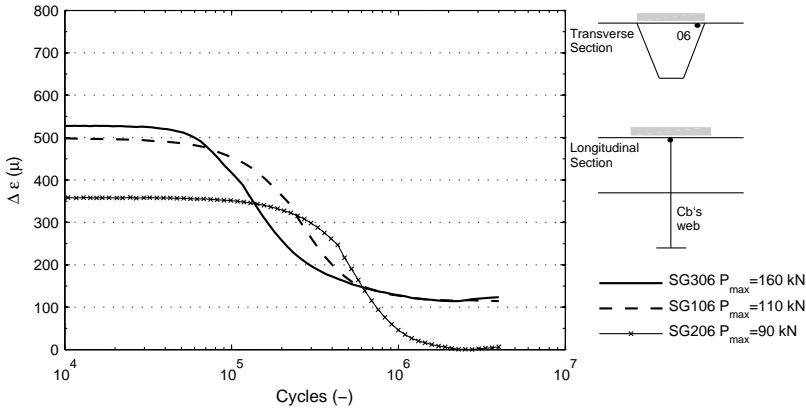
Figure 7.26: Strain ranges measured by the strain gauges _06 during fatigue tests at the crossbeam for three load levels on the bonded steel plates reinforced deck specimen.

Figure 7.26 compares the strain ranges measured by strain gauge SG_06 at the three load levels. At all load levels the strain range starts to decrease after a certain number of cycles. This number of cycles depends on the load level. The lower the load level, the more cycles are needed to the range to start decreasing. The decrease of strain range is related with the loss of stiffness close to deck-plate-to-stiffener weld at the crossbeam location.

Figure 7.27 shows the strain ranges measured during the fatigue test at midspan between crossbeams on the bonded steel plates reinforced deck. The selection of strain gauges represents the typical results from the most important deck details: strain gauges close to the deck-plate-to-stiffener weld root, SG8 and SG9 and close to the weld toe, SG3 and SG4; and strain gauge between the stiffener webs, SG12 and SG13. The load level is $P_{max} = 160$ kN ($\Delta P = 144$ kN).

There were no significant changes during testing in any of the strain gauge results. The strains close to the welds are significantly lower than those at any load level at the crossbeam location (SG9 is lower than 100μ, while SG_06 is approximately 500μ for the same load level). The stress concentration is considerably lower at midspan between crossbeams than at the crossbeam, since there is no crossbeam web which is a point of very high stiffness. The strain between the stiffener webs is higher at midspan between crossbeams than at the crossbeam (SG13 is approximately 900μ, while SG_10 is 600μ at the crossbeam for the same load level).
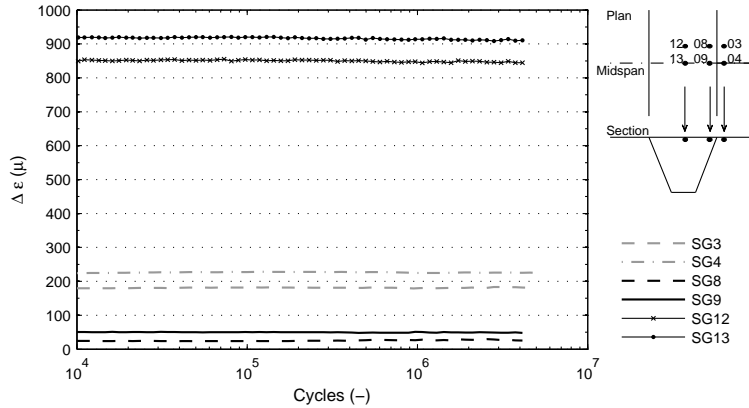
Figure 7.27: Strain ranges measured during fatigue tests at midspan between crossbeams on the bonded steel plates reinforced deck specimen $P_{max} = 160$ kN ($\Delta P = 144$ kN).

Figures 7.28, 7.29 and 7.30 show the results of the ultrasonic NDT A-scan performed on the loaded areas of the bonded steel plates reinforced deck. The interpretation of the amplitude levels from 0 to 80 is presented in Table 7.7. The amplitude interpretation was based on a small reference panel (100 mm by 100 mm) of bonded steel plates in which a delamination was deliberately simulated by two neoprene sheets placed inside the adhesive layer.

Table 7.7: Interpretation of the amplitude levels.

Amplitude levels	Interpretation
0	not scanned
20 – 40	good bonding
60 – 80	partially to full delaminated

Figure 7.28 shows the amplitude levels at the crossbeam A. Figure 7.28(a) shows some delaminated areas before testing (n=0 cycles). After the fatigue tests, Figure 7.28(b), no significant changes were observed. Hence, there was no further delamination induced by the fatigue testing. The areas where the bonding was considered good, kept the same good quality after the fatigue test. Therefore, one can conclude that the fatigue tests at crossbeam A did not induce any damage in the adhesive layer. At midspan between crossbeams, shown in Figure 7.29, the bonding quality was good before the fatigue tests and no considerable changes were found after the fatigue tests (no delamination). Finally, Figure 7.30 shows the results at crossbeam B. Once more there are no significant changes in the results before and after the fatigue tests. Also at this location no delamination in the adhesive layer was detected after the fatigue tests.

(a) n=0 cycles

(b) n=4 to 5 million cycles
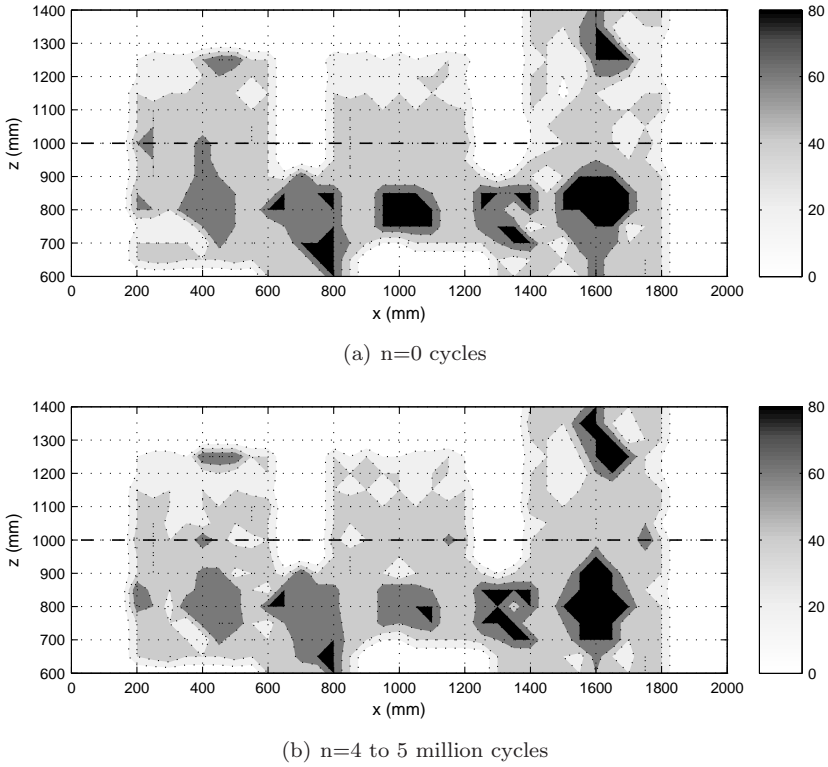
Figure 7.28: NDT performed at the crossbeam A of the bonded steel plates reinforced deck (a) before and (b) after the fatigue tests (crossbeam web at z=1000 mm).
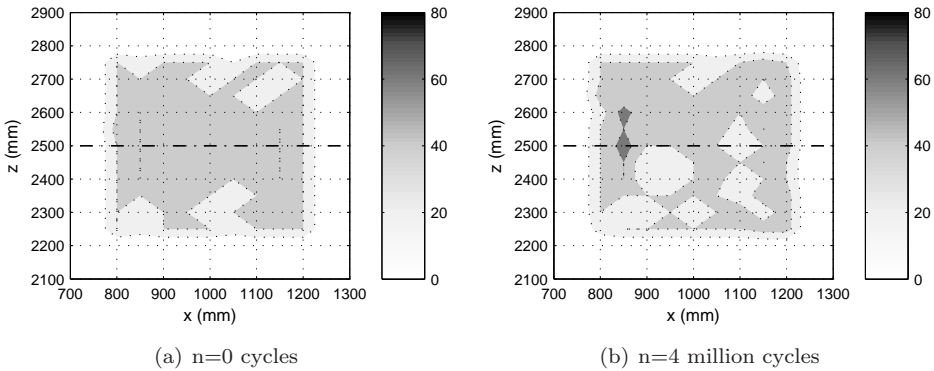

(a) n=0 cycles

(b) n=4 million cycles

Figure 7.29: NDT performed at midspan of the bonded steel plates reinforced deck (a) before and (b) after the fatigue tests (midspan at z=2500 mm).
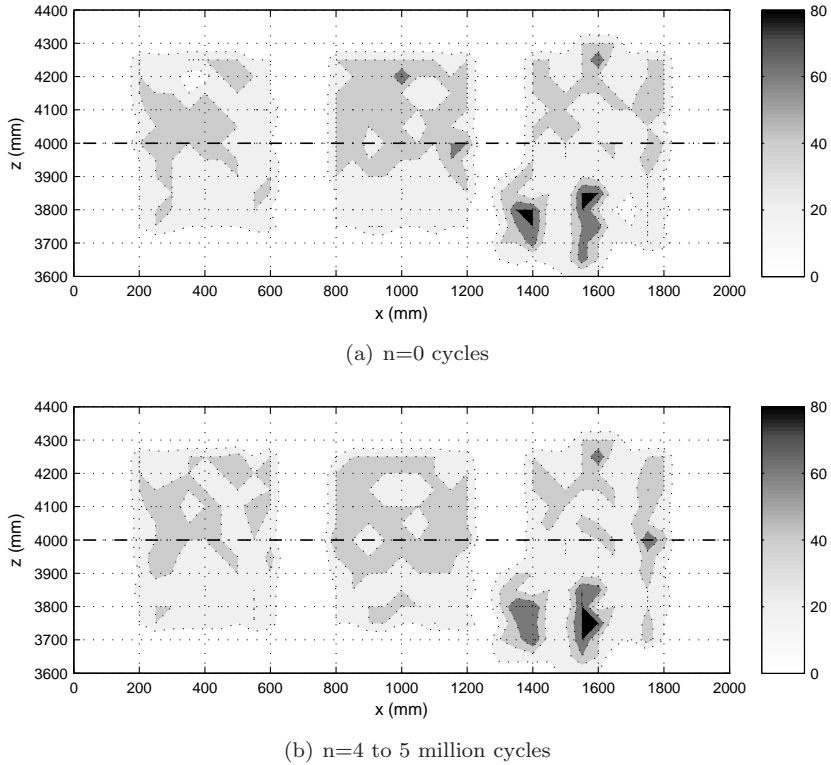
(a) n=0 cycles

(b) n=4 to 5 million cycles

Figure 7.30: NDT performed at the crossbeam B of the bonded steel plates reinforced deck (a) before and (b) after the fatigue tests (crossbeam web at z=4000 mm).

Sandwich steel plates reinforced steel deck

Figure 7.31 shows the strain ranges measured during fatigue tests at the crossbeam location on the sandwich steel plates reinforced deck. The results are from the same selection of strain gauges as the one presented for the bonded steel plates specimen. Figures 7.31(a), 7.31(b) and 7.31(c) show the results for three load levels, $P_{max} = 160$ kN, 110 kN and 90 kN, respectively.
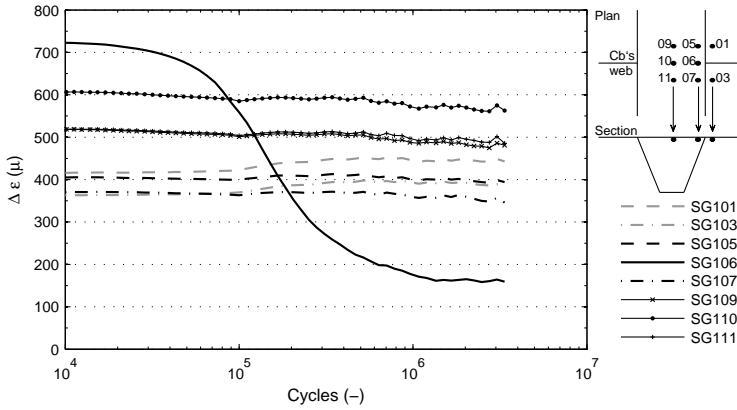
(a) crossbeam trough 3, $P_{max} = 160$ kN ($\Delta P = 144$ kN)
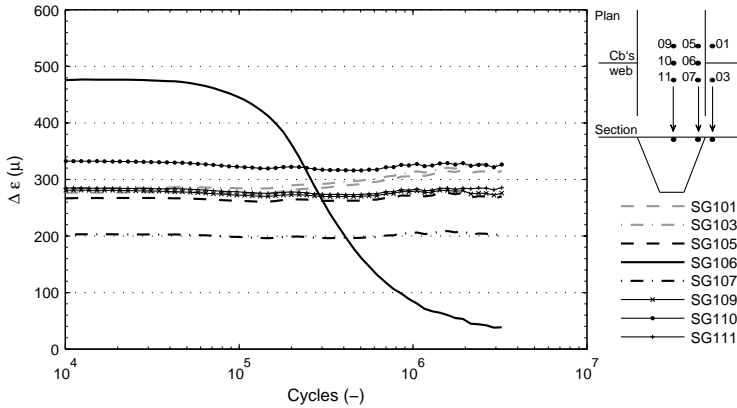
(b) crossbeam trough 1, $P_{max} = 110$ kN ($\Delta P = 99$ kN)
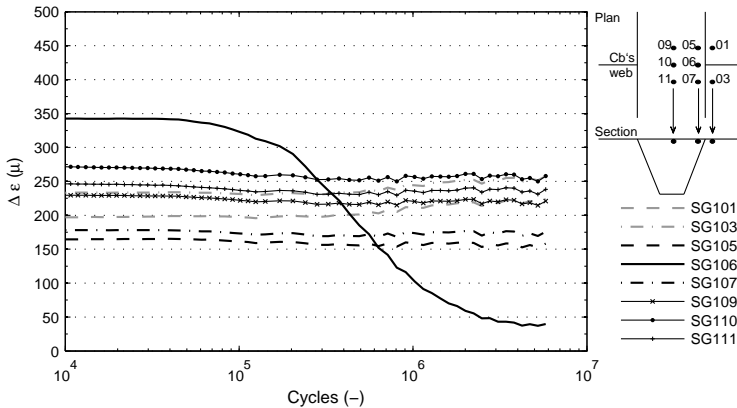
(c) crossbeam trough 2, $P_{max} = 90$ kN ($\Delta P = 81$ kN)

Figure 7.31: Strain ranges measured by strain gauges (SG) during fatigue tests at the crossbeam on the sandwich steel plates reinforced deck specimen.

The biggest change in the strain range occurred in strain gauge SG 06. The same was observed for the bonded steel plates reinforcement. The range also started to decrease in an early stage of the fatigue tests. As a response to that decrease, mainly the strain range of strain gauges SG 01 and SG 03 increased. As in the bonded steel plates specimen, the increase of the strain ranges of these strain gauges is a consequence of stress redistribution due to the local loss of stiffness close to strain gauge SG 06. The results of the repeated tests at the same load level are very similar to the ones presented, except for one at the load level 90 kN, where at one of the welds there was no significant change at any strain gauge, including SG 06.

Figure 7.32 compares the strain range measured by strain gauge SG 06 at the three load levels. The results are very similar to the corresponding ones for the bonded steel plates deck specimen. At all load levels the strain range starts to decrease after a certain number of cycles. The lower the load level, the more cycles are needed to the range to start decreasing.

Figure 7.33 shows the strain ranges measured during the fatigue test at midspan between crossbeams on the sandwich steel plates reinforced deck. The results are given for the same selection of strain gauges as the one presented for the bonded steel plates specimen. The load level is $P_{max} = 110$ kN ($\Delta P = 99$ kN).

There were no significant changes during testing in any of the strain gauge results. The strains close to the welds are significantly lower at midspan between crossbeams than at any load level at the crossbeam location (SG9 is lower than 100μ, while SG 06 is approximately 500μ for the same load level). The strain between the stiffener webs is higher at midspan between crossbeams than at the crossbeam (SG13 is approximately 550μ, while SG 10 is approximately 320μ at the crossbeam for the same load level).

Overall the strain ranges measured at the sandwich steel plates deck specimen are very similar to the corresponding ones measured at the bonded steel plate deck specimen.

The ultrasonic scan was not performed on the sandwich steel plates deck specimen. After a trial test on a reference sandwich panel, it was concluded that the damping of the sound wave when crossing the interface between the steel plate and the core material was as high as when crossing an interface between steel plate and air. Therefore, no distinction could be made between good and bad quality adhesion at the interface between the steel and the core.
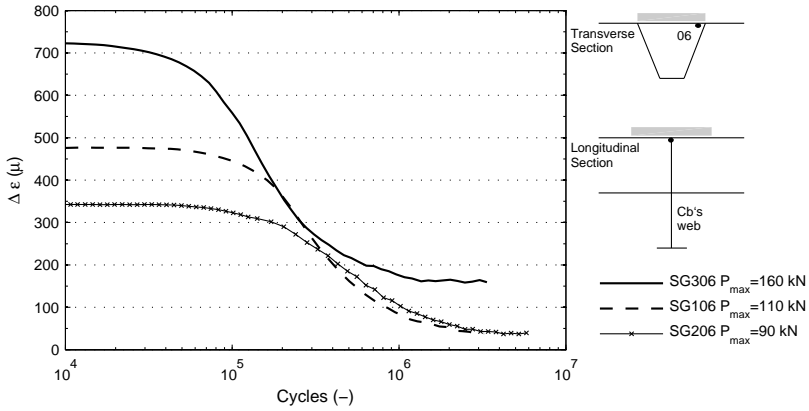
Figure 7.32: Strain ranges measured by the strain gauges _06 close to the weld during fatigue tests at the crossbeam for three load levels on the sandwich steel plates reinforced deck specimen.
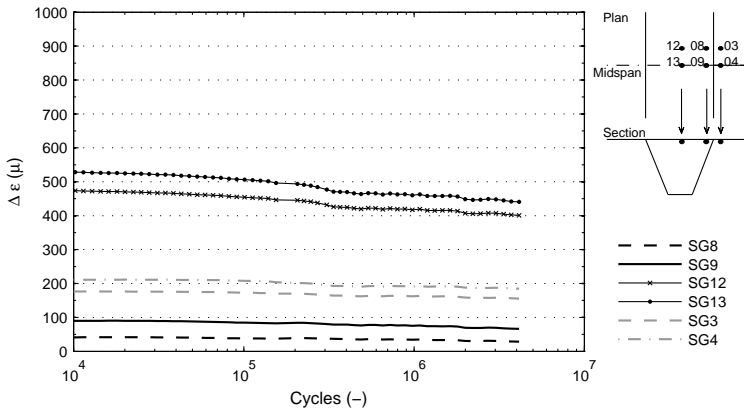

Figure 7.33: Strain ranges measured during fatigue tests at midspan between crossbeams on the sandwich steel plates reinforced deck specimen $P_{max} = 110$ kN ($\Delta P = 99$ kN).

During and after the fatigue tests, both bridge deck specimens were visually inspected for fatigue cracks at the welds. At the crossbeam location, several fatigue cracks were observed at the deck-plate-to-stiffener welds. The fatigue cracks at this location were observed on both bridge deck specimens. Figure 7.34 shows pictures of the fatigue cracks close to those welds on both reinforced deck-panels. These picture were taken after cutting a part of the deck specimens at the crossbeam. The fatigue cracks in the deck plate are clearly shown. At midspan locations no cracks were observed.

(a) bonded steel plates reinforced deck   (b) sandwich steel plates reinforced deck
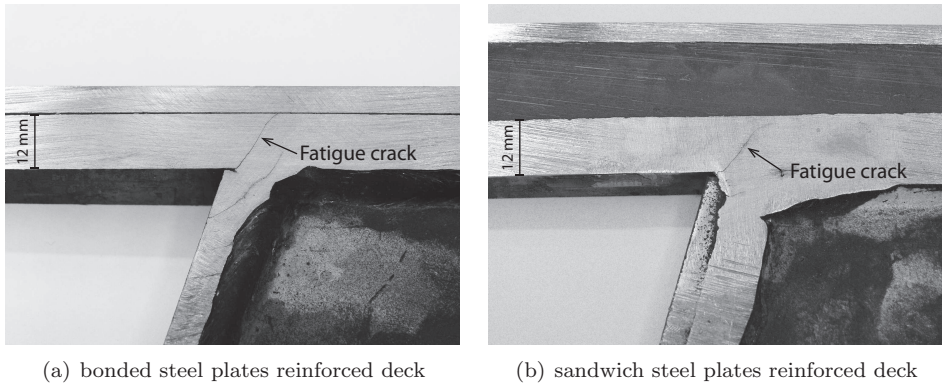
Figure 7.34: Fatigue cracks in the deck-plate-to-stiffener welds at the crossbeam location (wheel load type C $P_{max} = 160$ kN $- \Delta P = 144$ kN).

The strain gauges showing major changes are always close to the deck-plate-to-stiffener welds where fatigue cracks were observed. No delamination was detected in the adhesive layer by the ultrasonic NDT. Therefore, it can be concluded that the decrease of strain range close to the welds is caused by fatigue crack initiation at the deck-plate-to-stiffener weld. Although at the sandwich steel plates deck specimen, there was no NDT inspection to the interface between the core and the steel plate, the fact that the corresponding strain range pattern is very similar to the bonded steel plates deck panel and that fatigue cracks were also observed at the deck-plate-to-stiffener welds, it can be concluded that: there was no fatigue damage on the sandwich steel plates reinforcement.

Tables 7.8 and 7.9 summarise all fatigue results of the bonded and sandwich steel plates reinforced deck specimens. The fatigue life n_f is based on the strain ranges measured by the strain gauges close to the deck-plate-to-stiffener welds root, aligned with the crossbeam or with midspan between crossbeams (for example SG_06 and SG09, crossbeam and midspan location, respectively). The results are presented for two different failure criteria: 10% and 25% strain fall. These failure criteria were used by Kolstein (2007) to define the fatigue design classification of this type of fatigue crack (cracks at deck-plate-to-stiffener weld that grow through the deck-plate thickness). The main difference is that Kolstein (2007) used strain gauges on

the top side of the deck plate and in this thesis strain gauges on the bottom side of the deck-plate were used. At each fatigue test, two deck-plate-to-stiffener welds were tested and therefore the fatigue results are presented for both welds (one at each side of the stiffener).

Figure 7.35 shows the relationship between the fatigue lives n_f and the maximum load P_{max} for both deck specimens.

At midspan between crossbeams, there were no changes on the strain ranges during fatigue tests and no cracks were detected on both reinforced decks. Therefore, the tests are considered run-out tests. At the crossbeam, the major part of the strain gauges showed significant changes on the strain range during testing. There is one exception on the sandwich steel plates reinforced deck at the lowest load level. On this test at the crossbeam location, the strain gauges showed no changes during testing and no cracks were observed at the welds. Therefore it was considered a run-out test.

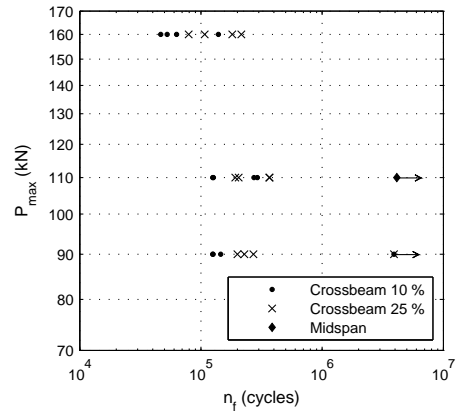Table 7.8: Maximum load versus fatigue lives of the welds at the bonded steel plates reinforced deck.

| Location | P_{max} | n_f (cycles) | |
		10%	25%
	160	72883	112354
	160	63225	108994
	160	64535	107649
	160	48368	72561
	110	402821	529840
Crossbeam	110	65392	124920
	110	107940	189030
	110	120544	239029
	90	227845	378262
	90	98259	203896
	90	211682	336889
	90	116726	217144
Midspan	160	> 5072367 (run out)	
	160	> 5072367 (run out)	

Table 7.9: Maximum load versus fatigue lives of the welds at the sandwich steel plates reinforced deck.

Location	P_{max}	n_f (cycles)	
		10%	25%
Crossbeam	160	139565	181320
	160	62955	107528
	160	52692	79330
	160	46573	215155
	110	125051	204498
	110	274344	369033
	110	126719	192044
	110	291973	365773
	90	125083	228472
	90	145685	271185
	90	125784	200292
	90	> 3918743 (run out)	
Midspan	110	> 4136051 (run out)	
	110	> 4136051 (run out)	
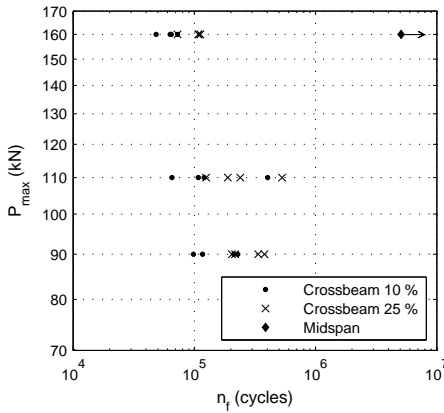
(a) bonded steel plates   (b) sandwich steel plates

Figure 7.35: Maximum load versus fatigue life of the welds.

7.4.4   Fatigue behaviour of the reinforcement

The aim of the full-scale fatigue tests was to study the fatigue behaviour of the bonded and sandwich steel plates reinforcement when applied to the actual geometry of an OBD and subjected to wheel loads.

As studied in Chapter 4, the main fatigue failure mode of the bonded steel plates reinforcement is the adhesive shear failure. Therefore, the fatigue behaviour of this reinforcement should be evaluated in terms of the shear stress in the adhesive layer. This shear stress distribution was presented in Figure 7.21, on page 138. For 100 kN wheel load type C, the maximum equivalent shear stress on the adhesive layer (τ_{yeq}) is approximately 8 MPa and 7 MPa when the load is at the crossbeam and at midspan between crossbeams, respectively (see Figure 7.23). The end of the fatigue life of the bonded steel plates reinforcement should be taken at the moment when delamination occurs in the adhesive layer. As no delamination was detected after any of the full-scale fatigue tests, it is considered that no fatigue damage occurred on the bonded steel plates reinforcement during full-scale fatigue testing.

Considering the sandwich steel plates reinforcement, the main fatigue failure mode is delamination between the steel plate and the polyurethane core, as presented in Chapter 5. Therefore, the fatigue behaviour of this reinforcement should be evaluated in terms of the shear stress present at that interface. These shear stress fields were presented in Figure 7.22, on page 139. For 100 kN wheel load type C, the maximum shear stress at the interface between plate and core (τ_{yeq}) is approximately 2.4 MPa (see Figure 7.24). The end of the fatigue life of the sandwich reinforcement should be taken when delamination occurs. As no delamination was detected during the full-scale fatigue tests, it is considered that no fatigue damage occurred on the sandwich steel plates reinforcement during full-scale fatigue testing.

Figure 7.36 shows the stress-cycle SN diagrams for both reinforcements. Figure 7.36(a) plots the fatigue life n_f of each bonded steel plates fatigue test against the shear stress range at the adhesive layer $\Delta\tau_{ad}$. Figure 7.36(b) plots the fatigue life n_f of each sandwich steel plates fatigue test against the shear stress range at the interface between core and steel plate $\Delta\tau_c$. The shear stress is the maximum equivalent shear stress multiplied by the amplitude load ($\Delta \cdot P = 0.9 \cdot P_{max}$). The results from the full-scale tests are plotted together with the fatigue results from the beam fatigue tests described in Chapters 4 and 5, for the bonded and sandwich steel plates reinforcement, respectively.

For the bonded steel plates reinforcement, the results from the full-scale tests are close to the run-outs of the beam tests. The equivalent shear stress present at the full-scale tests is close to the value of fatigue threshold of the adhesive layer determined in the beams tests. From the SN diagram of the beam tests, one could predict the fatigue life during full-scale testing based on the equivalent shear stress present at the adhesive layer.

For the sandwich steel plates reinforcement, the shear stress at the interface on the full-scale tests is lower than the fatigue threshold determined in the beams tests. It
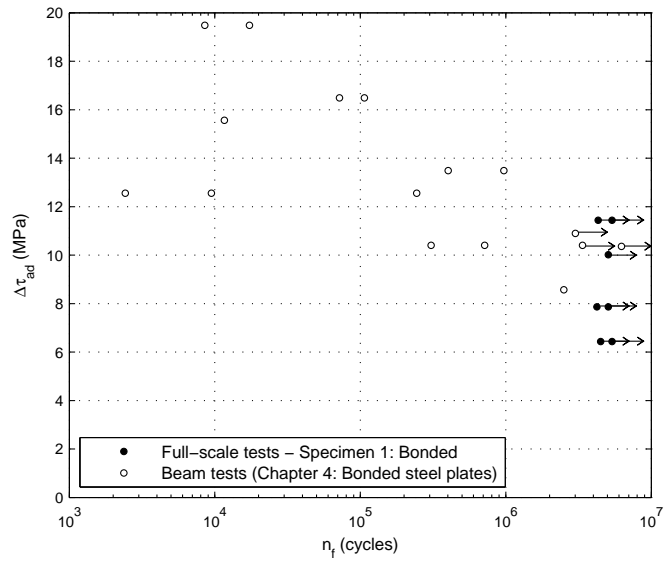
(a) Bonded steel plates reinforcement
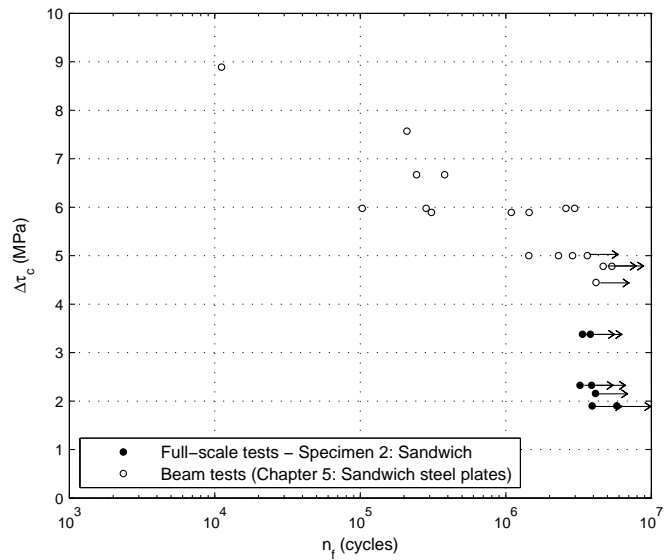
(b) Sandwich steel plates reinforcement

Figure 7.36: SN diagram of the reinforcements at the full-scale tests and at the beam tests.

could be predicted from the SN diagram of the beams tests that no fatigue damage would occur on the full scale tests, as confirmed during testing.

7.4.5   Fatigue life of the welds

It was not the main aim of the full-scale tests to determine the fatigue life of the welded joints in orthotropic steel bridge decks. However, as several fatigue cracks were found during testing, a brief analysis of their fatigue behaviour is made in this section.

As shown in Figure 7.34, the crack found at the crossbeam location is the well known fatigue crack at the deck-plate-to-stiffener weld at the crossbeam location. The crack starts at the root of the weld between the longitudinal stiffener and the deck plate at the point where it intersects with crossbeam web. The crack grows through the thickness of the deck plate, from the bottom to the top side of the plate.

In this study, the fatigue life n_f of the welds is the number of cycles when the strain range falls 10% or 25% at the strain gauge closest to fatigue crack initiation point (for example SG_06 – see Figure 7.26). The 10% strain fall failure criterium was used by Kolstein (2007) to define the fatigue design classification of these type of fatigue cracks. The main difference is that Kolstein (2007) used strain gauges on the top side of the deck plate and in this thesis strain gauges on the bottom side of the deck-plate were used.

Figure 7.37 shows the fatigue results of the welds at the crossbeam as $\Delta\sigma - n_f$ diagrams (SN-curves) for the bonded and sandwich steel plates reinforced deck specimens. The stress range $\Delta\sigma$ is taken at the point where the crack initiates, which means at the deck-plate-to-stiffener weld root on the bottom side of the deck plate. For this typical detail, as the stress gradient close to the weld is very high, the stress is determined based on the geometrical stress range – hot spot method. The hot spot method is recommended by Hobbacher (2009) for fatigue assessment of general welded joints and by Kolstein (2007) for this specific fatigue crack of orthotropic steel bridge decks. The method consists in extrapolating the structural stress from two measuring points to where the crack initiates, called hot spot point. The two measuring points are $0.4 \cdot t$ and t from the hot spot point, t being the plate thickness. The stress at the measuring points is taken from the FEA presented in Chapter 6. In this case study, the deck plate is 12 mm thick (t=12 mm). The measuring points are therefore 4.8 mm ($0.4 \cdot t = 0.4 \cdot 12 = 4.8$ mm) and 12 mm (t) from the weld root.

Figure 7.37(a) shows the results of the fatigue life using the 10% failure criterium and Figure 7.37(b) using the 25% failure criterium. From the fatigue results a linear regression analysis was made. The fatigue life of the welds in the bonded and sandwich reinforced decks is compared with the fatigue strength SN curve defined at EN1993-1-9 (2005). The detail category is defined as the fatigue strength at 2 million cycles. The detail category 125 is the one recommended by Kolstein (2007) for the fatigue crack found in this study at the crossbeam location: crack at the deck-plate-to-stiffener weld that starts at the weld root and grows through the deck-plate thickness.
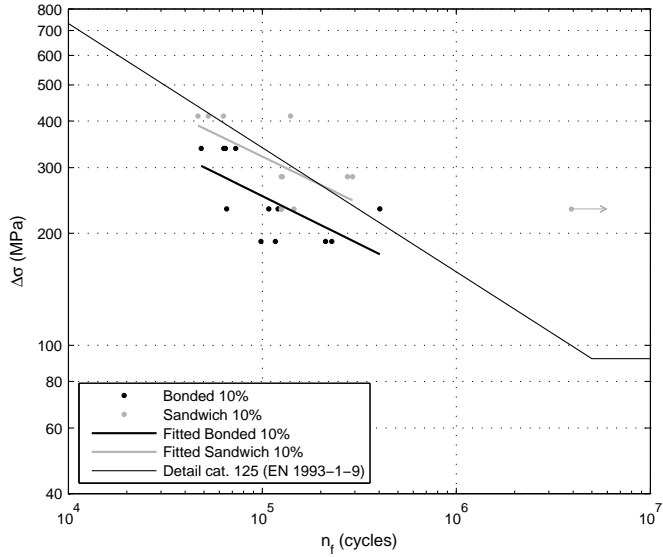
(a) 10% strain fall failure criterium
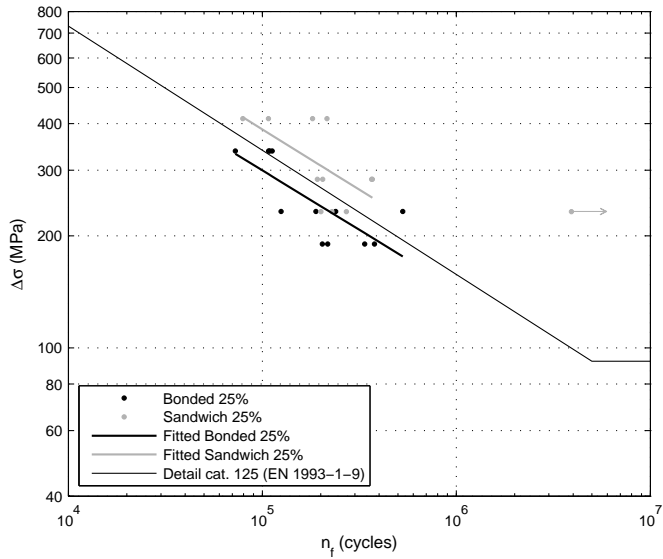
(b) 25% strain fall failure criterium

Figure 7.37: SN fatigue results of the welds at the crossbeam location from the bonded and sandwich steel plate deck specimens for (a) 10% and (b) 25% strain fall failure criteria and comparison with the detail category 125 defined in EN1993-1-9 (2005).

Table 7.10: Equations of the SN curves from the bonded and sandwich fatigue results and from the detail category 125 defined in EN1993-1-9 (R^2 – statistics coefficient of determination).

$\Delta\sigma = k \cdot n_f^{-1/m}$	m		k		R^2	
	10%	25%	10%	25%	10%	25%
Bonded	3.96	3.09	4901	11801	0.43	0.59
Sandwich	3.88	3.13	5869	16023	0.37	0.36
Detail cat. 125 ($n_f < 5 \cdot 10^6$)	3		15749		–	

Table 7.10 shows the results from the linear regression analysis fitted to the fatigue results and compares them with the SN fatigue strength of the detail category 125.

The fatigue results of the welds in the bonded and sandwich reinforced deck follow the same tendency when considering the same fatigue life criterion (slope m 3.9 for the 10% and 3 for the 25%). The fatigue life of the welds in the sandwich reinforced deck is slightly longer than in the bonded reinforced deck. But the R^2 coefficient is higher for the fitted curve of the bonded reinforced deck than for the sandwich reinforced deck (approximately 0.5 and 0.4, respectively). The slope of the fatigue results is closer to the fatigue strength detail category when the 25% strain fall failure criterium is used. In both graphs, the fatigue results are on the area of the fatigue strengths of the 125 detail category, spread above and under this line.

These fatigue results are worse than expected, since the detail category 125 should give a conservative fatigue strength of the fatigue life of these welds. This is related with the fact that, in this study the failure criteria are based on strain falls measured at the bottom side of the deck plate, very close to the weld root. While Kolstein (2007) based his recommendation on strain falls measured at the top side of the deck plate, and therefore farther away from the weld root. As this type of crack initiates at the weld root, the strain measured in this study are much more sensitive to the crack initiating at the weld root than the ones used by Kolstein (2007). Therefore the strain fall occurs earlier in the strain gauges used on this thesis (at the bottom side of the deck plate) than in the ones used by Kolstein (2007) (at the top side of the deck plate).

From extrapolation of these SN curves, one can predict the fatigue life of the welds at any stress range present at the weld root in a bonded or sandwich steel plates reinforced deck. This means that with the stress or strain reduction factor, one can predict the improvement in the fatigue life of the welds just by using the stress reduction factor on these SN curves.

Figure 7.38 shows the fatigue results of the deck-plate-to-stiffener welds at midspan between crossbeams as $\Delta\sigma - n_f$ diagrams (SN-curves), for the bonded and sandwich steel plates reinforced deck specimens. As no fatigue cracks were found at this location, all results are run-out tests. The stress range was determined by the nominal stresses at the deck plate at the stiffener web location. The results are compared with the details category for the fatigue strength of these welds recommended by

Kolstein (2007) (125 detail category) and by EN1993-1-9 (2005) (71 detail category). The results are below the constant amplitude fatigue limit ($\Delta\sigma$ at $n = 5 \cdot 10^6$) of the 125 detail category, which explains the absence of fatigue cracks at this location.
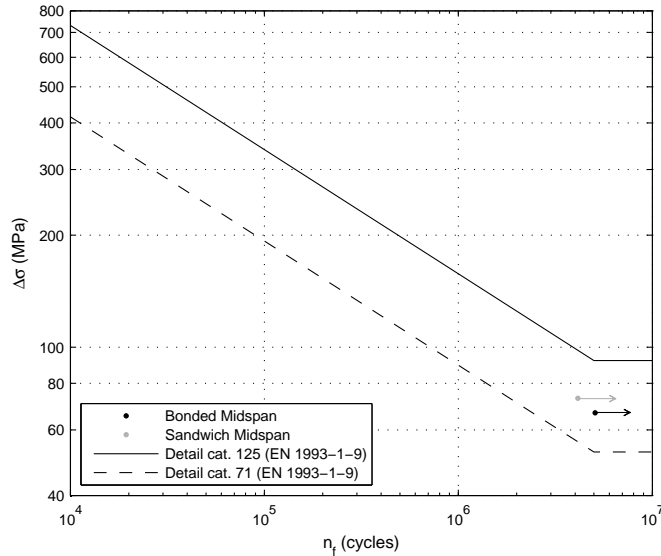

Figure 7.38: SN fatigue results of the welds at midspan between crossbeams location from the bonded and sandwich specimens and comparison with the detail categories defined in EN1993-1-9 (2005).

7.5 Parametric study

In the previous sections, the numerical analysis described in Chapter 6 was validated by experimental values. Once the FEA is validated, they can be used to predict the behaviour of different reinforcement.

In this section, the behaviour of several reinforcement scenarios is simulated using FEA. The orthotropic deck geometry is exactly the same as presented in Chapter 6. The load is 100 kN wheel type C aligned with the middle trough (see Figure 7.8(b), page 119) and positioned either at the crossbeam or at midspan between crossbeams.

The parametric study investigates the influence of the thickness of the reinforcement and of the environmental temperature on the behaviour of the reinforced deck panel. Predictions are made for the stress reduction factors and for the fatigue behaviour of the reinforcements.

7.5.1 Influence of the reinforcement thickness

For the bonded steel plates reinforcement, the influence of the second steel plate thickness was investigated. The adhesive thickness was kept 2 mm, since this is the nominal value to be applied in actual reinforcements. The thickness of the second steel plate was varied between 6 mm and 12 mm.

For the sandwich steel plates reinforcement, the influence of the thickness of the core and of the second steel plate were investigated. The thickness of the core was varied between 15 mm and 30 mm. The thickness of the second steel plate was varied between 5 mm and 8 mm.

The reinforcement weight was used to compare the two types of reinforcement. The combination of thicknesses was chosen to investigate solutions with comparable weights. For all cases studied, the thickness of the existing deck plate is 12 mm.

Tables 7.11 and 7.12 show the studied bonded steel plates reinforcement solutions and the studied sandwich steel plates reinforcement solutions, respectively.

Table 7.11: Bonded steel plates reinforcements.

Reinforcement	Deck plate	Adhesive	2nd steel plate	Weight
B1226	12 mm	2 mm	6 mm	49.4 kg/m^2
B1228	12 mm	2 mm	8 mm	65.1 kg/m^2
B12210	12 mm	2 mm	10 mm	80.8 kg/m^2
B12212	12 mm	2 mm	12 mm	96.5 kg/m^2

Table 7.12: Sandwich steel plates reinforcements.

Reinforcement	Deck plate	Core	2nd steel plate	Weight
S12155	12 mm	15 mm	5 mm	56.5 kg/m^2
S12205	12 mm	20 mm	5 mm	62.3 kg/m^2
S12255	12 mm	25 mm	5 mm	68.0 kg/m^2
S12305	12 mm	30 mm	5 mm	73.8 kg/m^2
S12158	12 mm	15 mm	8 mm	80.1 kg/m^2
S12306	12 mm	30 mm	6 mm	81.6 kg/m^2
S12308	12 mm	30 mm	8 mm	97.3 kg/m^2

Stress reduction factor

The stress reduction factor (SRF) is one of the most important parameter to evaluate the performance of the reinforcements. The SRFs can be used in the SN curves of the fatigue sensitive details to determine how much the fatigue life of the welds will be extended.

The SRF was determined using equation 7.6. The SRF was determined at the four deck locations – see Figure 7.39. The values were determined at the crossbeam location and at midspan between crossbeams.

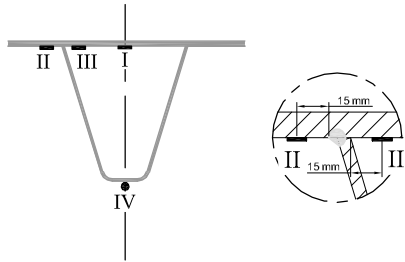$$SRF = 1 - \frac{\sigma_{Reinforced\ deck}}{\sigma_{Unreinforced\ deck}} \tag{7.6}$$

Figure 7.39: Deck locations: stiffener and close to the deck-plate-to-stiffener welds.

Table 7.13 shows the stress reduction factor (SRF) at the crossbeam location of the bonded steel plates solutions. The equivalent values for the sandwich steel plates solutions are shown in Table 7.14. Figure 7.40 plots the relationship between the weight of different reinforcements and their SRF at the crossbeam location.

Table 7.15 shows the stress reduction factor (SRF) at midspan between crossbeams of the bonded steel plates solutions. The equivalent values for the sandwich steel plates solutions are shown in Table 7.16. Figure 7.41 plots the relationship between the weight of different reinforcements and their SRF at midspan between crossbeams.

SRFs higher than 100% occur when the stress value changes the signal from negative to positive, or the other way around, after the reinforcement – see Equation 7.6.

The SRF of details I, II and III gives an indication of the reinforcement performance at the transverse stresses due to local bending of the deck plate. Concerning these details both at the crossbeam and at midspan between the crossbeam, the results show that: increasing the thickness of the second steel plate of the bonded steel plates reinforcement by 2 mm adds on average 6% to the SRFs; each increase of 5 mm of core thickness of the sandwich steel plates adds on average 3% to the SRFs. Increasing the thickness of the second steel plate of the sandwich steel plates from 5 mm to 8 mm adds 7% to the SRFs.

Table 7.13: SRF at the crossbeam of the bonded steel plates solutions (W – weight).

SRF (%)	B1226	B1228	B12210	B12212
I	54%	61%	67%	71%
II	53%	61%	67%	73%
III	60%	68%	75%	80%
W (kg/m^2)	49.4	65.1	80.8	96.5

Table 7.14: SRF at the crossbeam of the sandwich steel plates solutions (W – weight).

SRF (%)	S12155	S12205	S12255	S12305	S12158	S12306	S12308
I	45%	49%	52%	55%	53%	56%	60%
II	43%	46%	50%	52%	52%	54%	59%
III	45%	48%	51%	53%	53%	55%	58%
W (kg/m^2)	56.5	62.3	68.0	73.8	80.1	81.6	97.3

Table 7.15: SRF at midspan between crossbeams of the bonded steel plates solutions (W – weight).

SRF (%)	B1226	B1228	B12210	B12212
I	53%	60%	65%	69%
II	67%	76%	82%	87%
III	88%	98%	105%	111%
IV	19%	23%	27%	30%
W (kg/m^2)	49.4	65.1	80.8	96.5

Table 7.16: SRF at midspan between crossbeams of the sandwich steel plates solutions (W – weight).

SRF (%)	S12155	S12205	S12255	S12305	S12158	S12306	S12308
I	51%	55%	58%	61%	58%	62%	65%
II	53%	56%	59%	62%	63%	64%	69%
III	58%	60%	62%	63%	71%	66%	72%
IV	27%	30%	32%	34%	31%	35%	37%
W (kg/m^2)	56.5	62.3	68.0	73.8	80.1	81.6	97.3
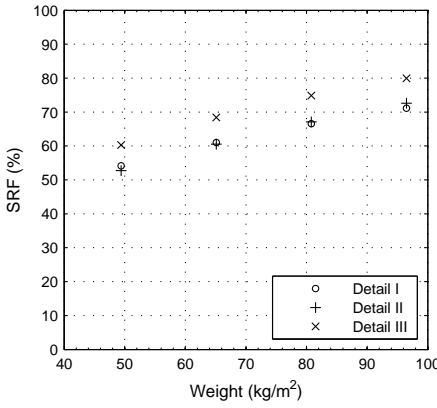
(a) bonded steel plates
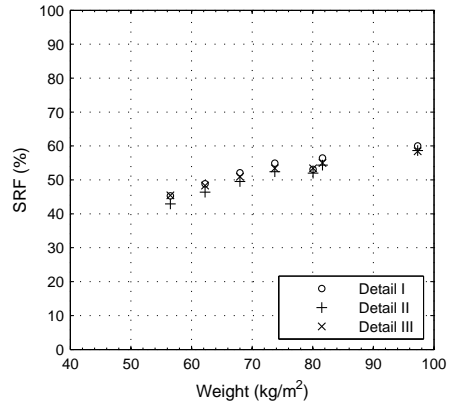
(b) sandwich steel plates

Figure 7.40: Relationship between the weight of different reinforcements and their stress reduction factor (SRF) at the crossbeam location.
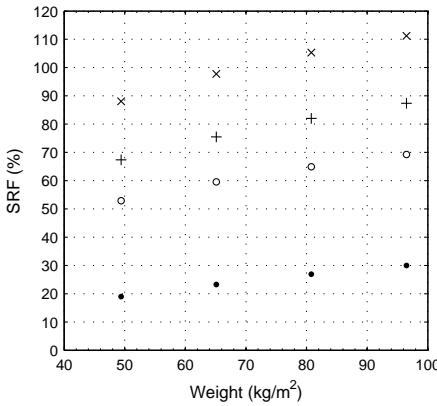
(a) bonded steel plates (for key see Figure (b))
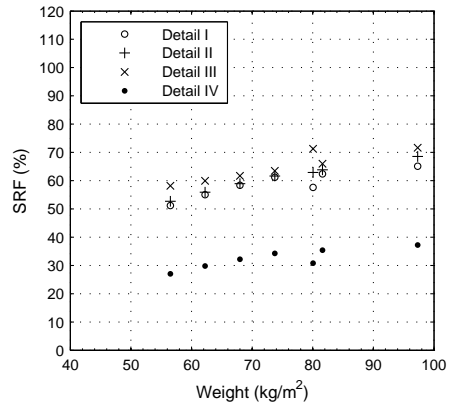
(b) sandwich steel plates

Figure 7.41: Relationship between the weight of different reinforcements and their stress reduction factor (SRF) at midspan between crossbeams.

Comparing two systems with the same weight, for details I, II and III at the crossbeam location, the SRFs are higher when using the bonded steel plates than when using the sandwich steel plates. The sandwich steel plates system can achieve on SRF similar to the ones of the bonded steel plates system but needs double the weight. At midspan between crossbeams, the SRF of details II and III increases

significantly when compared to the ones at the crossbeam location, especially that of detail III of the bonded steel plates. Also at midspan between crossbeams when comparing two systems with the same weight, details II and III have higher SRF in the bonded steel plates system than in the sandwich steel plates system. The SRF of detail I are similar in the sandwich steel plates reinforcement and in the bonded steel plates systems.

For detail IV, the sandwich steel plates system performs better than the bonded steel plates system. This detail gives an indication of the global effect of the reinforcement (longitudinal stress due to global bending of the OBD).

Figure 7.41(b) shows that the SRF of the solution S12158 (80.1 kg/m^2) at midspan between crossbeams is slightly out of the tendency. The overall tendency of the graph gives an idea of the effect of the core thickness, while the S12158 gives an indication of the effect of the second steel plate thickness. The results indicate that this effect is positive for detail III and negative for details I and IV.

Overall, the bonded steel plates reinforcement has a good performance in reinforcing the structure locally, as close to the deck-plate-to-stiffener welds. The sandwich steel plates reinforcement is more a global reinforcement. It affects not only the local stresses, but also the global stresses. The sandwich steel plates reinforcement improves its performance, when the existing steel deck becomes flexible (less stiff), and the bending of the deck becomes stronger. This is the case in detail I and detail IV at midspan between crossbeams.

In general, the SRFs obtained from the bending static tests performed on reinforced beams (described in Chapter 4 and 5) are lower than the ones at the OBD details. This difference is higher for the sandwich reinforcement than for the bonded reinforcement. As mentioned before, this is related to the fact that the stiffness of the existing deck plate amplifies the 'zig-zag' effect of the sandwich steel plates. The existing deck plate is stiffened by the longitudinal stiffeners and by the transverse crossbeams. At beam specimens, the lower steel plate is only a steel plate without any stiffeners.

However, the effect of the reinforcement thickness can be predicted by the beam specimens. Adding 2 mm of second steel plate thickness of the bonded steel plates added 7% to the SRF, which is very close to the effect predicted in the actual OBD. The difference between the SRF of the S12155 and S12305 solutions is also similar between the OBD and beam specimens, approximately 8%.

Fatigue life of the reinforcement

Besides extending the fatigue life of the welds, the reinforcements should not give rise to new fatigue problems. Therefore it is important to evaluate their fatigue life.

In Section 7.4, the full-scale fatigue tests showed no fatigue damage in the reinforcement. Moreover, this behaviour could have been predicted based on the SN diagrams of each reinforcement obtained from the fatigue tests on reinforced beams. The maximum shear stresses in the adhesive layer and in the core present during the

fatigue tests were below the fatigue thresholds of those SN diagrams. In general, in order to predict the fatigue behaviour of different reinforcements, one only needs to evaluate the shear stress field in the interface layers, adhesive or core, and compare it with the corresponding fatigue threshold.

Table 7.17 shows the maximum equivalent shear stress τ_{yeq} at the adhesive layer obtained from the FEA of the bonded steel plates reinforcements. The values correspond with a 100 kN wheel load type C aligned with the stiffener either at the crossbeam location or at midspan between crossbeams. The maximum shear stresses at the steel-core interface of the sandwich steel plates reinforcements are shown in Table 7.18.

Table 7.17: Maximum equivalent shear stress τ_{yeq} at the adhesive layer of the bonded steel plates reinforcement (100 kN load, wheel type C).

τ_{yeq} (MPa)	Crossbeam location	Midspan between crossbeams
B1226	7.95	6.95
B1228	7.63	6.66
B12210	7.14	6.18
B12212	6.61	5.64

Table 7.18: Maximum equivalent shear stress τ_{yeq} at the steel-core interface of the sandwich steel plates reinforcement (100 kN load, wheel type C).

τ_{yeq} (MPa)	Crossbeam location	Midspan between crossbeams
S12155	2.35	2.18
S12158	2.23	1.97
S12205	2.06	1.92
S12255	1.88	1.74
S12305	1.74	1.59
S12306	1.69	1.55
S12308	1.57	1.43

The reinforcement solutions tested on the full-scale fatigue tests, B1226 and S12155 for the bonded and sandwich respectively, have the highest values of shear stress. Therefore, if no fatigue damage was observed during the fatigue tests performed on those reinforcement solutions, no fatigue damage is expected to occur on all the other reinforcements with lower shear stresses.

7.5.2   Temperature effect

The temperature effect was studied by changing the Young's modulus of the adhesive or of the core materials to the corresponding values at -10 °C, room temperature (RT) and +50 °C. The Young's modulus are based on the tensile testing performed on the adhesive and core materials. These tests are described in Chapters 4 and 5 for the adhesive and for the core, respectively. Table 7.19 shows the Young's modulus of both materials at the three temperatures.

The study was performed on three reinforced decks: B1226, S12155 and S12305. The SRFs at the three temperatures were determined for each reinforcement. The SRF was determined at the same deck details I, II, III and IV, as shown in Figure 7.39. The results are shown in Figure 7.42 for the crossbeam location and in Figure 7.43 for midspan between crossbeams location.

Table 7.19: Young's modulus E of the adhesive (B1226) and core (S12155 and S12305) materials.

E (MPa)	-10 °C	RT	+50 °C
Adhesive	3378	2929	2451
Core	1049	721	471

The results show that both at the crossbeam and at midspan between crossbeams, the temperature effect is negligible in all details of the B1226 reinforced deck. These results are in accordance with the ones obtained from the beam specimens described in Chapter 4. In these tests, the temperature did not have any influence on the bending stiffness of the bonded steel plates reinforced beams.

The Young's modulus of the core material of the sandwich steel plates reinforcement has a significant effect on the SRF of details I, II and III. Both at the crossbeam and at midspan between crossbeams, the SRF of these details varies approximately 10% when varying the Young's modulus. In the beam tests described in Chapter 5, the effect of -10 °C was lower (around 2%) and the effect of +50 °C was higher, especially for the S12155 solution (around 15%), when compared to RT.

For detail IV the SRF is less affected by the temperature since the detail is farther away from the temperature-dependent materials.

The temperature effect on the fatigue behaviour of the reinforcements cannot be evaluated. The fatigue tests were all performed at RT and therefore the SN diagrams of the reinforcements are only available at this temperature.
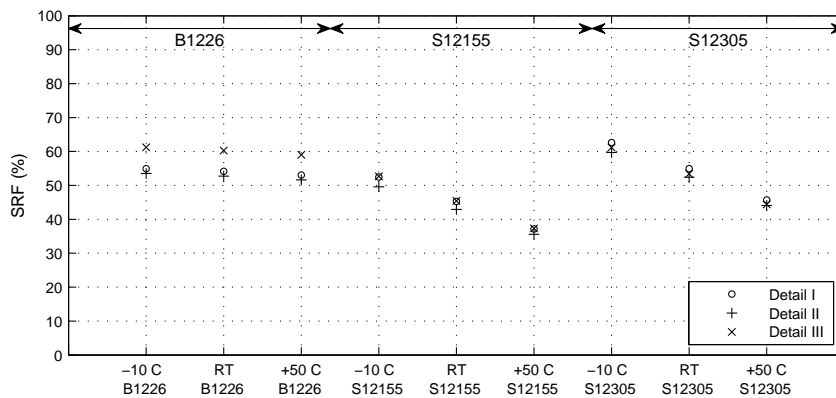
Figure 7.42: Stress reduction factor of details at the crossbeams of B1226, S12155 and S12305 reinforcements at -10 °C, room temperature (RT) and +50 °C.
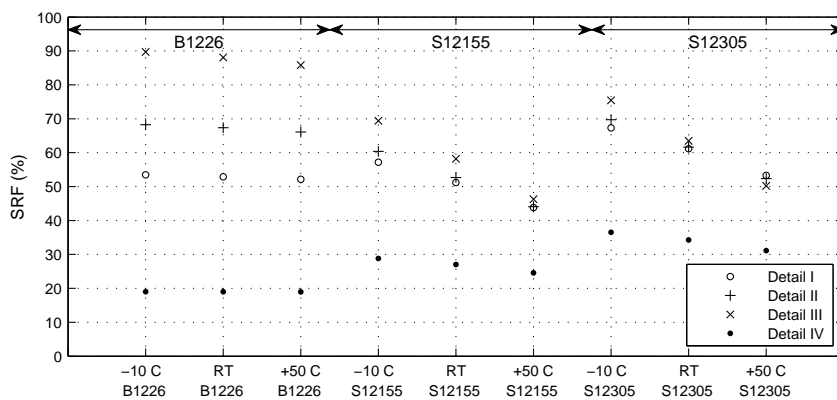

Figure 7.43: Stress reduction factor of details at midspan between crossbeams of B1226, S12155 and S12305 reinforcements at -10 °C, room temperature (RT) and +50 °C.

7.6   Conclusions

The aim of this part of the thesis was to study the effect and the behaviour of the bonded and sandwich steel plates reinforcement systems when applied to the actual geometry of an OBD. The bonded steel plates system consisted of bonding a 6 mm thick second steel plate using a 2 mm thick adhesive layer. The sandwich steel plates system consisted of adding a 5 mm thick second steel using a 15 mm thick polyurethane core. Full-scale tests were performed on both reinforced decks using wheel loads to simulate the heavy traffic loading on a reinforced OBD with a deck plate thickness of 12 mm. The FEA described in Chapter 6 were validated using the experimental data and used to perform a parametric study on the influence of the reinforcement geometry and of the environmental temperature on the reinforcements performance.

The results from the full-scale static tests on the bonded steel plates reinforcement system showed a significant reduction of the transverse stresses at the deck plate close to the deck-plate-to-stiffener welds. The stresses at this deck location were reduced by 50% to 60% at the crossbeam and by 60% to 80% at midspan between crossbeams, after the reinforcement. The longitudinal stresses at the bottom of the stiffener at midspan between crossbeams were reduced by 20% after the reinforcement. During the full-scale fatigue tests, no delamination occurred in the adhesive layer when the reinforced deck was subjected to fatigue wheel loads at the crossbeam and at midspan between crossbeams.

The results from parametric study showed that increasing the thickness of the second steel plate of the bonded steel plates reinforcement by 2 mm adds on average 6% to the SRFs close to the deck-plate-to-stiffener welds. The SRF of the transverse and longitudinal stresses is not expected to be significantly affected by temperatures between -10 °C and +50 °C. Moreover, it also showed that if a second steel plate thickness between 6 mm and 12 mm is used, no delamination is expected to occur in the adhesive layer due to wheel loads.

The results from the full-scale static tests on the sandwich steel plates reinforcement system also showed a significant reduction of the transverse stresses at the deck plate close to the deck-plate-to-stiffener welds. The stresses at this location were reduced by 45% at the crossbeam location and by 55% at midspan between crossbeams, after the reinforcement. The longitudinal stresses at the bottom of the stiffener at midspan between crossbeams were reduced by 30% after the reinforcement. During the full-scale fatigue tests, no delamination occurred between the core and the steel plates when the reinforced deck was subjected to fatigue wheel loads at the crossbeam and at midspan between crossbeams.

The results from parametric study showed that increasing the thickness of core of the sandwich steel plates reinforcement by 5 mm adds on average 3% to the SRF close to the deck-plate-to-stiffener welds. Increasing the second steel plate thickness from 5 mm to 8 mm adds on average 7% to the same SRF. The SRF of the transverse stresses at the deck plate is expected to be affected by temperature between -10 °C and +50 °C. Those values are expected to increase on average 9% at -10 °C and

decrease on average 10% at +50 °C when compared with RT. The temperature effect is lower at the SRF of the longitudinal stresses at the bottom of the stiffener (3%). The parametric study also showed that, if sandwich steel plates solutions with up to 30 mm core thickness and 8 mm second steel plate thickness are used, no delamination is expected to occur between the core and the steel plates due to wheel loads.

Considering reinforcement solutions with approximately the same weight: the bonded steel plates solutions reduce the local stresses close to the welds more than the sandwich steel plates solutions; the sandwich steel plates reinforcement reduces the global stresses more than the bonded steel plates reinforcement. The sandwich steel plates can be considered as a global reinforcement, while the bonded steel plates is more a local reinforcement.

The SRFs of the reinforced OBD are lower than the ones obtained from the beams specimens, especially for the sandwich steel plates reinforcement. This is caused by the amplification of the 'zig-zag' effect due to the high stiffness of the existing deck in comparison with an unstiffened steel plate. Nevertheless, the influence of the reinforcement geometry and temperature effect can be predicted by the beam specimens.

The increase of the fatigue life of the welds can be predicted by determining the SRF at the welds and using it on the SN curves of the same weld detail. The fatigue behaviour of the reinforcements can be predicted by determining the shear stress at the interface layers, adhesive or core, and comparing it with the correspondent fatigue threshold. This value is determined from the beam specimens fatigue tests.

Chapter 8

French five-point bending tests on sandwich steel plates reinforcement

8.1 Introduction

In this Chapter, French five-point bending tests (5pbt) performed on sandwich steel plates reinforcement are described. The aim was to understand if this type of tests can be directly used to evaluate the performance of reinforcement systems for OBD. If that is the case, the French 5pbt can be used for characterizing and optimizing reinforcement systems, avoiding the time and cost of a full-scale experimental program. A trial experimental program was performed on a sandwich steel plates reinforcement solution to assess the viability of performing these tests on other type of reinforcements. A sandwich steel plates solution with 30 mm core thickness and 5 mm second steel plate thickness was used.

The French five-point bending test was developed by the 'Laboratoire Central de Ponts et Chaussées' in the early 80's (Hameau et al., 1981). The aim was to perform a laboratory scale test that would allow studying the fatigue resistance of surfacing layers on orthotropic bridge decks. Hameau et al. (1981) report that the most severe load case for surfacing layers of OBD is when they are subjected to negative moments. This occurs at the alignment of the stiffener web when each of the wheel of a double-tyre is positioned at each side of the web. In the French five-point bending tests, this 'worst-case scenario' is simulated by a small test set-up which includes one 'deck-plate-to-stiffener' weld and therefore, the high stress concentration at this deck location due to the transverse moments caused by wheel loads. Recently, this methodology became a French standard test method (NF-P98-286, 2006). The five-point bending test has been used in several studies. It was recently used for the design of the asphalt surfacing of the OBD of the Millau Viaduct in France (Pouget

et al., 2010). Arnaud et al. (2009) also used French 5pbt to evaluate the resistance of concrete overlays as reinforcement techniques for orthotropic steel bridge decks.

8.2   Specimens

The specimens consisted of 12 mm thick steel plates, reinforced with sandwich steel plates of 30 mm thick core and 5 mm thick second steel plate (S12305). The sandwich beam is stiffened at the centre by a T-stiffener, connected to the bottom surface of the sandwich by two fillet welds. The specimens are 100 mm wide and 850 mm long. Figure 8.1 shows a drawing with the specimens' dimensions including a detail close to the stiffener. The geometry of the specimens is very similar to the one recommended by the French standard NF-P98-286 (2006). The main differences is the width of the specimens. In this study, the specimens are 100 mm wide and in the standard 200 mm is recommended.
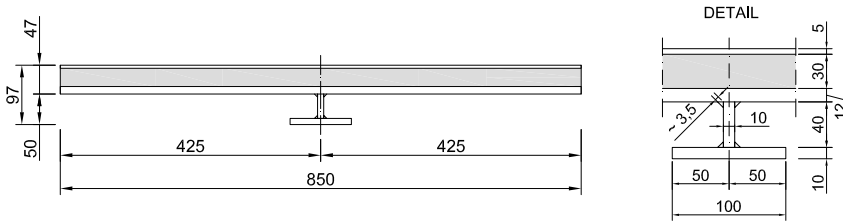
Figure 8.1: Geometry of the specimens (dimensions in mm).

8.3   Experimental procedure

Fatigue tests were carried out on four specimens. According to NF-P98-286 (2006), the fatigue tests should run a minimum of 2 million cycles and, if no fatigue damage occurs, the overlay is suitable to be applied in real orthotropic bride decks.

Figure 8.2 shows a drawing and a photograph of the test set-up. The specimens are clamped at the centre at the bottom of the T-stiffener flange, and simply supported at 270 mm distance from the stiffener. This distance is simulating the distance between stiffeners webs in the actual geometry of an OBD. Two equal pressure loads are applied on each side of the stiffener. Steel plates and rubber layers are used to distribute the load on the top of the specimen. These shoe prints are simulating the double-tyre wheel load.

According to the French standard, the maximum load of the fatigue test should be the one that would cause approximately $\varepsilon = 625\mu$ on the top side of the steel plate at the alignment of the stiffener of a specimen without any overlay. For a 12 mm thick steel plate, this corresponds with a pressure load of 0.72 MPa (Pouget et al.,
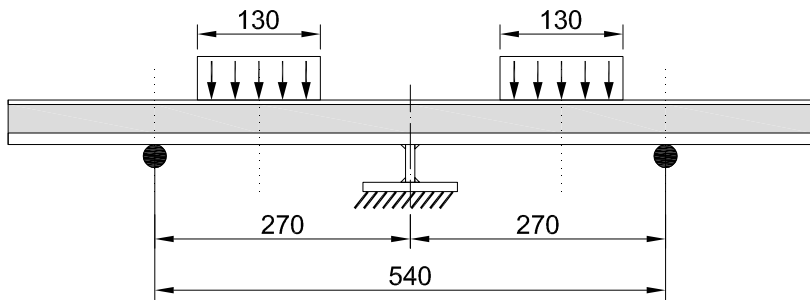
(a)
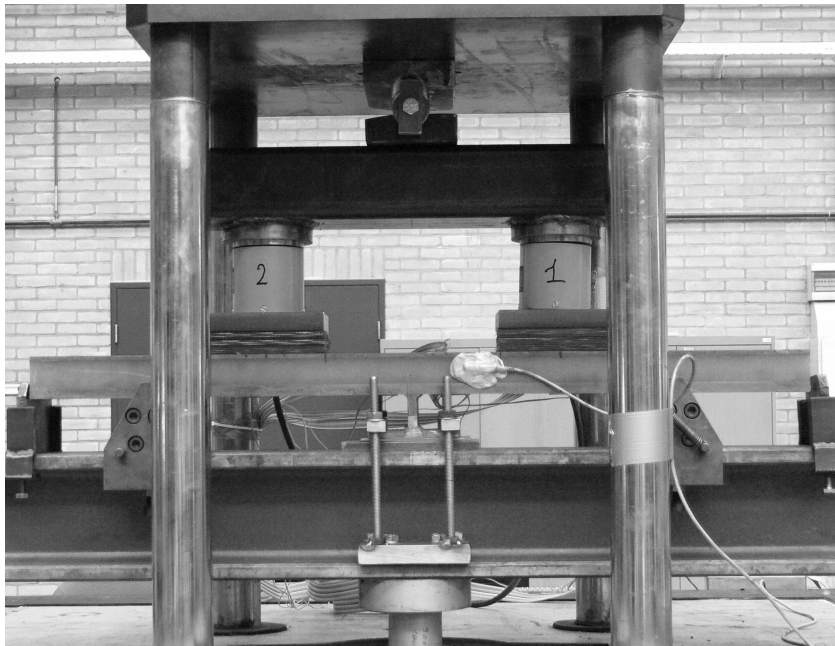
(b)

Figure 8.2: Five-point bending test set-up (dimensions in mm).

2010). In the standard test set-up, the load is applied by two shoe prints, with a length of 130 mm and a width of 200 mm.

In this experimental program, the specimens were 100 mm wide and therefore each shoe print was 130 mm long and 100 mm wide. The pressure load used on these shoe prints was 0.77 MPa, which is slightly higher than recommended by the standard. This pressure load corresponds with 10 kN on each shoe (0.77 MPa x 130 mm x 100 mm), which means a total of 20 kN ($P_{max} = 20$ kN). If the same pressure load of 0.77 MPa is applied on a wheel print type B (double tyre 220 mm by 320 mm), it corresponds with 108 kN wheel load.

All four fatigue tests were performed at the same load level ($P_{max} = 20$ kN). The fatigue tests were carried out in load control with a constant applied load ratio of $R = 0.1$ ($R = P_{min}/P_{max}$). The wave form was sinusoidal with a frequency of 2 Hz. The fatigue tests were performed at room temperature. Prior to the fatigue tests, static tests were performed until a maximum load of 20 kN. The static tests were carried out under load control and with a speed of 0.3 kN/s.

The instrumentation consisted mainly of strain gauges applied to the specimens. The aim was to monitor the strain ranges during the fatigue tests and to validate the numerical simulations using experimental results. A detail of the strain gauges close to the stiffener is shown in Figure 8.3. Temperature sensors were applied to the surface of the polyurethane core to monitor the temperature of this material during testing.

(a)   (b)
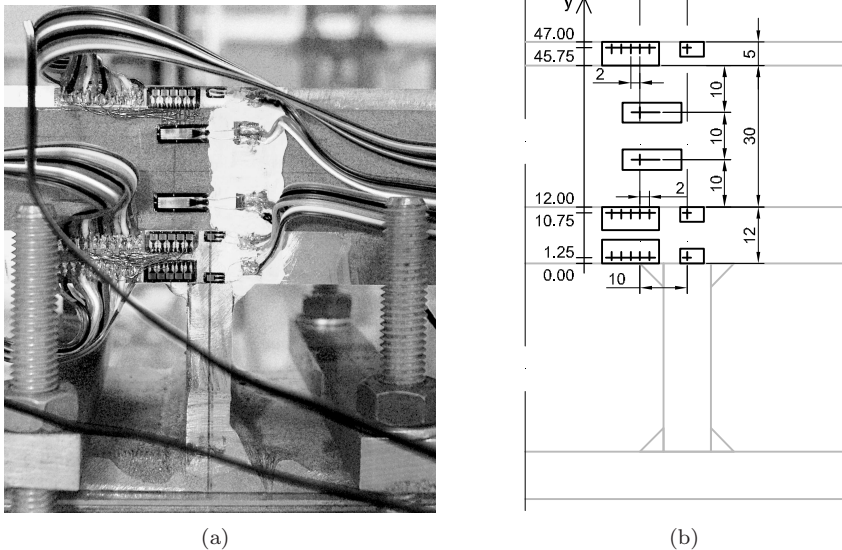
Figure 8.3: Detail of strain gauges in alignment of the stiffener (dimensions in mm).

8.4 Finite element analysis

A finite element analysis (FEA) was made in order to better understand the fatigue results and describe the stress distribution in the specimens.

The analysis simulates the elastic behaviour of the five point bending tests when subjected to static loads. The ABAQUS finite element code was used.

The Young's modulus and Poisson's ratio of all the steel parts are the ones recommended by EN1993-1-1 (2006), $E_{steel} = 210$ GPa and $\nu = 0.3$. The core material properties were defined by the tensile Young's modulus obtained from the material tests at room temperature ($E_{core} = 721$ MPa – see Table 5.3) and by the Poisson's ratio given by the manufacturer ($\nu = 0.36$ – see Table 5.2).

The steel plates, the stiffener and the core were modelled using continuum 20-nodes brick (solid) elements, quadratic (second-order) with reduced integration. These elements are available in the ABAQUS library as C3D20R. Quadratic elements were used in order to avoid problems of shear locking. Shear locking affects the performance of linear elements subjected to bending loads (ABAQUS, 2008). The elements simulating the welds are 15-nodes triangular prism elements, quadratic (second-order) with full integration. These elements are available in the ABAQUS library as C3D15. Full integration is recommended in limited areas of the model where high stress concentration is expected, as is the case for the welds (ABAQUS, 2008).

Figure 8.4 shows the 3D FE-model of the five point bending tests and the mesh zones used in the model. A mesh convergency study was carried out following the same methodology as previously described in Chapter 6. The mesh was refined until the difference in stresses between two refined meshes in the pertinent areas was insignificant (less than 0.5%). Table 8.1 gives the element dimensions (length and thickness) in the several zones of the FE-mesh. The element width is 5 mm for all zones (20 elements per specimen width). The element length was varied according to the expected stress pattern along the length, smaller elements close to the stiffener than at locations far from the pertinent areas. The mesh has 186433 nodes and 42120 elements (41800 C3D20R and 320 C3D15). The maximum aspect ratio of the elements is 5, which is enough to avoid errors due to artificial stiffening.
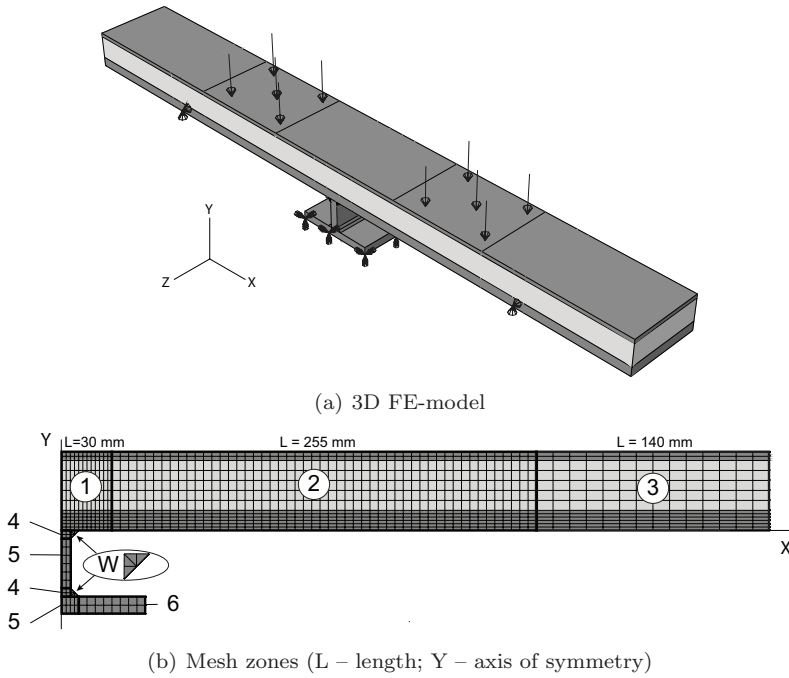
(a) 3D FE-model

(b) Mesh zones (L – length; Y – axis of symmetry)

Figure 8.4: Finite element model of the five point bending tests.

Table 8.1: Dimension of the elements in the mesh zones.

length(x)× thickness(y) (mm)	Zone 1	Zone 2	Zone 3
bottom steel plate	2.5×2	5×2	10×2
core	2.5×6	5×6	10×6
top steel plate	2.5×2.5	5×2.5	10×2.5
length(x)× thickness(y) (mm)	Zone 4	Zone 5	Zone 6
web	2.5×2.5	2.5×5	–
flange	–	2.5×5	5×5
length(x)× thickness(y) (mm)	W		
welds	2.5×2.5		

8.5 Experimental and numerical results

In this section the FEA is compared with the results from the static tests (static behaviour) and fatigue tests' results are presented (fatigue behaviour).

8.5.1 Static behaviour

The static tests were performed before the fatigue tests until a maximum total load of 20 kN. The strains recorded by the strain gauges during the static tests can be compared with the strain predictions from the FEA.

Figure 8.5 shows the longitudinal strains ε_{xx} along the sandwich thickness obtained from the FEA and recorded during static tests (Exp). Figure 8.5(a) shows the strains on the alignment of the stiffener web. Figure 8.5(b) shows the strains on the alignment of the weld toe. The FEA strain distribution is in agreement with the strain values given by the strain gauges during tests.

In both locations, the strains present a 'zig-zag' shape. This is the same effect that was observed in the sandwich beams loaded in short spans (see Figure 5.8, page 74) and in the full scale tests close to the welds between the deck plate and the stiffener (see Figure 7.19, page 135).
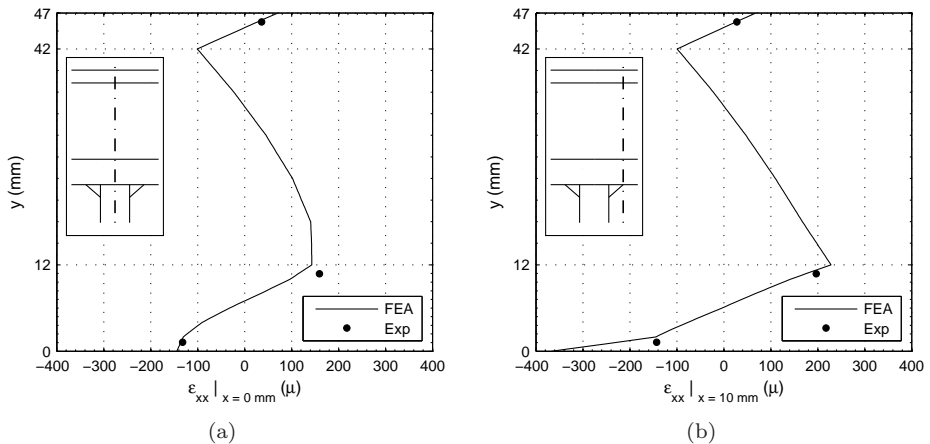
Figure 8.5: Longitudinal strains ε_{xx} along the sandwich thickness (a) on the alignment of the stiffener web (x = 0 mm) and (b) on the alignment of the weld toe (x = 10 mm).

Figure 8.6 shows the longitudinal strains ε_{xx} along the specimen length close to the stiffener, 1.25 mm from the top side of the 5 mm thick steel plate (top plate) and 1.25 mm from the top side of the 12 mm thick steel plate (bottom plate). The strains are plotted at the locations of the strain gauges – see Figure 8.3(b).

The FEA predicts the strain pattern close to the welded stiffener. The FEA predictions are closer to the experimental values in the 5 mm thick steel plate than in the 12 mm thick steel plate. This difference is not so significant if looking to the strain distribution along the thickness in Figure 8.5. Due to the high strain gradient, this difference is amplified when plotting the strain along the length in Figure 8.6. In the 12 mm thick steel plate, the maximum strain occurs close to the weld toe, and the strain values decrease by almost 50% in the vicinity of the stifferner. A similar strain pattern was observed by Hameau et al. (1981) at five-point bending tests of 10 mm thick steel plates without any reinforcement. The maximum strains were also observed close to the weld toe and the strains rapidly decreased close to the stiffener. This strain pattern is not present in the 5 mm thick steel plate. The strains at this plate are much lower than in the 12 mm steel plate and the maximum occurs in the alignment of the stiffener.
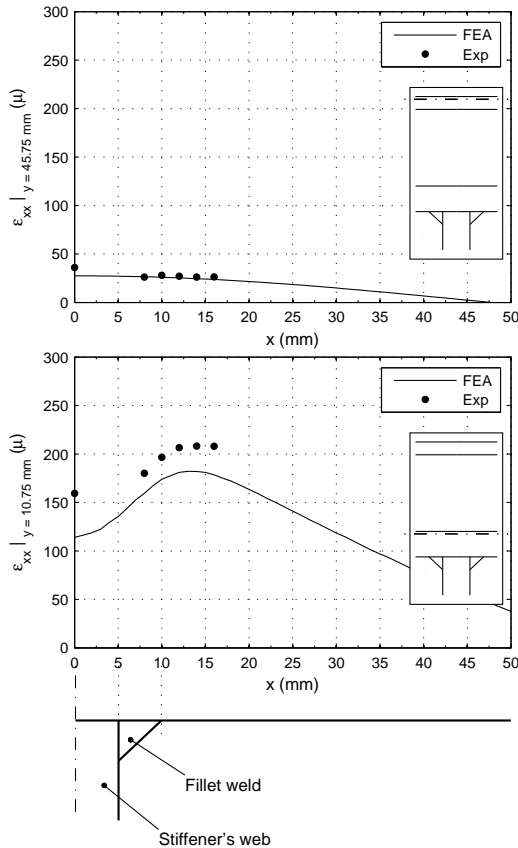
Figure 8.6: Longitudinal strains ε_{xx} close to the stiffener 1.25 mm from the top side of the 5 mm thick steel plate (top plate, y = 45.75 mm) and 1.25 mm from the top side of the 12 mm thick steel plate (bottom plate, y = 10.75 mm).

8.5.2   Fatigue behaviour

Four fatigue tests were performed, all at the same load level. Fatigue failure did not occur in any of the the fatigue tests. The four fatigue tests were stopped after approximately 3 million cycles. The strain values of the strain gauges were continuously recorded during the fatigue tests. Figure 8.7 shows one example of the displacement and strain ranges measured during one of the fatigue tests. The strains were measured by a strain gauge positioned 1.25 mm from the top side of the 12 mm steel plate, close to the weld toe (y = 10.75 mm – see Figure 8.3(b)). In order to monitor the damage of the specimen, the displacement of the piston of the hydraulic jack was also controlled δ_{piston}.
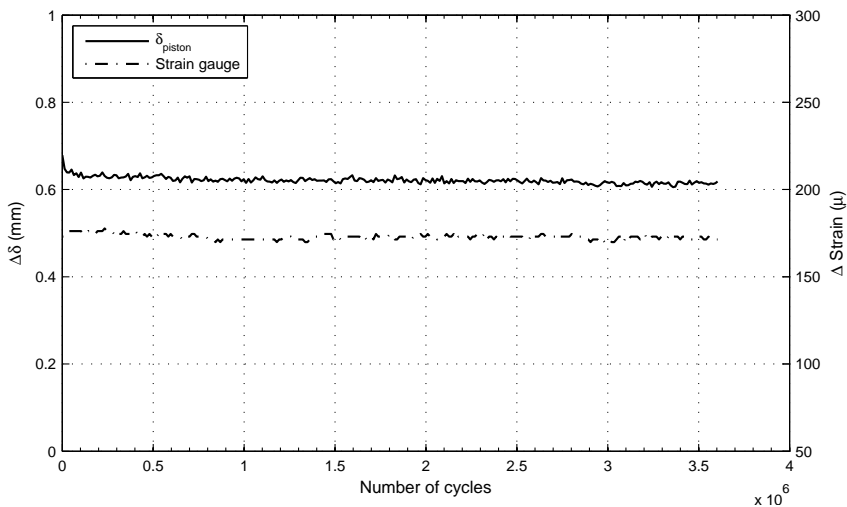
Figure 8.7: Displacement and strain range recorded during the fatigue test of specimen number 2.

There are no significant changes during the entire fatigue test. Also the temperature of the core did not show any significant change during testing. The same was observed in all four fatigue tests that were performed. No visual fatigue damage was observed in any of the four specimens after the fatigue tests. No cracks grew at the welds between the steel plate and the stiffener. No delamination was observed between the core and the steel plates. Table 8.2 summarizes the results of the four fatigue tests performed.

As no fatigue damage occurred in any of the tests, according to the French standard NF-P98-286 (2006) the sandwich overlay is suitable to be applied in real orthotropic bridge decks.

Table 8.2: Results of the five point bending tests.

Specimen	P_{max}	Fatigue life (cycles)
1	20 kN	>3047260 run out
2	20 kN	>3604610 run out
3	20 kN	>3085659 run out
4	20 kN	>3130531 run out

8.6   Discussion

In the previous section, the FEA was validated using experimental data of the static tests. The FEA can now be used to better understand the fatigue results. In this section, the fatigue results are discussed by evaluating the shear stress distribution in the core during the 5pbt and comparing it with the SN diagrams of the reinforcement presented in Chapter 5 and with the full-scale deck panels.

8.6.1   Shear stress distribution in the core

The fatigue analysis presented in Chapter 5 showed that the fatigue failure mode of the sandwich beams starts by delamination at interfaces between the core and the steel plates. Therefore, the fatigue evaluation of the sandwich steel plates reinforcement should use the shear stress at these interfaces.

Figure 8.8 shows the shear stresses distribution in the core during the five-point bending tests given by the FEA. The absolute shear stress distribution τ_{xy} at the core of the sandwich at 20 kN static load is given (by equilibrium $\tau_{yx}=\tau_{xy}$). The maximum shear stress is at the interface between the core and the 12 mm thick steel plate, in the area between the support and the load. The maximum shear stress is approximately 0.74 MPa, for a 20 kN load.

8.6.2   Comparison with SN diagrams

In order to better understand the fatigue results of the 5pbt, the shear stress range at the interface during the fatigue 5pbt should be compared with the SN diagram of the sandwich steel plates reinforcement presented in Chapter 5. This SN diagram was obtained from 4pbt performed on sandwich beams at several stress levels.

In the French 5pbt, the maximum fatigue load was 20 kN (P_{max}) with a load ratio of $R = 0.1$ ($R = P_{min}/P_{max}$), therefore the shear stress range at the interface during the fatigue tests was $\Delta\tau_{core} = 0.74 \cdot 0.9 = 0.666$ MPa ($\Delta P = 0.9 \cdot P_{max}$). Figure 8.9 plots the results from the fatigue five-point bending tests in the SN digram obtained from the beam tests in Chapter 5. The shear stress range at the interface during the fatigue 5pbt is below the fatigue threshold of 4 MPa, obtained from the fatigue tests on the sandwich beams. This is the reason why no delamination was observed at the interface during the fatigue five-point bending tests.

Figure 8.8: Shear stress at the core of the sandwich close at 20 kN static load.

Figure 8.9: SN diagram of the five point bending tests and of the beam tests.

8.6.3   Comparison with full-scale tests

The five-point bending test has been developed to simulate the fatigue loading of an orthotropic bridge deck (OBD). The load case used is wheel type B (double-tyre) positioned at midspan between crossbeams with one load at each side of the stiffener web. In order to understand if this simulation is successful, the stress patterns of the orthotropic deck at this load case need to be compared with the five point bending tests.

As mentioned before, the 20 kN maximum load of the five point bending tests is equivalent to a pressure load of 0.77 MPa (shoe prints: 2 x 130 mm x 100 mm). In order to obtain the same pressure load with an actual wheel print type B (double-tyre: 2 x 220 mm x 320 mm), we have to apply approximately 108 kN wheel load. This is the starting point for comparison between the 5pbt and the full-scale tests.

Figure 8.10 shows the result of the shear stress τ_{xy} at the core of the S12305 sandwich steel plates reinforced deck at midspan between crossbeams when loaded with 108 kN wheel type B at midspan. These stress fields were determined using the FEA described in Chapter 6.

If the stresses at the core of the OBD shown in Figure 8.10 are compared with the same stresses at the core of the five-point bending tests shown in Figure 8.8, it can be observed that they are in reasonable agreement. Their shear stress distribution is similar. In both cases, the maximum shear stress occurs at the interface between the core and the 12 mm thick steel plate. This maximum value occurs between the wheel loads and the supports. However, the maximum shear stress at the core of the OBD
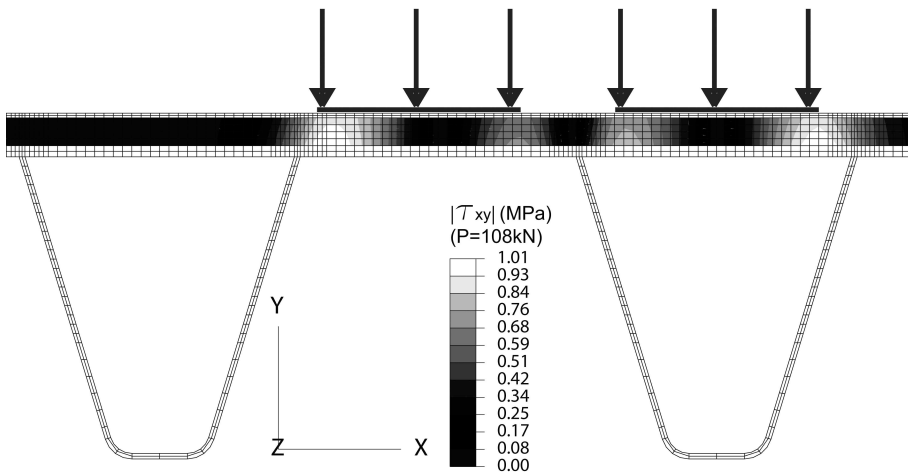
Figure 8.10: Shear stress τ_{xy} at the core of the S12305 sandwich steel plates reinforced deck at midspan between crossbeams when loaded by 108 kN wheel type B at midspan.

is 1.01 MPa and at the five point bending tests is 0.74 MPa (see maximum values of τ_{xy} in Figures 8.10 and 8.8, respectively). Therefore, the shear stress level is lower at the five point than at the OBD, with comparable pressure load levels of wheel prints. This might be related to the fact that the distance between the supports and the edge of the wheel loads is higher on the five-point than on the real load situation. On the five point this distance is 70 mm (270 mm support span for 130 mm load) and in the OBD it is approximately 40 mm (300 mm support span for 220 mm load). Overall, the 5pbt gives a good indication of the stress pattern of an OBD loaded at midspan between crossbeams using a wheel print type B (double-tyre).

This is the worst load case for surfacing layers of OBD (Hameau et al., 1981). However, this is not the case for the reinforcement systems studied in this thesis. Figures 7.21 (page 138) and 7.22 (page 139) showed that for both bonded and sandwich steel plates systems, the wheel print type C causes higher shear stresses at the interface layer than the wheel print type B. Moreover, this shear stress is higher if the OBD is loaded at the crossbeam location than if it is loaded at midspan between crossbeams. Hence, the five point bending tests do not simulate the worst load case for the fatigue damage of the interface layer, neither for the bonded nor for the sandwich steel plates systems.

8.7 Conclusions

Five-point bending static and fatigue tests were performed according to the French standard NF-P98-286 (2006) on S12305 sandwich steel plates reinforcement (12 mm steel plate + 30 mm PU core + 5 mm steel plate). The static strain distribution along the sandwich thickness close to the welded stiffener presents the same 'zig-zag' shape as observed in the sandwich beams and in the full-scale deck panels close to the deck-plate-to-stiffener weld. The peak of maximum strain on the 12 mm steel plate occurs close to the weld toe and decreases significantly in the vicinity of the stiffener web. During the four fatigue tests performed, no visual fatigue damage was observed. According to the French standard, this result indicates that the sandwich overlay is suitable to be applied in real orthotropic bride decks.

The five-point bending fatigue tests give a good indication of the shear stress distribution at the interface layer when the OBD is loaded at midspan between crossbeams by a wheel print type B (double-tyre). This is important taking into account that it is a promising test set-up to replace the fatigue full-scale tests, which are costly, limited and time consuming.

The five-point bending test simulates only one load case, the wheel print type B at midspan between crossbeams. However, this is not the worst load case for the fatigue damage of the interface layers of bonded and sandwich steel plates systems. For these reinforcements, the worst load case occurs when the OBD is loaded at the crossbeam with wheel print type C (super-single).

Therefore, the five-point bending test, as it is defined in the French standard NF-P98-286 (2006), should not be used to evaluate the fatigue behaviour neither of the

sandwich nor of the bonded steel plates systems.

Future works should improve the test set-up to obtain better agreement with the actual structure and to be able to simulate not only one but also alternative load cases that can lead to more severe fatigue damage in the reinforcement systems.

Part III

Monitoring of a reinforced orthotropic bridge

Chapter 9

Structural monitoring of the reinforced Scharsterrijn bridge *

9.1 Introduction

This chapter presents the results of the structural monitoring performed during the renovation of the Scharsterrijn bridge. The renovation consisted of repairing the existing fatigue cracks and strengthening the movable orthotropic steel deck using the bonded steel plates reinforcement system. This was the first time that this reinforcement was applied on a real bridge. Structural monitoring was carried out in order to evaluate the short- and long-term performance of the strengthening system on a real application.

9.2 Structural monitoring

Structural monitoring is essential in the assessment of the actual structural condition and performance of a fatigue cracked steel bridge. Through the strain data obtained from bridge monitoring, one can better understand the actual behaviour of the bridge, the actual stresses and stress distribution during normal traffic conditions (DeWolf et al., 2002; Farhey, 2005). The real input, obtained from structural monitoring, has been used for several applications, such as validation of bridge design models (Leander et al., 2010) or predicting the fatigue life of steel bridges based on their real strain history (Guo et al., 2008; Li et al., 2003).

---

*This chapter is based on Teixeira de Freitas et al. (2012b).

187

Structural monitoring is also very important to decide whether or not renovations are required (Cardini and DeWolf, 2009; Sartor et al., 1999) and, if so, to evaluate their performance, as it has been done in the present study (Guo and Chen, 2011; Lee et al., 2007). Long-term continuous health monitoring gives the possibility to predict when, where and how the failure might occur. Due to the high instrumentation costs, the decision for long-term monitoring is only justified for bridges with significant interest to research the performance of innovative technologies, such as this new type of strengthening system (Farhey, 2005).

In the present study, the monitoring consisted of two stages, a short-term measurements campaign, immediately before and after applying the reinforcement, and a long-term measurements campaign, during the year after the reinforcement. Strain data at the deck plate was recorded during controlled load tests and during normal traffic conditions. The aim was to determine the reinforcement effect on reducing the strains at the bridge deck and to detect changes in the strain data due to degradation of the strengthening system. The goal was to evaluate the short and long performance of the reinforcement system and to decide about further applications.

The monitoring was carried out by the Stevin Laboratory of the Faculty of Civil Engineering and Geosciences at the Delft University of Technology by order of Takke LSBV Brugdekken VOF. Takke LSBV Brugdekken VOF was commissioned by the Ministry of Transport and Public Works in the Netherlands to carry out the complete renovation of the orthotropic deck of the movable bridge Scharsterrijn.

9.3   Description of Scharsterrijn bridge and renovation technique

The Scharsterrijn bridge is located in Friesland, a northern province of the Netherlands. The bridge was built in 1970. After periodical inspections, fatigue cracks were observed around the year 2000. The decision of renovating the movable orthotropic deck of the bridge was taken in 2008 and the renovation took place in March 2009.

The bridge is composed of two independent bridges (one per traffic direction) and each one with a fixed and a movable part. Figure 9.1 shows a picture of the movable part of Scharsterrijn bridge that was repaired (open position). Figure 9.2 shows a drawing of the typical cross-section of the movable orthotropic steel deck. The main girders of the movable bridge have a total span of 8300 mm. The bridge deck consists of an orthotropic steel plate of 12 mm thickness, stiffened by 'U-shape' longitudinal stiffeners of 6 mm thickness and 4 transverse crossbeams distanced 2530 mm.

The strengthening system consisted in bonding a second steel plate on the heavy traffic lane of the movable bridge with the North traffic direction (Lemmer to Joure). Figure 9.3 shows a schematic plan view of the movable Scharsterrijn bridge including the second steel plate position. The second steel plate was 6 mm thick, 4200 mm wide and 8200 mm long. The bonding layer was 2 mm thick and made of Epikote resin EPR 04908 with hardener Epikure curing agent EPH 04908.

Figure 9.1: Picture of the movable deck of Scharsterrijn Brigde.
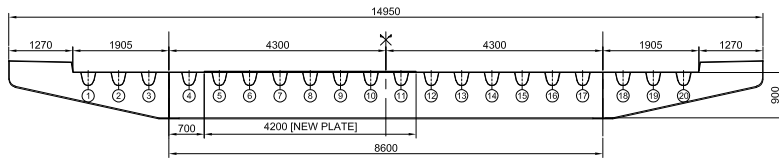
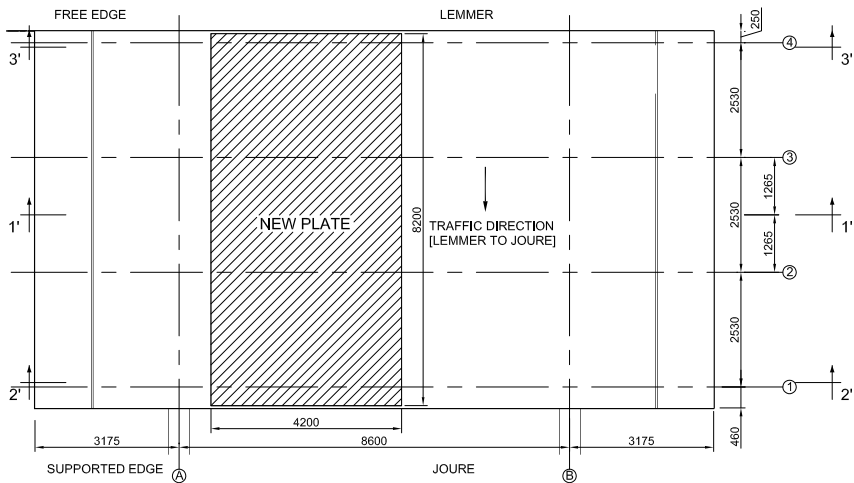Figure 9.2: Cross-section of the movable orthotropic deck (dimensions in mm).

Figure 9.3: Plan view of the movable orthotropic deck and new plate position (dimensions in mm).

The reinforcement procedure was very similar to what has been described up to now for the bonded steel plates reinforcement. The renovation consisted of the following chronological steps: (1) remove the existing wearing course; (2) examine the bridge deck for existing cracks; (3) repair cracks if needed; (4) grit blast the steel top surface of the existing deck plate (Sa 2 1/2 – ISO-8501 (2007)) followed by primer application; (5) glue steel spacers of 2 mm thickness to the deck plate; (6) place the new steel plate in the correct position above the steel spacers; (7) prepare the cavity between steel plates to create vacuum; (8) vacuum inject the adhesive into the cavity; (9) cure during 16 hours between $40\,^{\circ}\mathrm{C}$ to $50\,^{\circ}\mathrm{C}$ temperature; (10) place the new wearing surface on top of the new steel plate.

9.4   Monitoring plan

A monitoring plan was carried out on the movable orthotropic bridge deck to evaluate the performance of the strengthened deck. The monitoring plan included short-term and long-term measurements.

The short-term measurements were carried out immediately before and after the renovation. Strain values were recorded from controlled static load tests and strain history measurements were recorded from the normal traffic running on the bridge. The goal is to evaluate the short-term structural performance of the renovation.

The long-term measurements were carried out during one year, starting immediately after the renovation. Controlled dynamic load tests were carried out once every month and strain history measurements were recorded continuously. The goal is to evaluate the durability of the renovation.

9.4.1   Instrumentation

The instrumentation consisted of applying strain gauges to the orthotropic bridge deck. Strain gauges were applied to three transversal cross-sections of the movable deck, one at the middle of the deck, referred to as the Middle-span cross-section (Figure 9.3 - cut 1-1'), one at the beginning of the deck, referred to as the Lemmer cross-section (Figure 9.3 - cut 3-3') and finally one at the end of the deck, referred to as the Joure cross-section (Figure 9.3 - cut 2-2'). The short-term monitoring was carried out at the Middle-span cross-section. The long-term monitoring was carried out at all three cross-sections.

Two strain gauges were placed unattached to the bridge deck and they were used as witness strain gauges. Their strain data is used as reference to compare with the strain data from the deck plate. The witness strain gauges record strain variation due to temperature effects caused by thermal cycles. They also record irregular occasional peaks caused by external interference. The strain data from the deck plate was corrected based on these witness measurements (peaks and temperature

effects are removed). This procedure has proven to be extremely important for long-term monitoring in order to better understand changes in continuous data (Farhey, 2006).

Middle-span cross-section

Sixteen strain gauges were applied to the middle-span cross-section. They were applied close to the right wheel track (traffic direction) and to different deck details in order to determine the stress reduction at different orthotropic deck details. The positions of the 16 strain gauges are shown in Figure 9.4. The strain gauges close to the deck-plate-to-stiffener welds (2, 3, 5, 6, 8, 9, 11 and 12) measured transverse strains 15 mm from the weld toe – Figure 9.5. The strain gauges 1, 7 and 13 measured transverse strains at middle span between stiffener webs. Strain gauges 43 and 44 are at the same position as 1 and 7, respectively, but measuring longitudinal strains. Strain gauges 4, 10 and 14 measured longitudinal strains at the bottom of the stiffeners.

The strain data from the middle-span cross-section was used to determine the stress reduction immediately after the deck's strengthening.
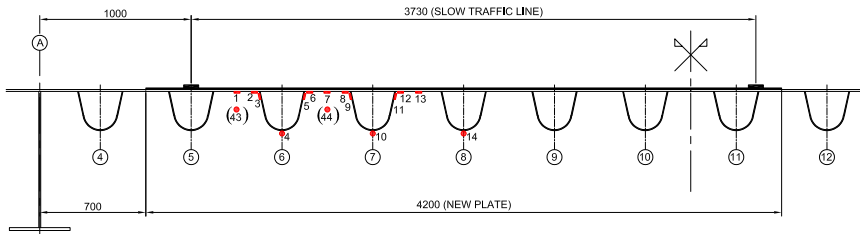
Figure 9.4: Middle-span cross-section: plan view and transverse cut of strain gauges positions 1 to 14, 43 and 44 (dimensions in mm).
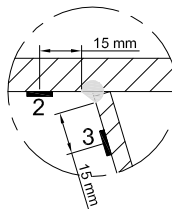
Figure 9.5: Strain gauges positions close to the deck-plate-to-stiffener welds.

Joure and Lemmer cross-sections

In the long-term, the critical points of the strengthening system are at the longitudinal edges of the new steel plate, at the beginning and at the end of the deck. High stress levels at the adhesive layer are expected where the end of the second steel plate meets the crossbeam location (stiffer deck plate). If degradation of the strengthening system due to delamination of the adhesive layer occurs it will most probably start there. Therefore, for the long-term monitoring, strain gauges were applied at the beginning (Lemmer cross-section) and at the end (Joure cross-section) of the strengthened deck. They measured only strains at the deck plate because these were expected to be the most sensitive to the strengthening performance. The strain gauges were positioned at the normal traffic wheel track, both left and right, where high strains are expected due to the wheel loads.

Figure 9.6(a) shows the 15 strain gauges that were applied on the Joure cross-section. The strain gauges close to the deck-plate-to-stiffener welds (16, 18, 19, 21, 22, 24, 25 and 27) measured transverse strains 15 mm from the weld toe, as shown in Figure 9.5. Strain gauges 17, 20, 23 and 26 measured transverse strains at the midspan between stiffener webs. Strain gauges 15 and 28 measured transverse strains 50 mm from the end of the new plate. Strain gauge 45 is at the same position as strain gauge 17 but measuring longitudinal strains. All 15 strain gauges were distanced 100 mm from crossbeam 1 (see Figure 9.3).

Figure 9.6(b) shows the 16 strain gauges which were applied on the Lemmer cross-section. The strain gauges positions are very similar to those in the Joure cross-section. The strain gauges close to the deck-plate-to-stiffener welds (30, 32, 33, 35, 36, 38, 39, and 41) measured transverse strains 15 mm from the weld toe. Strain gauges 31, 34, 37, and 40 measured transverse strains at the midspan between stiffener webs. The strain gauges 29 and 42 measured transverse strains 50 mm from the end of the new plate. Strain gauges 47 and 48 are at the same position as strain gauges 31 and 34, but measuring longitudinal strains. Overall, the strain gauges were distanced 100 mm from crossbeam 4, except 39, 40 and 41, which were 200 mm and 33, 34, 35 and 48, which were between the crossbeam 4 and the free edge of the bridge.
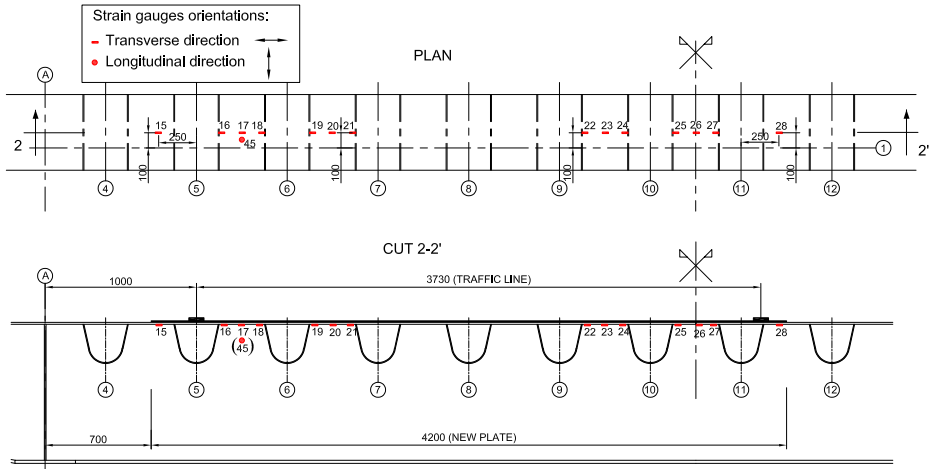
(a) Joure cross-section (strain gauges 15 to 28 and 45)
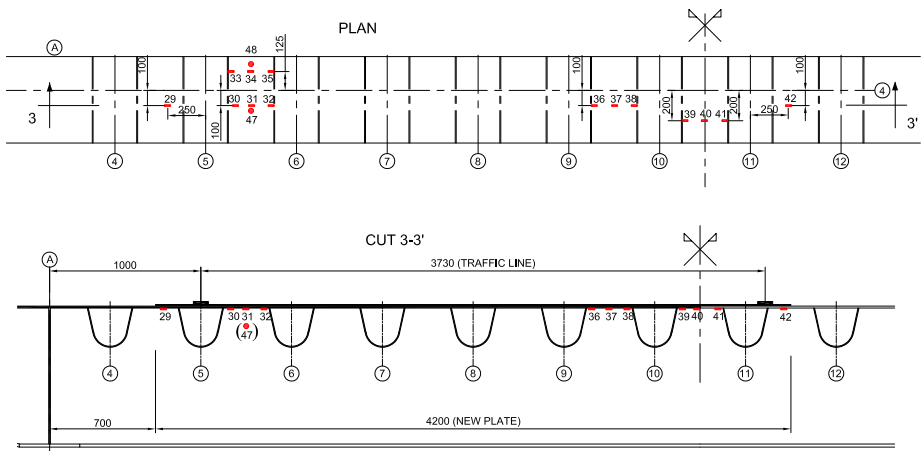
(b) Lemmer cross-section (strain gauges 29 to 42, 47 and 48)

Figure 9.6: Plan view and transverse cut of strain gauges positions at Joure and Lemmer cross-sections (dimensions in mm).

9.4.2   Controlled load tests

Static and dynamic load tests were performed during the structural monitoring. The tests were carried out using a calibrated truck.

Static loads

Static strains were recorded when the calibrated truck was positioned at stationary load configurations. The tests were carried out at the Middle-span cross-section, immediately before and after the renovation. No traffic was running on the bridge during the tests.

The truck was placed on 15 different positions along the same cross-section of the deck. The positions were distanced 150 mm, hence a total length of 2100 mm was covered during testing. Figure 9.7 shows the 15 positions of the truck. The positions refer to the left wheels of the truck axles. The wheel positions were controlled by visual observation and using laser equipment. The x-axis measured the distance from the beginning of the traffic line to the reference point of the wheel loads, which is is the middle of the single-tyre and the middle of the left double-tyre (see Figure 9.7).

The calibrated truck was a four axle lorry, with one axle at the front with single-tyres and three axles at the rear with double-tyres. Figure 9.8 shows a truck silhouette pointing out the front and rear axles used for the static tests and respective axle loads (axle loads=2·wheel loads). The front axle was used to perform the single-tyre load case and the heaviest rear axle was used to perform the double-tyre load case. At each deck condition (renovated and non-renovated) four static tests were carried out, two tests using the single-tyre and two tests using the double-tyre. Exactly the same tests (same positions and same calibrated truck) were performed before and after the renovation, hence eight tests in total were performed, four tests before the renovation plus four tests after the renovation. The wheel loads and wheel prints used in each test are shown in Table 9.1.

The wheel loads can be compared with the set of standard lorries defined at the Fatigue Load Model 4 of Eurocode 1 (EN1991-2, 2003) used for the fatigue calculations of bridges. The single-tyre wheel load, 37.75 kN on average, is slightly heavier than the 35 kN standard (70 kN front axle load). The double-tyre wheel load, 37.5 kN on average, is lighter than the minimum standard, 45 kN (90 kN rear axle load). The single-tyre and the double-tyre have approximately the same load.

The wheel prints are the load area of the wheel (contact area of the wheel with the deck plate). The area of the wheel prints is 864 cm^2 for the single-tyre and 972 cm^2 for the double-tyre. These wheel prints are in accordance with the classification given by the same Fatigue Load Model 4. The single-tyre is comparable with the wheel print type C (270 mm width and 320 mm length) and the double-tyre is comparable with the wheel print type B (540 mm width and 320 mm length). The axle spacing and the transverse distance between wheels are in accordance with the values of the same standard load model.
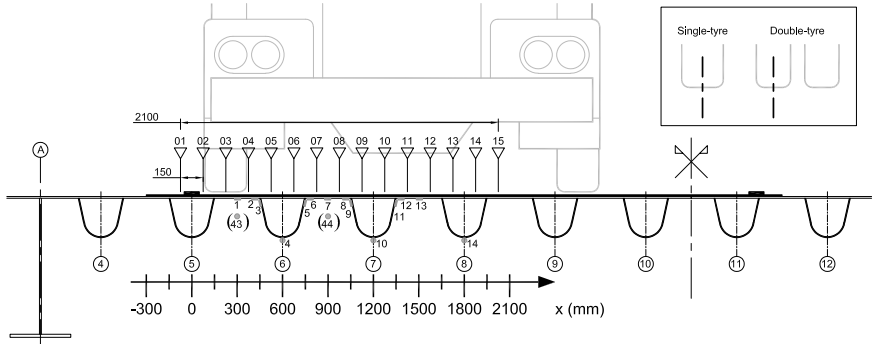
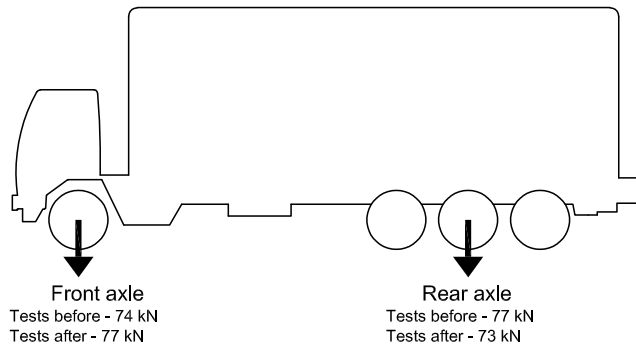Figure 9.7: Fifteen truck positions at the Middle-span cross-section and the reference x-axis (dimensions in mm).

Figure 9.8: Axle loads of the calibrated truck used for the static test before and after the renovation (axle loads=2·wheel loads).

Load case	Wheel Loads		Wheel Prints		Distance between	
	Before	After	Width	Length	Wheels	Axles
Single-tyre (Front axle)	37 kN (Tests 1 and 2)	38.5 kN (Tests 5 and 6)	270 mm	320 mm	2155 mm	5320 mm
Double-tyre (Rear axle)	38.5 kN (Tests 3 and 4)	36.5 kN (Tests 7 and 8)	620 mm	180 mm	1830 mm	

Table 9.1: Calibrated truck used in the static tests.

Dynamic loads

Controlled dynamic load tests were carried out once every month over a period of one year, starting immediately after the renovation. Dynamic strain values were triggered when the calibrated truck crossed the movable bridge. On each 'test-day' of the month, eight tests were performed. Up to September 2009, the tests were carried out at the same transverse position. After analysing the data, this truck position showed to be outside the relevant measuring area of the deck, causing insignificant strain values at the strain gauges positions. Therefore the results up to September 2009 are not presented. After September 2009, the tests were performed varying the transverse position of the calibrated truck. This procedure allowed covering different deck details and determining the dynamic stress influence lines of the deck plate. The calibrated truck transverse position was recorded using laser equipment positioned at the side of the bridge. The speed of the calibrated truck was, in all cases, approximately 80 km/h. The calibrated truck was a four axle lorry similar to the one shown in Figure 9.8, with an extra coupled three axle trailer. Table 9.2 lists the wheel loads. The deviation between wheel loads, in the different dynamic tests, is less than 5%.

Dynamic Tests		Wheel Loads (kN)						
			Truck			Trailer		
number	Month	Front Wheel (single-tyre)	Rear Wheels (double-tyre)			Rear Wheels (double-tyre)		
7	Sept 2009	38.0	19.5	33.5	20.5	51.0	52.5	53.5
8	Oct 2009	37.0	19.5	34.0	20.0	49.0	53.0	57.0
9	Nov 2009	37.0	20.0	34.0	20.5	51.0	53.5	58.0
10	Dec 2009	38.0	20.5	35.0	20.5	49.0	50.5	58.5
11	Feb 2010	38.5	20.5	32.5	20.0	47.5	53.5	57.0
12	Mar 2010	38.5	20.5	33.0	20.0	49.5	54.5	58.5
13	April 2010	36.5	19.0	34.0	20.0	53.0	55.0	57.0

Table 9.2: Calibrated truck used in the dynamic tests.

9.4.3   Strain history measurements

Strain history measurements were recorded continuously under normal traffic conditions at all strain gauges applied to the bridge deck. The strain values recorded correspond with the successive maximum and minimum values caused by each axle load crossing the bridge. From these measurements, stress spectra for each strain gauge can be derived using cycle counting methods.

Strain history measurements were used on the short-term monitoring for comparison of the stress spectrum before and after the renovation and on the long-term monitoring for detecting changes in the stress spectrum over the period of one year.

9.5   Results and analysis

The results and analysis of the strain data were gathered in five main groups, each group represents a typical detail of an orthotropic steel bridge deck. Figure 9.9 shows a drawing where the four groups are defined. Table 9.3 gives the list of strain gauges included in each group of results, at the three cross-sections, Middle-span, Joure and Lemmer (see Figure 9.4, page 191 and Figure 9.6, page 193).

Group I gathers the results from the transverse strains at the deck plate between stiffeners webs. Group II gathers the results from the transverse strains close to the deck-plate-to-stiffener weld toe at the deck plate side. Group III gathers the results from the transverse strains close to the deck-plate-to-stiffener weld toe at the stiffeners side. This group contains only strain gauges from the Middle-span cross-section. Group VI gathers the results from the longitudinal strains at the bottom of the stiffener. Also this group contains only strain gauges from the Middle-span cross-section. Finally Group V gathers the results from the longitudinal strains at the same position as Group I, such as for example strain gauges 43 and 44 at the Middle-span cross-section.
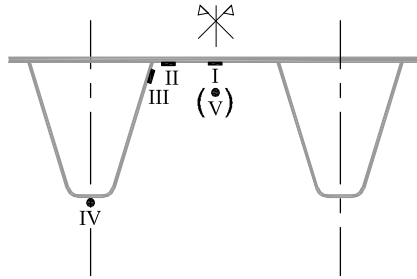
Figure 9.9: Groups of strain gauges according to the deck detail.

Table 9.3: Strain gauges' groups.

Group	Middle-span	Joure	Lemmer
I	1, 7, 13	17, 20, 23, 26	31, 34, 37, 40
II	2, 6, 8, 12	16, 18, 19, 21, 22, 24, 25, 27	30, 32, 33, 35, 36, 38, 39, 41
III	3, 5, 9, 11	—	—
IV	4, 10, 14	—	—
V	43, 44	45	47, 48

9.5.1   Short-term monitoring

On the short-term monitoring, static influence lines and stress spectra were determined to evaluate the immediate performance of the strengthening system. The measurements were recorded for the strain gauges applied at the Middle-span cross-section (see Figure 9.4).

Static Influence lines

Strain data from the controlled static load tests was used to determine static influence lines due to wheel loads.

Figure 9.10 shows one example of the strain influence lines that can be determined from one strain gauge. Figure 9.10(a) shows the results of the single-tyre load case (Tests 1 and 2 of Table 9.1) and Figure 9.10(b) of the double-tyre load case (Tests 3 and 4 of Table 9.1). The results shown are from strain gauge number 7 and were measured before the renovation.

The results of the single-tyre load case are less scatter than of the double-tyre. This might be related to the fact that the exact position of the rear axle (double-tyre) is more difficult to control than that of the front axle (single-tyre). Deviations of few millimetres from the intended tyre positions can lead to significant differences in strain values. This indicates that transverse strains at the deck plate are mainly caused by local loads (wheels) rather than global loads (truck).

(a) Single-tyre (37 kN)   (b) Double-tyre (38.5 kN)
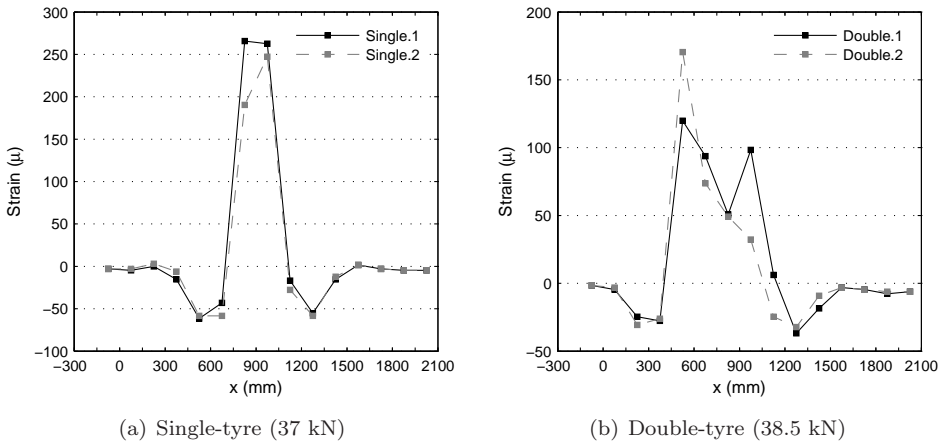
Figure 9.10: Strain influence lines of strain gauge number 7 before the renovation, for repeated tests using (a) single-tyre and (b) double-tyre.

Figure 9.11 compares, for each group, the strain influence lines due to single-tyre and due to double-tyre. Each graph shows the results of one representative strain gauge of the group.

There are two main differences between the two load cases, firstly the wheel prints, which are bigger on the double-tyre than on the single-tyre, and secondly the load configuration, which is one single load on the single-tyre and two loads side by side on the double-tyre. The wheel loads between the two load cases are comparable (37 kN and 38.5 kN).

Figure 9.11(a) shows the results of Group I (transverse strains at midspan between stiffeners), represented by strain gauge number 7 (see Figure 9.7). In the single-tyre load case, the maximum strain is reached when the load is aligned with the strain gauge ($x = 900$ mm). The results from the double-tyre load case show two peaks, the first ($x \approx 500$ mm) when the right double-tyre is approximately aligned with the strain gauge and the second ($x \approx 1000$ mm) when the left double-tyre is approximately aligned with the strain gauge. Note that the reference point for the double-tyre load case is the middle of the left tyre (see Figure 9.7). The strains are considerably lower when using the double-tyre than when using the single-tyre. This has to do with the fact that the individual tyre load is higher on the single-tyre than on each of the two double-tyres.

Figure 9.11(b) shows the results of Group II (transverse strains close to the deck-plate-to-stiffener weld toe at the deck plate side), represented by strain gauge number 8 (see Figure 9.7). The single-tyre load case presents two peaks of compressive strain, one before and one after the strain gauge ($x \approx 800$ mm and $x \approx 1250$ mm). The double-tyre load case presents three peaks, first ($x \approx 500$ mm) when the right double-tyre is before the strain gauge, second ($x \approx 800$ mm) when the strain gauge is just in between the tyres and finally a third when the left tyre is after the strain gauge ($x \approx 1250$ mm). For $x \approx 800$ mm the double-tyre leads to higher strains than the single-tyre because of its load configuration, with one load on each side of the weld. For $x \approx 1250$ mm the single-tyre leads to higher strains because, at this location, the left double-tyre is the only one affecting the strain and it has considerably less load than the single-tyre.

Figure 9.11(c) shows the results of Group III (transverse strains close to the deck-plate-to-stiffener weld toe at the stiffener side), represented by strain gauge number 9 (see Figure 9.7). Both load cases have a minimum peak and a maximum peak. The minimum strain occurs when the single-tyre is at midspan between different stiffeners (load 'outside' the stiffeners) and the maximum strain occurs when the single-tyre is at midspan between the same stiffener web (load 'inside' the stiffener). The strain for double-tyre load case is minimum when the right double-tyre is at the position 'outside'-midspan between stiffeners. The strain approaches zero when the web is just between the double-tyre (no bending of the web) and the strain is maximum when the left double-tyre is at the position 'inside'-midspan between stiffener. As the load is higher for the individual single-tyre than for each double-tyre, the strains are higher for the single-tyre load case than for the double-tyre load case.
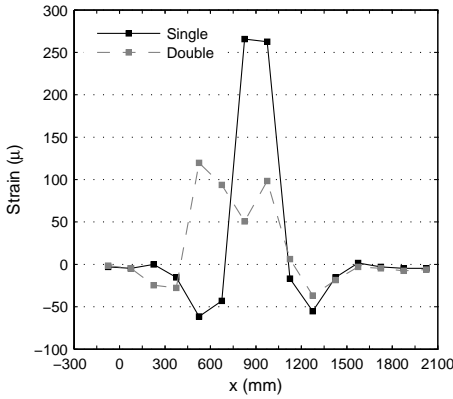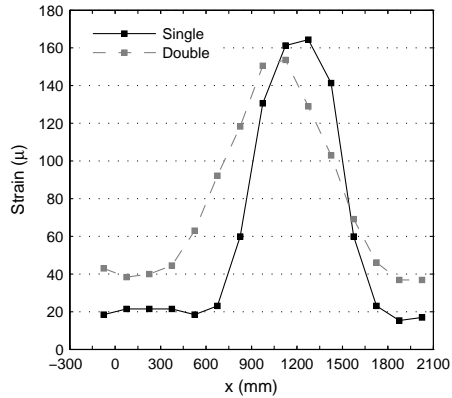
(a) Strain gauge 7 (Group I)
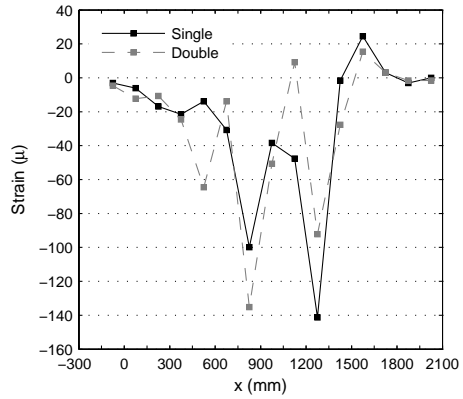
(b) Strain gauge 8 (Group II)
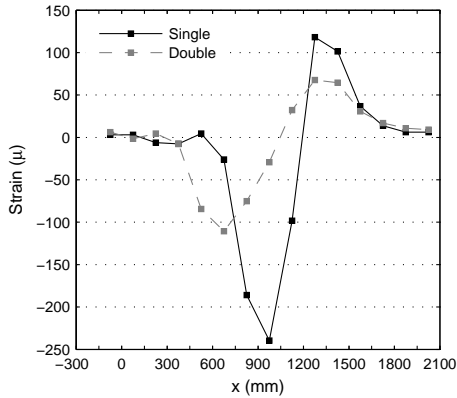
(c) Strain gauge 9 (Group III)

(d) Strain gauge 10 (Group IV)

Figure 9.11: Strain influence lines at different load cases (single-tyre - 37 kN and double-tyre - 38.5 kN).

Figure 9.11(d) shows the results of Group IV (longitudinal strains at the bottom of the stiffener), represented by strain gauge number 10 (see Figure 9.7). As expected, the longitudinal strains at the bottom of the stiffener are less load case dependent than the previous results. The strain at this location is more dependent on the total load than on the load configuration. Therefore, the single and double-tyre load cases present similar results.

Strain gauges from Group V present results that are very similar to the strain gauges from Group I as they are at the same position but measuring in the longitudinal rather than in the transverse direction. The main difference is on the magnitude of the strain values, which is less on the longitudinal direction than on the transverse direction.

Figure 9.12 compares the strain gauges' stress influence lines before and after the renovation. Each graph shows the results of two representative strain gauges of one group. The results are from the single-tyre load case. For the majority of the strain gauges this is the most severe load case and it is also the most reliable test concerning the wheel load position. The latter is especially important when tests before and after the renovation need to be compared. In order to compare strains within the same load level, the strain values measured before the renovation were corrected to a wheel load of 38.5 kN. The stress values were determined using the simplified Hooke's Law $\sigma = E \cdot \varepsilon$ using a Young's modulus for the steel 210 GPa recommended in Eurocode 3 (EN1993-1-1, 2006). These stress values are an approximation of the actual stresses on the deck, since the Hooke's law for plates takes also into account the strain in the perpendicular direction, which was not measured.

Figure 9.12(a) shows the results of strain gauges 1 and 7 which represent Group I. The pattern of the influence line is the same for the two strain gauges. The maximum strain depends on the strain gauge position (strain gauge 1, maximum at $x \approx 300$ mm and strain gauge 7, maximum at $x \approx 900$ mm). As the geometry of the deck plate is repeated along the transverse direction, the pattern of the influence line is repeated for the same deck details. Strain gauges 43 and 44 (Figure 9.12(b)) measured strains at the same location as strain gauges 1 and 7, but in the longitudinal direction. The stress influence lines of 43 and 44 are very similar to the ones from 1 and 7, but with approximately half the stress magnitude.

Figure 9.12(c) shows the results of strain gauges 2 and 12, which represent Group II. These strain gauges measured transverse strains close to the deck-plate-to-stiffener weld toe of the deck-plate side. Figure 9.12(d) shows the results of strain gauges 3 and 5 which measured the transverse strains close to the the deck-plate-to-stiffener weld toe of the stiffener side – Group III. It can be observed that the stress values are considerably higher on the weld toe of the stiffener side than on the weld toe of the deck-plate side, Group III and II, respectively. This can be explained by the fact that, the thickness of the stiffener is 6 mm and the thickness of the deck plate is 12 mm. Due to the stiffener's geometric symmetry, the stress influence lines of strain gauges 3 and 5 are symmetric (same stiffener, left and right web). Figure 9.12(e) shows the results of strain gauges 4 and 10 which measured longitudinal stresses on the bottom of the stiffener (Group IV). The two stress influence lines are very similar. The results show that the wheel load is totally carried by one stiffener if the load is positioned just above the stiffener and when the load is between stiffeners 50% is carried by one stiffener and 50% by the other stiffener.

Significant stress reduction can be observed for all deck details after the renovation. The reduction is higher at the deck-plate details, as Groups I and II, than at the stiffeners details as Group III and Group IV.

(a) Group I

(b) Group V

(c) Group II

(d) Group III

(e) Group IV
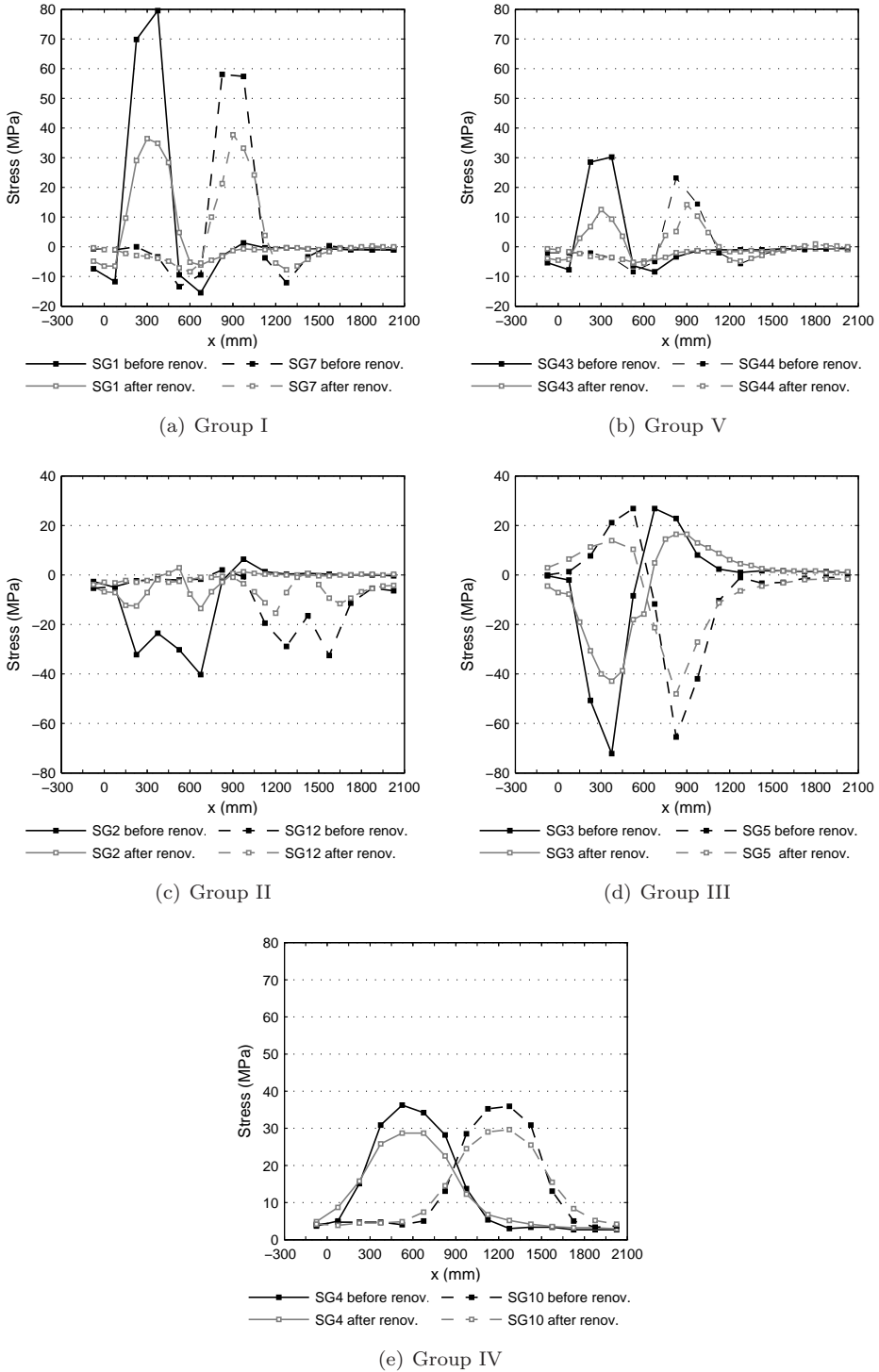
Figure 9.12: Strain gauges' stress influence lines before and after the renovation.

Strain history measurements

Strains were continuously recorded at all strain gauges applied to the bridge deck. The measurements started one week before the renovation and continued for one year after the renovation. The results of the strain gauges applied at the middle span cross-section were analysed for the short-term monitoring.

Figure 9.13 shows one example of the strain history measurements recorded during one day. The x-axis corresponds with 24 hours plotted in seconds, starting at midnight. The data shows the successive maximum and minimum values caused by each axle load running on the bridge. The data was previously corrected to take the temperature effects into account. The results are from strain gauge number 7 and were recorded before the renovation.

The stress spectrum of each strain gauge is obtained after subjecting the strain history measurements to cycle counting. In this study, the Range-Pair counting method was used for the cycle counting (ASTM-E1049, 2005).

The week stress spectrum is determined gathering the stress history of the 7 days of the week. Figure 9.14 shows the week stress spectra of all strain gauges at Middle-span cross-section gathered in the five main groups. The stress spectrum of the week before the renovation is compared with the stress spectrum of the week after the renovation.

For all groups, the maximum stress ranges obtained from the history measurements are considerably higher than those produced by the controlled static load tests.

As observed in the controlled load tests, the transverse stresses are the principal stresses on the deck plate (Figure 9.14(a) Group I vs. Figure 9.14(b) Group V) and the stresses close to the deck-plate-to-stiffener weld are higher at the weld toe of the stiffener side than at the weld toe of the deck plate side, Figure 9.14(d) and 9.14(c) respectively.
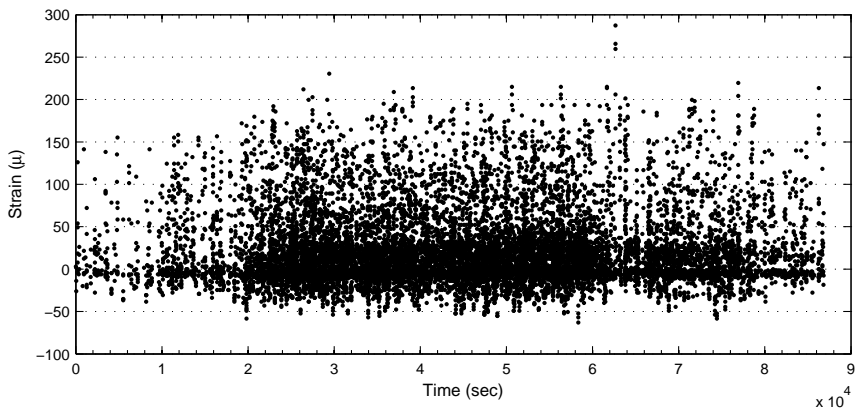
Figure 9.13: Strain history measurements of one day from strain gauge number 7.
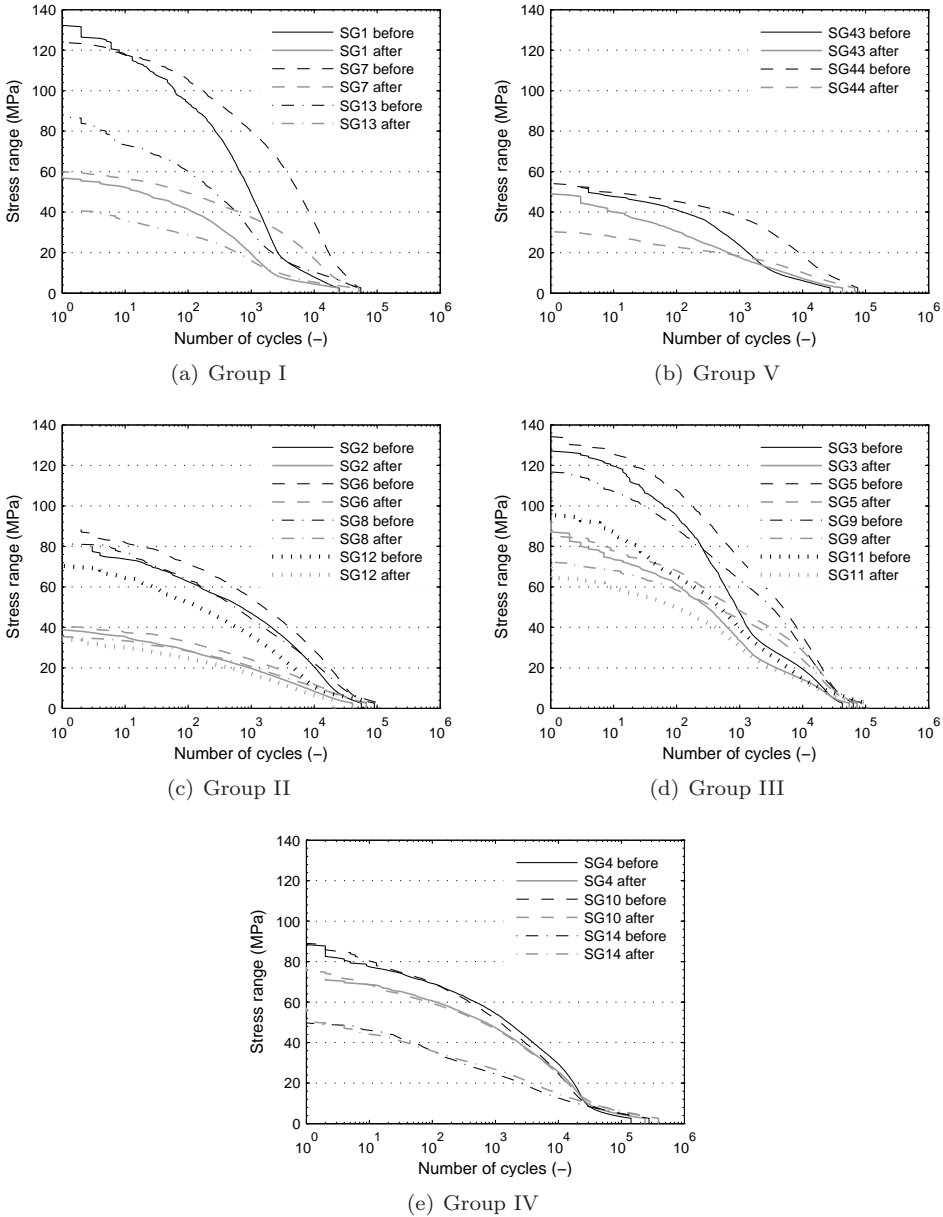
Figure 9.14: Strain gauges week stress spectra 'before' and 'after' the renovation.

Results show that there is a significant stress range reduction after the renovation for Groups I, II and III. The results from Group IV do not show significant changes after the renovation – see Figure 9.14(e). These results are in accordance with the static influence lines.

Stress reduction factor

One way to quantify the performance of the strengthening system is to determine the stress reduction factor. These values can be determined for each strain gauge i by Equation (9.1).

$$SRF_i = 1 - \frac{\sigma_i^{After}}{\sigma_i^{Before}} \qquad (9.1)$$

The stress reduction factor was determined using the maximum values obtained from the controlled static load test (see Figure 9.12) and using the stress ranges at 10, 100 and 1000 cycles from the stress spectra (see Figure 9.14). Table 9.4 presents the results of the sixteen strain gauges belonging to the five main group locations.

Group	Strain gauge	Controlled tests	$SRF_i(\%)$ Strain history n=10	n=100	n=1000	SRF_{Group} $ave \pm std$ (%)
I	1	55	56	56	61	
	7	38	52	53	54	50±6
	13	45	52	52	48	
	$ave \pm std$	46±7		54±3		
II	2	63	53	55	58	
	6	53	54	54	55	
	8	59	57	56	54	56±3
	12	57	53	52	52	
	$ave \pm std$	58± 4		54±2		
III	3	37	39	36	30	
	5	37	38	37	35	
	9	35	36	34	30	35±5
	11	39	32	24	23	
	$ave \pm std$	37±1		33±5		
IV	4	18	11	13	13	
	10	14	15	16	10	11±6
	14	7	4	2	0	
	$ave \pm std$	13±5		9±5		
V	43	57	53	55	54	
	44	47	44	51	51	52±4
	$ave \pm std$	52±5		51±3		

Table 9.4: Stress reduction factors.

Controlled load tests and strain history measurements give approximately the same results in terms of stress reduction factor. The highest stress reduction is at the deck plate (Groups I, II and V) varying from 45% to 55%, approximately. The transverse stress on the stiffeners web is reduced by approximately 35% (Group III). The lowest reduction is at the longitudinal stresses at the bottom of the stiffener, Group IV. This reduction decreases in the direction of the midspan between main girders.

The stress reduction is higher at the deck plate details (Groups I and II) than at the stiffeners details (Groups III and IV). The stress reduction decreases as we get farther away from the strengthening (deck plate level).

The aim of the reinforcement is to extend the fatigue life of the bridge. This fatigue life is limited by the fatigue cracks that grow at the deck-plate-to-stiffener welds. Therefore the most important stress reduction factors for the fatigue life of the bridge are from Group II and Group III, which represent strain gauges measuring strains close to these welds at the deck plate side and at the stiffener side, respectively (see Figure 9.5). Table 9.4 shows that the stress ranges close to the deck-plate-to-stiffener weld are reduced by 55% at the deck plate side and by 35% at the stiffener web side.

According to Eurocode 3: Part 1-9 Fatigue (EN1993-1-9, 2005), the fatigue strength curve of these welds is defined by the following Equation 9.2:

$$\Delta\sigma = k \cdot n_f^{-1/3} \tag{9.2}$$

$\Delta\sigma$ is the stress range, n_f is the fatigue life and K is a parameter which depends on the detail of the welds. Taking into account the stress reduction factor SRF close to the welds and rewriting Equation 9.2, one can determine how much is the increase of the fatigue life of the welds by Equation 9.3:

$$\frac{\Delta\sigma^{After}}{\Delta\sigma^{Before}} = \frac{k}{k} \cdot \left(\frac{n_f^{After}}{n_f^{Before}}\right)^{-1/3} \Longleftrightarrow n_f^{After} = \frac{n_f^{Before}}{(1-SRF)^3} \tag{9.3}$$

Due to the reinforcement, the fatigue life of the deck-plate-to-stiffener welds is expected to increase 11.9 times at the deck-plate side ($SRF_{II} = 56\%$; $n_f^{After} = 11.9 \cdot n_f^{Before}$) and 3.6 times at the stiffener web side ($SRF_{III} = 35\%$; $n_f^{After} = 3.6 \cdot n_f^{Before}$). These results were determined for welds at midspan between crossbeams.

The stress reduction factors can be compared with the values determined from the full-scale tests described in Chapter 7. One of the deck-panels used in the full-scale tests was reinforced with the same system: bonded steel plates with a 6 mm thick second steel plate and a 2 mm thick adhesive layer. Table 9.5 presents the stress reduction factors for both studies. The full-scale test results are taken from Table 7.5 on page 134, using the strain reduction factors of experiments carried out with wheel

Group	Scharsterrijn	Full scale deck panels (EXP1)	Deck detail
I*	50±6	50±3	transverse stress at midspan between stiffener webs
II	56±3	66±3	transverse stress close to the weld toe at the deck plate side
IV	11±6	18±5	longitudinal stress at the bottom of the stiffener

Table 9.5: Stress reduction factors (%) determined from the monitoring program and from the full-scale tests (Chapter 7, Table 7.5 on page 134); * similar deck details: for the Scharsterrijn bridge is outside the stiffener and for the full-scale deck panel is inside the stiffener.

loads at the midspan between crossbeams, as is the case on the Scharsterrijn bridge (middle-span cross-section and measured values before and after the renovation).

The reduction factors obtained from both studies are in reasonable agreement. The deck detail of Group I has the same reduction on real-scale and deck-scale, even if the detail is not exactly the same (for the Scharsterrijn bridge is outside the stiffener and for the full-scale deck-panels is inside the stiffener). The reduction close to the deck-plate-to-stiffener welds is higher on the deck-scale than on the real-scale. The same can be said for the reduction at the bottom of the stiffeners.

Similar structural monitoring was performed on bridges which were reinforced with Reinforced High Performance Concrete (RHPC). Jong and Kolstein (2004) report the renovation of the fixed orthotropic steel deck of Caland bridge (the Netherlands). The results show significant stress reduction after replacing the 50 mm thick surfacing of mastic asphalt (MA) by 60 mm thick layer of RHPC. The same type of reinforcement was applied in another fixed orthotropic deck in the Netherlands on the Moerdijk bridge (Kolstein and Sliedrecht, 2008). In this case, the 60 mm thick surfacing system of mastic asphalt was replaced by an RHPC overlay with 47 mm to 100 mm thickness. Kolstein and Sliedrecht (2008) report also significant stress reduction on the orthotropic deck after renovation. Table 9.6 compares the stress reduction factors reported in these studies with the ones determined on Scharsterrijn.

SRF	Scharsterrijn	Moerdijk	Caland
Group I	50%	91%	—
Group II	56%	86%	80%
Group III	35%	79%	64%
Group IV	11%	51%	—
Before renovation	7 mm MA	60 mm MA	50 mm MA
After renovation	B1226	50-100 mm RHPC	60 mm RHPC
Reinforcement weight (kg/m^2)	49	188	150

Table 9.6: Stress reduction factors, deck status before and after the renovation and reinforcement weight of three bridge renovations: Scharsterrijn, Moerdijk and Caland bridges.

The reinforcement systems of the fixed bridges Moerdijk and Caland are 3 to 4 times heavier than that of the movable deck of Scharsterrijn. The heavy solutions of RHPC lead to higher stress reduction factors than the lightweight solution of bonded steel plates reinforcement. On one hand they are comparable since all reinforcements are applied to extend the fatigue life of the orthotropic decks. On the other hand, reinforcements with such weight differences should not be compared since they are not applied in the same type of bridge. RHPC overlay with 50 to 100 mm thickness is not a possible reinforcement system for movable bridges.

9.5.2   Long-term monitoring

Long-term monitoring was performed during one year starting immediately after the renovation. The goal was to evaluate the performance of the strengthening system during a certain period of time. The measurements were recorded for all strain gauges, applied at the three longitudinal sections of the deck, Middle-span cross-section, Joure cross-section and Lemmer cross-section (see Figures 9.4 and 9.6) .

However, a certain percentage of strain gauges failed before the long-term monitoring ended. From the 47 strain gauges applied to the bridge deck, 5 failed after six months (10%) and 5 more after 10 months. Hence, in total 20% of the instrumentation was lost before the end of the monitoring, caused by failure of the strain gauges.

The long-term measurement results of the strain gauges are gathered in the same five main groups, representing five deck details, as presented for the short-term monitoring.

Dynamic influence lines

Strain data from the controlled dynamic load tests was used to determine dynamic stress influence lines caused by the passage of the calibrated truck over the movable bridge deck.

Figure 9.15 shows the results of Group I, which is represented by strain gauges 1, 17 and 34. These strain gauges measured the transverse strains at the deck plate between stiffener webs. The three strain gauges are at exactly the same transverse position of the deck but at different cross-sections: strain gauge 1 is at the middle of the deck, strain gauge 17 is at the end of the deck and strain gauge 34 is at the beginning of the deck.

Figure 9.15(b) shows two strain signals, triggered by strain gauge number 1, when the calibrated truck crossed the movable deck at two different positions. The position is based on the distance measured by the laser ('x-axis' shown in Figure 9.7). The reference of the wheel position is the same as for the static load tests, i.e. the centre of the single-tyre (front axle) and the centre of the outside/left double-tyre (rear axles) – see Figure 9.7. From both signals shown in Figure 9.15(b), one can easily identify each axle of the calibrated truck: one front axle and three rear axles from the main truck, and three rear axles from the trailer.
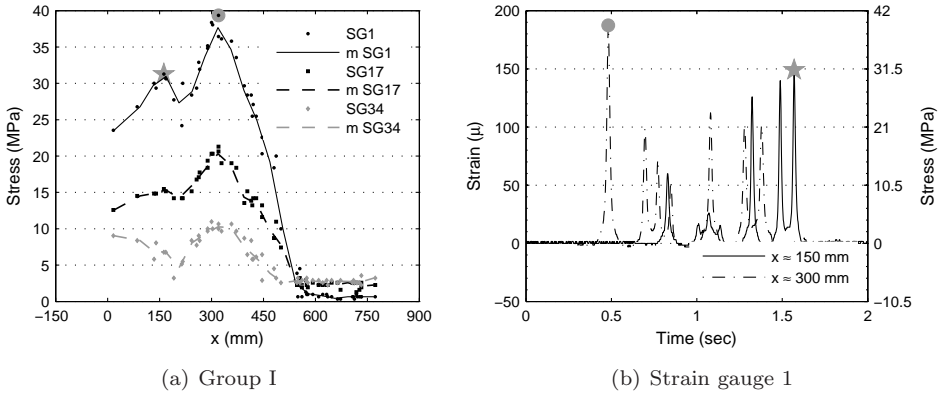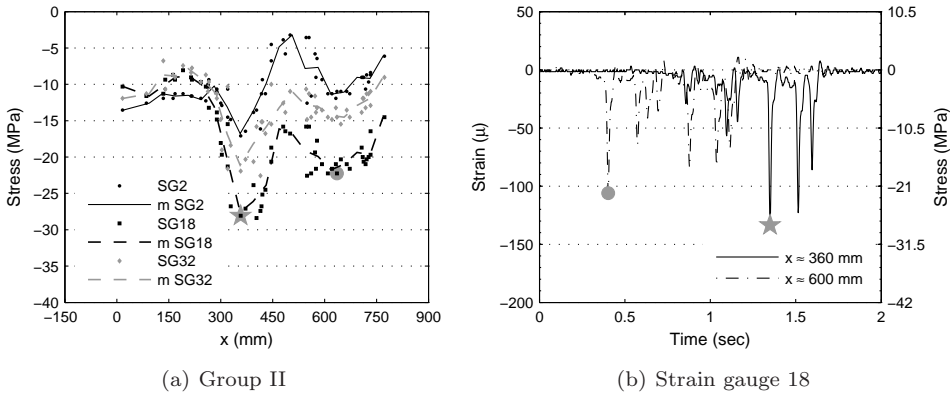
Figure 9.15: Dynamic strains measured on the deck plate at midspan between stiffeners (Group I): (a) Dynamic influence lines (m - mean) and (b) Strain gauge 1's triggered strains when the calibrated truck crossed the movable deck.

From each truck passage, the maximum strain value recorded was used to determine the dynamic stress influence line of each strain gauge. The results are shown in Figure 9.15(a) for strain gauges 1, 17 and 34. The points on the graph represent the maximum strain absolute values registered at the strain gauges during one dynamic test at the 'x-axis' calibrated truck position. The mean dynamic stress influence line was determined for each strain gauge (referred to as 'm' in Figure 9.15(a)) using all the results from one year.

Looking at the three dynamic influence lines, one can recognize a similar pattern, first peak at approximately $x \approx 150$ mm and the second peak at approximately $x \approx 300$ mm. In Figure 9.15(a) these peaks are highlighted for strain gauge number 1 (SG1). In order to better understand these maximum values, we need to look at the triggered strains recorded for each truck position in Figure 9.15(b). The triggered strains are plotted for the two peak truck positions of strain gauge 1 (highest values). At $x \approx 150$ mm, the maximum value is caused by the heaviest rear axle, i.e., by the double-tyre load case (see Figure 9.15(b), series '$x \approx 150$ mm'). This maximum value occurs when the inside tyre of the truck is approximately aligned with the strain gauge. At $x \approx 300$ mm, the maximum value is caused by the front axle, i.e. by the single-tyre load case (see Figure 9.15(b), series '$x \approx 300$ mm'). This maximum value occurs when the single-tyre is aligned with the strain gauge. The single-tyre load case causes higher stresses than the double-tyre because the individual load tyre is higher on the single-tyre (appr. 38 kN) than on each of the two double-tyres (appr. 29 kN = 58/2 kN). These results are in accordance with the static influence lines determined for the same group of strain gauges (see Figure 9.11(a)).

Taking into account the dynamic stress peak of strain gauge 1 caused by single-tyre (approximately 38 kN, $x \approx 300$ mm) and comparing it with the static stress peak

caused also by single-tyre at the same strain gauge (38.5 kN, $x \approx 300$ mm, see Figure 9.12(a), series 'SG1 after renov.'), we can observe that there is no significant difference between static and dynamic stresses (approximately 35 to 40 MPa). Therefore, we can conclude that the dynamic factors are low at the middle of the deck.

Although one can identify a similar pattern between the three dynamic influence lines, there is a significant difference in the absolute values of the three strain gauges. The strain values of strain gauge 1 are significantly higher than those of grain gauges 17 and 34. The transverse stresses between the stiffener webs are higher at midspan between crossbeams (strain gauge 1) than close to the crossbeams (strain gauges 17 and 34).

Figure 9.16 shows the corresponding results for Group II, which is represented by strain gauges 2, 18 and 32. These strain gauges measured transverse strains close to the deck-plate-to-stiffener welds toe at the deck plate side. The three strain gauges are exactly at the same transverse position of the deck, but at different cross-sections: strain gauge 2 is at the middle of the deck, strain gauge 18 is at the end of the deck and strain gauge 32 is at the beginning of the deck.

Figure 9.16(a) shows the mean dynamic stress influence lines of the three strain gauges and Figure 9.16(b) plots two strain signals triggered by strain gauge 18 at two truck positions.

(a) Group II   (b) Strain gauge 18

Figure 9.16: Dynamic strains measured on the deck plate close to the welds (Group II):
(a) Dynamic influence lines (m - mean) and (b) Strain gauge 18's triggered strains when the calibrated truck crossed the movable deck.

Also in this group, there is a similar pattern between the three dynamic influence lines, first minimum peak between $x \approx 350$ mm and $x \approx 400$ mm and second minimum peak at approximately $x \approx 600$ mm. These peaks are highlighted for strain gauge 18 in Figure 9.16(a). In Figure 9.16(b), the triggered strains are plotted for the two peak truck positions, $x \approx 360$ mm and $x \approx 600$ mm. At $x \approx 360$ mm, the minimum value is caused by the rear axles of the trailer, i.e. by the double-tyre load case (see Figure 9.16(b), series '$x \approx 360$ mm'). This minimum value occurs when the strain gauge is just in between the two double-tyres. At $x \approx 600$ mm, the minimum value is caused by the front axle, i.e. by the single-tyre load case (see Figure 9.16(b), series '$x \approx 600$ mm'). This minimum value occurs when the single-tyre is aligned with the stiffener. The double-tyre load case causes higher stresses than the single-tyre load case, with approximately 50 kN and 38 kN wheel loads, respectively. This is in accordance with the static influence lines of the same group of strain gauges (see Figure 9.11(b)).

Taking into account the dynamic stress peak of strain gauge 2 caused by single-tyre (approximately 38 kN, $x \approx 600$ mm) and comparing it with the static stress peak caused also by single-tyre (38.5 kN, $x \approx 600$ mm, see Figure 9.12(c), series 'SG2 after renov.'), we can observe that there is no significant difference between static and dynamic stresses (approximately 10 to 15 MPa). Therefore, we can conclude once more that at the middle of the deck the dynamic factors are low.

The difference between the stresses at the three longitudinal sections Joure, Lemmer and middle-span is less significant for Group II than for Group I. Nevertheless, strain gauges 18 and 32, which are close to crossbeams (Lemmer and Joure), have higher stress values than strain gauge 2, which is at midspan between crossbeams.

Concerning the strengthening performance during the year of monitoring, the results show that there is no significant scatter between all the points of each strain gauge collected over the year of monitoring. This indicates that the stresses at the deck plate remain approximately the same during the monitoring period. This was observed also for the rest of the strain gauges still functioning during the entire monitoring period.

Strain history measurements

The strain history was continuously recorded during the year after the renovation. The aim was to evaluate the performance of the strengthening system during a certain period of time. The measurements started in April 2009 and ended in April 2010. There was an interruption in the recording during the entire month of July 2009 due to power failure of the measuring equipment.

The strain history measurements were used to determine the week stress spectrum of each strain gauge. Figures 9.17 and 9.18 show typical results of strain gauges from Group I and Group II, respectively.

Figure 9.17(a) shows one-week stress spectra of strain gauges 1, 17 and 34 (Group I). The results are from the third week of September 2009 because it is the one with the

highest stresses observed for these strain gauges during monitoring. Figure 9.17(b) shows the evolution of the stress range at 100 cycles from April 2009 to April 2010, for the same strain gauges. No significant changes can be observed on the 100 cycles stress range and corresponding stress spectra, during the year of monitoring.
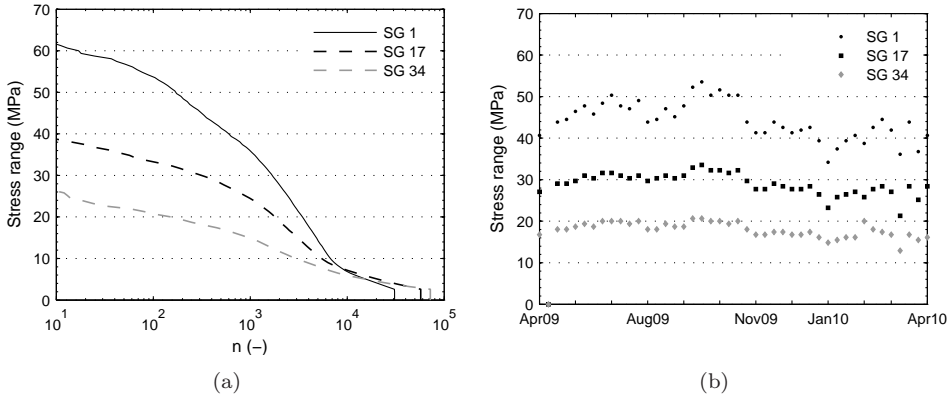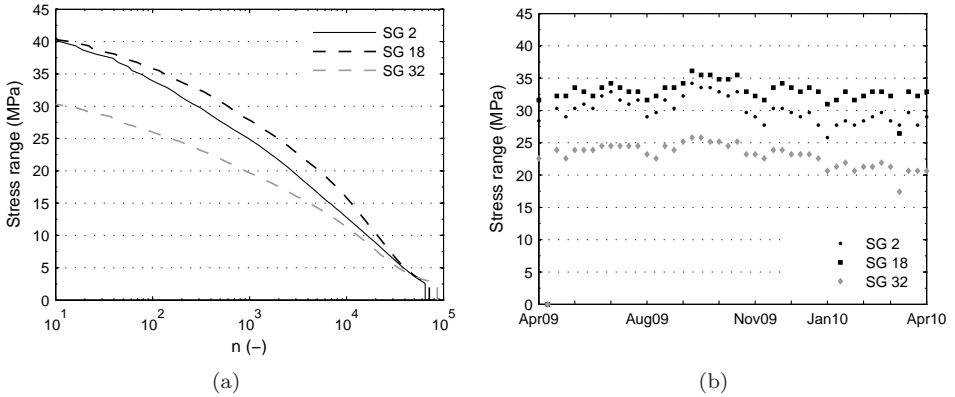

Figure 9.17: Typical results of Group I (a) Week stress spectra of week 38 (third week of September 2009) and (b) Stress range at 100 cycles of the week stress spectra from April 2009 to April 2010.

As observed for the dynamic load tests, there is a significant difference between longitudinal sections. The transverse stresses between stiffeners webs (Group I) are higher at midspan between crossbeams (SG 1) than close to the crossbeams (SG12 and 34). However, the maximum strains measured during normal traffic are considerably higher than those measured during the controlled dynamic load tests. The maximum dynamic stresses induced by the calibrated truck correspond approximately with the stress ranges at 1000 cycles per week. The maximum stress ranges registered during normal traffic are 1.6, 1.9 and 2.6 times higher than the maximum stresses measured during the dynamic tests, for strain gauges 1, 17 and 34 respectively.

Figure 9.18(a) shows one-week stress spectra of strain gauges 2, 18 and 32 (Group II). The results are also from the second week of September 2009 because it is the one with the highest stresses observed for these strain gauges during monitoring. Figure 9.18(b) shows the evolution of the stress range at 100 cycles from April 2009 to April 2010, for the same strain gauges. As for Group I, no significant changes can be observed on the stress range and corresponding stress spectra, during the year of monitoring.

Comparing the stress ranges of the three strain gauges, the highest was measured by strain gauge 18. This is in accordance with what was observed in the dynamic influence lines, although strain gauge 2 has closer values to strain gauge 18 than those measured from the dynamic tests (see Figure 9.16(a)) and it has higher values

Figure 9.18: Typical results of Group II (a) Week stress spectra of week 37 (second week of September 2009) and (b) Stress range at 100 cycles of the week stress spectra from April 2009 to April 2010.

than strain gauge 32. This is contrary to what was expected for this detail, which measured transverse stress close to the deck-plate-to-stiffener weld and, therefore, stresses were expected to be higher close to the crossbeams than at midspan between crossbeams.

As for Group I, the maximum strains measured, for strain gauges 2, 18 and 32, during normal traffic are considerably higher than those measured during the controlled dynamic load tests. The minimum stresses induced by the calibrated truck correspond approximately with the stress ranges at 1000 cycles per week. The maximum stress ranges registered during normal traffic are 2.3, 1.4 and 1.3 times higher than the minimum stresses measured during the dynamic tests, for strain gauges 2, 18 and 32 respectively.

Overall, there are no significant changes on the stress field of the deck plate during the year of monitoring. This indicates that the strengthening performance did not change during this period.

9.6   Conclusions

The orthotropic deck of the movable bridge Scharsterrijn was strengthened by bonding a second steel plate of 6 mm thickness to the existing 12 mm thick deck-plate. The results presented in this Chapter are part of the short and long-term monitoring plan carried out before and after the renovation. From these results, the following conclusions can be drawn.

The local transverse strains at the deck plate are mainly caused by individual wheel loads.

Overall, the single-tyre load case is worse than the double-tyre load case for the deck-plate details studied, except for the transverse strains close to the deck-plate-to-stiffener weld.

There is hardly any difference between comparable static and dynamic stresses at middle cross-section of the orthotropic deck.

The maximum strains measured under normal traffic conditions are considerably higher than those measured during the controlled dynamic load tests. The maximum stresses caused by the used calibrated truck correspond approximately with the stress ranges of 1000 cycles per week.

The short-term measurements reveal that after applying the reinforcement, the strains close to the deck-plate-to-stiffener weld toe, at midspan between crossbeams, are reduced by 56% at the deck plate side and by 35% at the stiffener side. Due to the reinforcement, the fatigue life of these welds is expected to increase 11.9 times at the deck plate side and 3.6 times at the stiffener side. The reinforcement is more efficient for details at the deck plate than at the stiffener web. The strengthening performance is lower for details away from the deck plate and influenced by the global behaviour of the structure. Overall, the short-term structural behaviour was within the expected performance of the strengthening system.

The long-term measurements do not show significant changes in the stress level of the bridge deck during the monitoring period. This indicates that there was no degradation of the strengthening system during the year after the renovation.

Based on this, the strengthening system has demonstrated good performance reliability to prolong the life span of movable orthotropic bridges and therefore can be considered satisfactory.

Chapter 10

Conclusions and Recommendations

The purpose of this research is to extend the fatigue life of orthotropic bridge decks (OBD) using lightweight reinforcements (50 to 80 kg/m^2), which are of special importance for application on movable bridges. The aim of applying the reinforcement is to stiffen the existing deck plate, in order to reduce the stress ranges at the welds to extend their fatigue life.

The reinforcement systems consist of adding a second steel plate to the existing steel deck. Two systems have been studied: bonded steel plates and sandwich steel plates. In the bonded steel plates system, the existing OBD is reinforced by adding the second steel plate using a thin epoxy adhesive layer (approximately 2 mm thick). In the sandwich steel plates system, the existing deck is reinforced by adding a sandwich overlay which is composed by a polyurethane core (PU-core, from 15 mm to 30 mm thick) and the second steel plate.

The research strategy used in this thesis was based on a multi-scale approach, in which the reinforcement behaviour was investigated on three structure-scales: (i) plate-scale, (ii) deck-scale and (iii) bridge-scale. The research was therefore divided into three main parts: Part I (plate-scale), Part II (deck-scale) and Part III (bridge-scale). In the following section the main outcome of each part of the research is presented and a design approach to evaluate the performance of OBD reinforcements is suggested. In the final section, recommendations are drawn for the future work on this research field.

10.1   Conclusions

Behaviour of reinforced steel plates – Part I

The main goal of this part of the research was to better understand the mechanical behaviour of the reinforcement systems. The static and fatigue behaviour of bonded and sandwich reinforced beams was investigated. The optimization of the systems was investigated using analytical studies. This optimization is based on maximizing the system stiffness by using a reinforcement with minimum weight. Stiffer solutions lead to more stress reduction at the deck which results in longer fatigue lives for the OBD. Bending tests were carried out under static and fatigue loading on both systems. Finite element analyses were performed in order to better understand the obtained experimental results.

For the bonded steel plates reinforcement system the following conclusions can be drawn. The optimization of the system can only be achieved by maximizing the second steel plate thickness. The actual application of the system restricts the adhesive nominal thickness to 2 mm. The maximum thickness of the second steel plate is related to the limit of weight of the reinforcement. For example, for a maximum reinforcement weight of 70 kg/m^2, the maximum stiffness is achieved using 8 mm thick second steel plate. Material testing show that the mechanical properties of the adhesive layer are temperature dependent. The material is brittle at -10 °C and ductile at +50 °C. At room temperature (RT), the material behaviour is closer to that at -10 °C than at +50 °C, which means that it is more brittle than ductile. However, since only 2 mm of adhesive thickness is used on the bonded system, the temperature effect has hardly any influence on the bending stiffness of the bonded steel plates reinforced beams. The static failure mode of the bonded steel plates reinforced beams occurs by yielding of the steel plates followed by shear failure of the adhesive layer. The major fatigue failure mode is shear failure of the adhesive layer and there is no significant stiffness degradation during the whole fatigue life until failure. The fatigue life of adhesive layers within the studied thickness between 1 mm and 3.5 mm is the same. The fatigue behaviour is determined by the shear stress at the adhesive layer, $\Delta\tau_{ad}$. Considering this parameter, the fatigue threshold appeared to be approximately $\Delta\tau_{ad}^{th} = 8$ MPa.

For the sandwich steel plates reinforcement system the following conclusions can be drawn. The analytical studies showed that the optimization of the system can be achieved by maximizing the core thickness until a certain maximum value. For cores thicker than the maximum value, the increase of shear displacement of the core counterbalances the increase of the moment of inertia of the sandwich section. The sandwich steel plates reinforcement decreases its performance as the shear increases its role on the flexural behaviour of the reinforced structure. The maximum core thickness is dependent on the maximum allowed weight of the reinforcement, the mechanical properties of the core material and the load conditions. For example, for the core material used in the sandwich steel plates system and for a maximum weight of 70 kg/m^2, the maximum core thickness is 30 mm when using a 5 mm thick second steel plate. This latter thickness is the minimum value allowed for real application

of the reinforcements. Material testing showed that the mechanical properties of the core material (polyurethane) are temperature dependent. The polyurethane stiffness (Young's modulus) decreases with increasing temperature. The bending stiffness of the sandwich beams is significantly affected by temperatures between $10\,^\circ$C and $+50\,^\circ$C, since the thickness of PU-core is significant on the total thickness of the sandwich (core thickness between 15 mm to 30 mm). When compared to RT, the bending stiffness of the sandwich beams increases on average 20% at $-10\,^\circ$C and decreases on average 50% at $+50\,^\circ$C. The static failure mode of the sandwich beams starts by yielding of the steel plates and near yielding of the PU-core, subsequently by delamination of the faces-to-core interfaces and, finally by shear failure of the core. The fatigue failure mode of the sandwich beams has three damage events. It starts by delamination of the interface between the core and the steel faces. In the second phase, the delamination crack progresses through the core thickness and in the last stage the crack crosses the complete core thickness (shear failure of the core). The stiffness degradation starts with the delamination event. For specimens with a fatigue life lower than 1 million cycles, the delamination occurs quite early, approximately 50% to 70% of the fatigue life. For specimens with longer lives, the delamination occurs mainly after 80% of the fatigue life. The fatigue life of sandwich beams with either 15 mm or 30 mm is the same. The fatigue behaviour is determined by the shear stress at the faces-to-core interface $\Delta\tau_c$. Considering this parameter, the fatigue threshold appeared to be approximately $\Delta\tau_c^{th} = 4$ MPa.

Behaviour of reinforced full-scale deck panels – Part II

The main goal of this part of the research was to study the behaviour and the effect of the reinforcement when applied to orthotropic bridge deck panels. The effect of the high stress concentrations at the welds of an OBD, on the reinforcement behaviour was investigated. The reinforcement of the deck panel using the bonded steel plates system consisted of bonding a 6 mm thick second steel plate using a 2 mm thick adhesive layer. The reinforcement of the deck panel using the sandwich steel plates system consisted of adding a 5 mm thick second steel using a 15 mm thick polyurethane core. Full-scale tests were performed on both reinforced deck panels using wheel loads to simulate the heavy traffic loading on a reinforced OBD with a deck plate thickness of 12 mm. Finite element analyses were performed in order to better understand the obtained experimental results. The FEA was validated using the experimental data and used to perform a parametric study on the influence of the reinforcement geometry and of the environmental temperature on the reinforcements performance.

The results from the full-scale static tests on the bonded steel plates reinforcement system showed a significant reduction of the transverse stresses at the deck plate close to the deck-plate-to-stiffener welds. The stresses at this deck location were reduced by 50% to 60% at the crossbeam and by 60% to 80% at midspan between crossbeams, after applying the reinforcement. The longitudinal stresses at the bottom of the stiffener at midspan between crossbeams were reduced by 20% after applying the reinforcement. During the full-scale fatigue tests, no delamination occurred in the

adhesive layer when the reinforced deck was subjected to fatigue wheel loads at the crossbeam and at midspan between crossbeams (wheel type C with maximum load of 160 kN).

The results from the parametric study showed that increasing the thickness of the second steel plate of the bonded steel plates reinforcement by 2 mm adds an average of 6% to the stress recution factors (SRF) close to the deck-plate-to-stiffener welds. The SRF of the transverse and longitudinal stresses is not expected to be significantly affected by temperatures between -10 °C and +50 °C. Moreover, it also showed that if a second steel plate thickness between 6 mm and 12 mm is used, no delamination is expected to occur in the adhesive layer due to the traffic loads on the bridge.

The results from the full-scale static tests on the sandwich steel plates reinforcement system also showed a significant reduction of the transverse stresses at the deck plate close to the deck-plate-to-stiffener welds. The stresses at this location were reduced by 45% at the crossbeam location and by 55% at midspan between crossbeams, after applying the reinforcement. The longitudinal stresses at the bottom of the stiffener at midspan between crossbeams were reduced by 30% after applying the reinforcement. During the full-scale fatigue tests, no delamination occurred between the core and the steel plates when the reinforced deck was subjected to fatigue wheel loads at the crossbeam and at midspan between crossbeams (wheel type C with maximum load of 160 kN and 110 kN, respectively).

The results from the parametric study showed that increasing the thickness of the core of the sandwich steel plates reinforcement by 5 mm adds an average of 3% to the SRF close to the deck-plate-to-stiffener welds. Increasing the second steel plate thickness from 5 mm to 8 mm adds on average 7% to the same SRF. The SRF of the transverse stresses at the deck plate is expected to be affected by temperature between -10 °C and +50 °C. Those values are expected to increase on average 9% at -10 °C and decrease on average 10% at +50 °C when compared with RT. The temperature effect is lower for the SRF of the longitudinal stresses at the bottom of the stiffener (3%). The parametric study also showed that, if sandwich steel plates solutions with up to 30 mm core thickness and 8 mm second steel plate thickness are used, no delamination is expected to occur between the core and the steel plates due to the traffic loads on the bridge.

Considering reinforcement solutions with approximately the same weight, the bonded steel plates solutions reduce the local stresses close to the welds more than the sandwich steel plates solutions and the sandwich steel plates reinforcement reduces the global stresses more than the bonded steel plates reinforcement.

At the end of this part of the research, the French five-point bending test carried out on a sandwich steel plates solution was described. The initial questions were: How well does it simulate the fatigue load on an OBD? Is it possible to use French 5pbt to evaluate the performance of OBD reinforcements?

It was concluded that, stress patterns in the reinforcement at the five point bending tests (5pbt) are similar to the ones at the full-scale deck panels when this is loaded at midspan between crossbeams by a wheel print type B (double-tyre). However for

the fatigue damage of the bonded and sandwich steel plates reinforcement, the worst load case occurs when the OBD is loaded at the crossbeam location by a wheel print type C (super single). Thus, the five point bending tests does not simulate the worst load case for these two types of reinforcements.

Therefore, the French five-point bending test, as it is defined in the French standard NF-P98-286 (2006) should not be used for evaluating the fatigue behaviour neither of the sandwich nor of the bonded steel plates reinforcement.

Monitoring of a reinforced bridge – Part III

In the last part of the research, a real case study of reinforcing an orthotropic bridge deck is described. The behaviour of the bonded steel plates reinforcement was evaluated on a real application. A movable orthotropic bridge deck in the Netherlands was strengthened using the bonded steel plates reinforcement. The solution consisted of bonding a 6 mm thick second steel plate to the existing deck with an adhesive layer of 2 mm nominal thickness. A monitoring campaign was performed on the bridge in order to evaluate the reinforcement performance. The monitoring consisted of two stages, a short-term measurement campaign, immediately before and after applying the reinforcement, and a long-term measurement campaign during the year after the reinforcement. Strain data at the deck plate was recorded during controlled load tests and during normal traffic conditions.

At midspan between crossbeams close to the deck-plate-to-stiffener weld, the strains after the reinforcement are reduced by 56% at weld toe on the deck plate side and by 35% at weld toe on the stiffener side. Due to the reinforcement, the fatigue life of these welds is expected to increase 11.9 times at the deck-plate side and 3.6 times at the stiffener-web side (proportional to a power 3 of the SN curve of the weld). The reinforcement is more efficient for fatigue cracks initiating at the deck plate than at the stiffener web. The SRF determined for the bridge are in agreement with the ones determined for the same reinforcement solution in the full-scale tests considering the same deck detail. In the bridge the strains are reduced by 56% and in the deck-specimens by 60%.

The strain data recorded during the year after the reinforcement does not show significant changes. This indicates that there was no degradation of the reinforcement system during the year after the renovation. This is also in agreement with the full-scale tests in which no delamination was found due to wheel loads.

Design approach to evaluate the performance of OBD reinforcements

In this section a new design approach is introduced to evaluate the performance of all kinds of reinforcement systems for OBD.

The performance evaluation of a reinforcement system should answer the following main questions: How much is the fatigue life of the orthotropic bridge deck increased after the reinforcement? Is the fatigue strength of the reinforcement high enough to survive the heavy traffic loading?

Determining the stress reduction factor (SRF) at the fatigue sensitive details of an OBD answers the first question. The increase of the fatigue life of the welds can be predicted by determining their SRF and using the SN curve of the relevant weld detail. The SRF is related to the weld detail and to the relevant starting point of the fatigue crack (weld toe, welt root, etc.). It is a misleading idea to think that reinforcement techniques on the deck plate will improve the detail category of the welded joints. The welds remain the same, the difference lies in the stress range at the welds, which depends on the reinforcement stress reduction factor. Implementing reinforcement on the deck plate is like walking through an SN curve of a welded joint. Higher stress reduction will lie at the high cycle fatigue life and lower stress reduction will lie at the low cycle fatigue life. Based on the research presented in this thesis, the SRFs can only be determined using the full-scale geometry of an OBD. The SRFs determined on reinforced beams at the plate-scale are higher than those at the fatigue sensitive details of an OBD, especially for the sandwich steel plates reinforcement. This is caused by the amplification of the 'zig-zag' effect, typical of sandwich structures, due to the high stiffness of the existing deck in comparison with an unstiffened steel plate. Nevertheless, the plate-scale studies can be used to predict the influence of the reinforcement geometry and of environmental temperature on the SRF.

The second question is related to the fatigue strength of the reinforcement. Fatigue tests on reinforced beams at the plate-scale showed that the fatigue life of the reinforcements is predicted by determining the shear stress at the interface layers, adhesive or core, and using the relevant fatigue threshold. This value can be determined by performing beam fatigue tests. The shear stress fields in the interface layers can be predicted by accurate finite element models of the reinforced OBD subjected to heavy wheel loads.

10.2   Recommendations for future work

The present thesis has contributed to the research of strengthening existing orthotropic bridge decks using lightweight solutions. The thesis establishes a design approach based on extensive experimental and numerical studies. Moreover, the outcome of the research on the behaviour of the steel plate reinforcement, as an autonomous structure, can be applied in several different applications beyond orthotropic bridge decks. Nevertheless, there are some aspects that can be further investigated.

An important issue is the influence of air voids and steel spacers on the fatigue resistance of the bonded steel plates reinforcement. The fatigue life of the bonded steel plates reinforcement is sensitive to the manufacturing quality of the adhesive layer. The presence of air flaws or steel spacers in the adhesive layer can decrease the fatigue life of the reinforcement, especially at stress levels higher than the fatigue threshold. Fatigue tests with several artificial void diameters should be performed and maximum design tolerances should be suggested for real applications.

The core material of the sandwich steel plates reinforcement system can be improved in order to obtain higher SRFs. Either stiffening the polyurethane material itself or adding reinforcements into the core, such as fibres, could improve the performance of the sandwich steel plates reinforcement.

Non-destructive testing techniques to monitor the quality of the sandwich steel plates reinforcement is another important aspect to be investigated. Major importance should be drawn to the interface quality between the core and the steel plates, since this is a fatigue sensitive area of these sandwich structures.

For the sandwich steel plates, the environmental temperature showed to be a relevant parameter on the static flexural behaviour. Temperature can also have a major influence on the fatigue resistance of the reinforcement. Fatigue tests at different environmental temperatures would clarify this effect. Another important factor is temperature gradients. They can induce stress patterns that can influence the flexural strength of the reinforcements.

Always an important issue on large-scale applications is how to connect different parts of the reinforcement. Joint details should be investigated to couple parts of the reinforcements. Attention should be paid to their effect on the fatigue life of the reinforcement systems.

Future works on the five-point bending test as it is defined in the French standard NF-P98-286 (2006) should improve the test set-up to get it closer to the actual structure and to be able to simulate not only one but also alternative load cases that can be more severe to the fatigue damage.

Bibliography

ABAQUS (2008). *Abaqus Version 6.8 Documentation*. U.S.A: Dassault Systèmes Simulia Corp.

Arnaud, L., A. Houel, and T. N. Guyen (2009). Monitoring and designing of wearing courses for orthotropic steel decks throughout the five-point bending test. In *Advanced Testing and Characterization of Bituminous Materials, Two Volume Set*, pp. 433–442. CRC Press.

ASCE (2008). The ASCE Orthotropic bridge home page. www.orthotropic-bridge.org.

ASTM-C393 (2006). C393-06: Standard test method for core shear properties of sandwich constructions by beam flexure.

ASTM-D638 (2008). D638-08 standard test method for tensile properties of plastics.

ASTM-E1049 (2005). E1049-85 standard practices for cycle counting in fatigue analysis.

Backer, H., A. Outtier, and P. Bogaert (2008). Alternatives for bridge surfacings with orthotropic plated deck: a fatigue point of view. *Foundations of civil and environmental engineering 11*, 5–16.

Battista, R., M. Pfeil, and E. Carvalho (2008). Fatigue life estimates for a slender orthotropic steel deck. *Journal of Constructional Steel Research 64*, 134–143.

Berggreen, C. and L. A. Carlsson (2010). A Modified TSD Specimen for Fracture Toughness Characterization - Fracture Mechanics Analysis and Design. *Journal of Composite Materials 44*(15), 1893–1912.

Boeters, T., R. Braam, H. Kolstein, and A. Romeijn (2009). Concrete overlay of movable steel orthotropic bridge decks. *Steel Construction 2*, 104–108.

Brischetto, S., E. Carrera, and L. Demasi (2009). Improved response of unsymmetrical laminated sandwich plates by using zig-zag functions. *Journal of Sandwich Structures and Materials 11*, 257–267.

Burman, M. and D. Zenkert (1997). Fatigue of foam core sandwich beams - 1: Undamaged specimens. *International Journal of Fatigue 19*(7), 551–561.

Cardini, A. J. and J. T. DeWolf (2009). Long-term structural health monitoring of a multi-girder steel composite bridge using strain data. *Structural Health Monitoring 8*(1), 47–58.

Carrera, E. (2003). Historical review of zig-zag theories for multilayered plates and shells. *Applied Mechanics Reviews 56*(3), 287–308.

Cheng, X., J. Murakoshi, and A. Moriyama (2004). Full-scale fatigue tests of orthotropic steel deck under running wheel loading. In *2004 Orthotropic Bridge Conference*, Sacramento, California, USA.

Cho, Y. and R. Averill (2000). First-order zig-zag sublaminate plate theory and finite element model for laminated composite and sandwich panels. *Composite Structures 50*, 1–15.

Choi, D.-H., H.-S. Na, H.-Y. Choi, and Y.-S. Park (2008). Fatigue life prediction of U-rib to crossbeam joints using fracture mechanics approach. In *International Orthotropic Bridge Conference 2008*, Sacramento, USA.

Choi, J.-H. and D.-H. Kim (2008). Stress characteristics and fatigue crack behaviour of the longitudinal rib-to-cross beam joints in an orthotropic steel deck. *Advances in Structural Engineering 11*(2), 189–198.

Cong, L., J. Yang, H. Zhu, and J. Cui (2009). A study on rutting prediction of the asphalt pavement for orthotropic steel bridge decks. *Journal of Testing and Evaluation 37*(5), 1–5.

Corte, W. D. (2011). Renovation techniques for rib to deckplate fatigue cracking in orthotropic bridge decks. *Scientific Research and Essays 6*(9), 1977–1986.

Cullimore, M. and J. Smith (1981). Local stresses in orthotropic steel bridge decks caused by wheel loads. *Journal of Constructional Steel Research 1*(2), 17 – 26.

DeWolf, J. T., R. G. Lauzon, and M. P. Culmo (2002). Monitoring bridge performance. *Structural Health Monitoring 1*(2), 129–138.

EN10002-1 (2001). EN 10002-1:2001 Metallic materials - Tensile testing - Part 1: Method of test at ambient temperature.

EN1991-2 (2003). Eurocode 1: Actions on structures – Part 2: Traffic loads on bridges.

EN1993-1-1 (2006). Eurocode 3: Design of steel structures Part 1-1: General rules and rules for buildings.

EN1993-1-9 (2005). Eurocode 3: Design of steel structures Part 1-9: Fatigue.

Farhey, D. N. (2005). Bridge instrumentation and monitoring for structural diagnostics. *Structural Health Monitoring 4* (4), 301–318.

Farhey, D. N. (2006). Instrumentation system performance for long-term bridge health monitoring. *Structural Health Monitoring 5* (2), 143–153.

Feldmann, M., G. Sedlacek, and A. Geler (2007). A system of steel-elastomer sandwich plates for strengthening orthotropic bridges decks. *Mechanics of Composite Materials 43 (2)*, 183–190.

Friedrich, H. (2007). Schönwasserparkbrücke: Untersuchungen zur thermischen Beanspruchung von SPS beim Einbau bituminöser Fahrbahnbeläge. *Stahlbau 76* (7), 472–477.

Gibson, L. and M. Ashby (1997). *Cellular solids: Structure and properties* (Second edition ed.). Cambridge University Press.

Gibson, R. F. (2011). A mechanics of materials/fracture mechanics analysis of core shear failure in foam core composite sandwich beams. *Journal of Sandwich Structures and Materials 13* (1), 83–95.

Grandt, A. (2004). *Fundamentals of structural integrity: damage tolerant design and nondestructive evaluation.* U.S.A: Jonh Wiley & Sons, Inc.

Guo, T. and Y.-W. Chen (2011). Field stress/displacement monitoring and fatigue reliability assessment of retrofitted steel bridge details. *Engineering Failure Analysis 18* (1), 354–363.

Guo, T., A. Q. Li, and J. H. Li (2008). Fatigue life prediction of welded joints in orthotropic steel decks considering temperature effect and increasing traffic flow. *Structural Health Monitoring 7* (3), 189–202.

Hameau, G., C. Puch, and A.-M. Ajour (1981). Revêtements de chaussées sur platelages métalliques. 2. Comportement à la fatigue en flexion sous moment négatif. *Bulletin de liaison des laboratoires des ponts et chaussées 111*, 29–38.

Hardy, S. and M. Pipelzadeh (1991). Static analysis of short beams. *The Journal of strain analysis for engineering design 26* (1), 15–29.

Hobbacher, A. (2009). The new IIW recommendations for fatigue assessment of welded joints and components - A comprehensive code recently updated. *International Journal of Fatigue 31* (1), 50 – 58.

Huang, C., A. Mangus, and C. Copelan (2010). Icons of movable bridges utilizing orthotropic bridge decks. In *2010 Structures congress*, Florida, USA, pp. 3415–3430.

Huurman, M., T. Medani, A. Molenaar, C. Kasbergen, and A. Scarpas (2004). APT Testing and 3D Finite Element Analysis of Asphalt Surfacing on Orthotropic Steel Deck Bridges. In *2nd International Conference on Accelerated Pavement Testing*, Minneapolis, USA.

Inokuchi, S., S. Kainuma, A. Kawabata, and D. Uchida (2008). Field measurements and development of an experimental system for fatigue cracking from weld roots between deck plate and U-rib in orthotropic steel decks. In *International Orthotropic Bridge Conference 2008*, Sacramento, USA.

Ishio, M., T. Tamakoshi, J. Murakoshi, A. Kawabata, and S. Inokushi (2008). Experimental study on durability of orthotropic steel decks and deckplate thickness. In *International Orthotropic Bridge Conference 2008*, Sacramento, USA.

ISO-527 (1996). EN ISO 527:1996 Plastics – Determination of tensile properties.

ISO-8501 (2007). ISO 8501-1:2007 Preparation of steel substrates before application of paints and related products.

Janss, J. (1988). Fatigue of welds in orthotropic bridge decks panels with trapezoidal stiffeners. *Journal of Constructional Steel Research 9*, 147–154.

Jong, F. (2004). Overview fatigue phenomenon in orthotropic bridge decks in the Netherlands. In *2004 Orthotropic Bridge Conference*, Sacramento, USA.

Jong, F. and M. Kolstein (2004). Strengthening a bridge with high performance concrete. In *2004 Orthotropic Bridge Conference*, Sacramento, USA.

Jong, F., M. Kolstein, and F. Bijlaard (2004). Strain measurement tests at orthotropic steel bridge decks with heavy vehicle simulator. In *10th Nordic Steel Construction Conference*, Copenhagen, Denmark, pp. 401–412.

Jong, F. B. P. (2006). Renovation techniques for fatigue cracked orthotropic steel bridge decks. PhD thesis, Delft University of Technology.

Kennedy, D., R. Dorton, and S. Alexander (2002). The sandwich plate system for bridge decks. In *2002 International Bridge Conference*, Pittsburgh, USA, pp. 1–13.

Kennedy, S. and T. Murray (2004). Ultimate strength of an SPS bridge – The Shenley bridge. In *2004 Annual Conference of the Transportation Association of Canada*, Québec, Canada, pp. 1–13.

Kiss, K. and L. Dunai (2002). Fracture mechanics based fatigue analysis of steel bridge decks by two-level cracked models. *Computers & Structures 80*(27-30), 2321 – 2331.

Kolstein, H. (2004). Stress reduction due to surfacing on orthotropic steel decks. In *10th Nordic Steel Construction Conference*, Copenhagen, Denmark, pp. 425–437.

Kolstein, H. (2007). Fatigue classification of welded joints in orthotropic steel bridge decks. PhD thesis, Delft University of Technology.

Kolstein, H., J. Wardenier, and H. Weijde (1998). A new type of fatigue failures in steel orthotropic bridge decks. In *Fifth Pacific Structural Steel Conference*, Seoul, Korea.

Kolstein, M. and H. Sliedrecht (2008). Reduction of traffic induced stresses using high strength concrete. In *2008 International Orthotropic Bridge Conference*, Sacramento, USA.

Kulkarni, N., H. Mahfuz, S. Jeelani, and L. A. Carlsson (2004). Fatigue failure mechanism and crack growth in foam core sandwich composites under flexural loading. *Journal of Reinforced Plastics and Composites 23*(1), 83–94.

Labordus, M. (2006). Vacuum infused bonded steel reinforcing plates for bridge rehabilitation. In *International Bridge Technology Conference and Trade Show*, Rotterdam, The Netherlands. Bridge Engineering.

Leander, J., A. Andersson, and R. Karoumi (2010). Monitoring and enhanced fatigue evaluation of a steel railway bridge. *Engineering Structures 32*(3), 854–863.

Lee, L. S., V. M. Karbhari, and C. Sikorsky (2007). Structural Health Monitoring of CFRP Strengthened Bridge Decks Using Ambient Vibrations. *Structural Health Monitoring 6*(3), 199–214.

Li, Z. X., T. H. T. Chan, and R. Zheng (2003). Statistical analysis of online strain response and its application in fatigue assessment of a long-span steel bridge. *Engineering Structures 25*(14), 1731–1741.

Liu, X., T. Medani, A. Scarpas, M. Huurman, and A. Molenaar (2008). Experimental and numerical characterization of a membrane material for orthotropic steel deck bridges: Part 2. *Finite Elements in Analysis and Design 44*(9-10), 580–594.

Mangus, A. and S. Sun (2000). Orthotropic Deck Bridges. In W.-F. Chen and L. Duan (Eds.), *Bridge engineering handbook*, pp. 1–47. CRC Press.

Matuschek, J., T. Stihl, and S. Bild (2007). Verstärkung der orthotropen Stahlfahrbahn der Schönwasserparkbrücke mittels Stahl-Elastomer-Sandwich (SPS). *Stahlbau 76*(7), 465–471.

Medani, T. (2006). Design principles of surfacings on orthotropic steel bridge decks. PhD thesis, Delft University of Technology.

Medani, T., X. Liu, M. Huurman, A. Scarpas, and A. Molenaar (2008). Experimental and numerical characterization of a membrane material for orthotropic steel deck bridges: Part 1: Experimental work and data interpretation. *Finite Elements in Analysis and Design 44*(9-10), 552–563.

Miki, C. (2006). Fatigue damage in orthotropic steel bridge decks ad retrofic work. *Steel structures 6*, 255–267.

Minten, J., G. Sedlacek, M. Paschen, M. Feldmann, and A. Geler (2007). SPS ein neues Verfahren zur Instandsetzung und Ertüchtigung von stählernen orthotropen Fahrbahnplatten. *Stahlbau 76*(7), 438–454.

Murakoshi, J., N. Yanadori, T. Ui, S. Inokuchi, T. Ishigaki, T. Kodama, and N. Oguri (2008). Research on steel fiber reinforced concrete pavement on orthotropic steel deck. In *International Orthotropic Bridge Conference 2008*, Sacramento, California, USA, pp. 359–371.

NF-P98-286 (2006). Essais relatifs aus chaussées - Produits d'étanchéité pour ouvrages d'art - Détermination de la résistance à la fatigue d'une étanchéité/roulement sur tôle métallique - Méthode d'essai sur banc de fatigue en flexion sous moment négatif.

Overduin, L., A. Romeijn, and M. Kolstein (1999). Modelling of bridge deck systems for orthotropic steel bridges. In *Proceedings National Conference on Computational Mechanics*, Volos, Greece.

Pfeil, M. S., R. C. Battista, and A. J. Mergulho (2005). Stress concentration in steel bridge orthotropic decks. *Journal of Constructional Steel Research 61*, 1172–1184.

Pouget, S., C. Sauzéat, H. Benedetto, and F. Olard (2010). Numerical simulation of the five-point bending tests designed to study bituminous wearing courses on orthotropic steel bridges. *Materials and Structures 43*, 319–330.

Pover, J. (2002). Rapportage mbt uitgevoerde analyses tbv levensduurverlengende oplossingen in het kader van het PSR-project (Problematiek Stalen Rijdekken). Technical report, Rijkswaterstaat.

Pover, J. (2004). Rapportage mbt uitgevoerde analyses tbv levensduurverlengende oplossingen in het kader van het PSR-project (Problematiek Stalen Rijdekken), Deel DPS02-scheur. Technical report, Rijkswaterstaat.

Prasad, S. and L. A. Carlsson (1994). Debonding and crack kinking in foam core sandwich beams–ii. experimental investigation. *Engineering Fracture Mechanics 47*(6), 825–841.

Reddy, J. (2004). *Mechanics of laminated composite plates and shells: theory and analysis*. New York: CRC Press.

Sartor, R. R., M. P. Culmo, and J. T. DeWolf (1999). Short-term strain monitoring of bridge structures. *Journal of Bridge Engineering 4*(3), 157–164.

Schrieks, M. (2006). Lifespan enlargement of deck plates of movable steel bridges. MSc thesis, Delft University of Technology.

Sharma, N., R. F. Gibson, and E. O. Ayorinde (2006). Fatigue of foam and honeycomb core composite sandwich structures: a tutorial. *Journal of Sandwich Structures and Materials 8*, 263–319.

Shenoi, R., S. Clark, and H. Allen (1995). Fatigue behaviour of polymer composite sandwich beams. *Journal of Composite Materials 29*(18), 2423–2445.

Shipsha, A., M. Burman, and D. Zenkert (1999). Interfacial fatigue crack growth in foam core sandwich structures. *Fatigue and Fracture of Engineering Materials and Structures 22*(2), 123–131.

Sim, H., C. Uang, and C. Sikorsky (2009). Effects of fabrication procedures on fatigue resistance of welded joints in steel orthotropic decks. *Journal of Bridge Engineering 14*(5), 366–373.

Smith, J. and S. Bright (2001). Upgrading orthotropic bridge decks with fiber reinforced composites. In *Proceedings of the international conference high performance materials in bridges*, Kona, Hawaii, pp. 463–472.

Smith, J. and M. Cullimore (1987). Stress reduction due to surfacing on a steel bridge deck. In *International Conference on Steel and Aluminium Structures*, Cardiff, UK, pp. 806–814.

Straalen, I. J. and G. J. Hagen (2003). TNO 2003-BC-R0062: Proeven op stalen rijdekken - levensduurverlengende oplossing met een 6 mm dikke staalplaat gelijmde op het rijdek. Technical report, TNO.

Teixeira de Freitas, S., H. Kolstein, and F. Bijlaard (2010). Composite bonded systems for renovations of orthotropic steel bridge decks. *Composite Structures 92*, 853–862.

Teixeira de Freitas, S., H. Kolstein, and F. Bijlaard (2011). Sandwich system for renovation of orthotropic steel bridge decks. *Journal of Sandwich Structures and Materials 13*(3), 279–301.

Teixeira de Freitas, S., H. Kolstein, and F. Bijlaard (2012a). Parametric study on the interface layer of renovation solutions for orthotropic steel bridge decks. *Computer-Aided Civil and Infrastructure Engineering 27*(2), 143–153.

Teixeira de Freitas, S., H. Kolstein, and F. Bijlaard (2012b). Structural monitoring of a strengthened orthotropic steel bridge deck using strain data. *Structural Health Monitoring* (accepted).

Tsakopoulos, P. and J. Fisher (2003). Full-scale fatigue tests of steel orthotropic decks for Williamsburg bridge. *Journal of Bridge Engineering 8*, 323–333.

Uchida, D., S. Inokuchi, A. Kawabata, M. Ishio, and T. Tamakoshi (2008). Field investigations and measurements of orthotropic steel decks to draft efficient method of stock management. In *International Orthotropic Bridge Conference 2008*, Sacramento, USA.

Vincent, R. and A. Ferro (2004). A new orthotropic bridge deck: Design, fabrication and construction of the shenley bridge incorporating an sps orthotropic bridge deck. In *2004 Orthotropic Bridge Conference*, Sacramento, California, USA.

Walter, R. (2005). Cement-based overlay for orthotropic steel bridge decks: a multi-scale modeling approach. PhD thesis, Technical University of Denmark.

Walter, R., J. F. Olesen, H. Stang, and T. Vejrum (2007). Analysis of an orthotropic deck stiffened with a cement-based overlay. *Journal of Bridge Engineering 12*(3), 350–363.

Wang, C. and Y. Feng (2008). Review of the fatigue behaviors and finite element analysis of orthotropic steel bridge decks. In *International Orthotropic Bridge Conference 2008*, Sacramento, California, USA.

Wolchuk, R. (1990). Lessons from weld cracks in orthotropic decks on three European bridges. *Journal of Structural Engineering 116*(1), 75–84.

Wolchuk, R. (2002). Structural behaviour of surfacings on steel orthotropic decks and considerations for practical design. *Structural Engineering Journal 2*, 124–129.

Xiao, Z.-G., K. Yamada, J. Inoue, and K. Yamaguchi (2006). Fatigue cracks in longitudinal ribs of steel orthotropic decks. *International Journal of Fatigue 28*, 409–416.

Xiao, Z.-G., K. Yamada, S. Ya, and X.-L. Zhao (2008). Stress analyses and fatigue evaluation of rib-to-deck joints in steel orthotropic decks. *International Journal of Fatigue 30*, 1387–1397.

Ya, S. and K. Yamada (2008). Fatigue durability of trough to deck plate welded joints of orthotropic steel bridge deck. *Structural Eng./Earthquake Eng. 25*(2), 33–46.

Ya, S., K. Yamada, and T. Ishikawa (2011). Fatigue evaluation of rib-to-deck welded joints of orthotropic steel bridge deck. *Journal of Bridge Engineering 16*(4), 492–499.

Yuge, T., F. Machida, H. Morikawa, C. Miki, T. Kamiki, and T. Masui (2004). Analyses of fatigue damage patters in orthotropic steel deck of Tokyo metropolitan expressways. In *2004 Orthotropic Bridge Conference*, Sacramento, California, USA.

Zenkert, D. (1991). Strength of sandwich beams with interface debondings. *Composite Structures 17*(4), 331 – 350.

Zenkert, D. (1997). *An Introduction to Sandwich Construction*. London: Chameleon Press, Ltd.

Zenkert, D. and M. Burman (2009). Tension, compression and shear fatigue of a closed cell polymer foam. *Composites Science and Technology 69*(6), 785 – 792.

Zhang, D., Y. Li, and C. Cui (2011). A retrofitted case study of orthotropic steel bridge decks strengthened with sandwich plate system. *Advanced Materials Research 163-167*, 410–416.

Zhang, Y., Y. Li, and D. Zhang (2011). Fatigue life estimation of rib-to-deck joints in orthotropic steel decks. *Advanced Materials Research 163-167*, 410–416.

Appendix A

Mesh convergency study

The convergency study analyses the mesh dependency of three geometrical parameters of the OBD-FEA: (i) crossbeam web and trough thickness, (ii) reinforcement thickness (bonded and sandwich steel plates overlay) and (iii) steel deck plate thickness. These are the parameters which influence the most the stress field of the deck plate close to the welds and the stress field of the reinforcement. Table A.1 shows the characteristics of the meshes studied. The standard mesh is the one described in Chapter 6 and used in the current thesis. Meshes 1 to 4 are refinements of the standard mesh. In each refined mesh, one parameter is studied.

Figures A.1 and A.2 show the meshes refinements close to the deck-plate-to-stiffener weld.

Table A.1: Mesh parameters values – elements per thickness.

Mesh	Crossbeam & Trough	Reinforcement		Deck Plate
		Bonded	Sandwich	
Standard	2	4 core	1 adhesive	2
		2 new plate	2 new plate	
Mesh 1	**4**	4 core	1 adhesive	2
		2 new plate	2 new plate	
Mesh 2	2	**6 core**	**2 adhesive**	2
		2 new plate	2 new plate	
Mesh 3	2	4 core	1 adhesive	**4**
		2 new plate	2 new plate	
Mesh 4	2	4 core	1 adhesive	> 4
		2 new plate	2 new plate	

(a) Standard   (b) Mesh 1   (c) Mesh 2   (d) Mesh 3   (e) Mesh 4
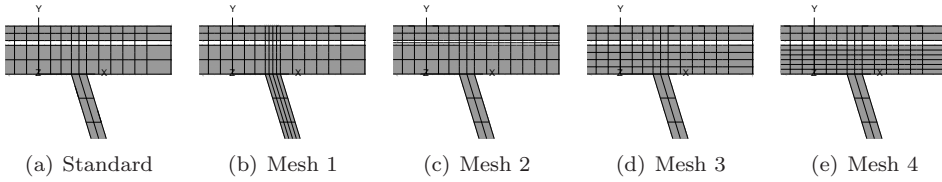
Figure A.1: Mesh refinement of the bonded steel plates reinforcement model.

(a) Standard   (b) Mesh 1   (c) Mesh 2   (d) Mesh 3   (e) Mesh 4
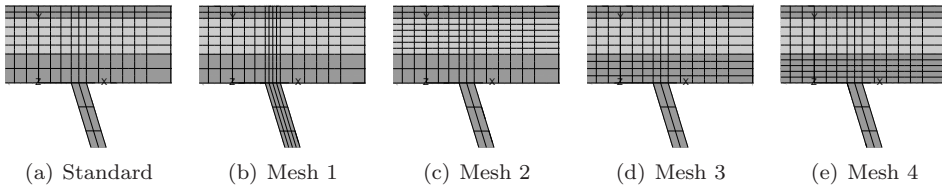
Figure A.2: Mesh refinement of the sandwich steel plates reinforcement model.

The load cases used for the mesh convergency study are shown in Figures A.3 and A.4 for the Crossbeam-FE model and for the Midspan-FE model, respectively. The results are presented to 100 kN wheel-loads.

In the Crossbeam-FE model, wheel type C (WC) is the worse load case and therefore it was selected for the convergency study. The stresses obtained for the several meshes are shown in Figures A.5 and A.6 for the sandwich and bonded steel plates reinforced deck-panels, respectively. In all cases the results of the standard mesh coincide with the four refined meshes, except for the point of stress concentration at the welds (see Figure A.5(a) and A.6(a) for the sandwich and bonded FE model, respectively). The transverse stresses at the deck-plate-to-stiffener welds at the crossbeam's web is an unstable point and does not converge even if the mesh is very fine (Mesh 3 and Mesh 4). Moreover, this unstable point is very local, if one takes the point 5 mm from the peak point, the stresses are stable and coincide for the various meshes. Therefore this point was not taken as a reference point for the convergency of the mesh, but 5 mm next to it.

The results of the Midspan-FE model are shown in Figures A.7 to A.10. Wheel type B (WB) is the worse load case for the welds, however wheel type C (WC) is the worse for the shear stresses at the reinforcement interface layer (core for the sandwich and adhesive for the bonded, see Figures A.7(e), A.8(e), A.9(e) and A.9(e)). Therefore, both load cases were analysed. In all cases the results of the standard mesh coincide with the three refined meshes (Mesh 1, 2 and 3), which proves the mesh independency of the analysis. In this case, it was not necessary to run models with Mesh 4, since the results from Mesh 3 are already coincident with the standard mesh results.

(a) longitudinal view

(b) transverse view
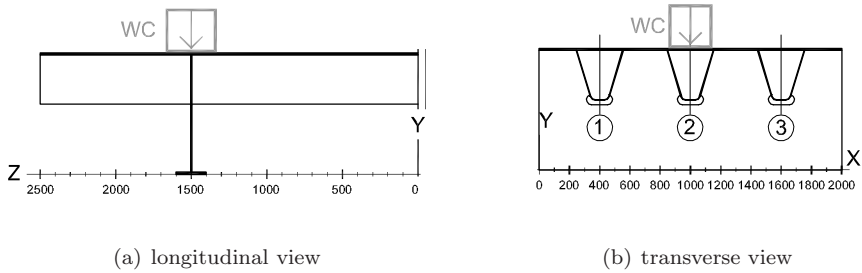
Figure A.3: Crossbeam's load case used for the mesh convergency study.

(a) longitudinal view

(b) transverse view
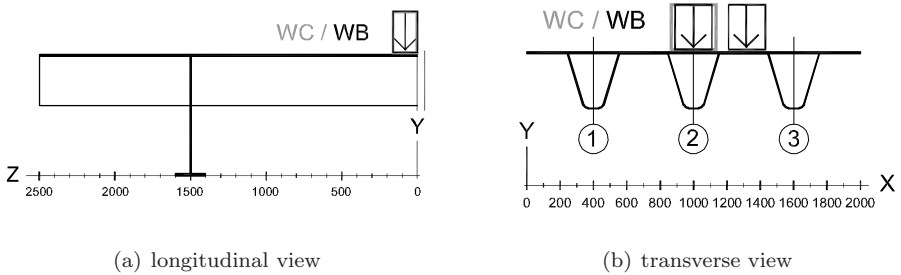
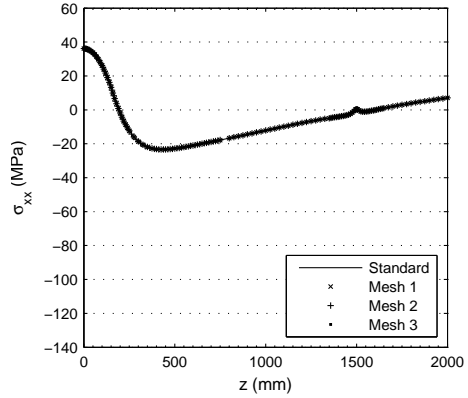Figure A.4: Midspan's load cases used for the mesh convergency study.
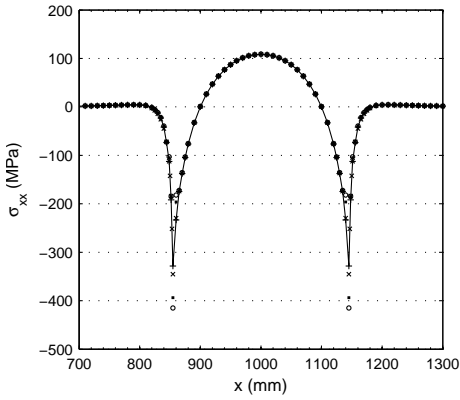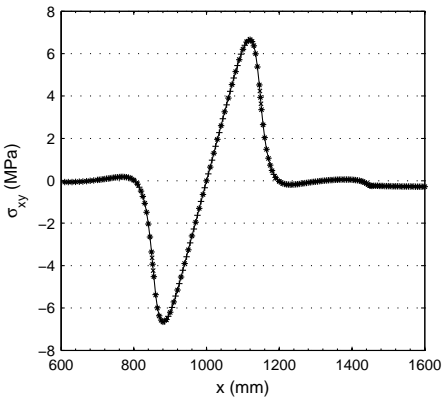
(a) bottom side of the steel deck
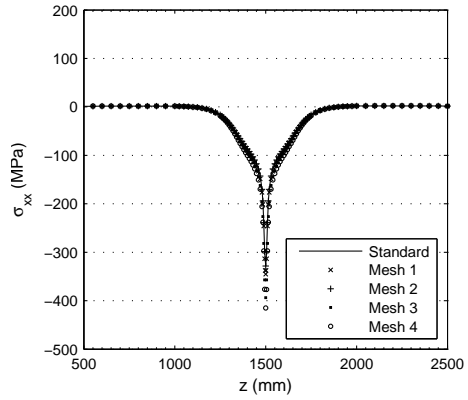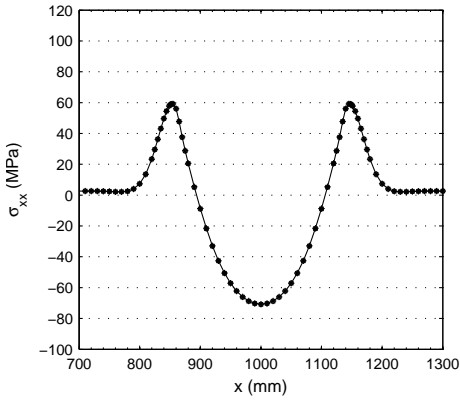
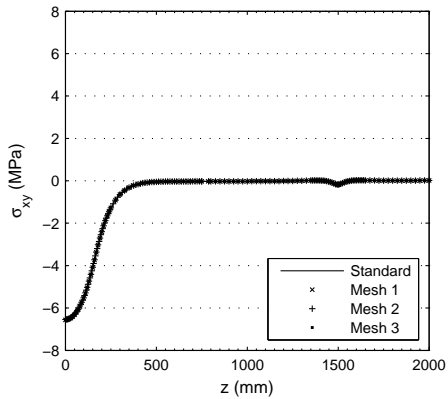(b) bottom side of the steel deck at the welds

(c) top side of the 2nd steel plate
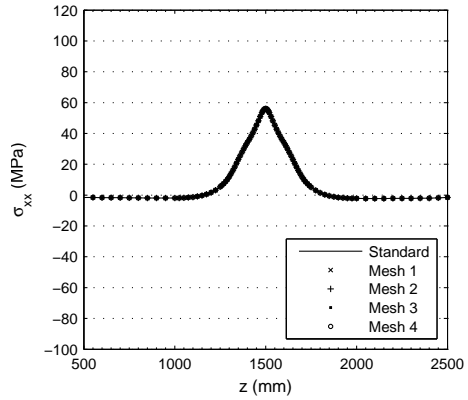
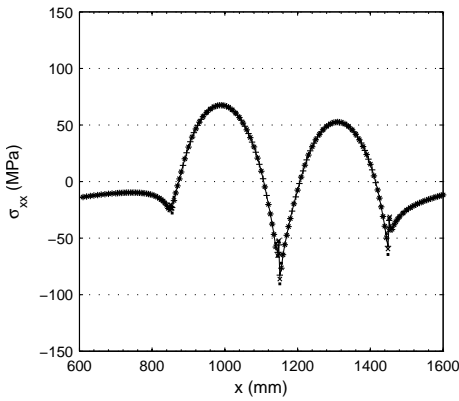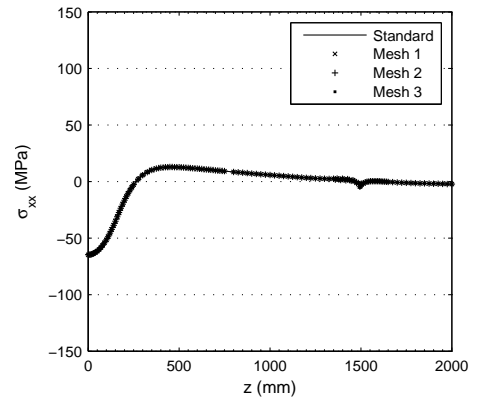(d) top side of the 2nd steel plate at the welds
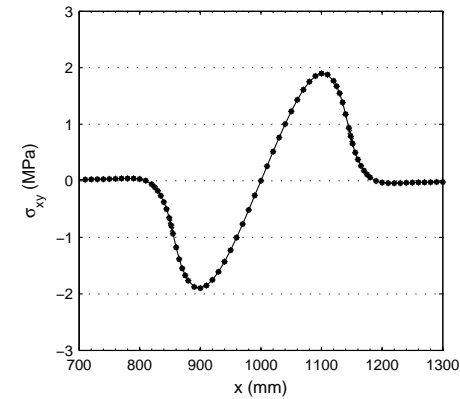
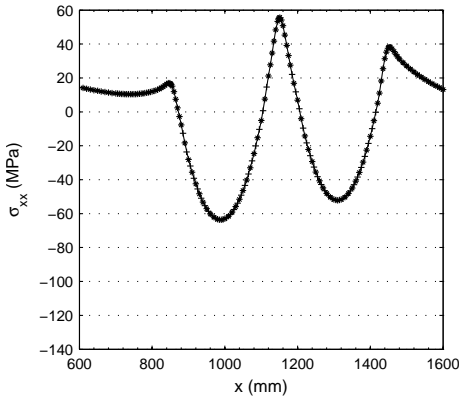(e) core mid-thickness
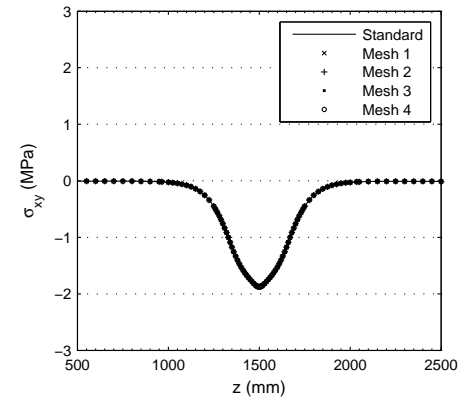
(f) core mid-thickness at x = 900 mm

Figure A.5: Stresses from the Crossbeam-FE model of the sandwich steel plates reinforced deck-panel loaded by WC (100 kN), along the crossbeam width close to the middle trough (x-axis) and along the model length close to the crossbeam (z=1500).
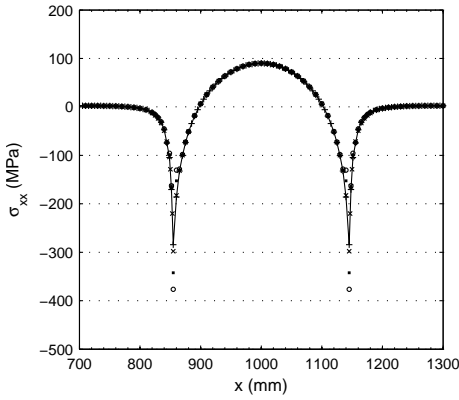
(a) bottom side of the steel deck
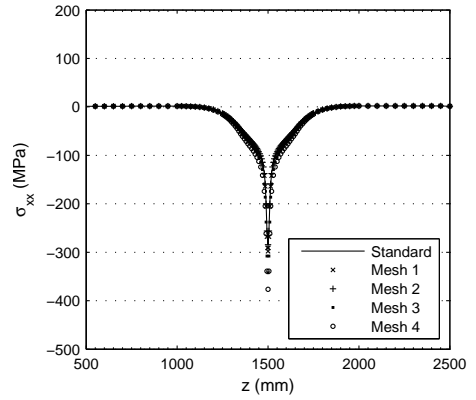
(b) bottom side of the steel deck at the welds
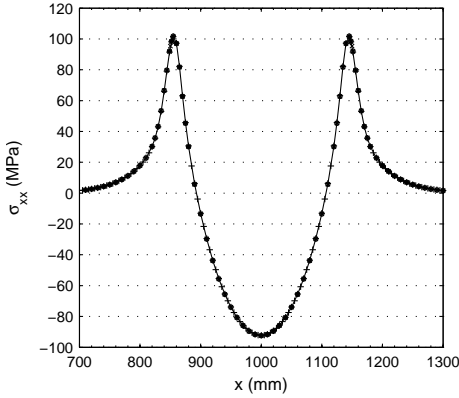
(c) top side of the 2nd steel plate
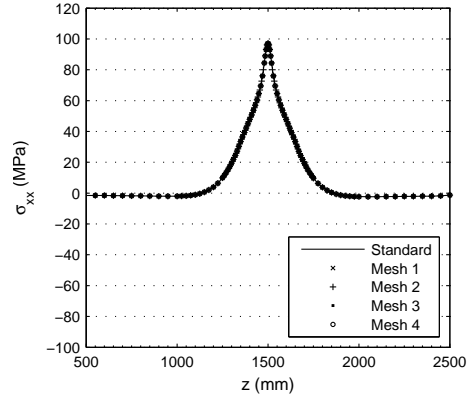
(d) top side of the 2nd steel plate at the welds
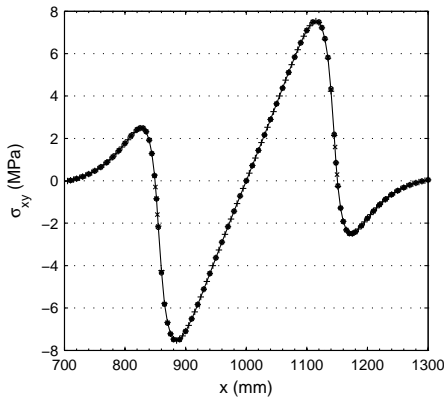
(e) adhesive mid-thickness
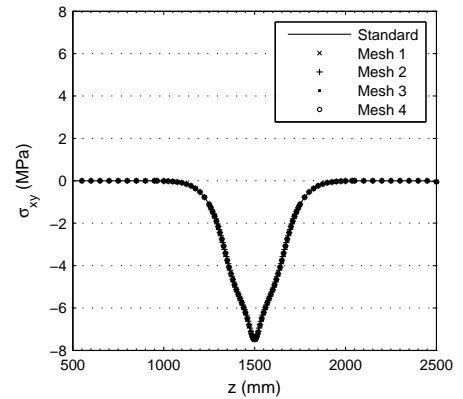
(f) adhesive mid-thickness at x = 900 mm

Figure A.6: Stresses from the Crossbeam-FE model of the bonded steel plates reinforced deck-panel loaded by WC (100 kN), along the crossbeam width close to the middle trough (x-axis) and along the model length close to the crossbeam (z=1500).
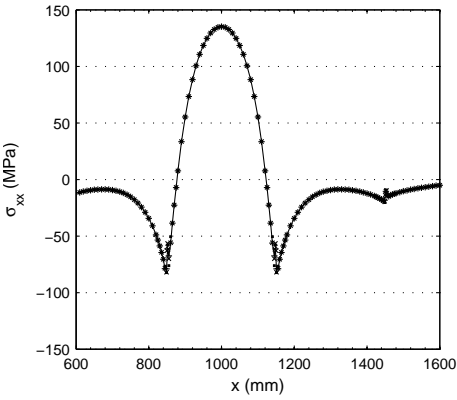
(a) bottom side of the steel deck
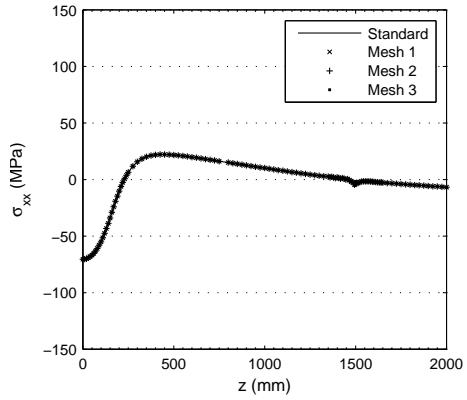
(b) bottom side of the steel deck at the welds
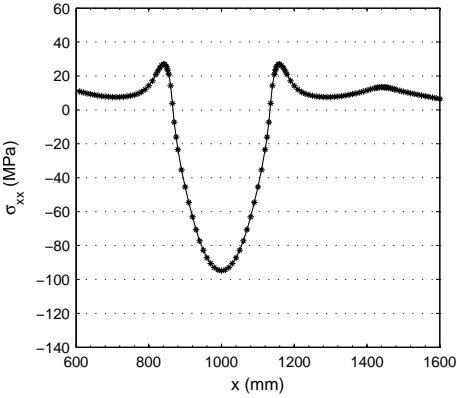
(c) top side of the 2nd steel plate
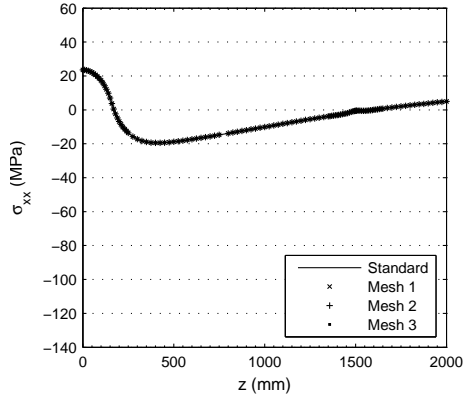
(d) top side of the 2nd steel plate at the welds
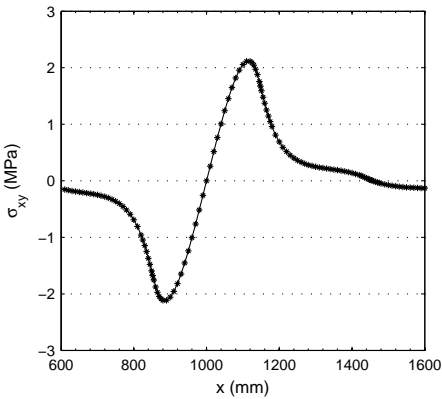
(e) core mid-thickness
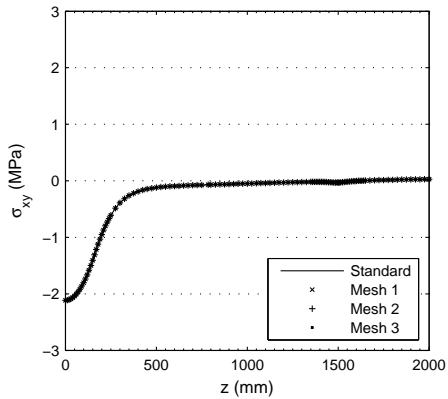
(f) core mid-thickness at x = 900 mm

Figure A.7: Stresses from the Midspan-FE model of the sandwich steel plates reinforced deck-panel loaded by WC (100 kN), along midspan width close to the middle trough (x-axis) and along the model length between midspan (z=0) and cross-beam (z=1500).
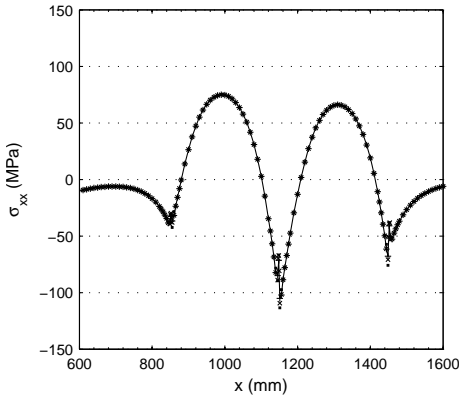
(a) bottom side of the steel deck
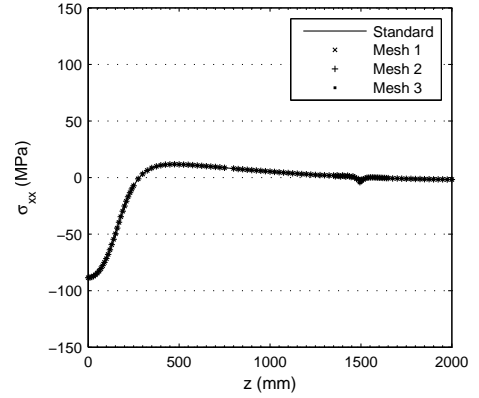
(b) bottom side of the steel deck at the welds
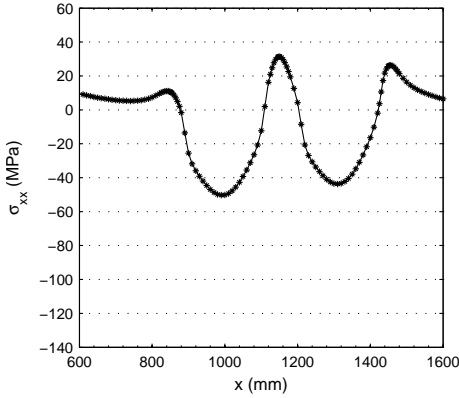
(c) top side of the 2nd steel plate
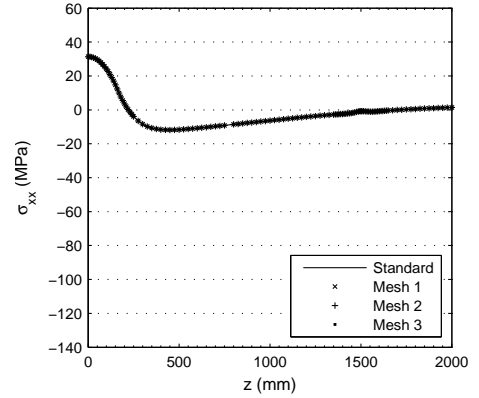
(d) top side of the 2nd steel plate at the welds
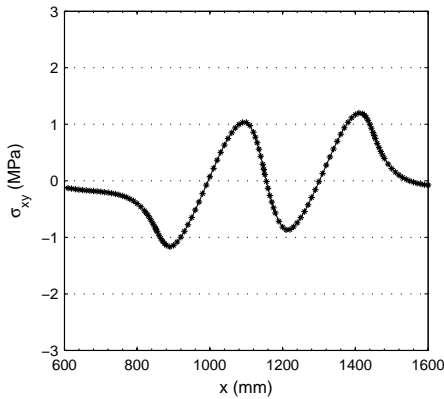
(e) core mid-thickness
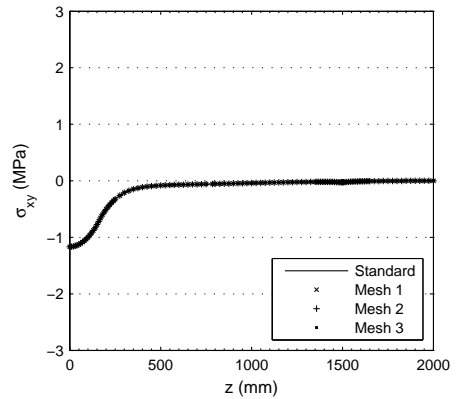
(f) core mid-thickness at x = 900 mm

Figure A.8: Stresses from the Midspan-FE model of the sandwich steel plates reinforced deck-panel loaded by WB (100 kN), along midspan width close to the middle trough (x-axis) and along the model length between midspan (z=0) and cross-beam (z=1500).
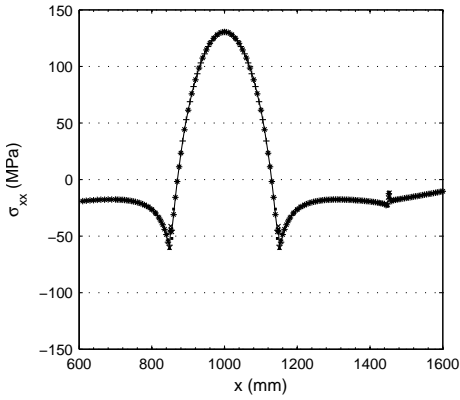
(a) bottom side of the steel deck
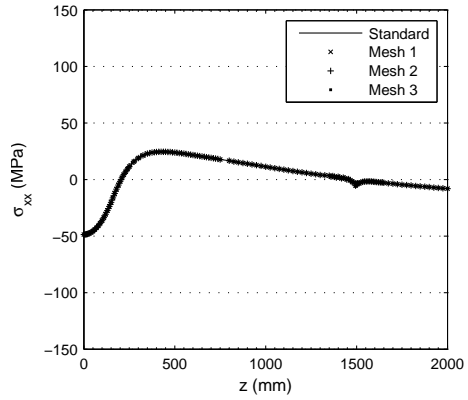
(b) bottom side of the steel deck at the welds
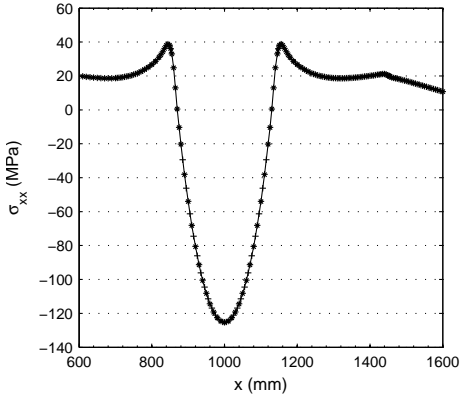
(c) top side of the 2nd steel plate

(d) top side of the 2nd steel plate at the welds

(e) core mid-thickness

(f) core mid-thickness at x = 900 mm

Figure A.9: Stresses from the Midspan-FE model of the bonded steel plates reinforced deck-panel loaded by WC (100 kN), along midspan width close to the middle trough (x-axis) and along the model length between midspan (z=0) and crossbeam (z=1500).

(a) bottom side of the steel deck

(b) bottom side of the steel deck at the welds

(c) top side of the 2nd steel plate
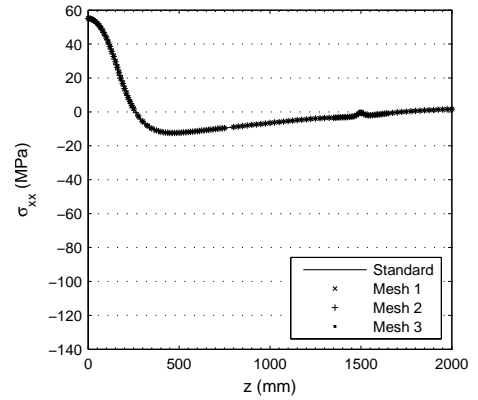
(d) top side of the 2nd steel plate at the welds
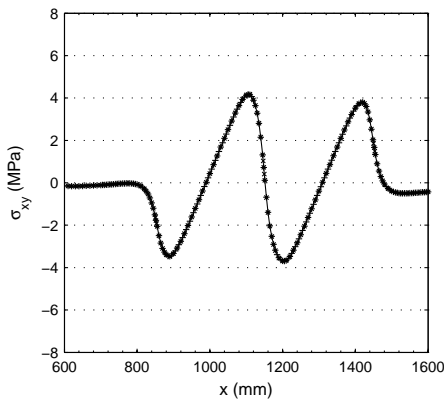
(e) core mid-thickness
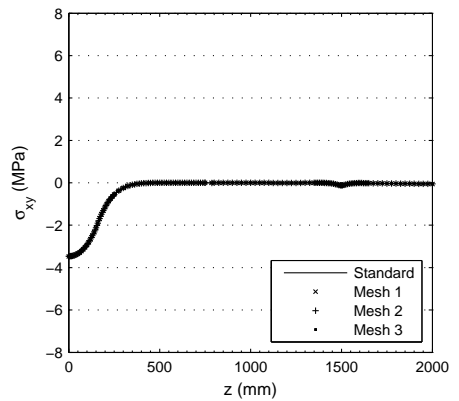
(f) core mid-thickness at x = 900 mm

Figure A.10: Stresses from the Midspan-FE model of the bonded steel plates reinforced deck-panel loaded by WB (100 kN), along midspan width close to the middle trough (x-axis) and along the model length between midspan (z=0) and cross-beam (z=1500).

Appendix B

Static full-scale tests

B.1   Pressure sensitive paper

Table B.1 shows photos of five typical pressure sensitive papers obtained during the full-scale static tests. For each type, a load distribution was determined. Table B.2 shows the load distribution corresponding to each load case and deck states. These loads distributions were used in the corresponding numerical simulations.

B.2   Static test results and numerical validation

Figures B.1 and B.2 show the results of the bonded steel plates reinforced deck when it is loaded at the crossbeam. The wheel load is 100 kN and it is aligned with the troughs 1 and 3, respectively. The wheel print is type C. The results are comparable with the ones obtained when the load is aligned with the middle trough (see Figure 7.13, page 126). The main difference is the location of the stress area, which in all cases is aligned with the loaded trough. The numerical prediction fits well with the experimental values, $n/e = 0.95 \pm 0.10$ for trough 1 and $n/e = 0.94 \pm 0.08$ for trough 3.

Figures B.3 and B.4 show the corresponding results for the sandwich steel plates reinforced deck (100 kN load wheel type C aligned with troughs 1 and 3). The results are once again comparable with ones obtained when the load is aligned with the middle trough (see Figure 7.15, page 128), only shifted to the correspondent loaded trough (troughs 1 and 3). The numerical prediction fits less good with the experimental values than for the bonded reinforcement. Nevertheless the deviation is still acceptable , $n/e = 1.07 \pm 0.17$ for trough 1 and $n/e = 1.10 \pm 0.12$ for trough 3.

Table B.1: Pressure sensitive paper tests: photos and load distribution for 100 kN.
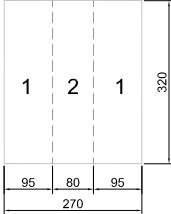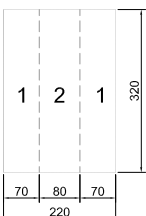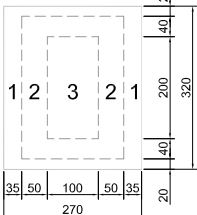
Wheel type	Photo print	Load distribution
Wheel C Uniform		$p_{uniform}^{C} = 1.15741\ \text{MPa}$
Wheel B Uniform		$p_{uniform}^{B} = 0.71023\ \text{MPa}$
Wheel C a		$p_{1a}^{C} =$ 0.89 MPa $p_{2a}^{C} =$ 1.7925 MPa
Wheel B a		$p_{1a}^{C} =$ 0.5195 MPa $p_{2a}^{C} =$ 1.044 MPa
Wheel C b		$p_{1b}^{C} =$ 0.62 MPa $p_{2b}^{C} =$ 1.23 MPa $p_{3b}^{C} =$ 1.8436 MPa

Table B.2: Wheel load distribution at each load case and corresponding FEA of the bridge deck specimens.

| Location	Unreinforced	Bonded	Sandwich
Midspan	Wheel C a Wheel B a	Wheel C a Wheel B a	Wheel C Uniform Wheel B Uniform
Crossbeam	Wheel C a	Wheel C a	Wheel C Uniform Wheel C b
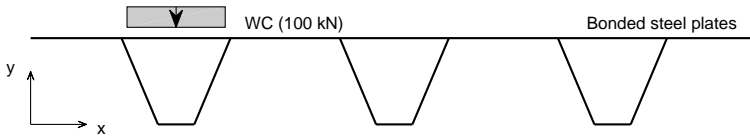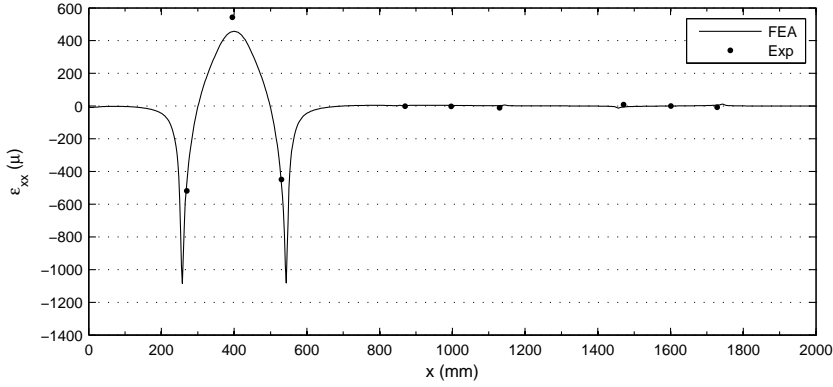
(a) crossbeam cross-section
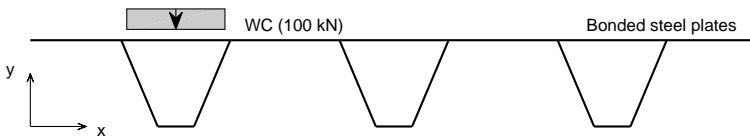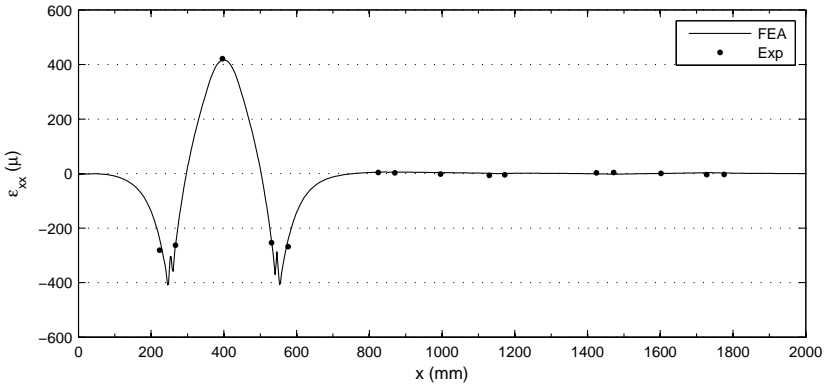
(b) 75 mm from crossbeam cross-section

Figure B.1: Transverse strains ε_{xx} at the bottom side of the bonded steel plates reinforced deck plate along the specimen width recorded during testing (Exp) and predicted by the FEA (100 kN wheel load type C aligned with trough 1 at the crossbeam – $n/e = 0.95 \pm 0.10$).
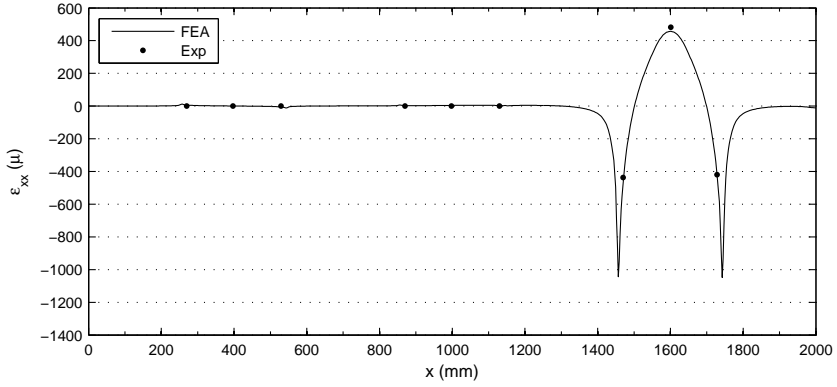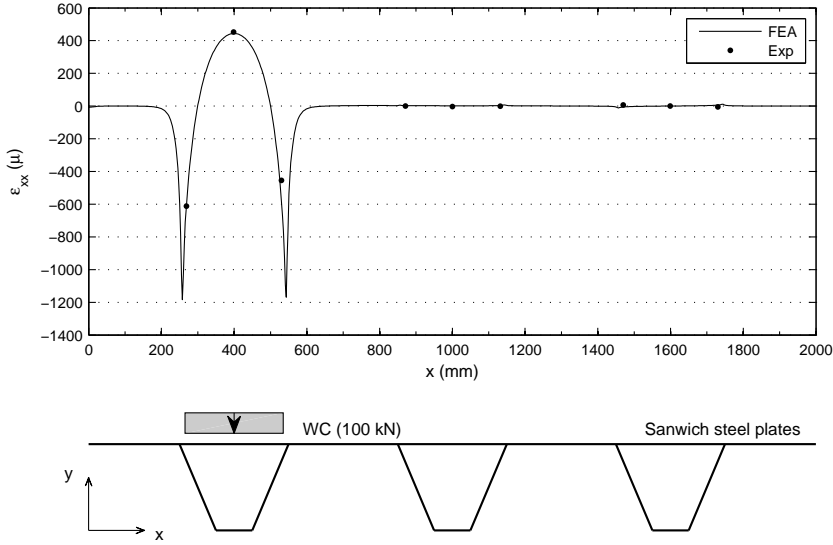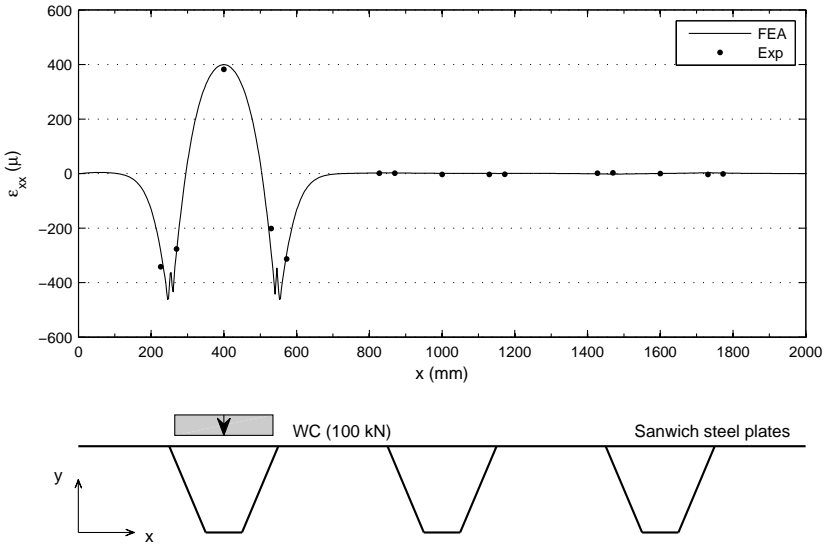
(a) crossbeam cross-section
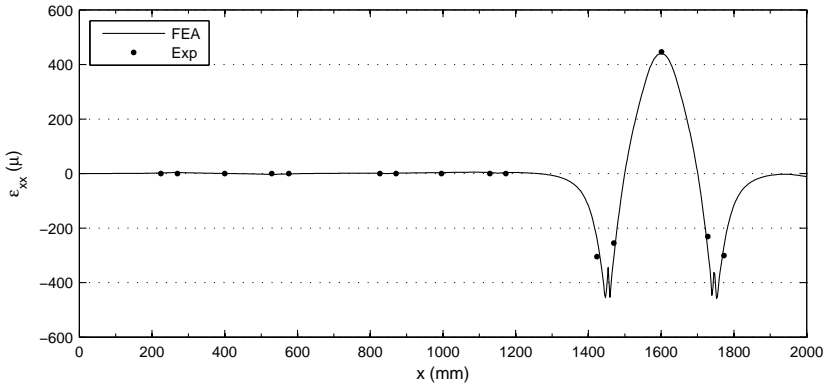
(b) 75 mm from crossbeam cross-section

Figure B.2: Transverse strains ε_{xx} at the bottom side of the bonded steel plates reinforced deck plate along the specimen width recorded during testing (Exp) and predicted by the FEA (100 kN wheel load type C aligned with trough 3 at the crossbeam – $n/e = 0.94 \pm 0.08$).
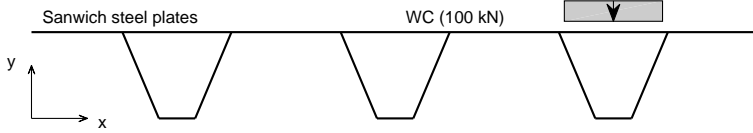
(a) crossbeam cross-section

(b) 75 mm from crossbeam cross-section

Figure B.3: Transverse strains ε_{xx} at the bottom side of the sandwich steel plates reinforced deck plate along the specimen width recorded during testing (Exp) and predicted by the FEA (100 kN wheel load type C aligned with trough 1 at the crossbeam – $n/e = 1.07 \pm 0.17$).
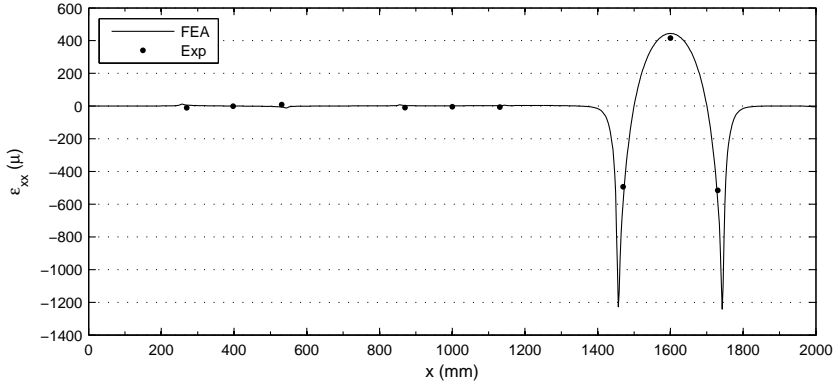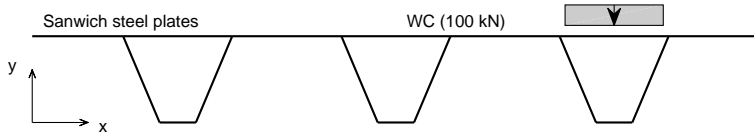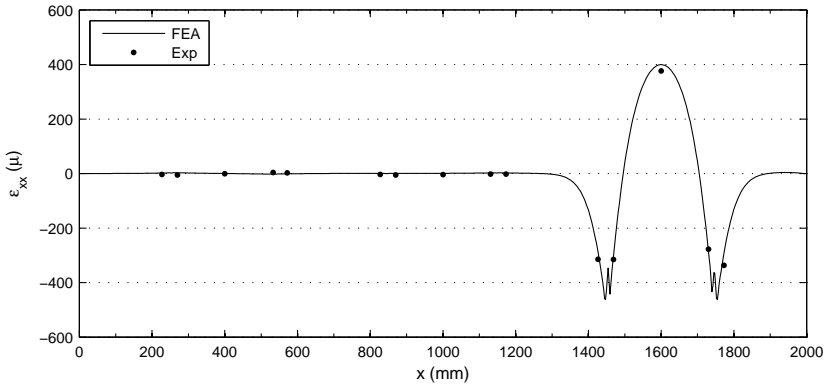
(a) crossbeam cross-section

(b) 75 mm from crossbeam cross-section

Figure B.4: Transverse strains ε_{xx} at the bottom side of the sandwich steel plates reinfor- ced deck plate along the specimen width recorded during testing (Exp) and predicted by the FEA (100 kN wheel load type C aligned with trough 3 at the crossbeam – $n/e = 1.10 \pm 0.12$).

Acknowledgements

First of all I would like to express my gratitude to Professor Frans Bijlaard and Dr. Henk Kolstein for giving me the opportunity to pursue this research. I am very thankful for their support, guidance and encouragement in all the key moments during my PhD.

This research included an extensive experimental program that was mainly conducted in the Stevin Laboratory II in the Faculty of Civil Engineering and Geosciences. As researchers, we must never forget the privilege of working in such unique facilities and with the help of an incredible team. I am extremely grateful to Arjen van Rhijn, John Hermsen and Kees van Beek for their daily support and for all the discussions during my research. Besides all, their friendship is one of the most valuable "outcomes of this research". I would also like to thank Intelligent Engineering for sponsoring all the material, fabrication and manufacturing of the sandwich specimens.

Over the last four years, besides being in the laboratory, I stayed long hours in my office. I would like to thank my office mates and most precious friends Edi, Neşen, Carmen, Richard, Xuhong and Xu. Thank you for your warm welcome and for your patience until the very last day.

Furthermore I would like to thank my parents for their guidance and support during all my life. My PhD would not have been the same without the incredible support of my father. His scientific guidance makes me who I am today as a researcher. He is my role model, giving me the right advices and the freedom to find my own way.

Finally, I would like to thank all my family and friends. A special thanks goes to João who is always supportive of all my decisions.

Curriculum vitae

Personal information

Name	Sofia Teixeira de Freitas
Email	sofreitas@gmail.com
Date of birth	30 November 1982
Nationality	Portuguese

Work experience

2008–2012	PhD researcher
	Delft University of Technology
	Faculty of Civil Engineering and Geosciences
	The Netherlands
2005–2007	Structural Design Engineer
	Teixeira Duarte, Engenharia e Construções, S.A.
	Portugal

Education

2000–2005	Degree in Civil Engineering
	Instituto Superior Técnico
	Portugal
	Final graduation thesis (February 2005–July 2005)
	Erasmus exchange program
	Delft University of Technology
	Faculty of Civil Engineering and Geosciences
	The Netherlands

List of Publications

Journal Publications

2012	Sofia Teixeira de Freitas, Henk Kolstein, and Frans Bijlaard. Structural Monitoring of a Strengthened Orthotropic Steel Bridge Deck using Strain Data. *Structural Health Monitoring* (accepted).
2012	Sofia Teixeira de Freitas, Henk Kolstein, and Frans Bijlaard. Parametric study on the interface layer of renovation solutions for orthotropic steel bridge decks. *Computer-Aided Civil and Infrastructure Engineering 27* (2), 143-153.
2011	Sofia Teixeira de Freitas, Henk Kolstein, and Frans Bijlaard. Sandwich system for renovation of orthotropic steel bridge decks. *Journal of Sandwich Structures and Materials 13*(3), 279-301.
2010	Sofia Teixeira de Freitas, Henk Kolstein, and Frans Bijlaard. Composite bonded systems for renovations of orthotropic steel bridge decks. *Composite Structures 92*, 853-862.

Conference Publications

2010	Sofia Teixeira de Freitas, Henk Kolstein, and Frans Bijlaard. Sandwich system for renovation of orthotropic steel bridge decks. In *9th International Conference on Sandwich Structures*, Pasadena, California, USA.
2009	Sofia Teixeira de Freitas, Henk Kolstein, and Frans Bijlaard. Sandwich and bonded systems in renovations of orthotropic steel bridges. In *15th International Conference on Composite Structures*, Porto, Portugal.
2009	Sofia Teixeira de Freitas, Henk Kolstein, Frans Bijlaard and Willem Souren. Orthotropic deck renovation of the movable bridge Scharsterrijn. In *Nordic Steel Construction Conference*, pp. 105-111, Malmo, Sweden.
2008	Sofia Teixeira de Freitas, Henk Kolstein, and Frans Bijlaard. Importance of the interface layer on behaviour and durability of orthotropic steel decks. In *International Orthotropic Bridge Conference 2008*, Sacramento, California, USA.
2005	Sofia Teixeira de Freitas, Peter de Vries, and Frans Bijlaard. Experimental Research on Single bolt connections for High Strength Steel S690. In *Actas do V Congresso de Construção Metálica e Mista*, pp. 679-688, Lisbon, Portugal.